DE GRUYTER

*Bireswar Banerjee (Ed.)*

# RUBBER NANO-COMPOSITES AND NANOTEXTILES

## PERSPECTIVES IN AUTOMOBILE TECHNOLOGIES

2ND EDITION

Bireswar Banerjee (Ed.)

**Rubber Nanocomposites and Nanotextiles**

## Also of interest


*Textile Chemistry*
Bechtold, Pham, 2019
ISBN 978-3-11-050067-7, e-ISBN 978-3-11-054989-8


*Chemical Product Technology*
Murzin, 2018
ISBN 978-3-11-047531-9, e-ISBN 978-3-11-047552-4


*Shape Memory Polymers*
Kalita, 2018
ISBN 978-3-11-056932-2, e-ISBN 978-3-11-057017-5


*Polymer Engineering*
Tylkowski, Wieszczycka, Jastrzab (Eds.), 2017
ISBN 978-3-11-046828-1, e-ISBN 978-3-11-046974-5


*e-Polymers*
ISSN 2197-4586
e-ISSN 1618-7229

# Rubber Nanocomposites and Nanotextiles

Perspectives in Automobile Technologies

Edited by
Bireswar Banerjee

2nd Edition

DE GRUYTER

**Editor**
Bireswar Banerjee
B-12/3 Karunamoyee Estate
Kolkata-700091
India

ISBN 978-3-11-064089-2
e-ISBN (E-BOOK) 978-3-11-064387-9
e-ISBN (EPUB) 978-3-11-064094-6

**Library of Congress Control Number: 2018966616**

**Bibliographic information published by the Deutsche Nationalbibliothek**
The Deutsche Nationalbibliothek lists this publication in the Deutsche Nationalbibliografie; detailed bibliographic data are available on the Internet at http://dnb.dnb.de.


Typesetting: Integra Software Services Pvt. Ltd.
Printing and binding: CPI books GmbH, Leck
Cover image: krystiannawrocki / E+ / Getty Images

www.degruyter.com

# Preface

In the early 1990s, a research team from Toyota Central Research Development Laboratories in Japan worked on Nylon 6–clay nanocomposites and revealed an improved process for producing Nylon 6–clay nanocomposites using *in situ* polymerisation similar to the Unichika Co. (Japan) method, who produced the first organoclay hybrid polyamide nanocomposite.

The first commercialisation of polymer nanocomposites took place in 1991 with the development of timing belt covers by Toyota Motor Co. In 2002, General Motors initiated a step-assist automotive component made of polyolefin reinforced with 3% nanoclay and, over the last decade, nanocomposite production has increased.

The objective of this book is to discuss the increasing demand for light weight automotive rubber parts and the role of polymer composites. Due to their advantages, e.g., superior strength and light weight, the application of polymer nanocomposites in automotive components enables the production of light weight vehicles, improved engine efficiency and decreased carbon dioxide emissions, which results in enhanced automobile performance.

It is forecasted that by the year 2022, the production of light vehicles on a global scale will reach 112 million units. In parallel, the global polymer nanocomposite market will be worth US $12,000 million by 2022.

Stringent government directives governing automotive emissions in a number of countries including, the USA, Germany, China, India and so on, have led to the growing use of polymer nanocomposites.

A team of ingenious scientists, professors and experienced rubber professionals, with extensive knowledge and research experience involving polymer nanocomposites and nanotextiles in automobile applications, have all contributed to this book.

The many advantages of nanocomposites over conventional composites, in terms of mechanical, electrical, thermal, barrier and chemical properties, e.g., increased tensile strength, improved heat deflection temperature, flame retardancy and so on, are reviewed in this book. In addition, examples of the scope and applications in the automobile industry, e.g., hoses, seals, tyres, tubes and flaps, are highlighted.

This book is comprised of six chapters that detail comprehensive views on the polymer nanocomposites and nanotextiles that feature in the fast-growing lighter automotive industry. Chapter 1 portrays the scope of application of elastomeric nanocomposites in automotive engineering with the utilisation of organoclay masterbatches that are light weight and exhibit balanced mechanical properties. Chapter 2 focuses on manufacturing tyre treads, with a description of elastomer nanocomposites, a vital component of pneumatic tyres that provide an extraordinary balance among three operational requirements, i.e., safety, comfort and cost.

https://doi.org/10.1515/9783110643879-201

Chapter 3 is a narrative on automotive components with respect to their mechanical characteristics. Chapter 4 discusses rubber–clay nanocomposites in relation to automobile components, and how the nanofillers, contrary to conventional ones, can significantly improve the functional properties of polymers. Rubber nanocomposites have also received considerable interest for strategic and critical applications in defence and aerospace sectors, which are also highlighted in this chapter. Chapter 5 details a comprehensive discussion regarding the advantages of ionic liquid(s) (IL)- mediated surface modification of multi-walled carbon nanotubes (CNT) over other methods, and the different roles of IL in CNT–rubber composites. An overview of CNT–elastomer composites is also presented.

Nanofibres (NF) or nanocomposite fibres for functional nanofinishing, nanocoatings or polymer nanocomposite coatings are gaining considerable interest for the development of smart, functional and high-performance textiles. Nanocomposite fibres have immense potential in automobile engineering components, and may transform the textile industry with new functionalities including: self-cleaning surfaces, conducting textiles, antimicrobial properties, controlled hydrophilicity and hydrophobicity, protection against fire and ultraviolet radiation, which are reviewed in Chapter 6.

The focus of this book is to offer concise information to the automobile component manufacturing industry, polymer technologists, students and researchers to obtain an overall view of polymer nanocomposites, its development and various applications in automobiles; in combination with the elaborate idea of NF and textiles engineered in the automobile industry. It is perceivable that future automobiles, railways and aerospace will endeavour to extensively employ nanotechnology.

I would like to express my sincere appreciation and gratitude to Ms Helene Chavaroche, Commissioning Editor, for her most sincere efforts to make this project successful and also to Mrs Eleanor Garmson, the Development Editor. We also appreciate the editorial service provided by Dr Liz Rees.

I indeed express my earnest thanks to all the staff of Smithers Rapra who assisted in the preparation and publication of this book.

# Contents

# Contributors

**Jiji Abraham**
International and Inter University Centre for
Nanoscience and Nanotechnology
Mahatma Gandhi University
P.D Hills, Kottayam
Kerala, 686560, India

**Bapan Adak**
Indian Institute of Technology
Department of Textile Technology
Hauz Khas
New Delhi, 110016, India

**Samar Bandyopadhyay**
A402, Mahalaxmi Apartment
Navratna Complex
Bedla Road, Udaipur
Rajasthan, 313001, India

**Bireswar Banerjee**
B – 12/3, Karunamoyee Estate
Salt Lake, Kolkata, 700091, India

**Bhagabat Bhuyan**
Indian Institute of Technology
Inorganic Materials and Nanocomposite
Laboratory, Department of Chemistry
Kharagpur, 721302, India

**Tuhin Chatterjee**
Indian Institute of Technology
Rubber Technology Centre
Kharagpur, 721302, India

**Mangala Joshi**
Indian Institute of Technology
Department of Textile Technology
Hauz Khas, New Delhi
110016, India

**Yadavendra Nath Gupta**
Defence Materials and Stores
Research & Development Establishment
DMSRDE Post Office
G.T. Road, Kanpur
208013, India

**Hanna J. Mariya**
International and Inter University Centre for
Nanoscience and Nanotechnology
Mahatma Gandhi University
P.D Hills, Kottayam
Kerala, 686560, India

**Kinsuk Naskar**
Indian Institute of Technology
Rubber Technology Centre
Kharagpur, 721302, India

**Dipak Kumar Setua**
Defence Materials and Stores
Research & Development Establishment
DMSRDE Post Office
G.T. Road, Kanpur
208013, India

**Suneel Kumar Srivastava**
Indian Institute of Technology
Department of Chemistry
Kharagpur, 721302, India

**Sabu Thomas**
International and Inter University Centre for
Nanoscience and Nanotechnology
Mahatma Gandhi University
P.D Hills, Kottayam
Kerala, 686560, India

https://doi.org/10.1515/9783110643879-202

Samar Bandyopadhyay

# 1 Applications of Rubber Nanocomposites in Automotives

## 1.1 Introduction

In the present global scenario, all vehicle manufacturers are striving to produce automobiles that exhibit enhanced safety with lower emissions and superior interior design along with an extended service warranty. Rubber is a preferred material for automotive manufacturers due to its many advantages, and is mainly used in tyres, tubes, flaps and many other auto components. The superior performance properties of synthetic rubbers compared with natural rubber (NR) makes them suitable for under-hood applications, whereas NR is used for general purpose rubber items. Due to its high resilience properties, NR enables superior braking performance and ride comfort. The proportion of different types of rubbers in a modern car is shown in Figure 1.1.

Elastomers are not only used in cars but are also extensively employed in all types of vehicle components from small bicycles to very large off-road tyres.

Carbon black(s) (CB) is the preferred reinforcing filler in the rubber industry because of its cost performance; however, it originates from petroleum oils which are now becoming increasingly scarce. The pollution caused as a result of utilising carbon has forced research scientists to use 'white' filler, with silica being a more competitive white filler than CB. Clay has poor reinforcing ability due to its big particle size and low surface activity. It was recently reported that researchers succeeded in intercalating polymers into clay layers, thus producing polymer–clay nanocomposites (PCN). This material has outstanding mechanical properties along with good barrier, thermal and ageing characteristics.

## 1.2 Rubber in Automobiles

The use of rubber in automobiles, as well as the potential application of rubber–clay nanocomposites in the automotive industry, is described later on in the chapter. This section describes the different types of rubber auto parts.

Elastomeric products in automobiles include tyres, tubes, flaps, hoses, belts, engine interiors, power train, chassis, interior trim, exterior trim and so on.

The different rubber parts used in cars is shown in Figure 1.2.

The engine, which is one of the most important automotive parts, contains different kinds of rubber parts [2].

Figure 1.3 shows the elastomers used in gasoline engines.

https://doi.org/10.1515/9783110643879-001

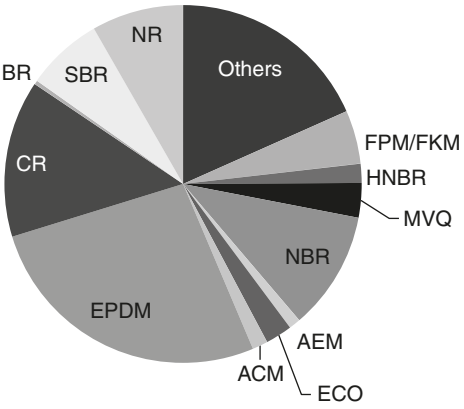


**Figure 1.1:** The share of different types of elastomers (excluding tyres) used in the Mercedes E-Class car [ACM: acrylic rubber (ester based); AEM: acrylic rubber (ether based); BR: polybutadiene rubber; CR: polychloroprene rubber; ECO: epichlorohydrin rubber; EPDM: ethylene propylene diene monomer rubber; FKM and FPM: fluorinated elastomers; HNBR: hydrogenated acrylonitrile-butadiene rubber; MVQ: methyl vinyl siloxane; NBR: acrylonitrile-butadiene rubber and SBR: styrene-butadiene rubber]. Reproduced with permission from *Rubber Science and Technology,* Ed., R. Mukhopadhyay, Shantinath Printing Udyog, Udaipur, Rajasthan, India, 2006. ©2006, Shantinath Printing Udyog [1].

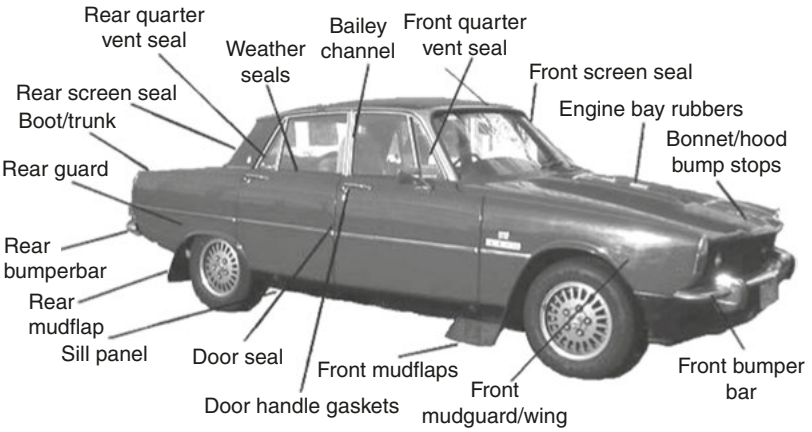


**Figure 1.2:** Pictorial presentation of the different rubber parts in a car. Reproduced with permission from *Rubber Science and Technology,* Ed., R. Mukhopadhyay, Shantinath Printing Udyog, Udaipur, Rajasthan, India, 2006. ©2006, Shantinath Printing Udyog [1].

## 1.2.1 Tyres, Tubes and Flaps

The major use of elastomers in automobiles is for tyres, tubes and flaps. A tyre is a ring-shaped object that fits around a wheel rim to enhance vehicle performance.

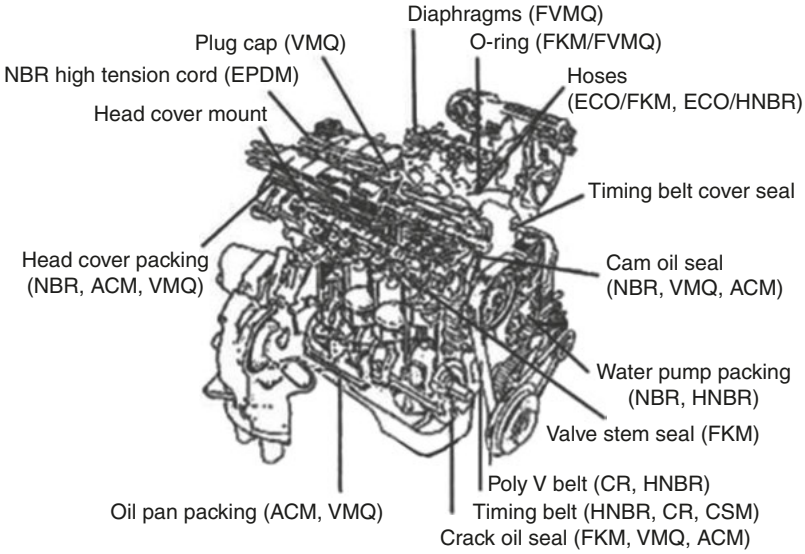


**Figure 1.3:** Elastomeric parts of a gasoline engine (CSM: chlorosulfonated polyethylene; FVMQ: fluoro vinyl methyl silicone rubber and VMQ: methyl silicone rubber). Reproduced with permission from *Rubber Science and Technology,* Ed., R. Mukhopadhyay, Shantinath Printing Udyog, Udaipur, Rajasthan, India, 2006. ©2006, Shantinath Printing Udyog [1].

Modern tyres are made of rubber, fabric, steel cord along with other compound chemicals. Tyres consist of tread and a carcass; the tread provides traction and the carcass gives strength. First-generation tyres were bands of metal fitted around wooden wheels to minimise wear and tear. Today, the majority of tyres are pneumatic, made of cords and wires combined with rubber and filled with air to form an inflatable device.

Tyres may be tube type or tubeless; a tube is a flexible membrane made of rubber that is fitted during the casing of a pneumatic tyre to contain the compressed air.

A flap is a rubber protector that prevents damage to the tube via the bead toes and the valve slot of the rim.

Pneumatic tyres are fitted on many types of vehicles, such as bicycles, motorcycles, cars, trucks, earthmovers and aircraft. Photographs of a tyre, tube and flap are shown in Figure 1.4.

## 1.2.2 Automotive Belts

The main function of the automotive belt is to transmit power. Automotive belts are classified as timing belts, V-belts and fan belts. A timing belt, timing chain or cam belt controls the timing of the engine's valves. The flat-4 engine used in


**Figure 1.4:** Picture of a tyre (A), tube (B) and flap (C). Reproduced with permission from *Rubber Science and Technology*, Ed., R. Mukhopadhyay, Shantinath Printing Udyog, Udaipur, Rajasthan, India, 2006. ©2006, Shantinath Printing Udyog [1].

the VW Beetle, uses timing gears. Timing belts are also used for power transmission or to interchange rotary motion and linear motion. Belts are mainly comprised of NBR, HNBR and CR elastomers, along with a reinforcing fabric as a composite.

## 1.2.3 Automotive Hose

### 1.2.3.1 Brake Hose

The function of the brake hose is to transmit a vacuum within the automotive power, which assists the braking system, and is made of CR reinforced with rayon fabrics.

### 1.2.3.2 Fuel Hose

The fuel hose operates from −30 to 100 °C and is made from NBR, FKM or CSM.

### 1.2.3.3 Fuel Injection Hose

The fuel injection hose carries automotive fuel and is run at high pressure and temperature. The inner cover is made from NBR and the outer cover is made from CSM and reinforced with fabric.

#### 1.2.3.4 Heater Hose

The heater hose operates as part of the vehicle's cooling system. It is used over the temperature range of −40 to +100 °C, is made from EPDM and is reinforced with a twin-braided spiral wrap. It is weather resistant and impervious to coolant system additives.

#### 1.2.3.5 Liquefied Petroleum Gas Vapour Hose

The function of the liquefied petroleum gas (LPG) vapour hose is to carry LPG vapour produced by automotive LPG conversions. A CR-based tube is used in the hose and is reinforced with braided cotton.

#### 1.2.3.6 Power Steering Hose

This hose is essential for the vehicle's power steering system. The tube is made from NBR rubber and polyester fabric is used for inner reinforcement. The cover rubber is made of CR which is resistant to oil, fuel and heat. It operates between −40 to +120 °C and at around 100 psi pressure.

Different types of hoses, seals, O-rings and belts are shown in Figure 1.5.

**Figure 1.5:** Different kinds of automotive hoses, seals, O-rings and belts. Reproduced with permission from *Rubber Science and Technology*, Ed., R. Mukhopadhyay, Shantinath Printing Udyog, Udaipur, Rajasthan, India, 2006. ©2006, Shantinath Printing Udyog [1].

### 1.2.3.7 Automotive Seals

Seals are used to prevent the leakage of liquid, solids or gases, and penetration of foreign matter into closed containers and pipe systems, and there are many types of seals available on the market. The selection of rubber for seals depends on the working pressure, temperature, corrosive atmosphere, material, shaft speed and so on. There are two types of automotive seals: static seals (O-rings, gaskets) and dynamic seals (radial lip seals). The main performance properties of automotive seals are low compression set, low volume swelling, low hardening or softening and good ageing resistance. NBR silicone rubber and fluorinated rubber are extensively used as seal materials.

### 1.2.3.8 Automotive Tubing

For the windscreen washer system, vacuum and washer tubing is used under vacuum due to its good heat and weather resistance.

### 1.2.3.9 Door Seal and Window Channels

EPDM rubber is used in door seals and window channels because of its good weather resistance. Figure 1.6 shows the door seal and rubber boots.

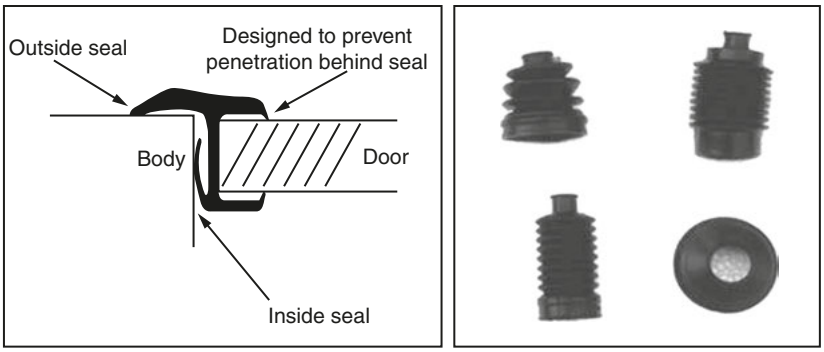


**Figure 1.6:** Door seal and rubber boots. Reproduced with permission from *Rubber Science and Technology*, Ed., R. Mukhopadhyay, Shantinath Printing Udyog, Udaipur, Rajasthan, India, 2006. ©2006, Shantinath Printing Udyog [1].

### 1.2.3.10 Diaphragms and Rubber Boots

EPDM and CR are used for rubber boots and different types of diaphragms because of their high ozone and chemical resistance and excellent physical properties.

#### 1.2.3.11 Other Miscellaneous Rubber Parts

In addition to the above-mentioned applications, there are many other rubber products used in the automotive industry, e.g., rubber bumpers, rubber engine mountings, rubber mats, grommets, rubber bellows, flexible couplings, mudflaps and so on.

## 1.3 Prime Requirements of Different Elastomeric Auto Components from an Application Point-of-View

Table 1.1 describes the general requirements of some important auto components, which vary based on product performance and cost. The table also details the stringent requirements of different auto rubber components [3].

## 1.4 Elastomeric Nanocomposites and the Rubber Industry

The buzz words 'nanocomposites', 'nanomaterials' and 'nanofillers' are relatively new but have been used from the beginning of this century (e.g., CB has been used as a reinforcing filler in rubbers since 1904). These materials have always existed in nature (in minerals and vegetation) [4]. The major advantages that nanocomposites have over conventional composites are:

- Lighter weight due to low loading.
- Improved properties (including mechanical, thermal, optical, electrical, barrier and so on) compared with conventional composites.

Three types of nanocomposites can be distinguished depending upon the number of dimensions of the dispersed particles that are in the nanometre range [5]:

- Isodimensional nanofillers have three dimensions on the nanometre scale, such as spherical silica nanoparticles obtained by *in situ* sol-gel methods or *via* polymerisation [6–8].
- When two dimensions are the same while the third is little larger in a nanocomposite, an elongated structure results, such as carbon nanotubes (CNT) or cellulose whiskers which have been extensively studied. [9–12].
- The third type of nanocomposite has only one dimension in the nanometre range. Here, the filler is in the form of sheets. Clays, clay minerals and layered silicates belong to this family and the resultant composites are called PCN or polymer-layered silicate nanocomposites.

**Table 1.1:** General requirements of some important auto components.

| Parts | Name | Current materials | Requirements | New material | Trend |
|---|---|---|---|---|---|
| Engine | Fuel hose | FKM/ECO/NBR/CR | Heat resistance | – | Low cost |
| | Emission control hose | ACM | – | – | – |
| | Air duct hose | NBR + PVC | Heat resistance | Thermoplastic olefins, ACM | – |
| | Water hose (radiator and so on) | EPDM (polyester) | Heat resistance | EPDM (aramid) | – |
| | Crank shaft rear | MVQ | Long life | FKM | – |
| | Crank shaft front | ACM | Long life | FKM | – |
| | Diaphragms | ECO, NBR, FVM | – | – | – |
| | Valve stem seal | FKM | – | – | – |
| | Valve cover gasket | NBR | Heat resistance | ACM | – |
| | Synchronous belt | CR | Heat resistance, long life | HNBR | Long life |
| | Accessory drive belt | CR | – | – | Heat resistance |
| Body | Fuel hose | NBR/CR | Permeability | FKM/ECO | – |
| | Filler hose | NBR + PVC | – | – | Low permeability |
| | Air condition hose | NBR/CR | Permeability | Polyamide 6/CIIR | – |
| | Weather strip | EPDM | Long life | – | – |
| | Glass rim | EPDM | Low abrasion | – | – |
| | Filler cap O-ring | NBR + PVC | – | – | – |
| | Intank pump cushion | NBR + PVC | – | – | – |
| | Hanger rubber | EPDM | – | – | – |
| | Wiper blade | CR, NR | – | – | Long-life heat resistance |
| | Engine mount | NR (SBR, BR) | – | – | – |
| | Mat | NR, SBR | Low abrasion | Use of recycled rubber | Low cost |
| | Bumpers | NR, SBR, EPDM | Weather resistance | – | Low cost, long life, weather resistance |

| | | | | | |
|---|---|---|---|---|---|
| Chassis | Oil cooler hose | ACM | – | – | Heat resistance |
| | Power steering hose | NBR | – | ACM | Heat resistance |
| | Brake hose | SBR/NR/CR + EPDM | Water permeability | EPDM | – |
| | Clutch hose | SBR/NR/CR + EPDM | Water permeability | EPDM | – |
| | Master vacuum hose | NBR/CR | Heat resistance | ECO | – |
| | Transmission oil seal | NBR | Heat resistance | ACM | – |
| | Power steering oil seal | NBR | – | – | Heat resistance |
| | Ball joint glass cover | CR, PU | – | – | – |
| | Constant velocity joint boot | CR | Heat, ozone | TPE | – |
| | Brake master cup | SBR | Heat, life | EPDM | – |
| | Caliper piston seal | SBR | Heat, life | EPDM | – |
| Wheel | Tyres | NR, SBR, BR | Light weight, low rolling resistance, high abrasion resistance, chipping and chunking resistance, higher flexibility | Solution SBR, BR | Fuel economy, higher mileage, longer life, low noise, high grip and so on |
| | Tube | Infared CIIR, brominated IIR, EPDM | High air retention, low growth | – | Tubeless tyre, puncture-proof tube |
| | Flap | NR, SBR | Heat and cut resistance | – | – |

CIIR: Chlorinated isobutyl-isoprene rubber
IIR: Isobutyl-isoprene rubber
PU: Polyurethane
PVC: Polyvinyl chloride
TPE: Thermoplastic elastomers
Reproduced with permission from *Rubber Science and Technology,* Ed., R. Mukhopadhyay, Shantinath Printing Udyog, Udaipur, Rajasthan, India, 2006.

## 1.5 Superiority of Clays/Clay Minerals *versus* Other Nanofillers

There are many reasons to choose clays/clay minerals as a potential nanofiller in comparison to CNT, nanographite, nano-calcium carbonate ($CaCO_3$) and so on.

Clays/clay minerals are cheap and abundant in nature, whereas most other nanofillers are produced *via* a complex synthesis process. The modification of clay minerals or clays is simple and they can be easily customised. Nanoclay (NC) composites show some unique properties with respect to other nanofillers, with clay nanocomposites exhibiting excellent air retention and barrier properties. These composites show very high elongation and anti-ageing properties.

## 1.6 Organo-modified Clay/Clay Minerals

Montmorillonite (MMT), and other layered silicate clays, are hydrophilic in nature. This property of the clay makes them poorly suited for interacting with polymer matrices, which are hydrophobic.

Moreover, electrostatic forces firmly hold the stacks of clay platelets. For the above-mentioned reasons, clay or clay minerals must be treated prior to making a nanocomposite; hence, a composite untreated clay material is not very effective as a material.

Ion exchange is a relatively easy method of modifying the surface of the clay/clay minerals, which allows the organic matrix to become more compatible. The cations present in the clay surface are not strongly bound and hence small cations of other molecules may replace the cations present in the clay. Using this process, MMT clay minerals can be compatibilised with a large number of polymer matrices. This process also results in easier intercalation and exfoliation.

## 1.7 Application of Elastomeric Nanocomposites in the Automotive Industry

Polymer nanocomposites are widely used in the automotive industry. However, these composites are modified by adding large amounts of supplements in the form of microparticles, thermal stabilisers, and chemical and flame resistance additives. Thus, improved performance often results due to the improvement in material density and fuel efficiency. Therefore, polymer nanocomposites offer higher performance with significant weight reduction, and hence these materials are very useful to transport industries, especially the automotive and aerospace sectors.

The following section describes the benefits of using elastomeric clay nanocomposites with respect to mechanical, physical, thermal, air retention, ageing and processing characteristics.

### 1.7.1 Lighter Weight and Balanced Mechanical Properties

Clay/clay mineral elastomeric nanocomposites have a low specific gravity compared with traditional fillers. Any weight reduction is very important in the automotive market as this will result in lower fuel consumption.

It has been reported that only 10 phr (parts per hundred parts rubber) of organoclay(s) (OC) was necessary to achieve a tensile strength (TS) comparable to an NBR compound loaded with 40 phr of CB [12]. It was also reported that a small loading of 7 wt%-modified clay was sufficient to achieve the mechanical properties exhibited by highly structured silica-filled and CB-filled NR vulcanisates [14]. Another author observed that organically modified interlayers of MMT were easily penetrated by NR chains, resulting in intercalated structures along with partial exfoliation [15]. A modulus increase, achieved by high loadings of conventional micrometre-sized fillers, was observed at only a 10 wt%-modified MMT loading due to the high surface area of the filler. Research scientists prepared NR-based nanocomposites with 10 wt% natural (sodium bentonite)- and synthetic (sodium fluorohectorite)-layered silicates using the latex compounding method [16]. Commercial clay minerals (an inert material) were used as a reference material. It was reported that the layered silicates showed an improvement in mechanical, thermal and swelling tests. CR–MMT nanocomposites exhibited high hardness, high modulus and high tear strength. Wang and co-workers suggested the potential application of these nanocomposites in inner tubes, inner liners and dumpers [17]. At an equivalent filler loading (20 phr), the rectorite/SBR nanocomposites showed better mechanical properties than SBR filled with CB N330 or calcium carbonate [18]. Wu and co-workers also prepared NBR/clay nanocomposites [19]. Transmission electron microscopy (TEM) showed that the silicate layers of clay were dispersed in the NBR in a planar orientation. The NBR/clay nanocomposites exhibited better physical and barrier properties, as determined by Nielsen's model. Varghese and co-workers reported the preparation of NR, PU rubber and NR/PU-based nanocomposites from the related lattices by adding 10 phr pristine synthetic sodium fluorohectorite (a layered silicate) [20]. It was reported that the silicate layers were preferentially embedded in the polar PU phase in a blend composed of polar PU and non-polar NR. The properties of the PU/NR-based nanocomposites were reported to be similar to plain PU; this observation is of great economic significance as NR latex is cheaper than PU latex. The preparation of clay/rubber nanocomposites *via* the latex route is described in patent US20030144401. The resultant materials have been used in tyre components such as tyre tread, sidewall and/or inner liner [21]. Another patent,

US2005065266, details the preparation of nanocomposites comprised of water swollen clay particles in aqueous emulsions such as anionic SBR or NR containing a novel amine to assist the intercalation and partial exfoliation of the clay particles [22]. Applications of such rubber nanocomposites include aircraft tyre treads, where the amount of CB reinforcement can be reduced to produce low heat build-up to enhance tyre durability; a reduction in tyre weight can also result in better fuel economy. Arroyo and co-workers prepared NR reinforced with 10 phr sodium montmorillonite (Na-MMT) (unmodified clay) and octadecylamine-modified Na-MMT (OC). The results were compared with NR loaded with 10 and 40 phr CB [23]. The rubber compounding was carried out on an open two-roll mill at room temperature (RT). The rheometer curve showed that the unmodified clay slightly changed the cure characteristics of NR, which was due to poor compatibility between the unmodified clay and hydrophobic polymer. However, the optimum cure time was sharply reduced in the presence of OC, which produced an accelerating effect on NR vulcanisation due to the presence of the ammonium groups of the organic cations. CB also caused a decrease of the optimum cure time to a lesser extent than OC. A nanocomposite of 10 phr OC showed higher torque values than the NR mix containing 40 phr CB, indicating a higher degree of crosslink formation by the nanocomposite, which was confirmed through swelling and by differential scanning calorimetry, i.e., OC behaved as an effective reinforcement agent. Other mechanical properties such as rebound resilience, hardness, compression set and abrasion loss reported by Arroyo and co-workers are detailed in Figure 1.7.

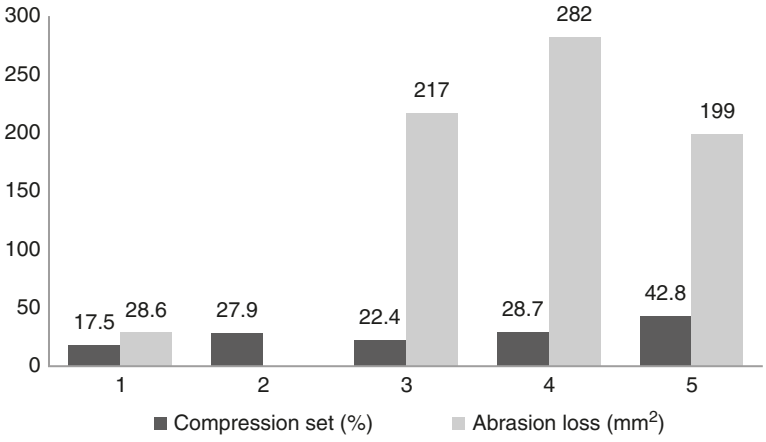


**Figure 1.7:** Comparison of compression set and abrasion loss for the various mixes [mixtures: 1) NR (unfilled); 2) NR + 10 phr unmodified clay; 3) NR + 10 phr OC; 4) NR + 10 phr CB and 5) NR + 40 phr CB]. Reproduced with permission from *Rubber-Clay Nanocomposites: Science, Technology, and Applications*, Ed., M. Galimberti, Wiley, New York, NY, USA, 2011. ©2011, Wiley [24].

The results indicated that *in situ* anionic polymerisation can enhance certain characteristics of exfoliated nanocomposites. The incorporation of OC obviously changed the microstructure of BR; the concentrations of the 1,2-unit, 3,4-unit and *trans*-1,4-unit dramatically increased with an increasing content of OC and the concentration of the *cis*-1,4-structure decreased. OC apparently strengthened the rubber matrix, e.g., the TS and hardness of nanocomposites increased greatly, but the permanent deformation exhibited little change.

EPDM/organophilic MMT hybrid nanocomposites were successfully prepared by a simple melt-compounding process by Chang and co-workers [25]. The hybrid nanocomposites showed improvement in TS and tear strength, modulus and elongation at break (EB).

BR/organically modified MMT nanocomposites along with polyisoprene and SBR nanocomposites were prepared by Liao and co-workers *via in situ* anionic-intercalation polymerisation [26].

Sadhu and Bhowmick described the effect of different concentrations of acrylonitrile (ACN) on the mechanical, dynamic mechanical and rheological properties of nanocomposites [27–29]. The polymers with the highest ACN content exhibited the greatest increase of properties.

The structure–property relationship for EPDM–layered double hydroxide (LDH) nanocomposites has been described by Acharya and co-workers [30, 31], who reported an improvement in TS and EB. The increase in stiffness in the corresponding nanocomposites was due to stress transfer from the polymer. The EB also increased with the modified LDH content due to the platelet orientation, chain slippage or plasticisation.

The effect of a MMT clay–polyacrylate hybrid material on the properties of a polyethylene octene copolymer was detailed by Ray and Bhowmick [32]. Maiti and co-workers reported the properties of organically modified NC and its nanocomposites, prepared using a polyethylene octene copolymer [33]. Excellent improvement in mechanical properties and storage modulus were reported and explained through morphology, dispersion of nanofillers and the interaction with rubber.

New nanocomposites from a polyethylene octene elastomer, MMT and biodegradable starch were reported by Liao and Wu [34], which was achieved through a melt-blending method. It was reported that the nanocomposites exhibited a stable TS with a starch content of up to 40 wt%. The production of microcellular foam from this elastomer was reported by Chang and co-workers [35]. CR–clay nanocomposites were prepared by co-coagulating the rubber latex and aqueous clay suspension, and the properties of the nanocomposites were compared with conventional CB-filled systems [17]. Cloisite® 10A hybrids and the terpolymeric nanocomposites demonstrated superior mechanical and dynamic mechanical properties. Higher thermal stability was shown by terpolymer–clay hybrids containing 9 wt% Cloisite® 10A. Nanocomposites prepared *in situ* showed better properties than those prepared by the solution method.

Organo-modified MMT nanocomposites have been prepared using dichloromethane at RT, *via* the solvent casting method. The nanocomposites showed a higher tensile modulus than the polymer matrix [36].

The effect of synthetic MMT on the properties of fluoroelastomers was reported by Maiti and Bhowmick [37]. The natural MMT-filled sample showed 65 and 51% improvement in TS and 100% modulus, respectively, over the control. The synthetic clay-filled samples showed better TS compared with natural clay-filled batches; in addition, better swelling and thermal resistance were also demonstrated by the synthetic clay-based nanocomposites. The natural clay-filled nanocomposites were found to be thermodynamically less stable than synthetic ones.

Linear block and star-shaped thermoplastic styrene-butadiene-styrene (SBS)/organophilic MMT clays were prepared using a solution approach by Liao and coworkers [38]. The star-shaped SBS/organophilic MMT nanocomposites showed significantly increased mechanical strength.

A rubber toughened, clay-filled nanocomposite material for use in automotive bumper application has been described in patent US6060549 [39]. The blend of a thermoplastic engineering resin (e.g., Nylon), a functionalised copolymer of $C_4$–$C_7$ isomonoolefine (e.g., isobutylene-*co-para*-methyl styrene) and layered clay made a toughened material as per the patent. Superior mechanical properties and enhanced impact strength were observed. The elastomeric component was in the range of 10–30% of the total polymer content.

## 1.7.2 Barrier or Air Retention Properties

Pneumatic tyres are inflated with air and this inflation pressure needs to be retained; this barrier property is the function of the inner liner or tube and is also required for critical safety and utility functions of the tyre. The inflation pressure can be maintained over a long period of time when air permeation through the tyre is minimised. Tyre damage and failure occurs when the inflation pressure becomes low. The permeation of air also causes oxidative degradation of the rubber and reinforcing fibres and an increase in internal defects.

OC elastomer nanocomposites show superior air retention and barrier properties; as a result, OC elastomer nanocomposites have huge scope as automotive tyre inner liners and tubes. The layer-like structure, with a high aspect ratio of the clay, results in better air retention characteristics. The sheet-like structure of the clay hinders the passing of air when the clay is distributed properly in the composite.

Butyl rubber [isobutyl-isoprene rubber (IIR)] and halogenated butyl rubbers are mainly used in tyre inner tube and liner applications. These rubbers are highly saturated and hence are difficult to process and co-crosslink with NR, SBR and BR, which are used in the tyre body sections. The air retention property of rectorite/SBR nanocomposites was reported to be excellent and higher than that of the CB N330/SBR

composite [18]. Thus, rectorite/SBR nanocomposites are expected to be good candidates for tyre tube and inner liner applications. A number of reports are available that detail the successful preparation of IIR–clay nanocomposites [40–44]. Kato and co-workers reported the production of maleic anhydride (MA)-grafted IIR and organophilic clay by melt processing. Higher gas barrier properties of the nanocomposites were reported, compared with MA-*g*-IIR, upon the addition of 15 phr clay [40]. The production of brominated polyisobutylene-*co-para*-methylstyrene (BIMS)-based nanocomposites was reported by Maiti and co-workers [45]. The solution processing method using various OC was used to prepare the nanocomposites. The mechanical, dynamic mechanical and rheological properties along with X-ray diffraction (XRD) and TEM were assessed. The modified clay-filled BIMS showed a remarkable increase in barrier properties compared with gum vulcanisates.

Several patents and papers are available that focus on the low permeability and improved barrier properties of butyl rubber nanocomposites [46–49]. In addition, Meneghetti and co-workers have reported SBR–OC nanocomposites with an enhanced gas barrier property [50].

Preparation of the tyre inner liner and tube compounds based on general purpose rubber and OC with no reduction in mechanical properties is reported in US patent US005576372A [51]. The authors mentioned the use of a reactive rubber to prepare OC nanocomposites for use in tyre inner liners. It was shown that the reactive rubber must have an active chemical group capable of reacting with the dispersed clay to form nanocomposites.

The use of BIMS and layered silicate to prepare nanocomposites is detailed in another patent. The authors described preparing clay–polymer nanocomposites *via* an organic aqueous emulsion method. It was mentioned that the polymer was available in the organic phase and the clay was present in the aqueous phase [52]. A significant improvement in permeation rate of the nanocomposites made them suitable for use in tyre inner liners and tube compounds.

The use of OC elastomer nanocomposites in tyre inner liners and tubes is described in several patents [53–55].

## 1.7.3 Ageing and Ozone Resistance

Products made of elastomeric composites are highly prone to attack by environmental ozone and oxygen due to unsaturation in the backbone, and therefore antioxidants and antiozonants are added to the formulation to protect the rubber components. It was reported that *in situ* resol-modified bentonite clay nanocomposites exhibited better ageing properties in comparison to regular compounds [56]. In addition, OC-filled SBR nanocomposites showed better retention of physical properties after thermal or thermooxidative ageing. The superior performance of the OC-filled compound was mainly due to the barrier property of the compound. The diffusion of oxygen inside

the rubber matrix was reduced by the exfoliated and intercalated clay layers; hence, the degradation process was less severe in the OC-filled compound. The ozone resistance of OC-filled compounds was found to be better than the CB-filled compound. The presence of OC (Cloisite® 20A) in the compound led to a superior barrier property, which decreased the ozone attack on the surface; hence, the OC compound exhibited better ozone resistance compared with the CB-filled compound. A description of the ozone cracked sample is given in Figure 1.8. The change in physical properties of the compounds after thermo and thermooxidative ageing is shown in Figure 1.9. The thermooxidative ageing properties of specimen TS and hardness were assessed at 105 °C for 7 days in a multicell ageing oven. The anaerobic ageing was achieved inside a compression mould for 30 h at 130 °C.

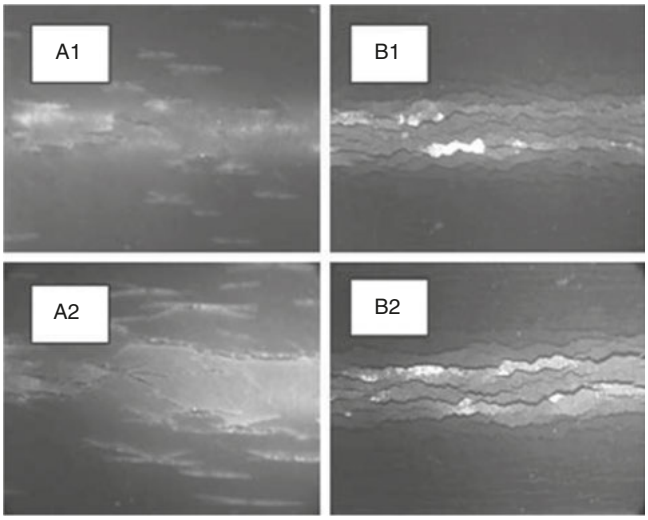


**Figure 1.8:** Ozone crack photograph of the OC compound (A1: 24 h and A2: 48 h) and CB compound (A1: 24 h and A2: 48 h) at 30 X magnification. Reproduced with permission from *Rubber-Clay Nanocomposites: Science, Technology, and Applications*, Ed., M. Galimberti, Wiley, New York, NY, USA, 2011. ©2011, Wiley [24].

The ageing performance of HNBR/clay nanocomposites at 178 °C in air, water and oil, respectively, has been reported [57]. The addition of OC significantly improved material performance for both air and oil ageing at high temperature; 80% of TS after ageing in air and 50% of TS after ageing in oil was reported. On the contrary, HNBR reinforced with CB showed a considerable deterioration of mechanical properties after ageing in air and oil. The ageing performance in water of HNBR nanocomposites was found to be similar to that of CB-filled HNBR. This may be due to the swelling of the material in the presence of OC, which counteracts with its

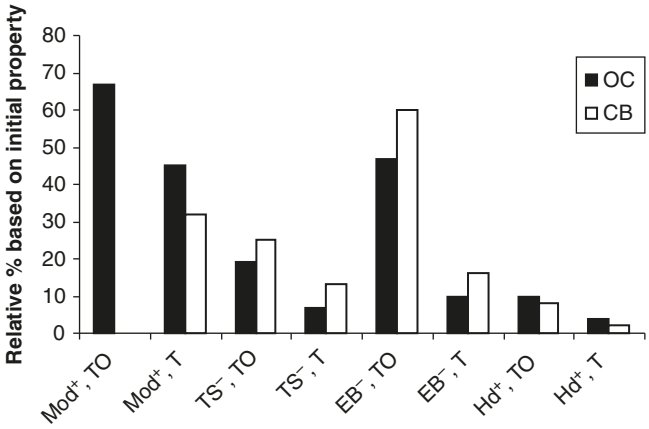


**Figure 1.9:** Relative decease/increase of physical properties after accelerated thermal and thermooxidative ageing ('+' sign indicates a relative increase, '–' sign indicates a relative decrease, 'Mod' stands for 300% modulus, 'Hd' stands for hardness, 'T' stands for thermal ageing and 'TO' stands for thermooxidative ageing). Reproduced with permission from *Rubber-Clay Nanocomposites: Science, Technology, and Applications*, Ed., M. Galimberti, Wiley, New York, NY, USA, 2011. ©2011, Wiley [24].

reinforcing effect. The retention of material properties hardly changed when the clay content was greater than 2.5 phr.

The OC-containing nanocomposites can be used in different automotive applications such as door/window sealing, automotive bumpers and so on.

## 1.7.4 Solvent Resistance

Most automotive rubber products require solvent resistance (rubber hose, tube and so on), in addition to other mechanical properties. It has been found that the elastomer clay nanocomposite exhibits an improved solvent-resistant property.

The effect of synthetic MMT on the properties of fluoroelastomers has been reported by Maiti and Bhowmick [58]. Better swelling and thermal resistance were also demonstrated by synthetic clay-based nanocomposites. The authors reported that synthetic clay-based nanocomposites were thermodynamically more viable than the natural clay-filled one. The addition of a small amount of clay reduced the swelling of the NR compound [59]. The swelling measurement of the thermoplastic elastomeric clay nanocomposite vulcanisate was conducted in toluene [60, 61], and the swelling decreased with clay content at RT as well as 100 °C.

Investigation of the diffusion and sorption of methyl ethyl ketone (MEK) and tetrahydrofuran in fluoroelastomer–clay nanocomposites over the temperature range of 30–60 °C *via* swelling experiments has been reported [61]. The addition of

NC decreased the overall sorption value. The sorption was at a maximum for the unmodified clay-filled sample, which also exhibited the lowest swelling. The swelling increased upon increasing the temperature in all the systems.

The morphological, rheological and swelling properties of nanocomposites based on NBR and organophilic-layered silicates using the melt-processing technique was reported by Kim and co-workers [62]. The swelling property was assessed using MEK. Vulcanised neat NBR and organo-MMT/NBR composites were immersed and the extent of swelling decreased upon increasing the organo-MMT loading. Thus, the organo-MMT/NBR nanocomposites have excellent barrier properties compared with vulcanised NBR.

The addition of layered NC to a neat polymer restricted the permeability of nanocomposites *via* a decreased area and increased path length. When a solvent diffuses across a polymer, it must travel the entire thickness of the sample. When the same solvent diffuses through a nanocomposite film containing NC, it takes a much longer time to cover the entire path length.

Thus, these nanocomposites have considerable potential to be used in automotive hoses and tubing due to the inherent solvent-resistant property.

### 1.7.5 Better Processability

The success of any new technology depends on its adoption by both the manufacturer and the end user. The same is also true for automotive component manufacturers. Auto component manufacturers not only ask for better performance, they also require ease of processability.

In the case of NBR–OC nanocomposites, shear viscosity continuously decreases with increasing shear rate, i.e., the shear thinning effect occurs, which was reported by Bhowmick and co-workers [63]. The extrudate profile was also better in the case of nanocomposites. It was reported that the processability improved upon incorporation of OC. The scanning electron microscopy (SEM) images of the extruded compounds are shown in Figure 1.10.

The melt rheological properties of ACM/silica and epoxidised natural rubber (ENR)/silica hybrid nanocomposites has been examined in a capillary rheometer at 100, 110 and 120 °C and at nine different shear rates [64]. The shear viscosity did not increase to a great extent for the rubber/silica nanocomposites even when the concentration of nano-silica was increased substantially. This is highly remarkable feature of these systems and, in general, is not observed with ordinary filler-loaded compounds. Both the nanocomposites exhibited pseudoplastic behaviour at experimental temperatures and followed the Power Law model. The ‘k’ value of the nanocomposite was not significantly higher than the gum compound and decreased upon increasing the temperature of extrusion. There was a lowering of die swell up to a critical shear rate for ACM/silica nanocomposites, and the die swell increased

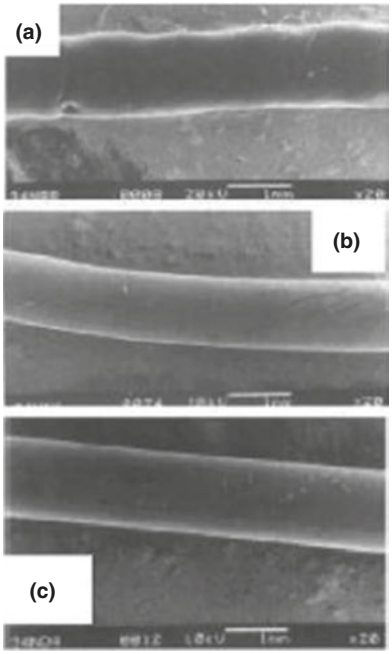


**Figure 1.10:** SEM images of the extruded compounds [compound (a) is the gum NBR compound (34 % ACN) containing no clay, compound (b) contains 4 phr of sodium MMT and compound (c) contains 4 phr of organo-modified MMT clay]. Reproduced with permission from *Rubber-Clay Nanocomposites: Science, Technology, and Applications*, Ed., M. Galimberti, Wiley, New York, NY, USA, 2011. ©2011, Wiley [24].

above this critical shear rate level. An increase in die swell at higher shear rates has been reported in ENR/silica nanocomposites. Both the nanocomposites displayed a decrease in die swell upon increasing the nanofiller content and temperature. The extrudate profile roughness decreased, due to the greater viscous nature of the nanocomposites compared with the gum rubbers. This is also supported by lowering of the first normal stress differences in the specimen at a particular temperature. A uniform distribution of silica was observed after extrusion of the nanocomposites. On the whole, the ENR/silica nanocomposites displayed regular flow compared with the conventional ACM/silica system due to the better polymer–silica interface in the nanocomposite. The activation energy of the flow decreased with the increase in shear rates (up to a certain shear rate) for both the nanocomposites. A linear increase in activation energy was observed with the silica content at a particular shear rate.

The OC nanocomposites act as a curing activator with a complex being formed between the amine moiety of the OC and the accelerator/activator. The activation energy of the vulcanisation reaction is reduced due to the formation of this complex [65].

For SBR–OC nanocomposites, a rheometric study was carried out by the authors (unpublished work) at 140 and 160 °C. The rheometric data is shown in Table 1.2. The data shows that a 20 °C reduction of curing temperature brought the

**Table 1.2:** Cure characteristics of different compounds.

| Material | $A4_{160}$ | $A5_{140}$ | $A5_{160}$ | $A6_{140}$ | $A6_{160}$ | $A7_{140}$ | $A7_{160}$ |
|---|---|---|---|---|---|---|---|
| Maximum torque (dN-m) | 6.17 | 7.9 | 6.5 | 7.7 | 6.5 | 7.6 | 6.6 |
| Minimum torque (dN-m) | 0.9 | 1.0 | 0.8 | 1.0 | 0.9 | 1.0 | 0.8 |
| $\Delta$Torque = $T_{max} - T_{min}$, (dN-m) | 5.3 | 6.9 | 5.7 | 6.7 | 5.6 | 6.6 | 5.8 |
| $TS_2$ (min) | 11.09 | 12.15 | 3.59 | 19.95 | 5.3 | 24.94 | 6.48 |
| $TC_{90}$ (min) | 22.85 | 24.48 | 10.26 | 33.50 | 12.1 | 40.61 | 12.89 |
| CRI ($min^{-1}$) | 8.5 | 8.1 | 15.0 | 7.4 | 14.7 | 6.4 | 15.6 |

Nomenclature: particular compound cured at a specific temperature
A4: Ordinary clay, control compound
A5: OC
A6: OC and 0.25 phr CTP
A7: OC and 0.5 phr CTP, all compounds contain 5 phr OC
Reproduced with permission from *Rubber-Clay Nanocomposites: Science, Technology, and Applications*, Ed., M. Galimberti, Wiley, New York, NY, USA, 2011. ©2011, Wiley [24]

cure rate index (CRI), scorch safety time ($TS_2$) and optimum cure time ($TC_{90}$) of compound A5 was very close to the control compound, A4. However, during curing at 140 °C, the CRI of A5, A6 and A7 was nearly half that of curing at 160 °C. The $TS_2$ of the $A7_{16}0$ is nearly double that of compound $A5_{160}$, which is due to the effect of cyclohexylthiopthalimide (CTP), i.e., the addition of CTP helped to increase the scorch safety of the compounds.

Manchado and co-workers reported that the addition of OC reduced the activation energy of the NR–OC nanocomposites [66]. They concluded that reduction of the curing temperature could match the curing parameter of the amine-modified clay-containing compound to that of the control compound. They also reported that the addition of CTP influences the curing parameters. The authors concluded that the OC nanocomposites can reduce the production cost either by reducing the temperature or by reducing the cycle time.

## 1.7.6 Elastomeric Polyurethane–Organoclay Nanocomposites

Thermoplastic polyurethanes (TPU) are also a member of the broader class of TPE, which have the processability of plastics combined with the flexibility and resilience of rubbers. Out of the TPE family, TPU materials currently comprise approximately 15% of the volume; hence, it is necessary to discuss elastomeric PU OC nanocomposites separately.

The most common automotive applications for TPE include automotive interiors, bumpers, covers, trim, constant velocity joint boots and so on. The use of TPE depend on several parameters including: flexibility, ultimate properties, adhesion, and compatibility with other part components, chemical resistance and price.

The properties of PU-based nanocomposites have been extensively studied [67–82]. The production of PU nanocomposites *via* the solvation of OC by polyol was first studied by Wang and Pinnavaia. Polyol loading of up to 10–20 wt% in clay results in a pourable mixture [68]. An XRD study showed that the intercalation of polyol into clay results in an increase of basal spacing from 1.8–2.3 nm to 3.2–3.9 nm. The formation of PU results in a further increase of basal spacing by more than 5 nm, which is considered to be exfoliation of clay or dispersal of nanolayers. For coupling with diisocyanate, the onium ions of the clay were considered to be active reagents X. A 2–3-fold improvement of tensile properties of a polymer can be achieved by loading PU with 5–10 wt% of clay. Inorganic fillers are generally used in PU chemistry to reduce formation cost and increase stiffness. The modulus increase of conventional PU composites are compromised by a sacrifice of elastomer properties. The nanocomposites were reported to exhibit an improvement in both elasticity and tensile modulus. Clay nanolayers, even when aggregated in the form of intercalated tactoids, strengthened, stiffened and toughened the matrix. The dispersion of clay nanolayers caused an enhancement in strength and modulus. The improvement in elasticity is due to the plasticising effect of onium ions, which contribute to dangling chain formation in the matrix, as well as to conformational effects on the polymer at the clay–matrix interface.

Millable PU–OC nanocomposites were prepared by Mishra and co-workers [83]. Wide-angle XRD results suggest intercalation of the polymer inside the OC; an improvement in TS, 100% modulus and EB were observed.

The incorporation of unmodified, low aspect ratio hectorite (Laponite$^{TM}$) into a number of TPU at up to 20 wt% using a novel solvent exchange technique was investigated by McKinley and co-workers [74, 84]. A substantial improvement in mechanical properties, heat distortion temperature and morphological characteristics of the nanocomposite system were reported.

The preparation of PU-based clay nanocomposites, along with the characterisation of mechanical and barrier properties, morphology and the effect of processing conditions have been reported [85–94]. Igor and co-workers reported that the coefficient of thermal expansion of PU elastomers increased by 85% upon the addition of 10 wt% of NC, and by 98% with 15 wt% of carbon nanofibres.

## 1.7.7 Use of Organoclay Nanocomposites in Tyres

The application of elastomeric nanocomposites in automotive tyres is the subject of great interest and a number of patents are available in this field. A brief discussion of some selected patents follows.

The use of OC to reduce the tan δ value at 1, 5 and 10% strain, in comparison to a CB-filled compound, is described in patent US006861462B2 [95]. A higher storage modulus value, which is an indication of a higher stiffness value of the compounds,

was also reported. A lower tan δ value results in lower rolling resistance, which in turn produces better fuel economy. The use of *in situ* elastomer–clay nanocomposites, generated by a latex-blending technique, further improved the result. The use of this type of nanocomposite in tyre tread has also been reported.

The use of vinyl pyridine-styrene-butadiene *ter* copolymer-type rubber and Cloisite® 30B OC nanocomposites is reported in another patent [96]. The elastomer–Cloisite® 30B–CB combination showed a superior tan δ value and storage modulus value according to rubber process analyser measurements. Higher TS and EB have also been claimed. When OC was treated with a coupling agent (Si69®), the tan δ value reduced substantially. OC and the coupling agent replaced around 15 parts of CB N299.

The preparation and use of OC–elastomeric nanocomposites in tyre tread, side wall and inner liners is reported in patent US006759464B2 [97]. For compounding purposes, *in situ*-generated OC nanocomposites were used. Preparation of the nanocomposite masterbatch was achieved using functionalised elastomers, such as epoxidised polyisoprene or BR latex. Improvement in the strength and tan δ values have been claimed.

The use of elastomeric–OC nanocomposites in the bead filler, side wall insert, tread base or tread under layer has been reported [98]. The use of epoxidised rubber along with a layered clay material improved the property, as detailed in the patent. Preparation of the epoxidised rubber and nanocomposites has also been reported, as has the use of organo-modified MMT clay nanocomposites in the tyre apex or side wall insert compounds [68]. The use of 5 parts of OC with 55 parts of CB in an NR-based compound increased the stiffness of the compound (storage modulus) with a marginal increase in tan δ value. A marginal drop in ultimate TS and EB with a large gain in modulus value were observed.

The use of rubber toughened thermoplastic nanocomposite materials for automotive bumper application is detailed in [39]. The product exhibited superior tensile and modulus properties along with improved impact strength. The materials were prepared based on a blend of one or more thermoplastic engineering resins, e.g., Nylon, a functionalised copolymer of a $C_4$–$C_7$ isomonoolefin, e.g., isobutylene, and a *para*-alkylstyrene, e.g., *para*-methylstyrene, and also contained a uniformly dispersed exfoliated-layered clay, such as MMT.

The use of the OC nanocomposites in racing tyre tread compounds is detailed in a US patent [99], and the compound formulation is given in Table 1.3.

The properties are summarised in Table 1.4.

Table 1.4 shows that the hardness of the CB-filled compounds is higher in comparison to the clay-filled compounds. In addition, the tan δ values of the clay-filled compounds are higher compared with the CB-filled compounds. A higher tan δ value results in a higher friction coefficient and skid resistance or increased grip of the tyre on the road. These compounds are particularly suitable for tyres requiring strong grip on the road such as racing tyres.

**Table 1.3:** Compound formulation.

| Materials (phr) | A | B | C | D |
|---|---|---|---|---|
| NR | 60 | 60 | – | – |
| BR | 40 | 40 | – | – |
| SBR 1500 | – | – | 100 | 100 |
| CB (N220) | 50 | – | 80 | – |
| MMT–clay modified with dimethyldioctadecyl ammoniums ions | – | 50 | – | 80 |
| Aromatic oil | 5 | 5 | 40 | 40 |
| Stearic acid | 2 | 2 | 2 | 2 |
| Zinc oxide | 3 | 3 | 3 | 3 |
| Antioxidant | 1 | 1 | 1 | 1 |
| Sulfur | 2 | 2 | 2 | 2 |
| Accelerator | 2.5 | 2.5 | 2.5 | 2.5 |

Reproduced with permission from *Rubber-Clay Nanocomposites: Science, Technology, and Applications,* Ed., M. Galimberti, Wiley, New York, NY, USA, 2011. ©2011, Wiley [24]

**Table 1.4:** Physical properties of the compounds.

| Property | A | B | C | D |
|---|---|---|---|---|
| TS (MPa) | 20.0 | 9.2 | 15.2 | 3.6 |
| 300% Modulus (MPa) | 15.04 | 5.35 | 6.83 | 2.35 |
| Tear strength (MPa) | 31.7 | 21.1 | 27.8 | 10.7 |
| Shore A hardness | 67.5 | 66.6 | 53.3 | 42.7 |
| Rebound at RT (%) | 58.1 | 48.7 | 47.0 | 17.0 |
| Rebound at 70 °C (%) | 64.5 | 38.1 | 60.6 | 29.2 |
| Tan δ, 0 °C | 0.109 | 0.160 | 0.278 | 0.393 |
| Tan δ, 30 °C | 0.065 | 0.248 | 0.237 | 0.433 |
| Tan δ, 60 °C | 0.061 | 0.210 | 0.194 | 0.334 |

Reproduced with permission from *Rubber-Clay Nanocomposites: Science, Technology, and Applications*, Ed., M. Galimberti, Wiley, New York, NY, USA, 2011. ©2011, Wiley [24]

The OC nanocomposites were used for the colour tyre side wall compounds [100]. The compound formulation is given in Table 1.5.

Physical properties are summarised in Table 1.6.

A higher strength property and better ozone resistance was observed for the nanocomposites, with the better ozone resistance explained in Section 1.7.3.

The preparation of clay/rubber nanocomposites *via* the latex route and use in tyre components, such as tyre tread and sidewall, has been described in patent US20030144401 [21].

The preparation and use of nanocomposites in aircraft tyre tread, where significant replacement of CB reinforcement is desired to reduce heat build-up to achieve

**Table 1.5:** Compound formulation.

| Materials (phr) | Sample A | Sample B |
|---|---|---|
| Natural rubber (SMR 5) | 35 | 0 |
| Chlorobuytl rubber | 50 | 50 |
| EPDM rubber | 15 | 15 |
| Silica | 20 | 20 |
| Titanium dioxide | 30.2 | 30.2 |
| Plasticiser | 5 | 5 |
| Wax | 3 | 3 |
| Nanocomposite masterbatch (35 phr NR) | – | 40 |

With the same curing package (i.e., both formulations have same sulfur and accelerator dosage).
Reproduced with permission from *Rubber-Clay Nanocomposites: Science, Technology, and Applications*, Ed., M. Galimberti, Wiley, New York, NY, USA, 2011. ©2011, Wiley [24]

**Table 1.6:** Physical properties of the compounds.

| Properties | Sample A | Sample B |
|---|---|---|
| TS (MPa) | 14.7 | 11.9 |
| EB (%) | 800 | 607 |
| 300% Modulus (MPa) | 2.6 | 4.8 |
| Shore A hardness | 48 | 56 |
| Rebound, RT (%) | 35 | 35 |
| Dynamic ozone test (0–60% strain, 48 h, 50 pphm, 40 °C) | Broken, edge crack | No crack |
| Taber abrasion test, weight loss after 1,000 cycles (gram) | 1.12 | 0.86 |

pphm: parts per hundred million
Reproduced with permission from *Rubber-Clay Nanocomposites: Science, Technology, and Applications*, Ed., M. Galimberti, Wiley, New York, NY, USA, 2011. ©2011, Wiley [24]

tyre durability and reduction in tyre weight for fuel economy, is described in patent US2005065266 [22]. The compounds containing an optimum loading of NC (~9 phr) exhibited lower abrasion loss.

A higher coefficient of friction and low abrasion loss of NR OC nanocomposites is reported in patent US200440147661A1 [101].

The use of OC elastomer nanocomposites in tyres is also detailed in several other patents [102–106].

## 1.8 Disadvantages of Using Organoclay Elastomeric Nanocomposites in the Automotive Industry

The main constraint of using OC elastomeric nanocomposites in the automotive industry is the 'cost', in addition to other disadvantages. NC composites exhibit a very high compression or tensile set property [18, 107], and the high set property restricts the use of OC in tyre tread, tubes and different kinds of seals where a low compression set property is required. OC nanocomposites exhibit a poor fatigue life in comparison to conventional CB-filled compounds [108]. The better fatigue life of CB-filled compounds can be explained by the relatively superior rubber–filler interaction [109]. CB are nanoparticles with a more or less spherical nature. The interaction of CB with rubber is a strong physico-chemical interaction, whereas the interaction of the clay with rubber is due to van der Waals forces. The interaction at the edge of the clay particles is the weakest.

Therefore, during cyclic deformation, the stress concentration is highest at the edge of the clay particles. Thus, flaws can easily be generated at these points in comparison to the strongly attached nearly spherical CB particles; hence, OC-containing compounds exhibit low fatigue life compared with CB-filled compounds.

A lower fatigue life limits the use of OC in dynamic automotive elastomeric components; however, treatment of OC with a silane coupling agent improved these properties [110].

The addition of OC nanocomposites produced relatively low RT and high-temperature self-self/self-carcass adhesion, which is explained by the same patent. Low adhesion is a serious concern related to product performance, as lower adhesion may cause early failure of the product.

## 1.9 Conclusion

There are not many OC elastomeric nanocomposites commercially available on the market, whereas there are numerous commercially available plastic nanocomposites. OC elastomer nanocomposites have many advantages but there are also disadvantages. The rubber parts in an automobile are used for dynamic applications, whereas the plastic parts are mainly for static applications. The main disadvantage of NC elastomer nanocomposites is poor dynamic mechanical characteristics. Rubber by its inherent nature is thermosetting, which also restricts the industrial use of OC elastomer nanocomposites. The biggest advantage of thermoplastic materials is reuse *via* remelting and reprocessing. The mixing time for OC elastomer nanocomposites is also high as it requires intense (time) mixing, which increases the production cycle time. A number of publications suggest that the preparation of nanocomposites *via* the masterbatch route and latex stage blending shows good potential [111–113].

There are a number of patents and publications focusing on OC elastomer nanocomposites [1, 24, 114–116], however, there are not many OC elastomeric nanocomposites available on the market for automotive applications. On the contrary, many thermoplastic nanocomposites are commercially available for automotive applications (FORTE$^{TM}$ nanocomposites from Noble Polymers, Nylon 6 nanocomposites from Ube Industry, Nylon 6 nanocomposites from Toyota Motors and so on).

Compared with a highly CB-loaded compound, a substantial improvement in physical properties is obtained using a low level of OC loading. The overall weight reduction of the tyre will, in turn, positively impact fuel economy. A low filler loading will reduce heat build-up and results in the development of a 'cooler running tyre'. The better air retention properties of elastomer nanocomposites makes them suitable for inner liner and tube applications; whereas, the better solvent-resistant property makes them suitable for use in automotive hose or inner liner applications. For tyre applications to achieve enhanced mileage, clay nanocomposites are used because of their low abrasion loss property. The superior ozone and ageing properties are exploited to produce tyre sidewalls. For enhanced grip and skid-resistant properties of tyres, elastomer nanocomposites are also used as they give a higher tan δ value and higher friction coefficient.

OC elastomer nanocomposites is a new technology for the automotive industry and requires considerable focus in order to overcome the different problems associated with their use. The big automotive giants and chemical companies are coming forward and taking an interest in systematic and intense research in the field of OC elastomer nanocomposites.

**Acknowledgements:** The author thanks Dr Sugata Chakraborty for heling to prepare this manuscript. The author also thanks the Indian Rubber Institute for giving permission to use certain figures in this chapter.

## References

1. S. Bandyopadhyay, S. Chakraborty and R. Mukhopadhyay in *Rubber Science and Technology*, Ed., R. Mukhopadhyay, Shantinath Printers, Udaipur, Rajasthan, India, 2006.
2. T. Akema and H. Yoshida, *Polyfile*, 1987, **25**, 24.
3. K. Hashimoto, A. Maeda, K. Hosoya and Y. Todani, *Rubber Chemistry and Technology*, 1998, **71**, 449.
4. J.B. Donnet, *Composite Science and Technology*, 2003, **63**, 1085.
5. M. Alexandre and P. Dubois, *Material Science and Engineering: R: Reports*, 2000, **28**, 1.
6. J.E. Mark, *Polymer Engineering & Science*, 1996, **36**, 2905.
7. J. Wen and G.L. Wilkes, *Chemistry of Materials*, 1996, **8**, 1667.
8. T. Von Werne and T.E. Patten, *Journal of the American Chemical Society*, 1999, **121**, 7409.
9. P. Calvert in *Carbon Nanotubes: Preparation and Properties*, Ed., T.W. Ebbesen, CRC Press, Boca Raton, FL, USA, 1992, p.277.

10. M.S. Dresselhaus, G. Dresselhaus and P. Avouris in *Carbon Nanotubes: Synthesis, Structure, Properties, and Applications*, Springer Verlag, Heidelberg, Germany, 2001, p.8.
11. V. Favier, G.R. Canova, S.C. Shrivastava and J.Y. Cavaille, *Polymer Engineering & Science*, 1997, **37**, 1732.
12. L. Chazeau, J.Y. Cavaille, G. Canova, R. Dendievel and B. Boutherin, *Journal of Applied Polymer Science*, 1999, **71**, 1797.
13. Y. Kojima, K. Fukumori, A. Usuki, A. Okada and T. Kurauchi, *Journal of Materials Science Letters*, 1993, **12**, 889.
14. R. Magaraphan, W. Thaijaroen and R.L. Ochakun, *Rubber Chemistry and Technology*, 2003, **76**, 406.
15. S. Joly, G. Garnaud, R. Ollitrault and L. Bokobza, *Chemistry of Materials*, 2002, **14**, 4202.
16. S. Varghese and J. Karger-Kocsis, *Polymer*, 2003, **44**, 4921.
17. Y. Wang, H. Zhang, Y. Wu, J. Yang and L. Zhang, *Journal of Applied Polymer Science*, 2005, **96**, 318.
18. Y. Wang, H. Zhang, Y. Wu, J. Yang and L. Zhang, *Journal of Applied Polymer Science*, 2005, **96**, 324.
19. Y.P. Wu, Q.X. Jia, D.S. Yu and L.Q. Zhang, *Journal of Applied Polymer Science*, 2003, **89**, 3855.
20. S. Varghese, K.G. Gatos, A.A. Apostolov and J. Karger-Kocsis, *Journal of Applied Polymer Science*, 2004, **92**, 543.
21. M. Ajbani, J.F. Geiser and D.K. Parker; inventors and assignees; US2003144401A1, 2003.
22. X. Yang, M.P. Cohen, M.L. Senyek, D. Kenton Parker, S.W. Cronin, L.T. Lukic, W.P. Francik and C. Gurer; inventors and assignees; US2005065266A1, 2005.
23. M. Arroyo, M.A. Lopez-Manchado and B. Herrero, *Polymer*, 2003, **44**, 2447.
24. *Rubber-Clay Nanocomposites: Science, Technology and Applications*, Ed., M. Galimberti, John Wiley & Sons, New York, NY, USA, 2011.
25. Y.W. Chang, Y. Yang, S. Ryu and C. Nah, *Polymer International*, 2002, **51**, 319.
26. M. Liao, W. Shan, J. Zhu, Y. Li and J.H. Xu, *Journal of Polymer Science, Part B: Polymer Physics*, 2005, **43**, 1344.
27. S. Sadhu and A.K. Bhowmick, *Journal of Polymer Science, Part B: Polymer Physics*, 2004, **42**, 1573.
28. S. Sadhu and A.K. Bhowmick, *Journal of Polymer Science, Part B: Polymer Physics*, 2005, **43**, 1854.
29. S. Sadhu and A.K. Bhowmick, *Rubber Chemistry and Technology*, 2005, **78**, 321.
30. H. Acharya, S.K. Srivastava and A.K. Bhowmick, *Composite Science and Technology*, 2007, **67**, 2807.
31. H. Acharya, S.K. Srivastava and A.K. Bhowmick, *Nanoscale Research Letters*, 2007, **2**, 1.
32. S. Ray and A.K. Bhowmick, *Rubber Chemistry and Technology*, 2001, **74**, 835.
33. M. Maiti, S. Sadhu and A.K. Bhowmick, *Journal of Applied Polymer Science*, 2006, **101**, 603.
34. H. Liao and C. Wu, *Journal of Applied Polymer Science*, 2005, **97**, 397.
35. Y. Chang, D. Lee and S. Bae, *Polymer International*, 2006, **55**, 184.
36. S.K. Lim, S.T. Lim, H.B. Kim, I. Chin and H.J. Choi, *Journal of Macromolecular Science, Part B: Physics*, 2003, **B42**, 1197.
37. M. Maiti and A.K. Bhowmick, *Composite Science and Technology*, 2008, **68**, 1.
38. M. Liao, J. Zhu, H. Xu, Y. Li and W. Shan, *Journal of Applied Polymer Science*, 2004, **92**, 3430.
39. D. Li, D.G. Peiffer, C.W. Elspass and H.C. Wang, inventors; Exxon Chemical Patents, Inc., assignee; US006060549A, 2000.
40. Y. Liang, Y. Wang, Y. Wu, Y. Lu, H. Zhang and L. Zhang, *Polymer Testing*, 2005, **24**, 12.
41. Y.P. Wu, Y. Ma, Y.Q. Wang and L.Q. Zhang, *Macromolecular Material and Engineering*, 2004, **289**, 890.

42. M. Kato, A. Tsukigase, H. Tanaka, A. Usuki and I. Inai, *Journal of Polymer Science, Part A: Polymer Chemistry*, 2006, **44**, 1182.
43. Y. Lu, Y. Liang, Y. Wu and L. Zhang, *Macromolecular Materials and Engineering*, 2006, **291**, 27.
44. Y. Liang, J. Ma, Y. Lu, Y. Wu, L. Zhang and Y. Mai, *Journal of Polymer Science, Part B: Polymer Physics*, 2005, **43**, 2653.
45. M. Maiti, S. Sadhu and A.K. Bhowmick, *Journal of Polymer Science, Part B: Polymer Physics*, 2004, **42**, 4489.
46. A.J. Dias, C. Gong, W. Weng, D.Y. Chung and A.H. Tsou, inventors; ExxonMobil Chemical Patents, Inc., assignee; WO02100935A1, 2002.
47. W. Weng, A.J. Dias, K.R. Karp, M.W. Johnston, C. Gong, C. Neagu and B.J. Poole, inventors; ExxonMobil Chemical Patents, Inc., assignee; WO2007064400A1, 2007.
48. S. Takahashi, H.A. Goldberg, C.A. Feeney, D.K. Karim, M. Farrell, K. O'Leary and D.R. Paul, *Polymer*, 2006, **47**, 3083.
49. T. Takashima, inventor; Nippon Petrochemicals, assignee; JP2005068237, 2005.
50. P. Meneghetti, S. Shaikf, S. Qutubuddin and S. Nazarenko, *Rubber Chemistry and Technology*, 2008, **81**, 821.
51. E.N. Kresge and D.J. Lohse, inventors; Exxon Mobil Chemical Patents Inc., assignee; US005576372A, 1996.
52. W. Weng, A.J. Dias, S. Neagu, B.J. Poole, C. Gong, J.R. Ayers, K. Randall Karp and M.W. Johnston; inventors and assignees; US20070015853A1, 2007.
53. E.N. Kresge and D.J. Lohse, inventors; Exxon Chemical Patents, Inc., assignee; US005665183A, 1997.
54. C.W. Elspass, D.G. Peiffer, E.N. Kersge, P.J. Wright, J.J. Chludzinski and C.H. Wang, inventors; Exxon Research and Engineering, assignee; US005807629, 1998.
55. C. Gong, A.J. Dias, A.H. Tsou, B.J. Poole and K.R. Karp, inventors; ExxonMobil Chemical Patents, Inc., assignee; US20050277723A1, 2005.
56. S. Chakraborty, R. Sengupta, S. Dasgupta, R. Mukhopadhyay, S. Bandyopadhyay, M. Joshi and S.C. Ameta, *Polymer Engineering & Science*, 2009, **49**, 1279.
57. H. Anmin, W. Xiaoping, J. Demin and L. Yanmei, *e-Polymer*, 2007, No. 051.
58. A. Ansarifar and N. Ibrahim, *Rubber Chemistry and Technology*, 2005, **78**, 793.
59. M. Bhattacharya, M. Maity and A.K. Bhowmick, *Rubber Chemistry and Technology*, 2008, **81**, 782.
60. J.K. Mishra, I. Kim, C.S. Ha, J. Ryou and G.H. Kim, *Rubber Chemistry and Technology*, 2005, **78**, 42.
61. M. Maiti and A.K. Bhowmick, *Journal of Applied Polymer Science*, 2007, **105**, 435.
62. J.T. Kim, T.S. Oh and D.H. Lee, *Polymer International*, 2003, **52**, 1203.
63. M. Maity, M. Bhattacharya and A.K. Bhowmick, *Rubber Chemistry and Technology*, 2008, **81**, 384.
64. A. Bandyopadhyay, M. De Sarkar and A.K. Bhowmick, *Rubber Chemistry and Technology*, 2005, **78**, 806.
65. M.A. Lopez-Manchado, B. Herrero and M. Arroyo, *Polymer International*, 2004, **53**, 1766.
66. M.A. Lopez-Manchado, B. Herrero, M. Arroyo and J. Biagiotti, *Journal of Applied Polymer Science*, 2003, **89**, 1.
67. J.H. Chang and Y.U. An, *Journal of Polymer Science, Part B: Polymer Physics*, 2002, **40**, 670.
68. Z. Wang and T.J. Pinnavaia, *Chemistry of Materials*, 1998, **10**, 3769.
69. Y.I. Tien and K.H. Wei, *Journal of Applied Polymer Science*, 2002, **86**, 1741.
70. L. Zhu and R.P. Wool, *Polymer*, 2006, **47**, 8106.
71. C.H. Dan, M.H. Lee, Y.D. Kim, B.H. Min and J.H. Kim, *Polymer*, 2006, **47**, 6718.

72. P. Ni, Q. Wang, J. Li, J. Suo, and S. Li, *Journal of Applied Polymer Science*, 2006, **99**, 6.
73. B. Finnigan, P. Halley, K. Jack, A. McDowell, R. Truss, P. Casey, R. Knott and D. Martin, *Journal of Applied Polymer Science*, 2006, **102**, 128.
74. L.T.Z. Korley, S.M. Liff, N. Kumar, G.H. McKinley and P.T. Hammond, *Macromolecules*, 2006, **39**, 7030.
75. W.J. Seo, Y.T. Sung, S.B. Kim, Y.B. Lee, K.H. Choe, S.H. Choe, J.Y. Sung and W.N. Kim, *Journal of Applied Polymer Science*, 2006, **102**, 3.
76. J. Jin, M. Song, K.J. Yao and L. Chen, *Journal of Applied Polymer Science*, 2006, **99**, 3677.
77. F.M. Uhl, P. Davuluri, S.C. Wong and D.C. Webster, *Polymer*, 2004, **45**, 6175.
78. A. Pattanayak and S.C. Jana, *Polymer*, 2005, **46**, 3275.
79. H. Tan and J. Nie, *Journal of Applied Polymer Science*, 2007, **106**, 2656.
80. A. Pattanayak and S.C. Jana, *Polymer*, 2005, **46**, 5183.
81. D.S. Kim, J.T. Kim and W.B. Woo, *Journal of Applied Polymer Science*, 2005, **96**, 1641.
82. F. Cao and S.C. Jana, *Polymer*, 2007, **48**, 3790.
83. J.K. Mishra, I. Kim and C.S. Ha, *Macromolecular Rapid Communication*, 2003, **24**, 671.
84. S.M. Liff, K. Nitin and G.H. McKinley, *Nature Materials*, 2007, **6**, 76.
85. V.Y. Kramarenko, T.A. Shantalil, I.L. Karpova, K.S. Dragan, E.G. Privalko, V.P. Privalko, D. Fragiadakis and P. Pissis, *Polymers for Advanced Technologies*, 2004, **15**, 144.
86. T.K. Chen, Y.I. Tien and K.H. Wei, *Journal of Polymer Science, Part A: Polymer Chemistry*, 1999, **37**, 2225.
87. Y.I. Tien and K.H. Wei, *Polymer*, 2001, **42**, 3213.
88. K.J. Yao, M. Song, D.J. Hourston and D.Z. Luo, *Polymer*, 2002, **43**, 1017.
89. R. Xu, E. Manias, A.J. Snyder and J.J. Runt, *Journal of Biomedical Materials Research Part A*, 2003, **64A**, 114.
90. M. Bertoldo, S. Bronco, P. Narducci, S. Rossetti and M. Scoponi, *Macromolecular Materials and Engineering*, 2005, **290**, 475.
91. A. Rehab and N. Salahuddin, *Material Science and Engineering*, 2005, **399**, 368.
92. T. Rihayat, M. Saari, A.R. Suraya, H.M. Mahmood, K.Z. Dahlan, W.M.Z.W. Yunus and S.M. Sapuan, *Polymer-Plastics Technology and Engineering*, 2006, **45**, 1323.
93. V. Igor, R. Khudyakov, D. Zopf and N.J. Turro, *Designed Monomers and Polymers*, 2009, **12**, 279.
94. G.C. Psarras, K.G. Gatos and J. Karger-Kocsis, *Journal of Applied Polymer Science*, 2007, **106**, 1405.
95. D.K. Parker, B.K. Larson and X. Yang, inventors; The Goodyear Tire & Rubber Company, assignee; US006861462B2, 2005.
96. M. Ajbani, W.L. Hsu, A.F. Halasa, G. Lee and E.S. Castner, inventors; The Goodyear Tire & Rubber Company, assignee; US007055566B2, 2006.
97. M. Ajbani, J.F. Geiser and D.K. Parker, inventors; The Goodyear Tire & Rubber Company, assignee; US006759464B, 2004.
98. M. Caprio, M. Galimberti, L. Grassi, S. Testi and D. Tirelli, inventors; Marathon Oil Company, assignee; WO1991006511A1, 2009.
99. B.K. Larson, inventor; The Goodyear Tire & Rubber Company, assignee; US006598645B1, 2003.
100. J. Zhao, M.J. Crawford, A.S. Puhala and M.P. Cohen; inventors and assignees; US20060135671A1, 2006.
101. A. Yaakub, C.P. Kuen, N. Keane and M. Ross; inventors and assignees; US20040147661A1, 2004.
102. C.W. Elspass, D.G. Peiffer, E.N. Kresge, D. Hsieh, J.J. Chludzinski and K.S. Liang, inventors; Exxon Research & Chemical Company, assignee; US005883173, 1999.

103. W. Weng, A.J. Dias, K.R. Karp, M.W. Johnston, C. Gong, C. Neagu and B.J. Poole, inventors and assignees; US20070129477A1, 2007.
104. X. Yang, M.P. Cohen, M.L. Senyek, D.K. Parker, W. Cronin, L.T. Lukich, W.P. Francik and C. Gurer, inventors; The Goodyear Tire & Rubber Company, assignee; US007342065B2, 2008.
105. D.K. Parker, B.K. Larson and X. Yang, inventors and assignees; US20040054059A1, 2004.
106. G. Heinrich, W. Herrmann, N. Kendziorra, T. Pietag and C. Recker, inventors; Continental Aktiengesellschaft, assignee; US20020095008A1, 2002.
107. Y. Wang, L. Zhang, C. Tang and D. Yu, *Journal of Applied Polymer Science*, 2000, **78**, 1879.
108. A.J. Dias, G.E. Jones, D.S. Tracey and W.H. Waddell; inventors and assignees; US20040132894A1, 2004.
109. S. Chakarborty, R. Sengupta, S. Dasgupta, R. Mukhopadhyay, S. Bandyopadhyay, M. Joshi and S.C. Ameta, *Journal of Applied Polymer Science*, 2010, **116**, 1660.
110. J. Karger-Kocsis and C.M. Wu, *Polymer Engineering & Science*, 2004, **44**, 1083.
111. H. Zhang, Y. Wang, Y. Wu, L. Zhang and J. Yang, *Journal of Applied Polymer Science*, 2005, **97**, 844.
112. Y.P. Wu, L.Q. Zhang, Y.Q. Wang, Y. Liang and D.S. Yu, *Journal of Applied Polymer Science*, 2001, **82**, 2842.
113. J.H. Koo in *Polymer Nanocomposites: Processing, Characterization, and Applications*, McGraw Hill, New York, NY, USA, 2006.
114. M. Galimberti, V. Cipolletti, S. Musto, S. Cioppa, G. Peli, M. Mauro, G. Gaetono, S. Agnelli, R. Theonis and V. Kumar, *Rubber Chemistry and Technology*, 2014, **87**, 417.
115. S. Thomas and H.J. Maria in *Progress in Rubber Nano Composites*, 1st Edition, Elsevier (Imprint Woodhead Publishing), Amsterdam, The Netherlands, 2016.
116. J.H. Koo in *Fundamentals, Properties and Applications of Polymer Nanocomposites*, Cambridge University Press, Cambridge, UK, 2016.

Suneel Kumar Srivastava and Bhagabat Bhuyan

# 2 Rubber Nanocomposites for Tyre Tread Applications

## 2.1 Introduction

### 2.1.1 Introduction to Tyres

A tyre is an assembly of a series of components, i.e., tread, tread shoulder, tread cushion, sidewall, curb guard, beads, shoulder belt wedge, liner tread and so on [1–3]. Tyre manufacturing is a complicated multi-step process involving several types of materials and processing steps. Overall, tyres perform a set of fundamental functions including: providing cushioning, dampening, cornering force and steering response; transmitting driving and braking torque, and minimising rolling resistance, abrasion resistance, noise and vibration, in addition to providing dimensional stability, load carrying capacity and durability. The ability of vehicles to start, stop and turn corners results from friction between the road and the tyres. Tyre tread designs need to deal with the complex effects of weather conditions, e.g., dry, wet, snow-covered and icy surfaces. Slick racing tyres or bald tyres may have good traction on dry surfaces, but may be undriveable in wet, rainy conditions due to hydroplaning. Tyre tread designs enable water to escape from the tyre–road contact area (the tyre footprint) to minimise hydroplaning, while providing a reasonable balance between the conflicting requirements of good dry traction, low wear and low noise. Tyres also act as a spring and damper system to absorb impacts and road surface irregularities over a wide variety of driving conditions. In view of this, the wheel remains unequivocally one of the key scientific inventions that has revolutionalised human life. Over time, changes to the wheel have taken place primarily to reduce power consumption and noise during usage. The demand for faster and safer wheels for military applications resulted in the development of spoked wheels with a cushioned envelope, such as a leather or elastomeric balloon, on the wheel frame referred to as a ‘tyre’. The process culminated in the development of the pneumatic tyre, in which an air-filled elastomeric balloon, called a tube, provides the necessary cushioning effect. Historically, the pneumatic tyre dates back to the late 1880s when small cross-section tyres with high pressures were reported for bicycle applications in Great Britain as an upgrade from solid rubber tyres. Larger ‘balloon’ tyres were introduced in the early 1920s with applications in the mushrooming motor vehicle industry. Tubeless tyres with improvements in rim design were introduced in the early 1950s, with belted bias tyres becoming popular in the late 1960s. Radial tyres, first introduced in Europe, became popular worldwide by the 1990s and now dominate the passenger tyre market. Today, the tyre is a composite engineering product that is essential for all sorts of bulk surface transportation systems. In view of this,

https://doi.org/10.1515/9783110643879-002

elastomers, specifically, natural rubber (NR) and styrene-butadiene rubber (SBR) and their elastomeric blends, find applications in different tyre components [4–121].

NR, synthetic rubber and its blends are the backbone of tyre tread compounds. Reinforcing fillers strengthen rubber compounds to give the compound unique properties – the most common being carbon black(s) (CB) and silica. Softeners such as petroleum oils, pine tar, resins and waxes are principally used as processing aids and to improve the tack of unvulcanised compounds. Antidegradants like waxes, antioxidants and antiozonants are added to protect tyres against deterioration by ozone, oxygen and heat. Curatives, during vulcanisation stage, crosslink the polymer chains transforming the viscous compounds into strong, elastic materials. Sulfur along with accelerators and activators help achieve the desired properties. Since the number of components in any tyre compound is very high, due to the different types of rubbers, CB, silica, oils, waxes, curatives and speciality chemicals, the potential variety of suitable compounds seems endless. The tyre compounder has a difficult task when finalising the formulation, as adjusting one of the properties often affects other performance areas. The best tread compound for dry traction and handling might lack wet/snow traction, chip/tear resistance or fuel economy. Thus, compounds must be engineered to meet all the performance criteria. Adding to the complexity, the chosen compound must be cost competitive and processable in manufacturing plants. Typical tyre tread compound formulations in three different types of passenger car radial tyres include: NR, SBR, polybutadiene rubber (BR), fillers (CB N220, CB N330, silica), processing aids, coupling reagents, activators, plasticisers, crosslinkers and accelerators.

Over the last two decades, nanotechnology has become an integral part of all research and development work in the field of science and technology, either directly or indirectly, and tyre technology is no exception. Surprisingly, there are a limited number of reports available that focus on the application of nanofillers such as clay [montmorillonite (MMT), kaolin and hectorite (Hc)], multi-walled carbon nanotubes (MWCNT), silica and graphene (GE) in different rubber matrices such as NR, SBR and their blends; with only a few are related to their application in tyre components. In all probability, the lack of sufficient reports detailing strong evidence of improvement in mechanical, dynamic mechanical, thermal and tribological properties can partially justify the reluctance of industries to switch over from conventional CB to newer, safer and eco-friendly substitutes. This clearly highlights why the 'nano-movement' has not yet been able to bring revolutionary change to the material components of a tyre.

Taking this into account, this chapter reviews all work, both at academic and industrial level, on nanofillers with regard to their suitability for use in tyre tread formulations. This is also expected to help material scientists develop new types of nanofillers, in addition to giving the tyre industry a complete overview on the recent developments in nanomaterials for tyre tread applications.

## 2.1.2 Brief History of Fillers in Tyre Tread Applications

CB is the major reinforcing filler used in the tyre industry and is available in different grades, e.g., thermal, furnace, channel and acetylene black. CB is composed of spherical particles of pure elemental carbon in colloidal dimension that coalesce into aggregates and agglomerates. Different grades differ in their particle size, aggregate form and aggregate shape. Conventionally, high abrasion furnace CB has been the major component of the filler system for tyre tread compounds, and the reinforcement is attributed to its dispersion in the rubber matrix during melt mixing. In addition, CB manufacturers have developed a new class of materials to meet a perfect balance among tyre performance indicators, i.e., rolling resistance, abrasion resistance, wet traction, snow traction and ageing resistance. The correct choice of CB is therefore crucial for the development of a polymer system that meets the performance specifications of a particular product, including tyres. As an empirical guide, an increase in CB-aggregate size or structure results in an improvement in cut growth and fatigue resistance. A decrease in particle size results in an increase in abrasion resistance, tear strength, hysteresis and heat build-up, and a drop in resilience. The general effect of CB loading on tyre performance properties will also be discussed. Furthermore, an ideal tread compound must fulfil many contradictory performance parameters, such as wet skid resistance, rolling resistance and so on. Therefore, synthesising CB with tailor-made particle size, aggregate size and surface area has a significant impact on industrial tyre research. In this context, CB grades such as N120, N234, LH30, N339 and N351 were specifically designed for tyre tread compounds for different types of tyres, i.e., they satisfy the tyre performance requirements either alone or in combination. However, its polluting nature, black colour and the quantity needed to enhance the mechanical properties are the drawbacks of CB.

Silica is the most important non-black reinforcing filler employed in tyre formulations. It improves mechanical properties, in particular, tear strength, abrasion resistance and rolling resistance. The reinforcement of rubber by silica can be attributed to the rubber network, hydrodynamic effect, volume fraction and aspect ratio of the filler, filler–filler and filler–rubber interactions. The filler–rubber interaction depends on the particle shape and size and surface characteristics of the filler, in addition to the chemical nature of the rubber. The abundance of available hydroxyl (–OH) groups on the silica surface makes it hydrophilic in nature and hence incompatible with organophilic polymers, which necessitates a coupling agent with one hydrophilic and another organophilic (i.e., hydrophobic) end. The presence of silane coupling agents, such as Si 69®, enhance the polymer–filler chemical interaction. Besides the use of silane coupling agents to control the surface energy of silica, treatment with glycols and esterification with monofunctional alcohols have also been extensively used. In addition to these two fillers, a large number of other inorganic or carbonaceous fillers, such as clays, carbon nanotubes (CNT) and GE, are used as part of the filler system. However, when polymers are reinforced by such individual fillers, they are often

unable to meet the desired performance expected of them. Therefore, a recent trend has involved using hybrid fillers consisting of two, or more, types of fillers for rubber reinforcement. Tables 2.1–2.3 provide all the details regarding the fillers and methodology adopted to prepare NR, SBR and its blend nanocomposites, respectively.

**Table 2.1:** Details of filler types and methods of preparing NR nanocomposites.

| Rubber | Nanofiller(s) | Method of preparation of rubber composite | Ref. |
|---|---|---|---|
| NR | Organo-modified MMT | Solution blending | [11, 12] |
| NR | Layered silicates (fluorohectorite and bentonite) | Open two-roll laboratory mill | [13] |
| NR | MMT | Processing using Banbury mixer | [14] |
| NR | Cloisite® 15A NC | Laboratory type Banbury mixer or a two-roll mixer | [15] |
| NR | OMMT | Dry mixing method | [16] |
| NR | ODA-modified fluorohectorite | Melt blending | [17] |
| NR latex | Layered silicates (sodium bentonite and sodium fluorohectorite) | Latex compound mixed with aqueous dispersions of silicates | [18] |
| NR | Na–MMT and organically modified layered silicates | Mixing in internal blender | [19] |
| NR | ZnO nanoparticle doped GE | Open two-roll mill method | [20] |
| NR latex | GE nanotubes and CNT | Latex mixing | [23] |
| NR | Fullerene, CNT and graphene nanoplatelets | Open two-roll mill method | [24] |
| NR | CB in the presence of NC and nanofibre | Open two-roll mill method | [25] |
| NR | Kaolin and CB | Melt blending | [26] |
| NR | CB and NC | Two-roll mill method | [27] |
| NR | Modified CG | Two-roll mill method | [28] |
| NR | rPET partially replaced with HNT | Two-roll mill method | [29] |
| NR | White tirade dust/CB | Open two-roll method | [30] |
| NR | Silica/CB | Two-roll mill method | [31] |
| NR | CB and NC | Melt compounding | [32] |
| NR | NC/CB | Laboratory mixer | [33] |
| NR | Marble waste/rice-husk-derived silica | Compounding | [34] |
| NR | CB/rice husk powder | Two-roll mill method | [35] |
| NR | MWCNT/silica | Two-roll mill method | [36] |
| NR | CB/NC | Two-roll mill method | [39] |
| NR | Na-MMT modified with cationic surfactants, DDA and ODA ammonium chloride | Electron beam dose of 250 kGy | [40] |
| NR | NR/PAT | Double-roller plasticator | [42] |

(continued)

**Table 2.1** (continued)

| Rubber | Nanofiller(s) | Method of preparation of rubber composite | Ref. |
|---|---|---|---|
| NR | MWCNT | Shear mixing techniques | [43] |
| NR | CB nanoparticles and GON | Solution mixing | [44] |
| NR | Functionalised CNT | Solution method | [45] |
| NR | CNC | Solution mixing and casting method | [46] |
| NR | Cellulosic nanoparticles | Casting evaporation method | [47] |
| NR | Pretreated CNT | Solvent mixing | [48] |
| NR | Organoclay | Grafting and intercalating in latex in the presence of a butyl acrylate monomer | [49] |
| NR | Organic vermiculite | Mixing | [50] |
| Unoxidised and oxidised NR latex | CNC | Casting/evaporation | [82] |
| NR | Gelatin–hydrazine hydrate–rGO | Water-based solution casting | [107] |
| NR latex | GO, rGO, substituting GO or rGO for CB | Latex mixing | [110] |
| NR latex | $SiO_2$ modified by $CeO_2$ | Latex mixing | [111] |
| NR | Thermally-reduced GE + ionic liquid modified CNT | Melt mixing | [116] |

$CeO_2$: Cerium(IV) oxide
CG: Coal gangue
CNC: Cellulose nanocrystals
DDA: *N,N*-dimethyldodecylamine
GO: Graphene oxide
GON: Graphite oxide nanosheets
HNT: Halloysite nanotube(s)
Na-MMT: Sodium montmorillonite
NC: Nanoclay(s)
ODA: Octadecylamine
OMMT: Organo-modified montmorillonite
PAT: Purified attapulgite
rGO: Reduced graphene oxide
rPET: Recycled polyethylene terephthalate
ZnO: Zinc oxide

**Table 2.2:** Details of filler types and methods of preparing SBR nanocomposites.

| Rubber | Nanofiller(s) | Method of preparation of nanocomposite | Ref. |
|---|---|---|---|
| SBR | OMMT | Solution blending | [11, 12] |
| SBR | ODA-modified fluorohectorite | Melt blending | [17] |

(continued)

**Table 2.2** (continued)

| Rubber | Nanofiller(s) | Method of preparation of nanocomposite | Ref. |
|---|---|---|---|
| SBR | Silica hybrid filler included bagasse ash and silica | Two-roll mill method | [35] |
| SBR Latex | TAG/HNT hybrid | Hybrid colloid co-coagulated with SBR emulsion | [38] |
| SBR | Modified Hc (modifier: ODA; by grafting with the silane coupling agent N-[3-(trimethoxysilyl) propylethylenediamine]) | Solution method | [51] |
| SBR | Clay/CB | Two-roll mill method | [52] |
| SBR | OMMT | Two-roll mill method | [53] |
| SBR | DDA–MMT | Latex method | [55] |
| SBR | Layered silicate surface-modified MMT with 75–70% clay and 25–30 wt% ODA | Mechanical mixing | [56] |
| SBR | Cloisite® 15A | Melt intercalation | [57] |
| SBR | Layered silicate | Latex mixing | [58] |
| SBR | Modified and unmodified MMT, sepiolite, Hc, CNF, EG | Mixing in the Brabender | [59] |
| SBR | Clay | SBR latex mixing | [60] |
| SBR | ODA-modified Na-MMT | Solvent casting | [61] |
| SBR | CNT | Coagulation method followed by mastication in a twin-screw extruder | [62] |
| SBR | EG and MEG with and without CB | Latex mixing | [63] |
| SBR | CB, CNT, GE, graphite | Banbury mixer | [64] |
| SBR | Nano-kaolin and precipitated silica | Roll mill method | [65] |
| SBR | Spherical and rod-like silica nanoparticles | Two-roll mill method | [66] |
| SBR | Nano-$CaCO_3$ | Two-roll mill method | [67] |
| SBR | GE | Latex mixing | [68] |
| SBR | CB–organoclay | Two-roll mill method | [69] |
| SBR | NC/CB | Two-roll mill method | [70] |
| SBR | EG and MEG with and without CB | Melt blending | [71] |
| SBR | CB/NC | Two-roll mill method | [74] |
| SBR | Kaolinite/silica | Melt blending | [75] |
| SBR | CB–GE | Two-roll mixing | [76] |
| SBR | Halloysite–zinc phthalocyanine and halloysite – chloroaluminophthalocyanine | Rolling mill method | [78] |
| SBR latex | MMT | Coagulating rubber latex and clay aqueous suspension | [79] |
| SBR latex | Bentonite | Latex stage blending | [80] |
| SBR | MWCNT/CB | Solvent method | [83] |
| SBR | HNT | Direct blending | [84] |

(continued)

**Table 2.2** (continued)

| Rubber | Nanofiller(s) | Method of preparation of nanocomposite | Ref. |
|---|---|---|---|
| SBR | CNT/thermally-reduced GE | Two-roll mill method | [89] |
| SBR | CB (65phr) + NC (1–3 phr) | Internal mixer | [90] |
| SBR/BR | Nano-$TiO_2$ | Two-roll mill method | [93] |
| SBR | MWCNT | Solvent method | [95] |
| SBR | Kaolin, calcined kaolin | Not mentioned | [97] |
| SBR | Bentonite clay | Latex stage blending | [100] |
| SBR | ODA-modified and unmodified Na-MMT | Solvent method | [101] |
| SBR (15, 23 and 40% styrene content) | ODA-modified Na-MMT clay | Solvent method | [102] |
| SBR | Bare wollastonite and modified wollastonite nanorods | Two-roll mixing mill mixing | [105] |
| SBR | MMT | *In situ* living anionic polymerisation | [112] |
| SBR | CB, MWCNT or their mixtures | Solvent method | [113] |
| SBR | Nano-silica | Roll-mill mixing | [116] |
| SBR | Rectorite | Coagulating SBR latex and rectorite/ water suspension | [118] |
| SBR | FG | Latex blend technique | [119] |

CNF: Carbon nanofibres
DDA: *N,N*-dimethyldodecylamine
EG: Expanded graphite
FG: Functionalised graphene
MEG: Modified expanded graphite
TAG: Tannic acid functionalised graphene

**Table 2.3:** Details on filler types and methods of preparing NR/SBR blend nanocomposites.

| Rubber Blend | Nanofiller(s) | Method of preparation of rubber nanocomposite | Ref. |
|---|---|---|---|
| NR/SBR | Organoclay | Direct compounding | [15] |
| NR/BR and NR/NBR | SRSO-MK | Open two-roll mixing mill | [22] |
| NR/SBR | Silica hybrid filler included bagasse ash silica and precipitated silica | Two-roll mill | [35] |
| NR/SBR | Organoclay | Two-roll mill | [54] |
| SBR/NBR | CB/silica | – | [87] |

(continued)

**Table 2.3** (continued)

| Rubber Blend | Nanofiller(s) | Method of preparation of rubber nanocomposite | Ref. |
|---|---|---|---|
| PS/SBR | Partial replacement of silica by rice husk powder | Brabender® Plasti-Corder® | [88] |
| SBR/BR | CB–$SiO_2$ | Rubber mill | [91] |
| SBR/BR and NR/BR | NC/CB | Two-roll mill method | [92] |
| NR/SBR | Organically functionalised MWCNT | – | [94] |
| PS/SBR | RHP | Mixing method | [96] |
| NR/SBR | Modified Na-bentonite | Roll-mill mixing | [99] |

MK: modified kaolin
NBR: acrylonitrile-butadiene rubber
PS: Polystyrene
RHP: Rice husk powder
$SiO_2$: Silicon dioxide
SRSO: Sodium salt of rubber seed oil

## 2.2 Morphology and Dispersion of Fillers in Natural Rubber, Styrene-Butadiene Rubber and their Blend Nanocomposites

### 2.2.1 Morphology and Dispersion of Fillers in Natural Rubber Nanocomposites

Srivastava and others [11, 12] in early work, studied the morphology of dodecylamine-intercalated montmorillonite (12C-MMT)-filled NR hybrids. Figure 2.1 represents scanning electron microscopy (SEM) micrographs of the fracture surface of NR [12]. The aggregation of the Na-MMT filler in an NR matrix is also well visualised in Figure 2.1. In the case of NR/12C-MMT, the filler exhibited uniform dispersion of 12-MMT in the polymer matrix. Mathew and co-workers [13] studied the dispersion of layered silicates in an NR latex and the corresponding transmission electron microscopy (TEM), illustrated in Figures 2.2a and 2.2b, showed excellent dispersion of the layered silicates in the NR latex compared with conventional composites. Sookyung and co-workers [16] achieved a homogeneous dispersion of ODA-modified Na-MMT (5 phr ODA – MMT) devoid of any agglomeration of nano-silicate layers in an NR matrix, as evident in the SEM and TEM images.

TEM micrographs of NR/ODA-modified fluorohectorite demonstrated exfoliation of the filler in the NR matrix [17]. High-resolution transmission electron microscopy

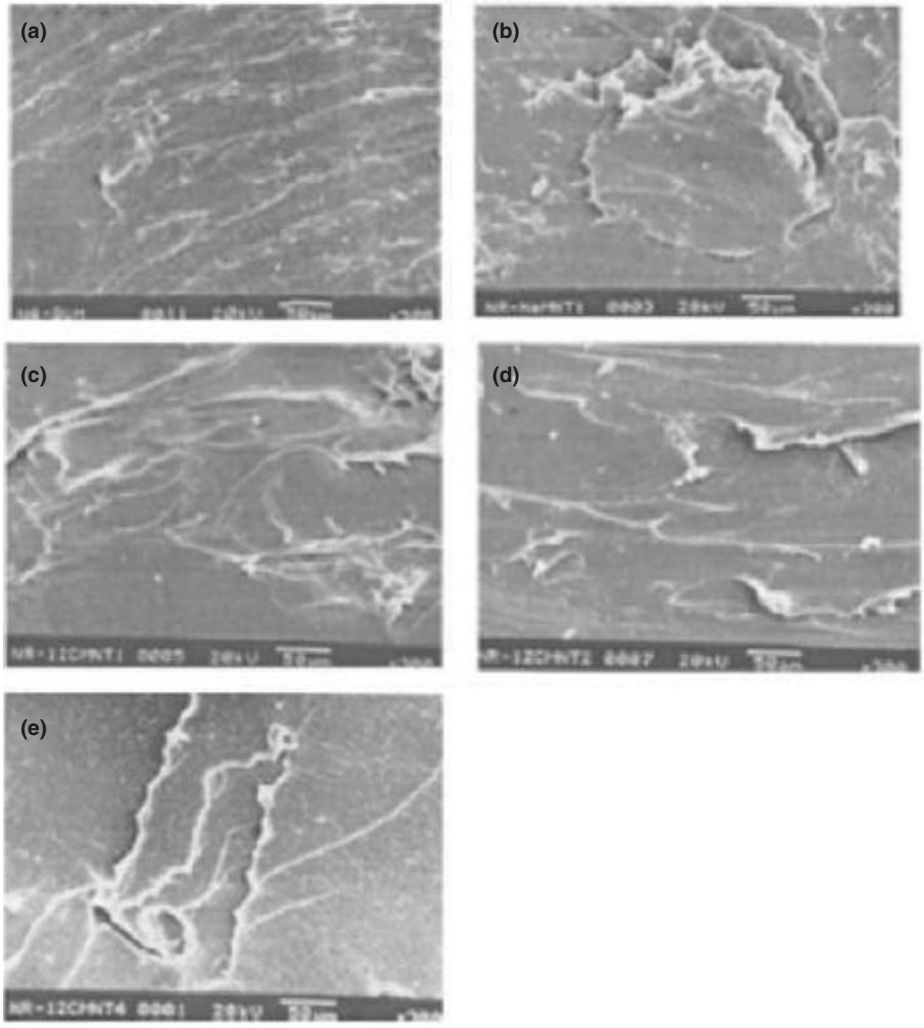


**Figure 2.1:** SEM micrographs of (a) virgin natural rubber (vNR); (b) NR–Na-MMT (1 wt%); (c) NR–12C-MMT (1 wt%); (d) NR–12C-MMT (2 wt%) and (e) NR–12C-MMT (4 wt%). Reproduced and adapted with permission from P. Bala, S.K. Srivastava, B.K. Samantaray and G.B. Nanda, *Journal of Applied Polymer Science*, 2004, **92**, 3583. ©2004, Wiley Periodicals, Inc. [12].

(HRTEM) images of the 1.5 phr filled nano-ZnO–GE NR nanocomposite clearly showed GE sheets existing as individual uniformly dispersed layers [20]. The TEM images indicate that the GE nanosheets are well exfoliated and homogeneously dispersed in the NR matrix [21]. The effects of substituting GO or rGO for CB on the performance of NR/CB composites has been studied using TEM [111]. Morphological observations revealed the dispersion of CB was improved by partially substituting nanosheets for CB.

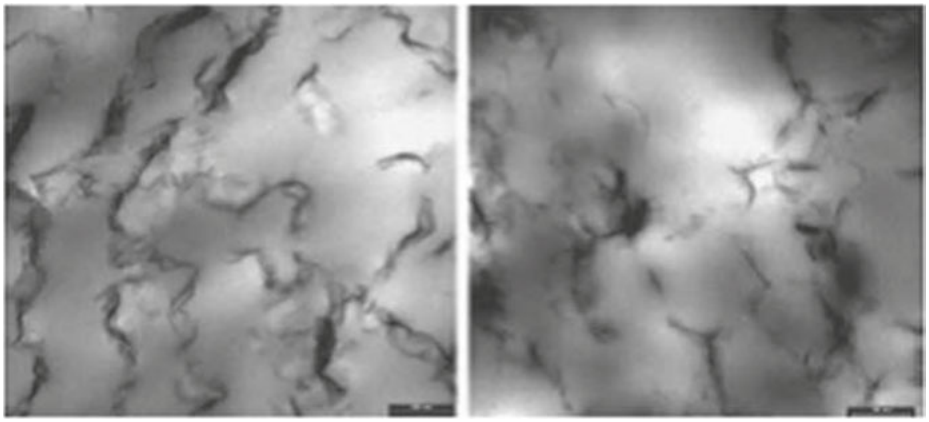


**Figure 2.2:** TEM pictures of (a) bentonite-filled NR and (b) fluorohectorite-filled NR composites. Reproduced with permission from S. Mathew, S. Varghese and R. Joseph, *Progress in Rubber, Plastics & Recycling Technology*, 2013, **29**, 1. ©2013, Smithers Rapra [13].

Li and co-workers [23] developed a modified latex-mixing method to disperse the GE/CNT hybrid in NR. They observed homogeneous dispersion of GE and CNT in the NR matrix in NR/GE (0.5 phr)/CNT (5 phr) and NR/GE (5 phr)/CNT (5 phr) through SEM and TEM, respectively. A kaolinite (10 phr)/CB (40 phr) hybrid filler produced a disorderly dispersion of kaolinite sheets covered by fine CB particles in the rubber matrix [26]. NR filled with 21 phr CB (N330) and 4 phr of Cloisite ® 15A showed well-dispersed CB aggregates with exfoliated clay layers (distributed in the unoccupied space of CB) [27]. Chen and co-workers [28] observed that SEM of the tensile fractured surface of NR/CG composites showed homogeneous dispersion of CG in NR. In the case of modified coal gangue (m-CG) (weight ratio of coupling agent: 2%, calcining temperature: 800 °C, calcining time: 1 h/CB hybrid filler in NR), the SEM image of the tensile fractured surface exhibited a blurry interface between the filler and rubber. Tensile fractured surfaces of rPET/HNT-filled NR composites observed through SEM revealed better adhesion and dispersion of HNT in the NR matrix at rPET:HNT ratios of 5:15 and 0:20 phr [29]. Waste tyre dust/CB [30] filler also exhibited improved filler dispersion in the NR matrix. SEM photomicrographs of fracture surface specimens of NR filled with silica/CB at ratios of 0/50, 10/40, 20/30, 30/20, 40/10 and 50/0 phr have been studied [31]. The samples containing 0, 10 and 40 phr of silica, compared with the sample containing 50 phr of silica, showed better filler dispersion. High-magnification tensile fractured SEM of NR/ silica/MWCNT hybrid nanocomposites of different silica/MWCNT (phr/phr) loading showed agglomerations of silica in the fractured surface at a 30/0 phr loading ratio [36]. In the case of silica/MWCNT (loading ratio: 29/1), a good dispersion of MWCNT and silica was evident in NR. The morphologies of the fracture surface of the NR and NR/PAT nanocomposites were examined

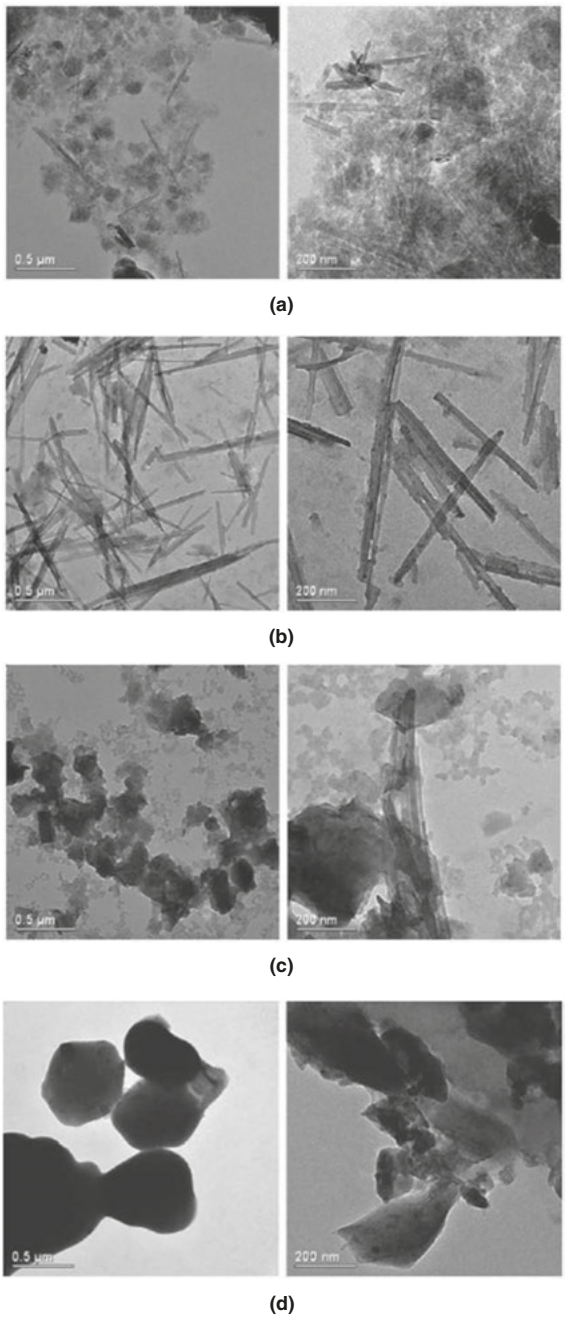


**Figure 2.3:** Fractographs of various nanocomposites with variations in the modified AT (a) NR; (b) NR/PAT-1%; (c) NR/PAT-450–1% and (d) NR/PAT- 850–1%. Reproduced with permission from J. Wang and D. Chen, *Journal of Nanomaterials*, 2013, Article ID:496,584. ©2013, Hindwai [42].

by SEM, as shown in Figure 2.3 [42]. These investigations suggested a smooth fractured section of pristine NR. In contrast, the fracture surface of an NR/1% PAT nanocomposite showed attapulgite (AT) fibres uniformly dispersed in NR. An X-ray diffraction (XRD) and SEM study indicated that a homogeneous dispersion state of GON in NR [44]. Abdullateef and co-workers [45] observed an improvement in dispersion acid-modified CNT in the NR matrix. NR/ cellulose nanocrystal (CNC) nanocomposites show a non-uniform dispersion with a lower CNC-rich layer and upper NR-rich layer structure [46]. Sui and co-workers [48] found that pretreated CNT showed good dispersion in the NR matrix.

### 2.2.2 Morphology and Dispersion of Fillers in Styrene-Butadiene Rubber Nanocomposites

Figure 2.4 shows SEM micrographs of the fracture surface of virgin styrene-butadiene rubber (vSBR) with Na-MMT, and 12C-MMT-filled NR nanocomposites [12]. It can be seen that aggregation of Na-MMT, used as the filler in the SBR matrix, is well visualised. It can also be observed that SBR shows behaviour very similar to that observed in NR/12C-MMT hybrids. However, the dispersion of 12C-MMT particles does not reach the same extent as that of NR, which may be due to intercalated MMT containing a dodecyl long aliphatic chain not being compatible with SBR.

As a result, the interaction of SBR does not occur to the same extent as NR, which causes poorer dispersion of 12C-MMT in SBR compared with NR. The TEM images of SBR nanocomposites show greatly improved dispersion of HNT in the presence of TAG [38]. In addition, TAG sheets were found to be uniformly dispersed around HNT to form a cosupporting and continuous hybrid network where the HNT are separated by the silk-like TAG. Srivastava and co-workers [51] prepared nanocomposites of SBR using 3 wt% of hectorite modified by octadecylamine (O-Hc), hectorite grafted by a silane coupling agent (S-Hc) and modified by both O-Hc and S-Hc (OS-Hc). XRD patterns of pristine and these modified Hc clay are displayed in Figure 2.5.

The diffraction peak (001) at $2\theta = 7.26$ corresponds to a 1.22 nm basal spacing of pristine Hc clay. The (001) diffraction peaks in O-Hc-, S-Hc- and Os-Hc-modified Hc correspond to 3.35, 1.79 and 3.08 nm basal spacing, respectively. The noted lowest basal spacing in S-Hc could be attributed to the smaller chain length of silane molecules.

Figure 2.6 displays the TEM micrographs of SBR/O-Hc and SBR/OS-Hc-modified nanocomposites with 3 wt% filler loading. It shows the presence of individual layers and stacking silicate layers with a thickness of about 5–20 nm and dispersion of filler reinforcement materials in the SBR matrix.

Das and co-workers [53] noted a good dispersion level of organoclay in the solution styrene-butadiene rubber (S-SBR) matrix by using carboxylated nitrile rubber (XNBR) as a vector to transfer silicate layers into the base polymer matrix. The dispersion of Na-MMT and DDA-modified MMT in the SBR/clay nanocomposites

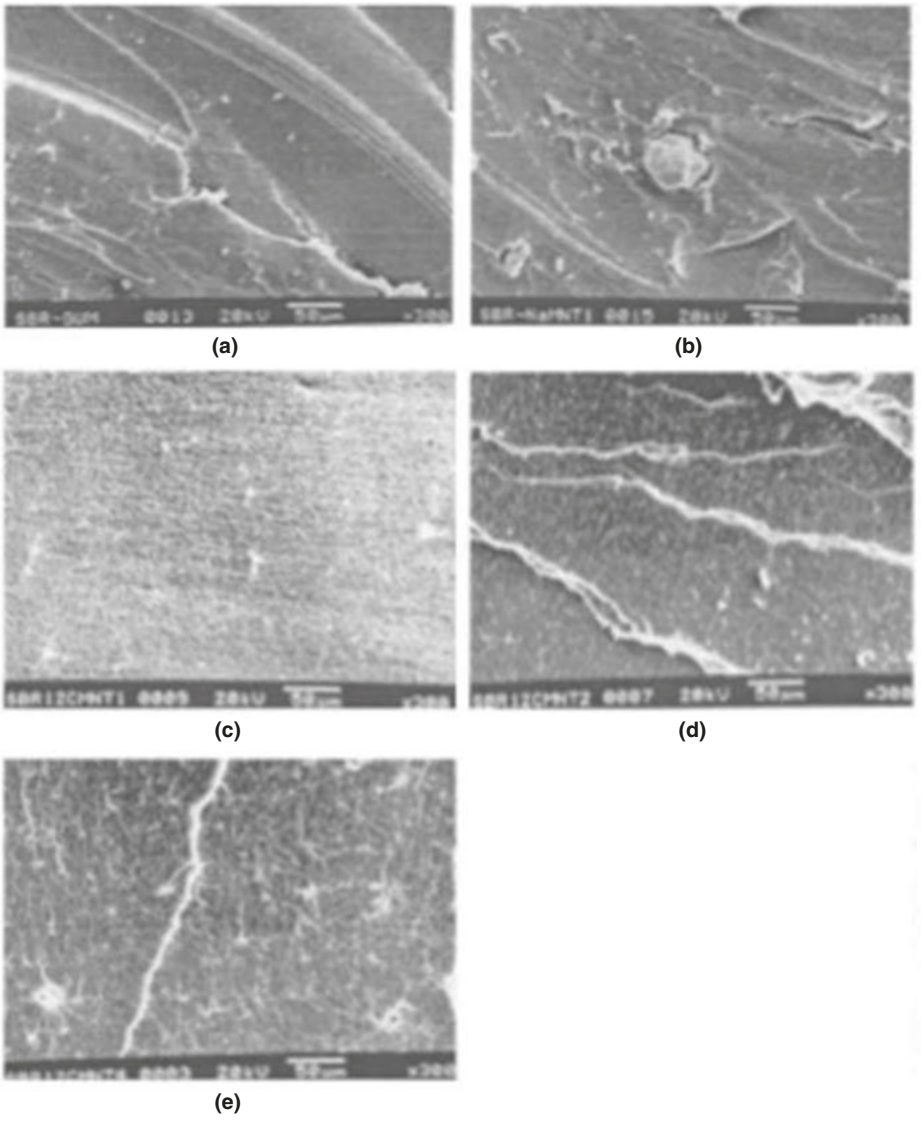


**Figure 2.4:** SEM micrographs (a) vSBR; (b) SBR–Na-MMT (1 wt%); (c) SBR–12C-MMT (1 wt%); (d) SBR–12C-MMT (2 wt%) and (e) SBR–12C-MMT (4 wt%). Reproduced and adapted with permission from P. Bala, S.K. Srivastava, B.K. Samantaray and G.B. Nanda, *Journal of Applied Polymer Science*, 2004, **92**, 3583. ©2004, Wiley Periodicals, Inc. [12].

has also been studied [55]. XRD/TEM images indicated the formation of an exfoliated morphology with a certain degree of intercalation of the filler in the prepared SBR composite. The results also showed that the loading clay distribution in the SBR matrix is poor at higher than 6 phr loading [56]. Scanning tunnelling electron

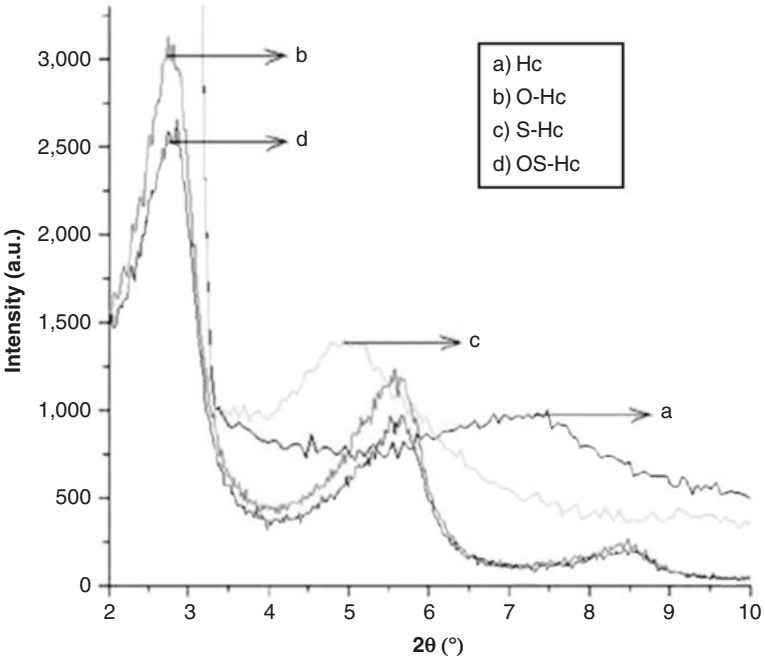


**Figure 2.5:** XRD of Hc. Reproduced with permission from P. Bharadwaj, P. Singh, K.N. Pandey, V. Verma and S.K. Srivastava, *Applied Polymer Composites*, 2013, 1, 207. ©2013, Smithers Rapra [51].

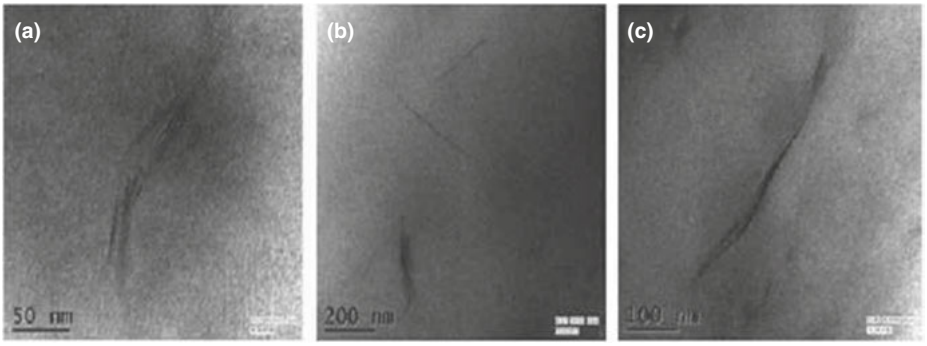


**Figure 2.6:** TEM micrograph of SBR/NC nanocomposites. (a) SBR/O-Hc nanocomposite; (b) SBR/OS-Hc nanocomposite and (c) SBR/S-Hc nanocomposite. Reproduced with permission from P. Bharadwaj, P. Singh, K.N. Pandey, V. Verma and S.K. Srivastava, *Applied Polymer Composites*, 2013, **1**, 207. ©2013, Smithers Rapra [51].

microscopy images of surface-modified MWCNT–SBR masterbatches revealed the presence of uniformly, well-dispersed MWCNT even at 15 wt% loading [62]. Malas and co-workers [63] reported HRTEM images of EG- and MEG-filled SBR composites in the presence and absence of CB. They noted that the uniform dispersion of MEG

nanosheets in the carboxylated styrene-butadiene rubber (XSBR) matrix. Further, EG/MEG flakes were found to be intercalated and delaminated in the SBR matrix in the presence and absence of CB. Atomic force microscopy pictures of NBR and SBR vulcanisates containing halloysite–zinc phthalocyanine or Hc hybrid fillers are characterised by a better dispersion of components [78]. Xing and co-workers [68] demonstrated the homogeneous dispersion of single GE layers in the SBR matrix, and calcium stearate was reported to be an excellent dispersion promoter for organoclay in SBR [69]. TEM of SBR/50 phr MK showed a fine dispersion of MK in the SBR matrix [75]. However, kaolinite sheets were covered by fine silica particles in MK hybridised with precipitated silica [75]. TEM indicated the homogeneous dispersion of GE sheets in the SBR matrix which was produced by the mechanical mixing method based on the application of CB–reduced graphene (RG) hybrid fillers in the SBR matrix [76]. TEM analysis demonstrated the partial exfoliation and/or intercalation in SBR/bentonite clay composites [80]. A significantly improved dispersion of HNT in SBR was achieved due to the interfacial hydrogen bonding between HNT and sorbic acids (SA) [84]. Abraham and others [89] studied the fractured surface morphology of SBR vulcanisates filled with a CNT-thermally-reduced GE hybrid. They observed that increasing thermally-reduced GE (>0.25 phr) decreased the rubber–filler interaction and led to poor filler dispersion. Schopp and co-workers [119] achieved emulsifier-free aqueous dispersions of FG, which exhibited predominantly uniform dispersion of single FG sheets in SBR.

### 2.2.3 Morphology and Dispersion of Fillers in NR/SBR, SBR/rNBR and PS/NBR Blend Nanocomposites

The XRD pattern confirmed the formation of exfoliated or well-intercalated nanocomposites at a lower clay content (1 and 2 wt%) and intercalated nanocomposites at a higher clay content (3 wt%) [15]. TEM of NR/SBR/NC (1 and 2 wt%) showed nanolayers of clay platelets were dispersed randomly in the matrix, which is in agreement with XRD data. At a higher clay loading (3 wt%), nanolayers of clays were arranged in parallel and formed an intercalated structure in the NR/ SBR blend. SEM micrographs of NR/NBR vulcanisates containing unmodified kaolin and SRSO–MK, respectively, showed a uniform and fine dispersion of particles of SRSO–MK in both NR/BR and NR/NBR blend rubber vulcanisates [22]. Noriman and Ismil [87] evaluated the morphological behaviour of hybrid filled, selected SBR/ recycled acrylonitrile-butadiene rubber (rNBR) blends at a fixed 85/15 blend ratio. The corresponding SEM of the tensile fracture surfaces indicated that the addition of Si 69® improved the dispersion of hybrid fillers and rNBR in the SBR/ rNBR matrix. SEM analysis on partially replaced silica by RHP in PS–SBR has also been investigated [88]. It showed that increasing the silica loading in the hybrid filler caused smaller agglomerate sizes and better distribution in the composite.

The morphological study of NR/SBR/modified Na-bentonite showed the intercalation of the NC NR/SBR blend chain [99].

## 2.3 Mechanical Properties of Natural Rubber, Styrene-Butadiene Rubber and their Blend Nanocomposites

### 2.3.1 Mechanical Properties of Natural Rubber Nanocomposites

The variation of tensile strength (TS) of NR upon altering the concentration of dodecyl alkyl ammonium filler is shown in Figures 2.7–2.9 [12]. It can be observed that the TS of the NR with 1 wt% 12C-MMT filler is almost the same as that of vulcanised NR without any filler. The TS of NR with 1 wt% of Na-MMT filler decreased to approximately 30% that of NR. It should also be noted that the TS of NR increased upon increasing the 12C-MMT filler content and reached a maximum at 4 wt%. The elongation at break (EB) of the NR with 1 wt% 12C-MMT indicated a lower value compared with vNR. It is also noteworthy that moduli for 1 wt% 12C-MMT content exhibited nearly the same value as that of NR without any filler, but these moduli increased with an increase of 12C-MMT filler content and become almost constant after 2 wt%. This study also showed that the modulus at elongation at 100% for 1 wt% of Na-MMT content is nearly the same as that of vNR and that of 1 wt% of 12C-MMT, but for 200%, it is smaller than the respective value of the 12C-MMT filler.

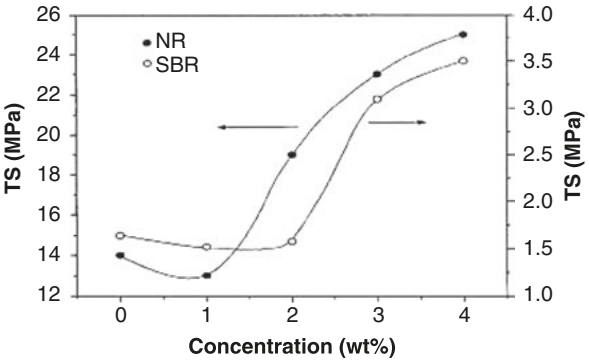


**Figure 2.7:** Variations of TS as a function of 12C-MMT filler concentration in NR and SBR. Reproduced with permission from P. Bala, S.K. Srivastava, B.K. Samantaray and G.B. Nanda, *Journal of Applied Polymer Science*, 2004, **92**, 3583. ©2004, Wiley Periodicals, Inc. [12].

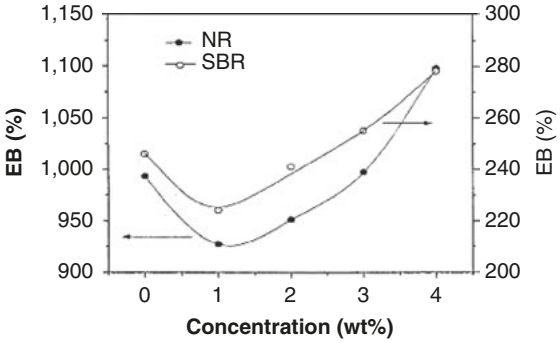


**Figure 2.8:** Variations of EB as a function of 12C-MMT filler concentration in NR and SBR. Reproduced with permission from P. Bala, S.K. Srivastava, B.K. Samantaray and G.B. Nanda, *Journal of Applied Polymer Science*, 2004, **92**, 3583. ©2004, Wiley Periodicals, Inc. [12].

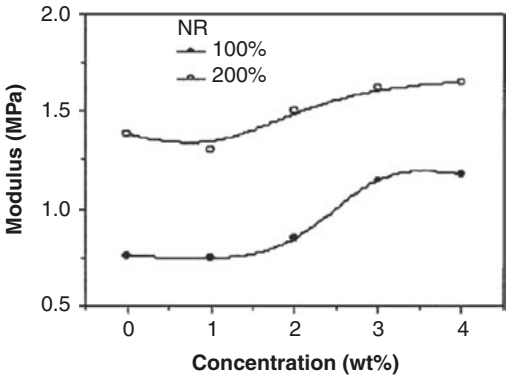


**Figure 2.9:** Variations of modulus of NR as a function of 12C-MMT filler concentration. Reproduced with permission from P. Bala, S.K. Srivastava, B.K. Samantaray and G.B. Nanda, *Journal of Applied Polymer Science*, 2004, **92**, 3583. ©2004, Wiley Periodicals, Inc. [12].

Mathew and co-workers [13] investigated the effect of thermal ageing on the mechanical properties of NR layered silicates. Figure 2.10 shows the percentage retention of TS after thermal ageing at 100 °C for 24 and 48 h. After 48 h, though the retention values of the composites decreased to more than 50% of the original, fluorohectorite and bentonite showed comparatively better retention values. This might be due to the protection of the polymer chains by the surrounding silicate platelets. The percentage retention of EB at 100 °C for two different intervals is given in Figure 2.11. At 24 h, the elongation values are mostly unaffected. Upon prolonged ageing (48 h), the percentage retention in EB follows the order: fluorohectorite > bentonite > English Indian clay. Even though the layers are 'inorganic' in nature, because of their very large aspect ratio and nanometre thickness, they behave mechanically more like thin sheets rather than thick rigid plates. This flexibility (elastic nature) of the silicate layers contributes to the elasticity of the rubber. It has been reported that intercalated and exfoliated clay

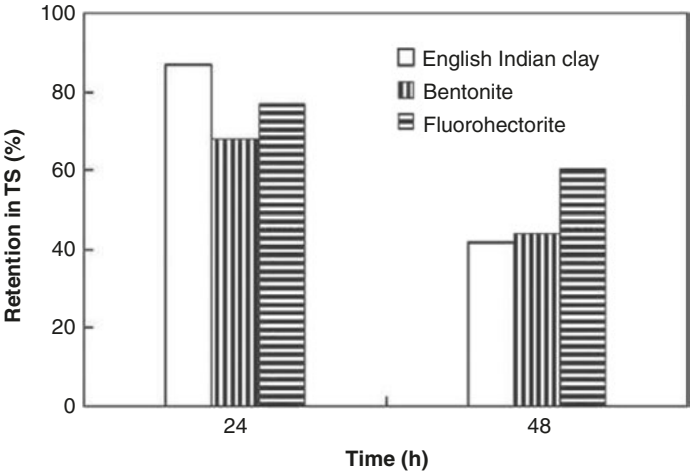


**Figure 2.10:** Percentage retention of TS on thermal ageing. Reproduced with permission from S. Mathew, S. Varghese and R. Joseph, *Progress in Rubber, Plastics & Recycling Technology*, 2013, **29**, 1. ©2013, Smithers Rapra [13].

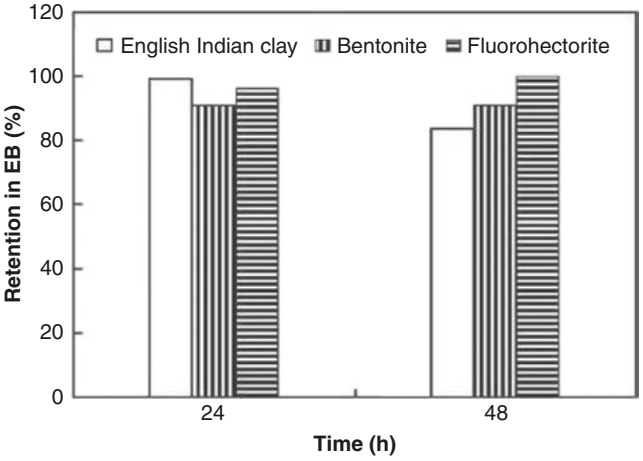


**Figure 2.11:** Percentage retention of EB on thermal ageing. Reproduced with permission from S. Mathew, S. Varghese and R. Joseph, *Progress in Rubber, Plastics & Recycling Technology*, 2013, **29**, 1. ©2013, Smithers Rapra [13].

layers in rubber orient along the strain direction during stretching. After 24 h of thermal ageing, a significant reduction in TS was noted for the English Indian clay-loaded composites, whereas the reduction was comparatively less in the nanocomposites. The better retention of physical properties by the nanocomposites during thermal ageing was attributed to the evenly distributed network of silicate layers.

NR/ODA-modified fluorohectorite exhibited a higher modulus, and lower TS and strain at break than pure NR [17]. The mechanical properties of the NR/ nano-ZnO–GE nanocomposite were significantly improved compared with NR/ conventional ZnO [20]. The addition of 1.5 phr of nano-ZnO–GE in NR enhanced the TS (12.7%), modulus at 300% strain (3.8%) and tear strength (32.3%). This is attributed to improved dispersion of GE sheets in the NR matrix which in turn increased the contact between the nano-ZnO and rubber additives. NR/NC and NR/ CNF nanocomposites were consolidated with CB to fabricate ternary nanocomposites [81]. These nanocomposites exhibited enhanced mechanical properties compared with those of either NR/clay, NR/ CNF or the NR/black control microcomposites. These nanocomposites exhibited an increment of 18% in tear strength and 40% in modulus at 300% elongation over the control microcomposite. The unique ternary architectural base, with the space between the clay/fibre occupied by small CB aggregates forming networks or '*nano-channels*', accounted for the synergistic improvements.

The mechanical properties of NR and its nanocomposites filled with GE/CNT hybrid fillers has also been investigated [23]. The findings demonstrated that hybridisation of CNT with GE resulted in pronounced reinforcement of the nanocomposites due to the synergistic effect. rPET was partially replaced with HNT as fillers in NR composites [29] and, due to the reinforcing effect and ductility of the HNT, the moduli, TS, EB and fatigue life were found to increase proportionally with increasing HNT content. Liu and co-workers [27] observed that the combination of 41 phr CB (N330 + 4 phr Cloisite® 15A) hybrid-filled NR show improved TS, EB, modulus (100, 200%), tear strength, elongation and modulus tear strength compared with neat NR gum or other NR composites. Both the modulus and TS of NR/CB/OMMT and NR/CB/organo-modified Laponite® RD (LRD) clay were shown to be considerably higher than their microcomposite counterparts [39]. However, without CB, the organoclay-reinforced NR vulcanisates exhibited only improved strength, with limited enhancement in modulus.

Liu and co-workers [32] noted a more significant reinforcing effect of an organoclay/ CB hybrid filler in NR with regards to mechanical testing. Modified-fumed silica was found to exhibit a greater reinforcement effect on the NR vulcanisate than the common fumed silica, which was evident from the mechanical properties [41]. The effect of adding MWCNT on the mechanical properties of the NR nanocomposite has also been studied [43]. It was noted that the TS of the rubber nanocomposites was augmented by up to 70% and EB improved up to 130% containing the maximum amount (1 wt%) of the MWCNT in NR. This was attributed to the uniform dispersion, large surface area, nanolevel interaction with the polymeric molecular chains and the filler–matrix compatibility of the MWCNT. The variation of TS (and EB) showed an increasing trend with silica/MWCNT loadings up to 29/1 phr/phr in NR [36]. This is possibly due to the larger surface area, together with the aspect ratio of MWCNT, compared with silica. The TS and EB of NR/PAT nanocomposites increased upon increasing the filler loading up to 1 phr [42]. It is suggested that PAT can be easily dispersed in the NR at this lower loading; however, the mechanical properties

marginally fell as the PAT loading increased to 10 phr. The mechanical properties of the GON-reinforced NR showed a considerable increase compared with neat NR [44]. The initial modulus of pure NR increased up to 53.6% in the NR/GON (7 wt%) nanocomposite. Furthermore, they noted that the modulus and strength of NR containing GON appeared to be superior to those of CB with the same filler content.

The thermal and mechanical properties of NR reinforced with CNC in NR increased the TS and modulus but marginally decreased EB [46]. Bendahou [47] examined the reinforcing effect of cellulose whiskers and microfibrillated cellulose in NR latex. It was seen that NR/microfibrillated cellulose nanocomposites exhibited a superior reinforcing effect compared with NR/cellulose whiskers due to the higher aspect ratio and possibility of entanglement of microfibrillated cellulose. Young's modulus, strain at break and strength of the CNT-reinforced NR showed a considerable increase compared with the neat NR and traditional CB/NR composites [48]. Organoclay-filled NR nanocomposites, prepared by grafting the intercalating method in latex, demonstrated remarkably improved mechanical properties compared with NR [49]. NR/organic vermiculite nanocomposites showed an improvement in mechanical strength, hardness and modulus [50]. The substitution of a small amount of GO or rGO nanosheets in place of CB in the NR/CB composite resulted in improvements in modulus and TS [110]. The mechanical properties of a hybrid consisting of thermally-reduced GO and ionic liquid [1-ethyl-2,3-dimethylimidazolium *bis*(trifluoromethylsulfonyl)imide]-modified CNT (5 wt%)-filled NR nanocomposites revealed a high TS, high modulus and low EB compared with neat NR, NR reinforced with graphite (5 wt %) and NR reinforced with rGO (5 wt%) systems owing to the synergistic hybrid effect [117].

### 2.3.2 Mechanical Properties of Styrene-Butadiene Rubber Nanocomposites

The mechanical properties of SBR-filled Na-MMT and 12C-MMT have been investigated [12]. It can be observed from Figure 2.7 that the TS of SBR with 1 wt% 12C-MMT filler is almost the same as that of vulcanised SBR without any filler, whereas a decrease in TS can be observed in the SBR/Na-MMT composite; however, it increases upon the further addition of 12C-MMT filler in SBR and reached a maximum value at 4 wt%. The variation of EB with 12C-MMT content in SBR was almost the same as in NR (Figure 2.8). In the case of SBR with 1 wt% of Na-MMT filler, the fall is not so drastic. The variation of modulus of SBR at an elongation of 100 and 200% is highlighted in Figure 2.12, and shows that the moduli for SBR with 1 wt% 12C-MMT filler are almost the same as that of SBR without any filler. It can also be observed that these moduli increase with an increasing concentration of 12C-MMT filler and reach maxima at 2 wt% of 12C-MMT filler; beyond this, it remains almost

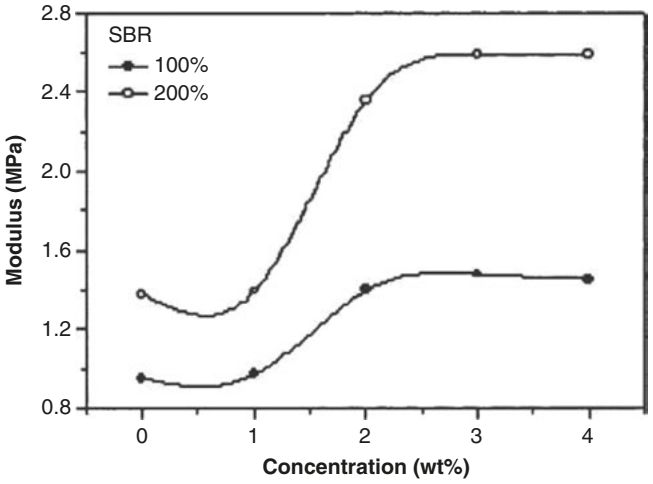


**Figure 2.12:** Variations of modulus of SBR as a function of 12C-MMT filler concentration. Reproduced with permission from P. Bala, S.K. Srivastava, B.K. Samantaray and G.B. Nanda, *Journal of Applied Polymer Science*, 2004, **92**, 3583. ©2004, Wiley Periodicals, Inc. [12].

unchanged. It is interesting to note that SBR with 1 wt% of Na-MMT filler shows a lower value compared with SBR without any filler.

The mechanical properties of nanocomposites of SBR have been studied by Bharadwaj and co-workers [51]. Figures 2.13–2.15 show the increases in mechanical strength of organo-modified O-Hc, S-Hc and OS-Hc-filled SBR nanocomposites compared with neat SBR. The observed increase in TS is probably due to the intercalation of silicate layers into the SBR matrix that reduce the slippage of polymer chains over the silicate layers. Table 2.4 details TS and EB data of SBR filled with O-Hc, S-Hc and OS-Hc. The order of improvement in TS and EB in all of these SBR nanocomposites are SBR < SBR/S-Hc (5 wt%) < SBR/OS-Hc (7 wt%) < SBR/O-Hc (3 wt%) and SBR < SBR/OS-Hc (6 wt%) < SBR/S-Hc (1 wt%) < SBR/ OHc (3 wt%), respectively.

Attharangsan and co-workers [35] reported that the TS and modulus at 100 and 300% elongation increases, whereas the EB decreases with increasing CB content in CB/RHP-hybrid-filled NR composites [35]. It is suggested that an increase in CB provides a better rubber–filler interaction and higher crosslink density, as supported by swelling studies. The improvement in the modulus and strength of the composites in a three-dimensional network consisting of HNT and TAG in the hybrid filler-reinforced SBR is attributed to synergistic effects [38].

Stress–strain plots indicated that the mechanical properties of the S-SBR + XNBR (9.4 phr) + organoclay (5.6 phr) nanocomposites are enhanced at higher elongations due to the presence of a small amount of organoclay in the rubber matrix [53]. In contrast, an equivalent amount of XNBR without any filler negatively impacted the corresponding mechanical properties of the composites. It is suggested that organo-

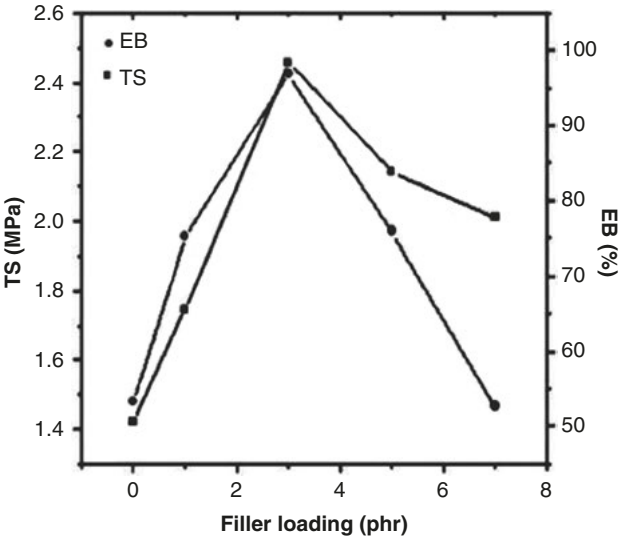


**Figure 2.13:** TS and EB for the O-Hc-modified nanocomposite at different filler loadings. Reproduced with permission from P. Bharadwaj, P. Singh, K.N. Pandey, V. Verma and S.K. Srivastava, *Applied Polymer Composites*, 2013, **1**, 207. ©2013, Smithers Rapra [51].

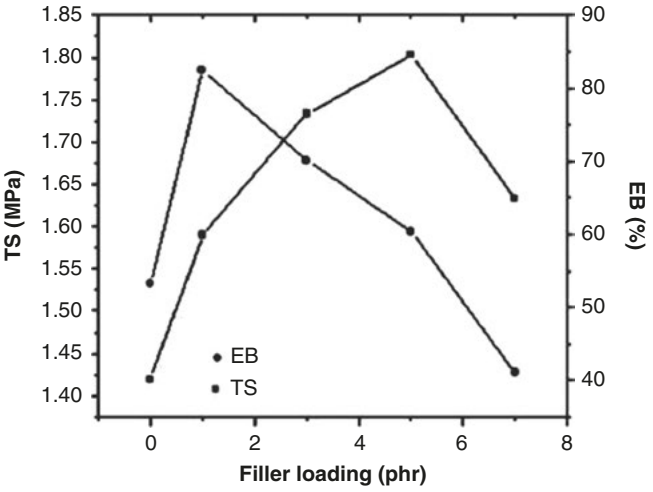


**Figure 2.14:** TS and EB for the S-Hc-modified nanocomposite at different filler loadings. Reproduced with permission from P. Bharadwaj, P. Singh, K.N. Pandey, V. Verma and S.K. Srivastava, *Applied Polymer Composites*, 2013, **1**, 207. ©2013, Smithers Rapra [51].

modified NC impart excellent reinforcement effects on the rubber matrix and also act as a compatibiliser. Kim and co-workers [55] studied the mechanical properties of DDA (tertiary amine)-modified MMT-reinforced SBR. They noted maximum values of

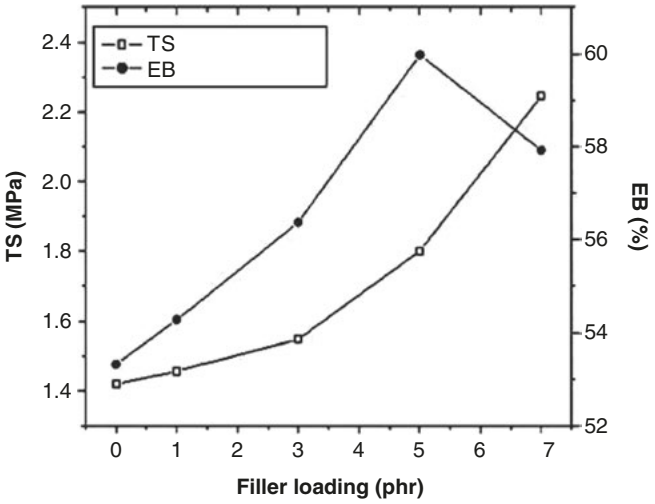


**Figure 2.15:** TS and EB for the OS-Hc-modified nanocomposite at different filler loadings. Reproduced with permission from P. Bharadwaj, P. Singh, K.N. Pandey, V. Verma and S.K. Srivastava, *Applied Polymer Composites*, 2013, **1**, 207. ©2013, Smithers Rapra [51].

**Table 2.4:** TS and EB of SBR/O-Hc, S-Hc and OS-Hc nanocomposites.

| Filler (phr) | TS (MPa) | | | EB (%) | | |
|---|---|---|---|---|---|---|
| | O-Hc | S-Hc | OS-Hc | O-Hc | S-Hc | OS-Hc |
| 0 | 1.42 | 1.42 | 1.42 | 53.32 | 53.32 | 53.3 |
| 1 | 1.744 | 1.59 | 1.456 | 75.20 | 82.5 | 54.28 |
| 3 | 2.456 | 1.733 | 1.548 | 96.9 | 70.1 | 56.37 |
| 5 | 2.141 | 1.803 | 1.802 | 75.93 | 60.33 | 59.98 |
| 7 | 2.011 | 1.633 | 2.245 | 52.66 | 41.01 | 57.98 |

Reproduced and adapted with permission from P. Bharadwaj, P. Singh, K.N. Pandey, V. Verma and S.K. Srivastava, *Applied Polymer Composites,* 2013, 1, 207. ©2013, Smithers Rapra [51]

TS at 2.5 g of DDA due to the increased dispersion of the silicate layers in the rubber matrix and the increased crosslinking of the SBR nanocomposites by DDA itself.

A higher degree of reinforcement of SBR upon the addition of NC was reflected in the static tensile properties [57]. The addition of CB on the optimised SBR–clay nanocomposite resulted in a tremendous improvement in the mechanical properties of the SBR–clay nanocomposite. Diez and co-workers [56] observed an increment of 265% in TS at 15 phr loading, which was attributed to the uniform dispersion of the nano-silicate layers in the rubber matrix. The EB of neat SBR (292%) increased to 437% at 15 phr loading. Xing and co-workers [68] achieved a remarkable

reinforcement effect at a GE filler loading of 0.3 phr in SBR, which was evident from the improvement of 260% in TS and 140% in EB. Such an improvement in the TS of SBR could be attributed to the strong rubber–GE interaction due to the better dispersion of GE layers in the rubber matrix. According to Zhang and co-workers [76], the TS and EB of SBR/CB–RG composites improved significantly compared with the SBR/CB blends [76]. Bhowmick and co-workers [79] prepared styrene-butadiene nanocomposites filled with a number of modified and unmodified inorganic fillers. Comparison of the mechanical properties of the nanocomposites against the gum illustrates that Cloisite® 15A, at 8 phr loading, produced an increment of 230% in the TS. At 6 phr loading, CNF increased the modulus by 101%, while tear strength increased by 79%. Upon modification, Cloisite® 15A resulted in a 146% increase in modulus and 303% in TS, while CNF led to a 150% increment in modulus and 113% in TS of the nanocomposite, over the gum control.

The tensile properties of SBR/CB/RG composites improved significantly and the volume resistivity decreased compared with the SBR/CB blends [76]. The mechanical properties of nanocomposites prepared with different grades of nitrile rubber with SBR, and with BR modified with stearyl amine showed improvement with the degree of filler loading up to a certain level due changes in the nature and polarity of the rubbers [103]. SA-modified SBR/HNT nanocomposites exhibited promising mechanical properties and correlated with the interactions between HNT and SA and the greatly improved dispersion of HNT [84]. Al-Yamanil and Goettler [85] also studied the mechanical properties of organo-modified layered silicates/SBR. Noriman and Ismail [87] examined the mechanical properties of SBR/recycled NBR blends reinforced with 50/0, 40/10, 30/20, 20/30, 40/10 and 0/50 phr of a CB/silica hybrid filler treated with and without a silane coupling agent (Si 69®). It was noticed that the incorporation of the silane coupling agent (Si 69®) enhanced the TS, EB, stress at 100% elongation (M100) and stress at 300% elongation (M300) of CB/silica hybrid filler-filled SBR/NBR bleds. The CB N330 (20 parts)-filled SBR-based nanocomposite registered a 20% higher TS with 4 parts of the modified NC. In addition, 4 phr of the ODA-modified NC also significantly improved the TS of SBR vulcanisates [104].

Tensile stress–strain measurements were made on nanocomposites of SBR containing various loadings of MWCNT [114]. The EB remained at the level of SBR (~460%) until about 7.5 wt% MWCNT, and subsequently decreased, while the stress at break increased by 210% up to 7.5 wt% MWCNT. The TS of SBR/ODA-modified fluorohectorite nanocomposites with a loading of 10 phr ODA-modified fluorohectorite was found to be about 4–5 times higher than the pure rubber vulcanisate [17], which was attributed to the slippage of the rubber molecules and the orientation of the intercalated ODA-modified fluorohectorite. Ahmed and co-workers [116] studied the TS and elongation properties of SBR/nano-silica and the findings are displayed in Figures 2.16 and 2.17, respectively. It should be noted that the addition of a small quantity of nano-silica increased the TS, which was followed by a decrease at higher loadings. It is thought that, in small quantities, the particles fill the spaces

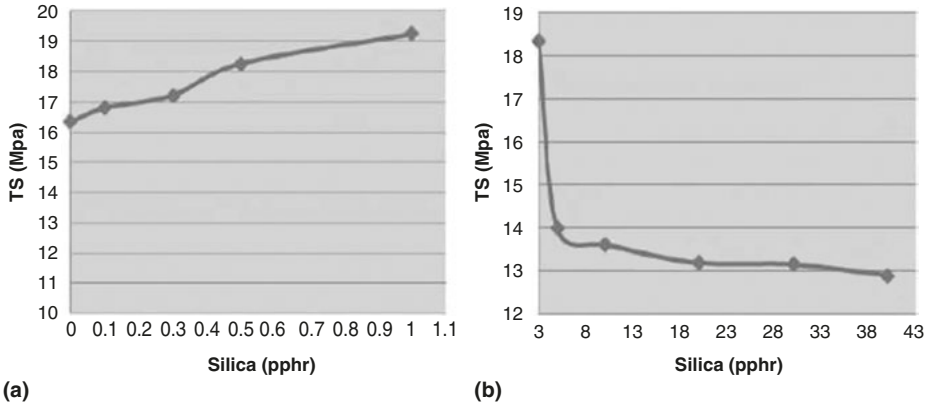


**Figure 2.16:** Effect of small and large quantities of nano-silica on the TS of the formulation. Reproduced with permission from J.K. Ahmed, M.H. Al-Maamori and H. Mohammed Ali, *International Journal of International Materials Science and Applications*, 2015, **4**, 15. ©2015, Science Publishing Group [116].

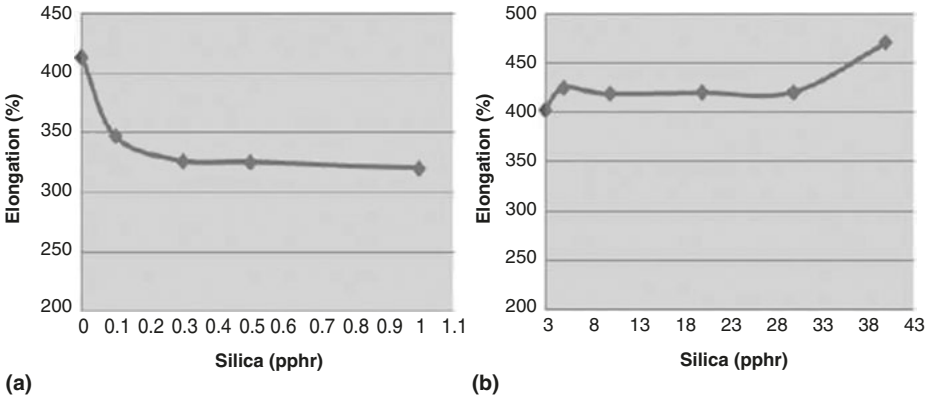


**Figure 2.17:** Effect of small and large quantities of nano-silica on the elongation of the formulation. Reproduced with permission from J.K. Ahmed, M.H. Al-Maamori and H. Mohammed Ali, *International Journal of International Materials Science and Applications*, 2015, **4**, 15. ©2015, Science Publishing Group [116].

between the rubber chains and give a rigid structure with better TS; however, at a higher loading of nano-silica, the TS decreases due to its aggregation. The elongation of SBR decreases upon the addition of small quantities of nano-silica due to the restricted mobility of chains, however, it increases at a higher loading of nano-silica in SBR. Their study also showed that the modulus and tear resistance increase with small amounts of the nano-silica in SBR.

The nanocomposite containing 20 phr of organo-modified NC in SBR gum showed a TS of 9.5 MPa and EB of 821% compared with neat SBR with values of 1.8 MPa and 219%, respectively [106]. Interestingly, the addition of NC resulted in a steady increase in per cent EB. The SBR nanocomposite loaded with 20 phr NC displayed a higher strength (8.6 MPa) and EB (261%) compared with the control SBR sample containing 20 phr CB. However, the SBR sample containing 20 phr CB exhibited a higher stress at 100% elongation compared with the SBR sample containing 20 phr NC. The highly effective FG dispersion in SBR produced an improvement in EB, TS and stress at 50 and 300% strain [119]. The mechanical performance of the rubber/silica composites was found to be significantly improved upon the addition of SA [121].

### 2.3.3 Mechanical Properties of Natural Rubber and Styrene-Butadiene Rubber Blend Nanocomposites

Mohan and co-workers [15] prepared NR/SBR NC (1, 2 and 3 wt%) blend nanocomposites and studied the mechanical properties. The TS of NC-filled NR/SBR showed no improvement. The EB values also continuously decreased as the clay concentration in the rubber increased. The modulus at 100% elongation continuously increased with increasing clay content and a rise of 70% was observed at 3 wt% NC in NR/SBR. Raji and co-workers [22] observed improvements in mechanical properties for blends of NR with SBR and NBR containing SRSO–MK in comparison to the blends containing unmodified kaolin. They noted that the TS, EB and tensile modulus of the NR/BR (and NR/NBR) blend with 4 phr of SRSO–MK, compared with blends/unmodified kaolin, were enhanced by 30.8 (53.5%), 3.6% (9.1%) and 5.6 (5%), respectively. The TS, tensile modulus and tear strength improved significantly for organoclay (<5.0 phr) in NR/SBR [54]. The TS and the tear strength of the nanocomposite with only 3.0 phr organoclay improved by ~93 and ~63%, respectively. It was also noted that the modulus (200%) of NR/SBR/organoclay increased compared with the neat blend, which was attributed to the reinforcing effect of the exfoliated organoclay and a high degree of organoclay dispersion in the rubber matrix. The TS, elongation and traction properties were improved with a low coupling agent Si 69® content in the SBR/BR blend of NC/silica [74]. Noriman and Ismail [87] observed that the incorporation of Si 69® improved the TS, EB, stress at 100% elongation (M100) and stress at 300% elongation (M300) of CB/silica hybrid filler-filled SBR/NBR blends. These properties were found to be influenced by the degree of crosslinked density, which increased with increasing silica content.

SBR/BR-based rubber nanocomposites filled with CB (65 phr) and MMT, treated with an alkyl ammonium salt (1 and 3 phr), were radiation cured at 100, 200, 389 and

800 kGy from a $^{60}$Co *y* radiation source and tested against a reference compound without NC (Figures 2.18–2.21) [90].

The TS and moduli measurements at 50% elongation of SBR/BR nanocomposites exhibit spectacular reinforcement, which derived from the NC

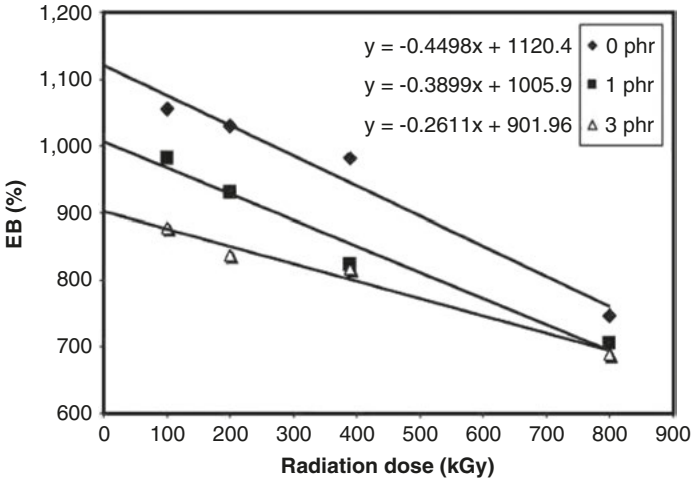


**Figure 2.18:** Effects of radiation dose on the EB of the rubber nanocomposites. The addition of 1 and 3 phr of NC caused a stiffening effect on the nanocomposite as indicated by the reduced elongation. Reproduced with permission from F. Cataldo, O. Ursini and G. Angelini, *Progress in Rubber, Plastics & Recycling Technology*, 2007, **23**, 209. ©2007, Smithers Rapra [90].

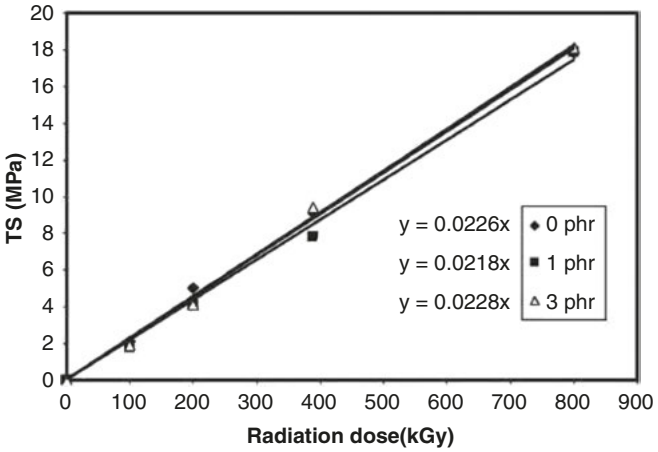


**Figure 2.19:** Effect of radiation dose on the TS of rubber composites with and without NC. Reproduced with permission from F. Cataldo, O. Ursini and G. Angelini, *Progress in Rubber, Plastics & Recycling Technology*, 2007, **23**, 209. ©2007, Smithers Rapra [90].

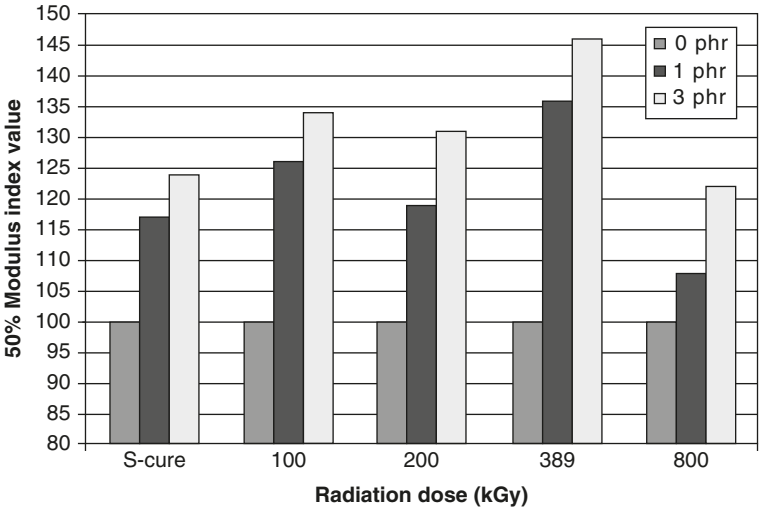


**Figure 2.20:** Moduli at 50% elongation: comparison with the sulfur-cured compound. The phr level of 1 and 3 refers to the amount of NC added. Reproduced with permission from F. Cataldo, O. Ursini and G. Angelini, *Progress in Rubber, Plastics & Recycling Technology*, 2007, **23**, 209. ©2007, Smithers Rapra [90].

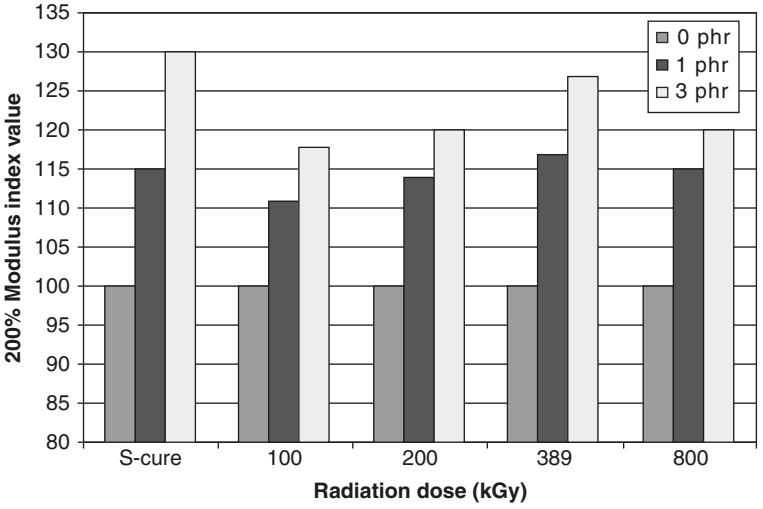


**Figure 2.21:** Moduli at 200% elongation: comparison with the sulfur-cured compound. The phr level of 1 and 3 refers to the amount of NC added. Reproduced with permission from F. Cataldo, O. Ursini and G. Angelini, *Progress in Rubber and Plastic Recycling Technology*, 2007, **23**, 209. ©2007, Smithers Rapra [90].

addition to the composite both in the radiation-cured compounds and in the sulfur-cured compound. Although the sulfur-cured composite showed a reduction in hysteresis after the NC addition, the radiation-cured compounds show the opposite trend. NR/SBR-modified Na-bentonite blend nanocomposites also exhibited improvements in the TS, modulus and EB [99]. Table 2.5 records the maximum improvement of mechanical properties of different rubber nanocomposites.

**Table 2.5:** Trend in improvement of mechanical properties of rubber nanocomposites.

| Rubber | Filler composition of best compound (phr)/(wt%#) | Rise@ in TS (%) | Rise@ in EB (%) | Rise@ in tear strength (%) | Ref. |
|---|---|---|---|---|---|
| NR/SBR | NC (2)# | 1 | * | 5 | [15] |
| NR | NC (11) | 40 | 10 | † | [16] |
| NR | NC (10) | 400 | 200 | † | [17] |
| NR | Nano-ZnO-GE (2) with respect to conventional ZnO (5) | 20 | 8 | 37 | [20] |
| NR/BR | SRSO–MK (4) with respect to kaolin (4) | 30 | 4 | † | [22] |
| S-SBR | NC (5.6) + XNBR (9.4) | 250 | 15 | † | [53] |
| NR/SBR | NC (3) | 93 | * | 63 | [54] |
| SBR latex | NC (5) + calcium stearate (0.5) | 200 | 25 | 300 | [55] |
| SBR | NC (15) | 164 | 50 | 139 | [56] |
| SBR | NC (6) + CB (30) | 1350 | * | † | [57] |
| SBR latex | MMT (20) | 679 | 47 | 200 | [58] |
| SBR, XSBR | XMEG (6) + CB (30) | 830 | 85 | 325 | [63] |
| SBR latex | GE (7) | 990 | * | † | [68] |
| SBR | CB (10) + rGO (3) | 39 | 11 | † | [76] |
| SBR | CB (20) + NC (10) | 1,111 | 195 | † | [106] |
| SBR | FG sheets (2)# | 450 | 50 | † | [108] |
| NR latex | GE (0.6) | 48 | * | † | [109] |
| NR latex | CB (39) + rGO (1) with respect to CB (40) | 18 | † | † | [110] |
| NR latex | $SiO_2$ (30) + $CeO_2$ (5) | 16 | * | 23 | [111] |
| SBR | CB (40 phr) | 370 | 41 | † | [114] |
| | CB (40 phr) + MWCNT (1 phr) | 490 | 12 | † | |
| SBR latex | Thermally-reduced GO (25) | 240 | * | † | [119] |
| SBR latex | MWCNT (10)# | 250 | * | † | |

* No improvement
# Composition in wt%
† Not reported
@ Improvement with respect to neat rubber or blend

# 2.4 Dynamic Mechanical Thermal Analysis of Natural Rubber, Styrene-Butadiene Rubber and its Blends

## 2.4.1 Dynamic Mechanical Thermal Analysis and Natural Rubber Nanocomposites

The storage moduli (E′) of NR/nano-ZnO–GE nanocomposites with a filler content higher than 1.0 phr are significantly improved compared with the NR/conventional ZnO (5 phr) composite, indicating a superior elastic response to deformation [20]. In comparison to the NR/conventional ZnO composite, the glass transition temperature ($T_g$) of the NR/nano-ZnO–GE nanocomposites shifted to a higher temperature. Their study also indicated a maximum improvement in wet skid resistance, i.e., the highest value of tan δ (0 °C) at a filler level of 1.0 phr and for rolling resistance (i.e., the lowest value of tan δ 60 °C) at a filler level of 2.0 phr. Fuquan and co-workers [111] reported that NR/$SiO_2$ nanocomposites containing $CeO_2$ promoted a $T_g$ shift to a high temperature, with the nanocomposites featuring a higher tan δ (0 °C) and lower tan δ (60 °C) and exhibiting comparable wet grip and lower rolling resistance when NR/$SiO_2$–$CeO_2$ nanocomposites were used in the tyre tread compound. The variation of storage modulus and tan δ curves of NR composites containing m-CG, m-CG/CB and CB has been studied over the temperature range of –120 to 100 °C [28]. It was found that the storage modulus and tan δ of CG in NR composites were higher than CB, but the $T_g$ was less than CB-filled NR vulcanisates. Liu and Wang [39] studied the temperature dependence of G′ and tan d for CB, CB/LRD, CB/Na–MMT, CB/organo-modified Laponite® RD (ORD) [polyethylene glycol (PEG)-modified LRD] and CB/OMMT (PEG-modified MMT)-filled NR composites over the temperature range of –100 to 60 °C. It was found that NR containing a hybrid filler exhibited superior mechanical properties compared with CB as a single-phase filler. According to these results, compared with the CB-filled rubber, the G′ increased significantly for hybrid-filled composites in the rubbery zone; whereas little G′ improvement in the glassy state was observed. Liu and co-workers [32] performed dynamic rheological tests to elucidate the mechanism of reinforcement in order to explain the superior performance of NR containing the organoclay and CB hybrid filler. They noted a three-order increase in magnitude of storage modulus of uncured rubber composites filled with 15 parts per hundred parts (phr) of rubber CB and 10 phr of rubber organoclay compared with gum rubber. The observed reinforcement was attributed to the formation of a more developed filler network in the hybrid filler system compared with the individual-phase filler.

The acid modification of CNT as a filler led to an improvement in the dynamic mechanical properties of neat NR [45]. The storage modulus of NR improved upon

the addition of CNC, indicating its reinforcing tendency [46]. According to Zhang and co-workers [46], both the glassy and rubbery modulus improved upon the addition of CNC to the NR matrix. Furthermore, they also noted that CNC addition insignificantly shifted the peak of tan δ to a lower temperature. A significant increase in the stiffness was observed above the glass–rubber transition temperature upon the addition of cellulose whiskers and microfibrillated cellulose to the NR latex [47]. Liu and co-workers [49] observed that the $T_g$ of the nanocomposites were higher than that of the NR vulcanisate. The $T_g$ of the 15 wt% organic vermiculite-filled NR nanocomposite remained unchanged [50].

### 2.4.2 Dynamic Mechanical Thermal Analysis of Styrene-Butadiene Rubber Nanocomposites

Dynamic mechanical thermal analysis of the NR/BR and NR/NBR blend rubber compositions containing SRSO-MK showed notable increases in storage modulus and decreases in loss modulus and tan δ in the presence of modified kaolin compared with unmodified kaolin [22]. Furthermore, the extent of the increase in storage modulus and decrease in loss modulus and tan δ of the vulcanisate containing SRSO-MK (from that containing unmodified kaolin) were greater in the case of the NR/NBR vulcanisate than the NR/BR vulcanisate.

The temperature dependence of the storage modulus of the composites show that HNT–TAG gave rise to a significant increase in the E′ of the SBR – HNT–TAG composites in both glassy and rubbery regions [38]. Das and co-workers [53] prepared nanocomposites of S-SBR with MMT layered silicate using XNBR as a compatibiliser and studied the temperature dependence of G′. They noted an insignificant difference in G′ in the sample consisting of 5 phr masterbatch (SB-10) and an unfilled S-SBR sample, SB-00, at room temperature. In contrast, the samples with higher loadings showed strong reinforcement effects resulting in higher G′ values. The SB-11 rubber composite showed a 1.65-fold increment of G′ compared with the S-SBR gum. They also examined the effect of XNBR on the dynamic mechanical performance of the SBR vulcanisates.

Mohanty and co-workers [69] observed improved dynamic properties, i.e., rolling resistance (tan δ at 60 °C) and wet skid resistance (tan δ at 0 °C), of an SBR/CB/ and NC (3 phr) composite. However, the mechanical properties and wear resistance, combined with the above-mentioned dynamic properties, were further improved by direct substitution of stearic acid with calcium stearate, which was attributed to the enhanced filler–rubber interaction. Dynamic mechanical analysis was carried out on MMT and silica fillers combined with Si 69® as a coupling agent in SBR/BR tread compounds [74]. The findings established that Si 69® promoted the crosslinking reaction of rubber molecules and enhanced the rubber modulus. As a result, ice traction and wet traction properties were improved with a low Si 69® content, whereas good

dry handling and rolling resistance were achieved at a high Si 69® content. The $T_g$ of the SBR/CB–RG blend was found to be higher in comparison to the SBR/CB blend [76], indicating the presence of strong interfacial interactions between RG and SBR due to the high surface area of GE and the π–π interaction between SBR and GE.

Dynamic mechanical thermal analysis of SBR and NBR and ODA-modified and unmodified Na-MMT clays was reported at 0.32 to 32 Hz over the temperature range of −80 to +80 °C and strains ranging from 0.001 to 10% [101]. The investigation showed significant changes in the tan δ peak temperature and height, and storage modulus, upon the addition of a small amount of the modified and unmodified fillers. The CB-filled SBR nanocomposite showed enhanced modulus in the range of 30 to 125% [104]. Tangudom and co-workers [115] investigated NR/SBR-filled with bagasse ash silica and precipitated silica as a coreinforcing filler and revealed an improved tensile modulus at 100% elongation, TS and elongation. Table 2.6 refers to data on the improvement of dynamic mechanical properties of different rubber nanocomposites.

**Table 2.6:** Trend in the improvement of dynamic mechanical properties of rubber nanocomposites.

| Rubber | Filler/special additive composition (phr/ wt%) | Wet skid resistance tan δ @ 0 °C | Rolling resistance tan δ @ 60 °C | Storage modulus [log E′(MPa)] | Ref. |
|---|---|---|---|---|---|
| NR | Nano-ZnO-GE (2) | 0.180 | 0.125 | – | [20] |
| NR/B | SRSO–MK (4) | – | – | 2.380 @ −48 °C | [22] |
| SBR latex | NC (5) + calcium stearate (2) | 0.332 | 0.151 | – | [55] |
| SBR | XMEG (3) + CB (30) | – | – | 1.097 @ 25 °C | [63] |
| SBR | NC (6) + CB (25) | – | 0.098 @ 70 °C | 1.214 @ 25 °C | [69] |
| SBR | NC (3) + CB (42) + CS (2) | 0.211 | 0.090 | 1.029 @ 60 °C | [69] |
| NR | GE (5) | – | – | 1.161 @ 10 °C | [109] |
| NR | $SiO_2$ (30) + $CeO_2$ (3) | 0.183 | 0.055 | – | [111] |

# 2.5 Thermogravimetric Analysis of Natural Rubber, Styrene-Butadiene Rubber and its Blend Nanocomposites

## 2.5.1 Thermogravimetric Analysis/Differential Thermal Analysis of Natural Rubber Nanocomposites

Mathew and co-workers [13] studied the degradation behaviour of NR latex nanocomposites in detail. Figure 2.22 shows the effect of nano-silicates on degradation.

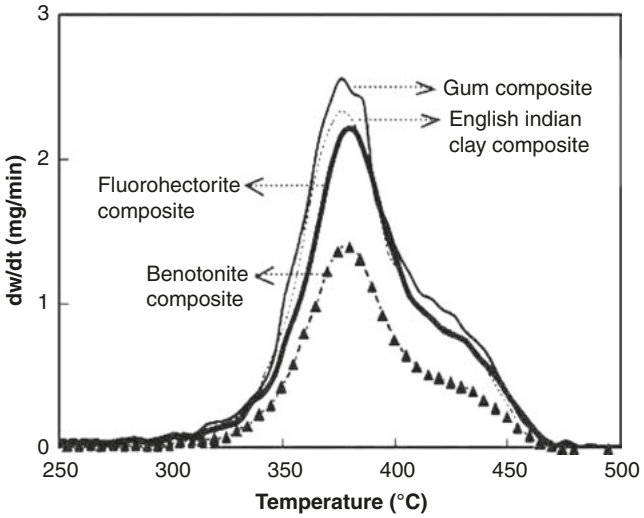


**Figure 2.22:** Thermogram of the layered silicate nanocomposites prepared from sulfur-prevulcanised NR latex nanocomposites at a loading of 5 phr. Reproduced with permission from S. Mathew, S. Varghese and R. Joseph, *Progress in Rubber, Plastics & Recycling Technology*, 2013, **29**, 1. ©2013, Smithers Rapra [13].

From this figure it is obvious that the decomposition rate (dw/dt) values are in the order: gum composite > English Indian clay composite > bentonite composite > fluorohectorite composite. It is clear that with the degradation temperature at 10 to 90%, the weight loss is higher for layered silicates than for gum and amorphous clay composites. At lower temperatures, filled NR shows a slight difference in thermal stability but at higher temperatures nanofilled NR shows enhanced thermal stability, which may be attributed to the improved layered silicate–matrix interaction. Nano-silicates can interact better with the matrix due to their higher surface area; this makes the matrix stiffer and the diffusion of heat and gases through the bulk more difficult, which retards the degradation of the composite.

NR/SBR/organoclay exhibits better stability compared with that of the neat NR/SBR blend [54]. Such an improvement in the initial thermal stability is attributed to the combined effect of the good gas barrier action of the organoclay layers, strong clay–polymer interaction and homogeneous dispersion. The effect of the ODA-modified Na-MMT-loading level on the thermal behaviour of NR/organoclay nanocomposites was an improved thermal stability compared with SR as well as NR/Na-MMT [16].

The thermal stability of the NR/BR blend nanocomposite was not affected significantly by the replacement of kaolin with Na-SRSO–MK [22]. Thermogravimetric analysis (TGA) of NR-2 (50 phr modified kaolinite), NR-3 (10 phr modified kaolinite + 40 phr CB) and NR-4 (50 phr CB) has been undertaken [26]. It was noted that the temperature corresponding to 5 wt% loss (T5) compared with neat NR increased by 31, 58 and 46 °C, respectively. The superior thermal stability of NR in the presence

of 10 phr modified kaolinite + 40 phr CB was attributed to the hybridisation of the CB particles with the kaolinite particles. Figure 2.23 shows thermograms of NR, NR/PAT–1%, NR/PAT–450–1% and NR/PAT-850–1% nanocomposites. It can be noted that the initial degradation temperature and degradation temperature of nanocomposites increased by the range of 70–113 and 17–21 °C, respectively.

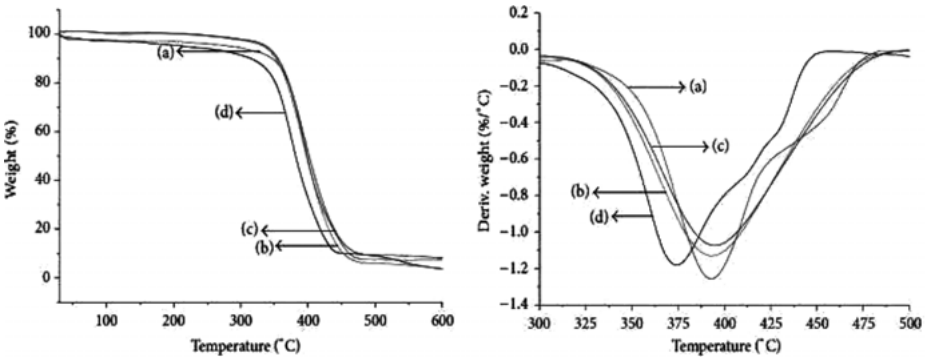


**Figure 2.23:** Thermograms of NR and NR/PAT nanocomposites: (a) NR/PAT-1%, (b) NR/PAT-450–1%, (c) NR/PAT-850–1% and (d) NR. Reproduced with permission from J. Wang and D. Chen, *Journal of Nanomaterials*, 2013, Article ID:496,584. ©2013, Hindwai [42].

TGA of rPET/HNT hybrid-filled NR composites under nitrogen showed that thermal stability increased and the maximum mass loss content reduced with a higher HNT loading, as observed from temperatures corresponding to 5, 50 and 80 wt% [29]. The improved thermal stability of rPET/HNT-filled NR composites could be due to the good dispersion and strong physical interaction of HNT. The thermal-oxidative stability of NR/$SiO_2$ nanocomposites in an air atmosphere showed that the initial weight loss temperature (323.6 °C) was enhanced with $SiO_2$/$CeO_2$ (30/05 weight ratio) and $SiO_2$/$CeO_2$ (30/10 weight ratio) to 326.8 and 337.7 °C, respectively [111]. NR/PAT nanocomposites displayed better thermal resistance than that of the pristine NR [42] and the thermal decomposition temperature of NR slightly increased upon the addition of the GON [44]. The acid modification of CNT as a filler led to an improvement in the thermal stability of neat NR [45]. The thermal stability of NR was also clearly improved upon the addition of treated CNT [48].

## 2.5.2 Thermogravimetric Analysis/Differential Thermal Analysis of Styrene-Butadiene Rubber Nanocomposites

Bhowmick and co-workers [61] reported that the decomposition of SBR-based vulcanisates in a nitrogen atmosphere occurs in multiple steps, as shown in Figure 2.24. The addition of the modified clay caused only a slight improvement in the major

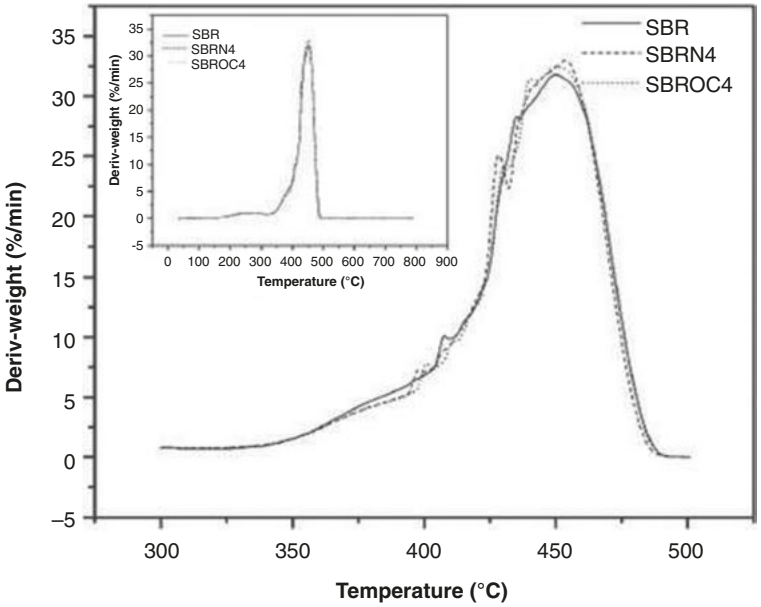


**Figure 2.24:** DTG curves of SBR and its nanocomposites at a heating rate of 20 °C/min in a nitrogen atmosphere. Reproduced with permission from S.S. Dey, R.S. Rajeev and A.K. Bhowmick, *Polymers & Polymer Composites*, 2008, **16**, 283. ©2008, Smithers Rapra [61].

degradation step (448 to 451 °C), in addition to shifting the first peak from 254 to 258 °C in the case of the modified clay-filled samples (SBROC4). Thus, clay affects both the degradation steps, although marginally, and the overall stability was improved. The degradation steps present inbetween the two peak degradation temperatures ($T_{max}$), in the case of the unmodified and modified clay-filled rubbers, were not so prominent, which is evident from the differential thermogravimetric analysis (DTG) curve. The value of onset decomposition temperatures of SBR/MMT nanocomposites containing 0, 1.0, 2.0, 2.5, 3.0 and 4.0 wt% OMMT were found to be 384.1, 385.8, 393.5, 399.6, 402.8 and 394.5 °C, respectively [72]. According to Bhowmick and Sadhu [73], the position of $T_{max}$ remains more or less the same for almost all the samples, but the rate of degradation decreased from 1.6 to 1.2% °C for the modified clay rubber nanocomposites. In either case, the thermal stability of the SBR/MMT nanocomposites was improved upon the addition of OMMT. SBR composites filled with modified kaolinite/precipitated silica hybrid fillers exhibited excellent thermal stability compared with the thermal stability of pure SBR [75].

Zhang and co-workers [76] observed a slight difference in the thermal stability of SBR composites filled with CB and/or CB–RG. SBR-modified MMT showed that the thermal stability of the nanocomposites depended on the spatial network structure as well as the content and type of nanoadditive in the vulcanisate [81]. In SBR (and NR)/kaolin nanocomposites, good interfacial links between the rubber and filler

contributed to the excellent thermal stability of the rubber composites [98]. TGA showed that the thermal stability of SBR/calcium carbonate ($CaCO_3$) nanocomposites increased, compared with pristine SBR, upon a reduction in size of $CaCO_3$ [67]. Xing and co-workers [68] observed an improvement of 26 °C in the initial degradation temperature (i.e., the temperature corresponding to 5 wt% mass loss) at a filler level of 1 phr of GE in SBR. This was attributed to increased paths for gas diffusion on account of the uniform dispersion of GE layers and p-p interaction between GE and the phenyl groups of SBR. No further increase in the initial degradation temperature was observed at higher GE loadings in SBR.

## 2.6 Differential Scanning Calorimetry of Natural Rubber, Styrene-Butadiene Rubber and its Blend Nanocomposites

### 2.6.1 Natural Rubber Nanocomposites

Liu and Wang [39] studied differential scanning calorimetry (DSC) of PEG, OMMT, NR/OMMT, NR/CB/OMMT, unfilled NR and PEG, ORD, NR/ORD, NR/CB/ORD and unfilled NR. An intense endothermic peak appeared in the first heating cycle of PEG and OMMT at 65 and 60 °C, respectively, corresponding to the melting transition of PEG chains. The melting transition of PEG almost disappears in NR/ORD and NR/CB/ORD, for both the initial and second heating cycles, indicating the absence of packed PEG chains as well as confined NR chains.

Sagar and co-workers [43] reported that $T_g$ and crystallisation temperatures were reduced upon the incorporation of MWCNT in the NR matrix by up to 7 and 6 °C, respectively. Furthermore, the first and second melting-phase temperatures were elevated up to 22 and 2 °C correspondingly. DSC NR/GON showed that the $T_g$ region in NR was enhanced upon increasing the filler content [44]. They found that the $T_g$ in NR GON (7 wt%) corresponds to −59.14 °C, which is 4.74 °C higher than that of the NR matrix (−63.88 °C). The $T_g$ of NR was not influenced by the presence of CNC [46]. DSC of a hybrid consisting of thermally-reduced GO and ionic liquid [1-ethyl-2,3-dimethylimidazolium *bis*(trifluoromethylsulfonyl)imide]-modified CNT (5 wt%)-filled NR composites showed no significant changes in the $T_g$ of neat NR [116].

### 2.6.2 Styrene-Butadiene Rubber Nanocomposites

Bharadwaj and co-workers [51] carried out DSC analysis of Hc-filled SBR nanocomposites. They recorded the $T_g$ of neat SBR as −45 °C whereas organo-modified

Hc, silane-grafted and double-modified NC filler-reinforced SBR nanocomposites exhibited $T_g$ at −38.46, −43.4 and −43.52 °C for 3 wt% filler loading, respectively. The shift in the $T_g$ may be attributed to the restricted mobility of the SBR chains within the Hc layers, indicating the intercalated/exfoliated nature of the SBR/O-Hc, SBR/S-Hc and SBR/OS-Hc nanocomposites. Schopp and co-workers [119] reported that the $T_g$ of SBR was not significantly altered by thermally-reduced GO even up to a level of 25 phr. An appreciable increase in $T_g$ has been observed in SBR reinforced with nano- $CaCO_3$ compared with pristine SBR [67], with the increment in $T_g$ due to the restricted mobility of nano-$CaCO_3$-filled SBR nanocomposites. Sadhu and Bhowmick [73] noted similar observations in clay-modified rubber nanocomposites, with the $T_g$ shifting by a few degrees to a higher temperature due to the filler–polymer interaction. SBR/clay nanocomposites exhibited increased $T_g$ compared with neat SBR [86]. Venter and co-workers [91] studied the thermal stability of a silica-filled SBR/BR composite, and found that the $T_g$ of SBR/clay nanocomposites increased compared with that of neat SBR. DSC under dynamic conditions has also been used to study the influence of GE loading on the vulcanisation kinetics of GE/SBR nanocomposites [120].

## 2.7 Abrasion Resistance of Natural Rubber, Styrene-Butadiene Rubber and its Blend Nanocomposites

Abrasion resistance is a key property of a tread compound and directly reflects the reinforcing efficiency (i.e., the degree of dispersion and degree of reinforcement) of the filler. The abrasion resistance was improved greatly for 3.0 phr of organoclay in NR/ SBR/organoclay nanocomposites providing a good prospect for application in the tyre industry [54]. Xing and co-workers [68] noticed that well-dispersed GE nanosheets in SBR enhanced the abrasion resistance of the corresponding nanocomposites. Gopi and co-workers [57] observed that a 6 phr organoclay and 25 phr CB (N330)-filled SBR nanocomposite marginally improved the abrasion resistance compared with a 40 phr CB-filled SBR.

Ahmed and co-workers [116] studied the abrasive properties of nano-silica-filled SBR. Figure 2.25 shows that the weight loss of rubber increases upon the addition of small amounts of silica (e.g., 0.1 pphr), and then decreases until it reaches 0.41% at 1 pphr of silica. In the case of an increasing amount of nano-silica (>3 pphr), the weight loss increases due to particle agglomeration. The formation of excess fillers weaken the link between the molecules and, in addition, reduces the tension and abrasion resistances. Bao and co-workers [74] also carried out abrasion resistance index investigations in MMT and silica fillers combined with Si 69® as their coupling agent in SBR/BR tread compounds. Table 2.7 records the trend in improvement of abrasion resistance of various rubber nanocomposites.

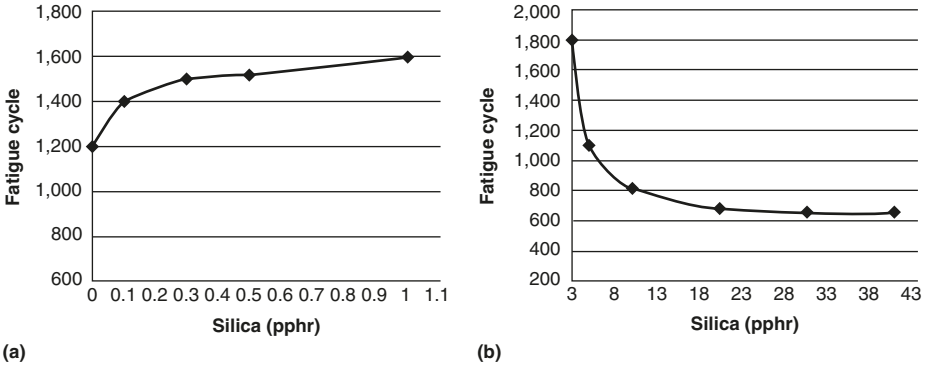


**Figure 2.25:** Effect of small and large quantities of nano-silica on the fatigue life of the formulation. Reproduced with permission from J.K. Ahmed, M.H. Al-Maamori and H. Mohammed Ali, *International Journal of International Materials Science and Applications*, 2015, **4**, 15. ©2015, Science Publishing Group [116].

**Table 2.7:** Trend in improvement of the abrasion resistance of rubber nanocomposites.

| Rubber | Filler composition of the reference compound (phr/wt%) | Filler composition of the best compound (phr/wt%) | Maximum improvement in abrasion loss/ abrasion resistance index/wear rate | Ref. |
|---|---|---|---|---|
| NR + SBR | CB (48) | NC (3) + CB (45) | 82 $mm^3$ | [54] |
| SBR latex | MMT (5) | NC (5) + calcium stearate (0.5) | 700 µg/rev | [55] |
| SBR | CB (40) | NC (6) + CB (25) | 5.0% | [57] |
| SBR, XSBR | CB (40) | XMEG (6) + CB (30) | 5.0% | [63] |
| SBR latex | WCB (40) | GE (7) | 122 $mm^3$ | [68] |
| SBR | CB (45) | NC (3) + CB (42) + calcium stearate (0.5) | –3.0% | [69] |
| SBR + BR | NC (22.5) + PS (22.5) + Si 69® (3.6) | NC (5) + PS (45) + Si 69® (3.6) | 45% | [74] |

WCB: White carbon black

## 2.8 Heat Build-up of Natural Rubber, Styrene-Butadiene Rubber and its Blend Nanocomposites

Heat build-up during cyclic loading and unloading of a filled rubber specimen is primarily due to friction between the filler particles. In view of this, several studies have reported different NR, SBR and rubber blend nanocomposites. Studies on CB- and NC-filled SBR nanocomposites established a substantial decrease in heat build-up values by replacing CB with NC [57]. Mohanty and co-workers [69] reported a heat build-up study on SBR/CB/organoclay (Cloisite® 20A) nanocomposites. The partial replacement of CB with NC in different proportions in the presence of calcium stearate led to a reduction in heat build-up. It was suggested that calcium stearate acts as a dispersion promoter for NC, enhancing the polymer–filler compatibility and thereby lowering the heat build-up value. The variation of heat build-up at ambient temperature (30 °C) as a function of compression time in SBR composites filled with different fillers such as CB, fumed silica/WCB and GE has been reported [68]. A 40 WCB/SBR composite exhibited the highest heat build-up due to the strong interfacial friction and interaggregation of filler particles. A 7 GE/SBR nanocomposite with mechanical properties comparable to that of 40 WCB/SBR showed a relatively lower heat build-up by about 5 °C. Sookyung and co-workers [16] observed a lower heat build-up in organoclay (<5 phr) NR nanocomposites. NR/CB/rGO, compared with NR/CB/GO composites, displayed a much lower heat build-up at a high load of nanosheets [110]. Raji and co-workers [22] observed that the temperature rise was 3 °C less for the SRSO-MK-based compound compared with that of unmodified kaolin at a content of 4 phr filler.

Table 2.8 records the trend in improvement of the heat build-up of various rubber nanocomposites.

## 2.9 Conclusions

It can be concluded from the detailed discussion on cure kinetics, mechanical properties, abrasion resistance, heat build-up and dynamic mechanical properties of different rubber nanocomposites that the homogeneous dispersion of fillers across the rubber matrix, high degree of polymer–filler interaction and polymer – polymer compatibility (in case of blends) are the primary parameters that dictate the morphology, processability and end properties. The use of compatibilisers (like XNBR and XSBR), coupling agents [like *bis*(triethoxysilylpropyl)tetrasulfane] to improve polymer–polymer and polymer–filler compatibility has been proved to be effective in improving the performance parameters of the tread compound. Organo-modified

**Table 2.8:** Trend in improvement of the heat build-up of rubber nanocomposites.

| Rubber | Filler composition of the reference compound (phr/wt%) | Filler composition of the best compound (phr/wt%) | Improvement in heat build-up | Ref. |
|---|---|---|---|---|
| NR | MMT (11) | NC (11) | –8.0 °C | [16] |
| NR/BR | Kaolin (4) | SRSO–MK (4) | 3.0 °C | [22] |
| SBR | CB (40) | NC (6) + CB (25) | 5.2 °C (base), 16.6 °C (centre) | [57] |
| SBR latex | WCB (40) | GE (7) | 5.5 °C | [68] |
| SBR | CB (45) | NC (3) + CB (42) + N-cyclohexyl-2-benzothiazole sulfenamide. (2) | 3.3 °C | [69] |
| NR latex | CB (35) + GO (5) | CB (35) + rGO (5) | 10.0 °C | [110] |

clays, functionalised MWCNT and functionalised GE nanosheets are three important fillers that show a synergistic effect in reinforcing the rubber matrix in combination with conventional fillers – CB and silica. Clays modified by amine/quaternary ammonium salts (like hexadecylamine, ODA and so on), Na-SRSO, have shown significant improvement in the degree of dispersion and polymer–filler interaction. Replacing the conventional compounding ingredients by their modified versions (like calcium stearate in place of stearic acid) also brings additional improvement in the morphology and end properties. A recent study showed the simultaneous use of two different nanofillers in a conventional tread formulation to be useful due to the synergistic effect.

**Acknowledgement:** S.K. Srivastava is thankful to his daughter Mili Srivastava, the Royal Bank of Canada, Toronto, Canada, for providing the necessary facilities to complete this task during his stay in the summer of 2016.

# References

1. J.M. Baldwin and D.R. Bauer, *Rubber Chemistry and Technology*, 2008, **81**, 338.
2. J.A. Brydson in *Rubbery Materials and their Compounds*, Springer, New York, NY, USA, 1988.
3. S. Ghosh, R.A. Sengupta and M. Kalike, *Rubber Chemistry and Technology*, 2014, **87**, 276.
4. S.K. Srivastava and T. Kuila in *Polymer Green Flame Retardants: A Comprehensive Guide to Additives and their Applications*, Eds., C.D. Papaspyrides and P. Kiliari, Elsevier, Amsterdam, The Netherlands, 2013, p.597.
5. S.K. Srivastava in *Natural Rubber Materials, Volume 2: Composites and Nanocomposites*, Eds., S. Thomas, H.J. Maria, J.P. Joy, C. Han Chan and L.A. Pothen, Polymer Chemistry Series No.8, Royal Society of Chemistry, Cambridge, UK, 2014, p.504.

6. K.G. Gatos and J. Korger-Kocsis in *Rubber-Clay Nanocomposites: Science, Technology, and Applications*, Ed., M. Galimberti, Wiley, New York, NY, USA, 2011, p.169.
7. *The Pneumatic Tyre*, DOT HS 810 561, National Highway Traffic Safety Administration/US Department of Transportation, Washington, DC, USA, February 2006. https://www.fueleconomy.gov/feg/pdfs/PneumaticTire_HS-810-561.pdf.
8. A.K. Bhowmick in *Current Topics in Elastomers Research*, CRC Press, Boca Raton, FL, USA, 2008.
9. M. Pramanik, S.K. Srivastava, B.K. Samantaray and A.K. Bhowmick, *Journal of Applied Polymer Science*, 2003, **87**, 2216.
10. H. Acharya, S.K. Srivastava and A.K. Bhowmick, *Composite Science and Technology*, 2007, **67**, 2807.
11. P. Bala, B.K. Samantaray, S.K. Srivastava and G.B. Nando, *Journal of Material Science Letters*, 2001, **20**, 563.
12. P. Bala, S.K. Srivastava, B.K. Samantaray and G.B. Nanda, *Journal of Applied Polymer Science*, 2004, **92**, 3583.
13. S. Mathew, S. Varghese and R. Joseph, *Progress in Rubber*, *Plastics & Recycling Technology*, 2013, **29**, 1.
14. Y. Wang, H. Zhang, Y. Wu, Y. Yang and L. Zhang, *Journal of Applied Polymer Science*, 2005, **96**, 318.
15. T.P. Mohan, J. Kuriakose and K. Kanny, *Journal of Industrial Engineering Chemistry*, 2011, **17**, 264.
16. U. Sookyung, C. Nakason, W. Thaijaroen and N. Vennemann, *Polymer Composites*, 2016, **37**, 1735.
17. Y. Wu, Y. Ma, Y. Wang and L. Zhang, *Macromolecular Materials Research*, 2004, **289**, 890.
18. S. Mathew, S. Varghese, K.E. George and T. Cherian, *Progress in Rubber, Plastics & Recycling Technology*, 2011, **192**, 177.
19. Y.T. Vu, J.E. Mark, H. Pham and M. Engelhardt, *Journal of Applied Polymer Science*, 2001, **82**, 1391.
20. Y. Lin, Y. Chen, Z. Zeng, J. Zhu, Y. Wei, F. Li and L. Liu, *Composites, Part A: Applied Science and Manufacturing*, 2015, **70**, 35.
21. R.K. Prud'Homme, B. Ozbas, I. Aksay, R. Register and D. Adamson, inventors; The Trustees of Princeton University, assignee; US7745528B2, 2010.
22. V.V. Raji, S. Ramakrishnan, R. Sukumar, M. Brahmakumar and A. Menon, *Polymer International*, 2015, **64**, 1585.
23. H. Li, L. Yang, G. Weng, W. Xing, J. Wu and G. Huang, *Journal of Materials Chemistry A*, 2015, **3**, 22385.
24. O.A. Al-Hartomy, A.A. Al-Ghamdi, A.S. Farha Al Said, N. Dishovsky, R. Shtarkova and V. Iliev, *Applied Polymer Composites*, 2014, **2**, 59.
25. J. Choi and A.I. Isayev, *Rubber Chemistry and Technology*, 2013, **86**, 633.
26. Y. Zhang, J. Xiang, Q. Zhang, Q. Liu and R.L. Frost, *Thermochimica Acta*, 2014, **576**, 39.
27. Y. Liu, L. Li, Q. Wang and X. Zhang, *Journal of Polymer Research*, 2011, **18**, 859.
28. J. Chen, K. Xu, R. Pan, Z. Peng and L. Ma, *Polymer Composites*, 2014, **35**, 1911.
29. H. Nabil and H. Ismail, *Journal of Thermoplastic Composite Materials*, 2013, **28**, 415.
30. H. Ismail, N.F. Omar and N. Othman, *Journal of Applied Polymer Science*, 2011, **121**, 1143.
31. N. Rattanasoma, T. Saowapark and C. Deeprasertku, *Polymer Testing*, 2007, **26**, 369.
32. Y.B. Liu, L. Li and Q. Wang, *Plastics*, *Rubber and Composites*, 2010, **39**, 370.
33. J. Sapkota, M. Poikelispa, A. Das, W. Dierkes and J. Vuorinen, *Polymer Engineering and Science*, 2013, **53**, 615.

34. K. Ahmed, M. Nasir, A. Imran and K. Mahmood, *Journal of Materials and Environmental Science*, 2014, **5**, 1085.
35. S. Attharangsan, H. Ismail, M.A. Bakar and J. Ismail, *Polymer-Plastic Technology Engineering*, 2012, **51**, 655.
36. H. Ismail, A.F. Ramly and N. Othman, *Journal of Applied Polymer Science*, 2013, **128**, 2433.
37. S.K. Srivastava and H. Acharya in *Rubber Nanocomposites: Preparation, Properties and Applications*, Eds., S. Thomas and R. Stephen, John Wiley, Hoboken, NJ, USA, 2010, p.551.
38. Z. Tang, Q. Wei, T. Lin, B. Guo and D. Jia, *RSC Advances*, 2013, **3**, 17057.
39. Y. Liu, L. Li and Q. Wang, *Journal of Applied Polymer Science*, 2010, **118**, 1111.
40. J. Sharif, W.M.Z.W. Yunus, K.Z.H.M. Dahlan and M.H. Ahmad, *Polymer Testing*, 2005, **24**, 211.
41. Z-X. Jia, Y-F. Luo, Y-B. Zhou, D. Jia and H. Ligong, *Daxue Xuebao*, *Ziran Kexueban*, 2008, **36**, 147.
42. J. Wang and D. Chen, *Journal of Nanomaterials*, 2013, Article ID:496584. http://dx.doi.org/10.1155/2013/496584.
43. S. Sagar, N. Iqbal, A. Maqsood and M. Bassyouni, *IACSIT International Journal of Engineering and Technology*, 2014, **6**, 168.
44. J. Bian, L.L. Hai, X. He Fei, L. Wang, W. Wei Xiao, I-T. Chang and Y. Lu, *Polymer Composites*, 2015, doi:10.1002/pc.23710.
45. A.A. Abdullateef, S.P. Thomas, M.A. Al-Harthi, S.K. De, S. Bandyopadhyay, A.A. Basfar and M.A. Atieh, *Journal of Applied Polymer Science*, 2012, **125**, E76.
46. C. Zhang, Y. Dan, J. Peng, L.S. Turng, R. Sabo and C. Clemons, *Advances in Polymer Technology*, 2014, **33**, 21448/1.
47. A.K. Bendahou, H. Kaddami and A. Dufresne, *European Polymer Journal*, 2010, **46**, 609.
48. G. Sui, W.H. Zhang, X.P. Yang, Y.H. Yu and S.H. Zhao, *Polymers for Advanced Technologies*, 2008, **19**, 1543.
49. L. Liu, Y. Luo, D. Jia, W. Fu and B. Guo, *Journal of Elastomers & Plastics*, 2006, **38**, 147.
50. H. Wei, L. Wei and W. Chi-Fei, *Acta Metallurgica Sinica*, 2006, **23**, 77.
51. P. Bharadwaj, P. Singh, K.N. Pandey, V. Verma and S.K. Srivastava, *Applied Polymer Composites*, 2013, **1**, 207.
52. S.J. He, Y.Q. Wang, J. Lin, and L.Q. Zhang, *Advanced Materials Research*, 2012, **393–395**, 28.
53. A. Das, R. Jurk, K.W. Stockelhuber, T. Engelhardt, J. Fritzsche, M. Kluppel and G.J. Heinrich, *Journal of Macromolecular Science, Part A: Pure and Applied Chemistry*, 2008, **45**, 144.
54. C. Shan, Z. Gu, L. Wang, P. Li, G. Song, Z. Gao and X. Yang, *Journal of Applied Polymer Science*, 2011, **119**, 1185.
55. D-S. Kim, D-H. Lee, I-J. Kim, M-J. Son, W. Kim and S-G. Cho, *Macromolecular Research*, 2009, **17**, 776.
56. J. Diez, L. Barral, R. Bellas, J. Lopez, C. Ramirez and A. Rodriguez, *Journal of Applied Polymer Science*, 2012, **125**, E705.
57. J.A. Gopi, S.K. Patel, D.K. Tripathy and A.K. Chandra, *Journal of Polymer Research*, 2011, **18**, 1625.
58. S-J. He, Y-Q. Wang, Y-P. Wu, X-H. Wu, Y-L. Lu and L-Q. Zhang, *Plastics*, *Rubber and Composites*, 2010, **39**, 33.
59. M. Bhattacharya, M. Maiti and A.K. Bhowmick, *Polymer Engineering and Science*, 2009, **49**, 81.
60. L. Zhang, Y. Wang, Y. Wang, Y. Sui and D. Yu, *Journal of Applied Polymer Science*, 2000, **78**, 1873.
61. S.S. Dey, R.S. Rajeev and A.K. Bhowmick, *Polymers & Polymer Composites*, 2008, **16**, 283.
62. S.K. Peddini, C.P. Bosnyak, N.M. Henderson, C.J. Ellison and D.R. Paul, *Polymer*, 2014, **55**, 258.

63. A. Malas, P. Pal, S. Giri, A. Mandal and C.K. Das, *Composites, Part B: Engineering*, 2014, **58**, 267.
64. S.H. Song, O.S. Kwon, H.K. Jeong and Y.G. Kang, *Korean Journal of Materials Research*, 2010, **20**, 104.
65. Q. Liu, Y. Zhang and H. Xu, *Applied Clay Science*, 2008, **42**, 232.
66. R. Scotti, L. Conzatti, M. D'Arienzo, B. Di Credico, L. Giannini, T. Hanel, P. Stagnaro, A. Susanna, L. Tadiello and F. Morazzoni, *Polymer*, 2014, **55**, 1497.
67. S. Mishra, N.G. Shimpi and U.D. Patel, *Journal of Polymer Research*, 2007, **14**, 449.
68. W. Xing, M. Tang, J. Wu, G. Huang, H. Li, Z. Lei, X. Fu and H. Li, *Composites Science and Technology*, 2014, **99**, 67.
69. T.R Mohanty, V. Bhandari, A.K. Chandra, P.K. Chattopadhya and S. Chattopadhy, *Polymer Composites*, 2013, **34**, 214.
70. S.P. Lee, O.S. Kwon, Y.G. Kang and S.H. Song, *Plastic and Rubber Composites*, 2016, **45**, 382.
71. A.R. Payne, *Journal of Applied Polymer Science*, 1962, **1**, 57.
72. Z. Zhang, L. Zhang, Y. Li and H. Xu, *Polymer*, 2005, **46**, 129.
73. S. Sadhu and A.K. Bhowmick, *Rubber Chemistry and Technology*, 2003, **76**, 860.
74. Z. Bao, J. Tao and C. Flanigan, *Polymer Composites*, 2015, doi:10.1002/pc.23653.
75. Y. Zhang, Q. Zhang, Q. Liu, H. Cheng and R.L. Frost, *Journal of Thermal Analysis and Calorimetry*, 2014, **115**, 1013.
76. H. Zhang, C. Wang and Y. Zhang, *Journal of Applied Polymer Science*, 2015, **132**, 41309/1.
77. D.V. Gura, L.A. Sokolova, V.I. Ovcharov and P.I. Soroka, *Kauchuk i Rezina*, 2014, **3**, 20.
78. P. Rybinski, A. Paja, G. Janowska and M. Jozwiak, *Journal of Applied Polymer Science*, 2015, **132**, 42593/1.
79. H. Zhang, Y. Wang, Y. Wu, L. Zhang and J. Yang, *Journal of Applied Polymer Science*, 2005, **97**, 844.
80. S. Chakraborty, R. Sengupta, S. Dasgupta, R. Mukhopadhyay, S. Bandyopadhyay, M. Joshi and S.C. Ameta, *Polymer Science and Engineering*, 2009, **49**, 1279.
81. M. Bhattacharya and A.K. Bhowmick, *Journal of Materials Science*, 2010, **45**, 6126.
82. M. Mariano, N.E. Kissi and A. Dufresne, *Carbohydrate Polymers*, 2016, **137**, 174.
83. L. Bokobza, M. Rahmani, C. Belin, J-L. Bruneel and N-E. El Bounia, *Journal of Applied Polymer Science*, 2008, **46**, 1939.
84. B. Guo, F. Chen, Y. Lei, X. Liu, J. Wan and D. Jia, *Applied Surface Science*, 2009, **255**, 7329.
85. F. Al-Yamani and L.A. Goettler, *Rubber Chemistry and Technology*, 2007, **80**, 100.
86. M. Alimardani and F. Abbassi-Sourk, *Journal of Composite Materials*, 2015, **49**, 1267.
87. N.Z. Noriman and H. Ismail, *Applied Polymer Science*, 2012, **124**, 19.
88. M. Zurina, H. Ismail and A.A. Bakar, *Journal of Reinforced Plastic Composites*, 2004, **23**, 1397.
89. J. Abraham, M.G. Maya, S.C. George, N. Kalarikkal and S. Thomas, *Research & Reviews: Journal of Engineering and Technology*, 2015. http://www.rroij.com/open-access/carbon-nanotubethermally-reduced-graphene-hybridstyrene-butadiene-rubber-nano-composites-mechanical-morphological-anddielectric-studies.php?aid=57853.
90. F. Cataldo, O. Ursini and G. Angelini, *Progress Rubber, Plastics and Recycling Technology*, 2007, **23**, 209.
91. S.A.S. Venter, M.H. Kunita, R. Matos, R.C. Nery, E. Radovanovic, E.C. Muniz, E.M. Girotto and A.F. Rubira, *Journal of Applied Polymer Science*, 2005, **96**, 2273.
92. M. Ghanbari, S.N. Khorasani, M.M. Talakesh and A. Farzadfar, *Journal of Elastomers and Plastics*, 2013, **45**, 551.
93. A. Yekrangi, M. Afrasiabi, A. Langari and M.K. Hafshejani, *Journal of Engineering and Applied Science*, 2014, **9**, 580.
94. M. Li, W. Tu, X. Chen, H. Wang and J. Chen, *Journal of Polymer Engineering*, 2016, **36**, 813.

95. N. Girun, F-R. Ahmadun and S.A. Rashid, *Fullerenes, Nanotubes, and Carbon Nanostructures*, 2007, **15**, 207.
96. M. Zurina, H. Ismail and A.A. Bakar, *Journal of Applied Polymer Science*, 2004, **92** 3320.
97. N. Ahmed and S.H. El-Sabbagh, *Society of Plastic Engineers Plastic Research*, 2014. http://www.4spepro.org/view.php?article=005234-2014-02-21.
98. Y. Zhang, Q. Liu, Z. Wu, H. Keji and D. Xuebao, *Ziran Kexueban*, 2006, **21**, 73.
99. A.I. Khalaf, M.A. Hegazy and D.E. El-Nashar, *Polymer Composites*, 2015, doi:10.1002/pc.23598.
100. K. Pal, R. Rajasekar, S.K. Pal, J.K. Kim and C.K. Das, *Journal of Nanoscience and Nanotechnology*, 2010, **10**, 3022.
101. S. Sadhu and A.K. Bhowmick, *Rubber Chemistry and Technology*, 2005, **78**, 321.
102. S. Sadhu and A.K. Bhowmick, *Journal of Applied Polymer Science*, 2004, **92**, 698.
103. S. Sadhu and A.K. Bhowmick, *Journal of Polymer Science, Part B: Polymer Physics*, 2004, **42**, 1573.
104. M. Maiti, S. Sadhu and A.K. Bhowmick, *Journal of Applied Polymer Science*, 2005, **96**, 443.
105. A. Chatterjee, P.S. Khobragade and S. Mishra, *Journal of Applied Polymer Science*, 2015, **132**, 42811/1.
106. S. Praveen, P.K. Chattopadhyay, P. Albert., V.G. Dalvi, B.C. Chakraborty and S. Chattopadhyay, *Composites*, *Part A: Applied Science and Manufacturing*, 2009, **40**, 309.
107. B. Dong, S. Wu, L. Zhang and Y. Wu, *Industrial Engineering Chemistry Research*, 2016, **55**, 4919.
108. B. Ozbas, C.D. O'Neill, R.A. Register, I.A. Aksay, R.K. Prud'homme and D.H. Adamson, *Journal of Polymer Science, Part B: Polymer Physics*, 2012, **50**, 910.
109. W. Xing, J. Wu, G. Huang, H. Li, M. Tang and X. Fu, *Polymer International*, 2014, **63**, 1674.
110. G. Yang, Z. Liao, Z. Yang, Z. Tang and B. Guo, *Journal of Applied Polymer Science*, 2015, **132**, 41832.
111. F. Zhang, L. Liao, Y. Wano, Y. Wang, H. Huang and P. Li, *Journal of Rare Earths*, 2016, **34**, 221.
112. I. Halász and T. Bárány, *Materials Science Forum*, 2015, **812**, 65.
113. C. Shan, Z. Gu, L. Wang, P. Li, G. Song, Z. Gao and X. Yang, *Journal of Applied Polymer Science*, 2011, **119**, 1185.
114. S.K. Peddini, C.P. Bosnyak, N.M. Henderson, C.J. Ellision and D.R. Paul, *Polymer*, 2015, **56**, 443.
115. P. Tangudom, S. Thongsang and N. Sombatsompop, *Materials and Design*, 2014, **53**, 856.
116. J.K. Ahmed, M.H. Al-Maamori and H. Mohammed Ali, *International Journal of International Materials Science and Applications*, 2015, **4**, 15.
117. S. Yaragalla, B. Sindam, J. Abraham, K.C.J. Raju, N. Kalarikal and S. Thomas, *Journal of Polymer Research*, 2015, **22**, 137.
118. Y. Wang, H. Zhang, Y. Wu, J. Yang and L. Zhang, *Journal of Applied Polymer Science*, 2005, **96**, 324.
119. S. Schopp, R. Thomann, K.F. Ratzsch, S. Kerling, V. Altstadt and R. Mulhaupt, *Macromolecular Materials and Engineering*, 2014, **299**, 319.
120. M. Tang, W. Xing, J. Wu, G. Huang, H. Li and S. Wu, *Chinese Journal of Polymer Science*, 2014, **32**, 658.
121. B. Guo, F. Chen, Y. Lei and W. Chen, *Polymer Journal*, 2010, **42**, 319.

Tuhin Chatterjee and Kinsuk Naskar

# 3 Nanofilled Thermoplastic Vulcanisates in Automotive Applications

## 3.1 Basic Concepts of Thermoplastic Elastomers and Thermoplastic Vulcanisates

### 3.1.1 Thermoplastic Elastomers

An elastomer is a material that exhibits a rapid and large recoverable strain in response to a stress. Softness, flexibility and the highly elastic nature of elastomeric materials make them suitable for various applications including tyres, seals, conveyor belts, gaskets, gloves and so on. Virgin rubbers have limited applications due to their sticky nature, low strength and high degree of solubility in solvents, in addition, they are highly prone to disentanglement even under a small stress, which leads to viscous deformation and permanent set. Typical elastomeric properties such as elasticity, strength and solvent resistance, are only obtained after crosslinking, as crosslinks severely restrict the motion of chain molecules. The formation of covalent crosslinks between the chain molecules prevents melt processing of elastomers or rubbers, which offers crosslinked elastomers a distinct disadvantage over thermoplastics. In addition, simple recycling of the waste material and scrap is not possible.

On the other hand, although thermoplastic materials possess better melt processability and good strength properties, the poor elastic behaviour, low flexibility and rigidity restricts the use of thermoplastics in dynamic applications. In this respect, thermoplastic elastomers (TPE) are an interesting class of material, as they combine the good elastic and mechanical properties of thermoset crosslinked rubber with the melt processability of thermoplastics. From another point-of-view, TPE can be defined as a class of polymers that combine the service properties of elastomers with the processing properties of thermoplastics [1]. As a result, TPE bridge the gap between conventional elastomers and thermoplastics.

In the late 1950s, the emergence of TPE provided a new horizon in the field of polymer science and technology. Most TPE meet the standard American Society for Testing and Materials, ASTM D1566, definition of a rubber because:

- They recover quickly and forcibly from large deformations.
- They can be elongated by more than 100%.
- Their tension set is less than 50%.

TPE have the following advantages:

- No vulcanisation and very little compounding are required.
- Properties can be manipulated by changing the ratios of the components.

https://doi.org/10.1515/9783110643879-003

– Scrap can be recycled or reused without any significant deterioration of properties, as shown in Figure 3.1.

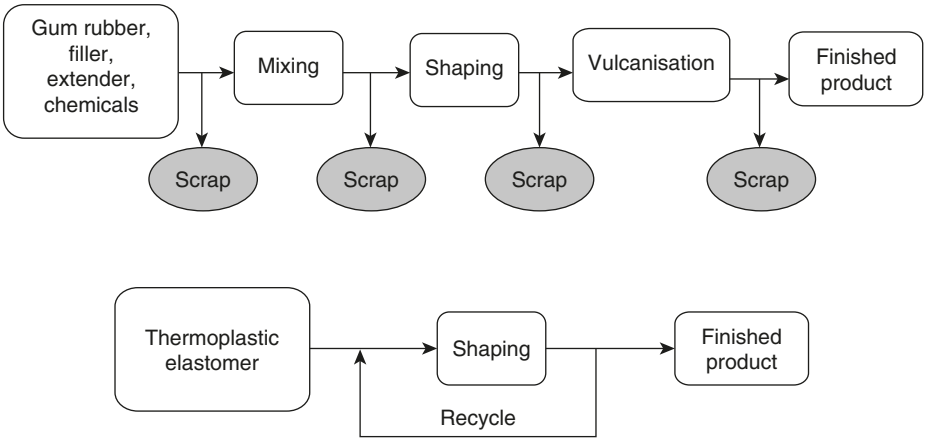


**Figure 3.1:** Processing scheme of vulcanised rubbers and TPE.

– Amenable to methods of thermoplastic processing such as injection moulding, blow moulding and thermoforming.
– Better quality control.

Due to the above-mentioned advantages, TPE are slowly replacing conventional rubber products and many leading plastic materials. In our day-to-day life, these materials are used on a large scale, without the public being aware of the fact that they are actually TPE and are different from the rubbers they see in the tyres of their car. Thus, TPE provide the easiest way to achieve tailor-made properties at low cost, by simply varying the blend compositions, viscosity of the components and compounding ingredients. TPE can also easily meet the physical, chemical and aesthetic requirements of several automotive products and provide cost advantages and design flexibility to the automobile engineer, which results in a growing demand for TPE in various automotive applications.

Commercial TPE can be classified into two main categories:

– TPE based on block copolymers (mainly triblock or multiblock copolymers).
– TPE based on polymer blends.

Triblock copolymers typically consist of a soft, flexible midblock end-capped with two rigid end-blocks, such as polystyrene-polybutadiene-polystyrene, i.e., styrene-butadiene-styrene. Multiblock copolymers are typically based on polyesters, polyamides (PA) or polyurethanes as hard blocks and polyethers as soft blocks. At

service temperature, the rigid blocks cluster together to form small domains that act as physical crosslinks between the soft blocks, as is schematically shown for a triblock copolymer in Figure 3.2.

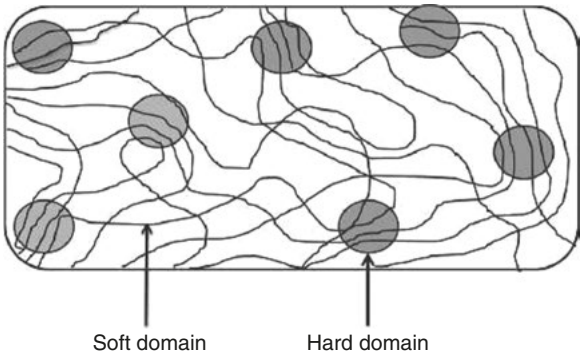


**Figure 3.2:** Schematic representation of the morphology of a triblock TPE.

Above the melting temperature of the hard blocks, the physical crosslinks disappear and the material becomes melt processable. This leads to a material with rubber-like properties at service temperature and allows (re)processability of the melt [2].

However, TPE also have the following disadvantages:

- TPE soften or melt at elevated temperature above which they lose their rubbery behaviour.
- TPE exhibit a creep response upon extended use.

In the case of TPE, as the elastomeric phase is not crosslinked, TPE do not provide sufficient resistance to compression set and tension set under prolonged deformation. However, the use of low-cost materials, combined with an easy production process (simple melt blending or large-scale reactor blending), makes thermoplastic polyolefins (TPO) a suitable class of materials for many applications, especially in the automotive industry. Hence, the concept of thermoplastic vulcanisates (TPV) was developed in which the elastomeric phase is crosslinked, which leads to superior elastic behaviour.

## 3.1.2 Thermoplastic Vulcanisates

TPV, a special class of TPE, are produced by 'dynamic vulcanisation' of non-miscible blends of a thermoplastic and an elastomer, i.e., selective crosslinking of the elastomer phase during melt mixing with the thermoplastic [3]. Simultaneous

vulcanisation of the rubber phase in the presence of a crosslinking agent (e.g., peroxide, diamine, sulfur accelerator and so on) during melt blending with the thermoplastic, leads to the generation of a dynamic vulcanisate that consists of dispersed crosslinked rubber particles in a continuous thermoplastic matrix phase, as shown in Figure 3.3.

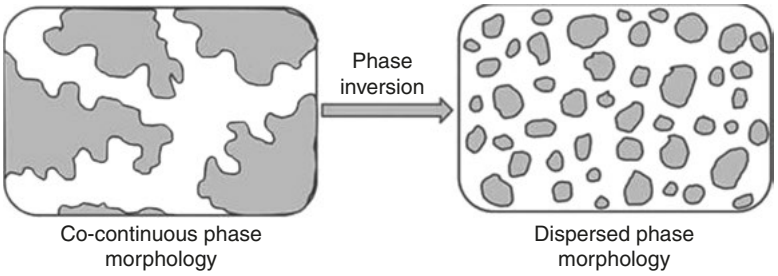


**Figure 3.3:** Development of TPV *via* phase inversion.

The dispersed rubber particle size generally varies over the range of 0.5–2.0 μm. The presence of dispersed rubber particles enhances the elasticity of the TPV, while the thermoplastic phase governs the melt processability. Therefore, compared with simple non-crosslinked blends, TPV have the following advantages [4]:

- Reduced permanent set and better elastic recovery.
- Higher ultimate mechanical properties.
- Improved fatigue resistance.
- Enhanced resistance to attack by fluids, e.g., hot oils.
- Improved high-temperature tolerance.
- Greater stability of phase morphology in the melt.
- Higher melt strength.

### 3.1.3 Concept of Dynamic Vulcanisation and Morphology Development of Thermoplastic Vulcanisates

During dynamic vulcanisation, the morphological development of TPV is primarily governed by two factors, i.e., the viscosity ratio of the elastomer/thermoplastic and the elastomer/thermoplastic composition ratio.

For TPV, the scheme of morphological development is depicted in Figure 3.4.

The beginning of the mixing process is characterised by the presence of non-molten thermoplastic pellets which ‘swim’ in the elastomer matrix. After complete melting of the thermoplastic phase, it is assumed that the two immiscible phases become thoroughly mixed resulting in the development of co-continuous morphology.

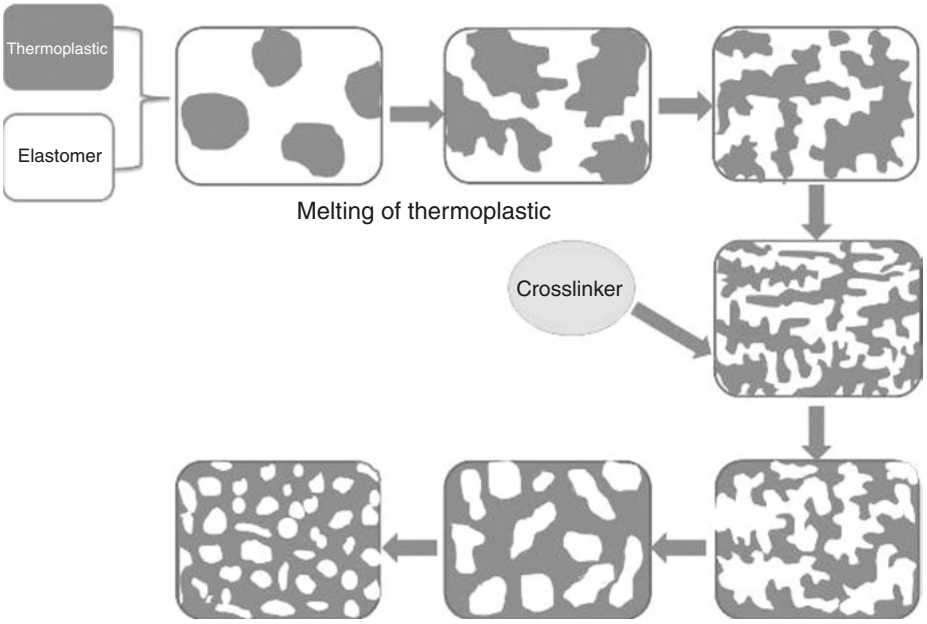


**Figure 3.4:** Scheme of morphological development during dynamic vulcanisation.

The combined effect of shear and elongational forces during mixing deforms the co-continuous morphology, which leads to the refinement of the co-continuous strands, i.e., preserving the cocontinuity, the strands become thinner. Crosslinking of the elastomer phase leads to an increment in the viscosity of this phase resulting in the simultaneous increment in shear and elongational forces acting on the system and thus, to an increased deformation of the co-continuous structure. After the threshold stress value is reached, the elastomer strands starts to break up into small particles which results in the dispersion of the crosslinked elastomer particles in a thermoplastic matrix. Thus, phase inversion occurs, resulting in final morphological changes from a thermoplastic dispersion in an elastomer matrix, *via* a co-continuous state, to dispersed crosslinked elastomer particles to a continuous thermoplastic matrix [5]. Hence, phase inversion enables the crosslinked elastomer to transition to the dispersed phase, even if the rubber phase or elastomeric component is the major component with volume fractions of ≥0.5. A finer particle size of the crosslinked elastomer particles depends upon the composition, viscosity ratio, interfacial tension, type of deformation and also the rates of deformation of the crosslinked elastomer particles. Thus, dynamic vulcanisation offers heterophasic morphology in the final commercial TPV, which is comprised of irregularly shaped elastomer particles with a broad size distribution.

### 3.1.4 Preparation of Thermoplastic Vulcanisates

In the case of TPV, a wider distribution of the rubber particles in the continuous thermoplastic matrix is crucial in order to obtain a high-quality product. Therefore, the processing conditions and parameters are important factors that govern the final TPV morphology. TPV can be prepared *via* three different mixing methods:

- Phase mixing
- Pre-blending
- Split addition

A flow diagram of the three mixing methods is shown in Figure 3.5.

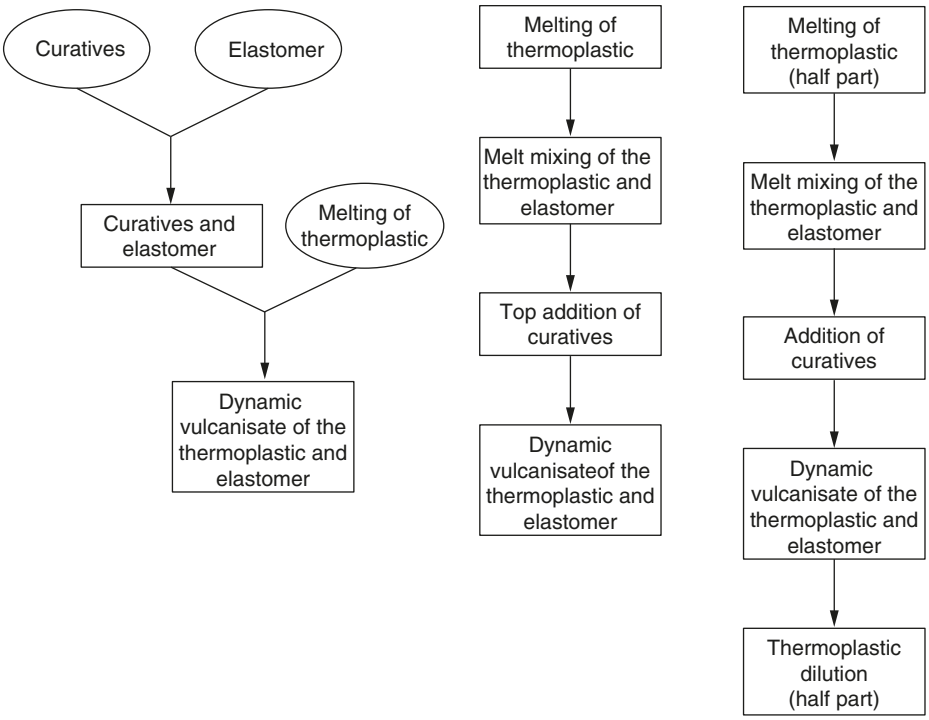


**Figure 3.5:** Preparation of TPV by different mixing methods.

For all the mixing processes, TPV showed better mechanical properties compared with its unvulcanised blends means TPE.

- Pre-blending method: the conventional method for preparing TPV. In this method, the first step involves melt mixing the thermoplastic and elastomer to obtain a homogeneous blend, a crosslinking agent is then added on top of the mix to form the TPV.

- Phase-mixing method: in this process, prior to mixing the thermoplastic and elastomer, a crosslinking agent is pre-blended with the elastomeric phase to form a curative masterbatch at low temperature. After that, the curative masterbatch is added to the molten thermoplastic phase at an elevated temperature to achieve dynamic vulcanisation under a high shear rate.
- Split addition method: firstly, half of the thermoplastic and all of the elastomer is melt mixed at an elevated temperature followed by the addition of the crosslinking agent. After completion of dynamic vulcanisation, the remaining half of the thermoplastic is added to the dynamic vulcanisate and mixing continues in order to facilitate the melting and mixing of the thermoplastic [6].

Among the above-mentioned three techniques, TPV produced using the split addition method exhibits poor mechanical behaviour, which may be due to the poor dispersion of the thermoplastic matrix phase that is added at a later stage of the mixing process. Even after increasing the mixing time, there was no significant improvement in the level of dispersion of the thermoplastic matrix phase. Generally, in the split addition method, the late addition of the half portion of the thermoplastic phase dilutes the matrix phase only. Few scientists have investigated the dilution effect of TPV, however, the dilution effect does not lead to a change in the final morphology of the TPV. The mean particle size remains more or less constant. The dilution effect results in an increment of mean particle distance only.

On the other hand, among the phase-mixed TPV and pre-blended TPV, the phase-mixed TPV shows a higher modulus value at low strain as well as non-linear behaviour. At the same time, in the phase-mixed TPV, the crosslink density of the dispersed elastomeric phase is higher than the crosslink density of the dispersed elastomeric phase of pre-blended TPV. Morphological analysis also demonstrates that the phase-mixed TPV exhibits smaller rubber domains whereas pre-blended TPV possess coarser rubber particles, as depicted in Figure 3.6 below.

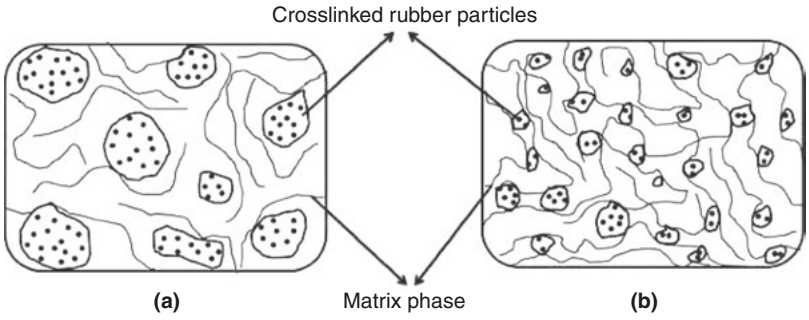


**Figure 3.6:** Possible structures of TPV prepared by (a) the pre-blending method and (b) the phase-mixing method.

Smaller crosslinked rubber domains have a higher tendency to adsorb the thermoplastic chains on the surface, forming more trapped thermoplastic chains by connecting the particles. The adsorbed chains on the surface of the domains, via physical or chemical adsorption, usually broaden the relaxation spectrum towards longer periods, which results in a higher dynamic modulus and viscosity in frequency and strain sweep experiments.

## 3.2 Various Types of Thermoplastic Vulcanisates

### 3.2.1 Polypropylene–Ethylene Propylene Diene Rubber-based Thermoplastic Vulcanisates

Most commercially applicable TPV are typically based on polypropylene (PP) and ethylene propylene diene monomer rubber (EPDM), in which EPDM rubber is selectively crosslinked during melt mixing with the PP phase. In the case of EPDM, the presence of a saturated main chain backbone results in excellent stability against heat, oxygen and ozone to the corresponding TPV. Dynamic vulcanisation of the EPDM rubber can be carried out in the presence of several crosslinking agents, such as activated phenol formaldehyde resins (commonly known as resol resins), co-agent-assisted peroxides, a sulfur-accelerator system, platinum-catalysed hydrosiloxane, vinyltrialkoxysilane/moisture, catalysed quinonedioxime and bisthiols, and so on.

#### 3.2.1.1 Phenolic Resin-cured Thermoplastic Vulcanisates

Phenolic resins are usually classified into two categories, namely resols and novolacs. Resols contain a reactive methylol group and dimethylene ether units, which are shown in Figure 3.7.

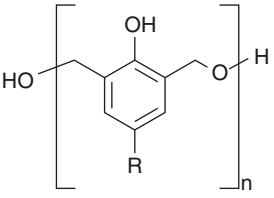


**Figure 3.7:** Typical structure of resol (R = iso-octyl, n = 1–3).

However, novolacs do not contain any reactive methylol functionalities and therefore cannot act as a crosslinking agent. Resols have been used extensively for the crosslinking of EPDM rubber during the manufacture of PP–EPDM TPV.

Abdou-Sabet and Fath demonstrated the improvement of rubber-like properties (compression set, oil resistance and processing characteristics) of PP–EPDM-based TPV in the presence of dimethylol octyl phenol curing resin [7]. Phenolic-resin curatives containing dibenzyl ether linkages were unexpectedly found to be much more effective in crosslinking the rubber in the PP–EPDM blend compared with that of the conventional phenolic resin.

Moisture absorption, even at an ambient temperature, and staining issues (the appearance of a dark brownish colour) excluded the application of conventional phenolic-resin-cured PP–EPDM TPV from various applications. Esterification (acetylation, tosylation, silylation) of phenolic-resin curatives eliminates the chance of staining.

#### 3.2.1.2 Sulfur-cured Thermoplastic Vulcanisates

Dynamic vulcanisation of PP–EPDM and PE–EPDM blends in the presence of a sulfur-accelerator system has been studied by Coran and Patel [8]. A typical composition of TPV is given in Table 3.1.

**Table 3.1:** Typical recipe for sulfur-cured TPV.

| Component | Amount (phr) |
|---|---|
| EPDM | 100 |
| Polyolefin resin | X |
| ZnO | 5 |
| Stearic acid | 1 |
| Sulfur | Y |
| Tetramethylthiuram disulfide | Y/2 |
| Mercapto benzothiazole | Y/4 |

ZnO: Zinc oxide

The amount of polyolefin resin (X phr) and sulfur (Y phr) were varied, with an increment of sulfur from 0 to 2.0 phr resulting in a drastic improvement of the physico-mechanical properties of PP–EPDM TPV. During dynamic vulcanisation, a reduction in particle size led to rapid improvement of elongation at break (EB) (from 190 to 530%) and tensile strength (TS) (from 4.9 to 24.3 MPa).

However, a sulfur-accelerator system is not commercially applied in PP–EPDM TPV, since PP has a high melting point and the crosslinks lack thermal and ultraviolet stability. Apart from during the production and processing of PP–EPDM TPV, the unpleasant odour is another issue.

### 3.2.1.3 Peroxide-cured Thermoplastic Vulcanisates

Unlike the reaction mechanism of accelerated sulfur vulcanisation, the basic chemistry of peroxide decomposition and subsequent crosslink-forming reactions is well established for various unsaturated and saturated elastomer systems. The general advantages of peroxide crosslinking systems can be summarised as follows [9]:

- Simple formulation.
- Rapid vulcanisation without reversion.
- Ability to crosslink saturated as well as unsaturated rubbers; the crosslinking mechanism is shown in Figure 3.8.

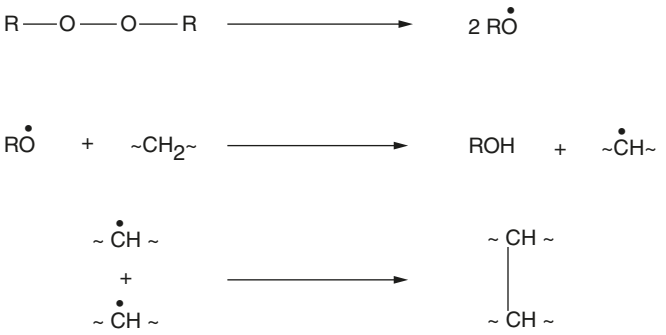


**Figure 3.8:** Mechanism of peroxide crosslinking.

- High-temperature resistance of the vulcanisates.
- Better compression set properties (elastic recovery) of the vulcanisates even at elevated temperature.
- No moisture uptake of the TPV.
- Ability to store the peroxide-containing compound over a long period without scorching.
- No staining or discolouration of the finished products.
- The influence of various peroxides with different chemical structures on PP–EPDM TPV at a fixed, as well as a varied, blend ratio was thoroughly explored by Naskar and Noordermeer [10]. Table 3.2 summarises the peroxide-cured TPV composition based on PP–EPDM at a fixed blend ratio.

The chemical and commercial names and structures of the various peroxides are detailed in Table 3.3.

Only a limited number of experiments could be performed with TTTP due to restricted availability. For peroxide crosslinked TPV it has been found that, in general, three different parameters (the solubility parameter of peroxide relative to the

**Table 3.2:** TPV composition (phr) at a fixed PP–EPDM blend ratio.

| Component | Amount (phr) |
|---|---|
| EPDM | 200.0 |
| PP | 50.0 |
| Irganox® 1076 | 0.4 |
| Irgafos® 168 | 0.4 |
| Peroxide | Varying doses (0.0–7.0) |
| Co-agent | 4.0 |

polymers, the decomposition mechanism of the peroxide and the kinetic aspects of the peroxide fragmentation) govern the final mechanical properties of the TPV [2, 11]. The closer the solubility parameter of the peroxide to that of the rubber, the higher the TS and the better is the compression set property. Table 3.4 summarises the physical properties of different peroxide-cured PP–EPDM TPV at varied blend ratios.

From the table, it can be seen that DCP in the presence of triallyl cyanurate (TAC) as a co-agent gives the overall best balance of physico-mechanical and elastic recovery properties of PP–EPDM TPV. In general, the commonly used peroxides produce volatile decomposition products, which lead to an unpleasant smell (for DCP) in the final TPV, or these peroxides can exhibit the blooming effect (for DTBPIB). Therefore, Naskar and co-workers also studied the influence of multifunctional peroxides to eliminate the drawbacks of commonly used peroxides.

Kajari and co-workers developed TPV based on a PP matrix and polar maleated-ethylene propylene rubber (m-EPM), which is basically a chemically-modified EPM rubber [12]. Incorporation of polar maleic groups resulted in additional features for m-EPM, such as moderate TS and EB. It also provided very high heat resistance, weather resistance and resistance to different aggressive chemicals such as acid, alkali and so on. Furthermore, it exhibits very good electrical properties and excellent fatigue resistance, as well as good abrasion resistance, low-temperature tolerance and adhesion characteristics, especially with polar substrates. All the PP–m-EPM-based TPV were developed in the presence of peroxide (DCP) using maleated-polypropylene (m-PP) as a compatibiliser. TPV were developed using a batch process at a fixed and varied blend ratios. Table 3.5 summarises the TPV compositions with different DCP concentrations (0–3 phr) at a fixed blend ratio of PP–m-EPM.

Stress–strain properties of the PP–m-EPM-based TPV are given in Table 3.6.

Table 3.6 clearly shows that the TS of m-EPM-based TPV varies from 3.5 to 7.3 MPa and EB varies from 120 to 240%. TS and EB reach a maximum at a DCP concentration of 2 phr, which may be due to β-chain scission of the PP thermoplastic phase at a higher concentration of peroxide. Other mechanical properties such as the moduli, hardness and tear strength of TPV have also been found to increase with increasing DCP concentration.

**Table 3.3:** Chemical/commercial names and structures of the peroxides used.

| Chemical/commercial name | Chemical structure |
|---|---|
| DTBPH (Trigonox® 101-40D) (40%) (dialkyl type) | 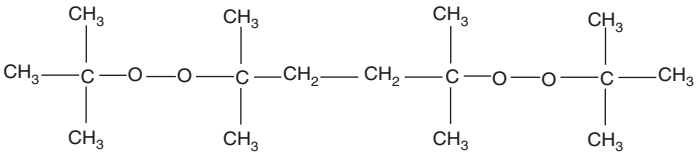 |
| DTBPHY (Trigonox® 145-45B) (45%) (dialkyl type) | 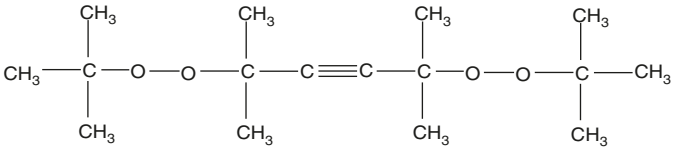 |
| DTBPIB (Perkadox® 14-40B) (40%) (alkyl-aralkyl type) | 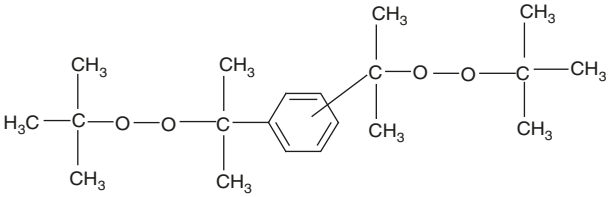 |
| DCP (Perkadox® BC-40B) (40%) (diaralkyl type) | 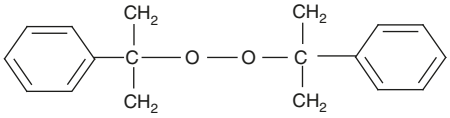 |
| TTTP (41%) (cyclic type) | 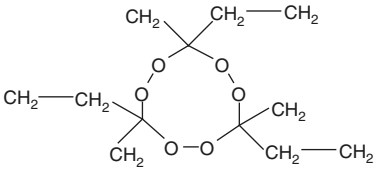 |

DCP: Dicumyl peroxide
DTBPH: 2,5-Dimethyl-2,5-di(*tert*-butylperoxy)hexane
DTBPHY: 2,5-Dimethyl-2,5-di(*tert*-butylperoxy)hexyne-3
DTBPIB: Di-(2-*tert*-butylperoxyisopropyl)benzene
TTTP: 3,6,9-Triethyl-3,6,9-trimethyl-1,4,7-triperoxonane

**Table 3.4:** TPV compositions (phr) at varied PP–EPDM blend ratios with peroxide concentrations of 9 milliequivalents and corresponding properties.

| | | | | | | | | |
|---|---|---|---|---|---|---|---|---|
| EPDM | 200 | 200 | 200 | 200 | 200 | 200 | 200 | 200 |
| PP | 50 | 100 | 50 | 100 | 50 | 100 | 50 | 100 |
| DTBPH | 3.3 | 3.3 | – | – | – | – | – | – |
| DTBPHY | – | – | 2.9 | 2.9 | – | – | – | – |
| DTBPIB | – | – | – | – | 3.8 | 3.8 | – | – |
| DCP | – | – | – | – | – | – | 6.1 | 6.1 |
| TAC | 4.0 | 4.0 | 4.0 | 4.0 | 4.0 | 4.0 | 4.0 | 4.0 |
| Irganox® 1076 (stabiliser) | 0.4 | 0.4 | 0.4 | 0.4 | 0.4 | 0.4 | 0.4 | 0.4 |
| Irgafos® 168 (stabiliser) | 0.4 | 0.4 | 0.4 | 0.4 | 0.4 | 0.4 | 0.4 | 0.4 |
| TS (MPa) | 4.2 | 6.7 | 3.9 | 6.2 | 4.5 | 6.6 | 4.7 | 7.4 |
| EB (%) | 455 | 419 | 401 | 387 | 440 | 416 | 472 | 375 |
| Modulus at 300% (MPa) | 3.3 | 5.9 | 3.5 | 5.7 | 3.5 | 5.6 | 3.4 | 5.5 |
| Hardness (Shore A) | 61 | 85 | 61 | 86 | 63 | 87 | 61 | 88 |
| Overall crosslink density (v + PP) × $10^5$(mol/ml) | 9.9 | 18.6 | 12.0 | 16.3 | 8.9 | 17.5 | 13.5 | 19.3 |

TAC: Triallyl cyanurate

**Table 3.5:** TPV compositions with different DCP concentrations at a fixed PP–m-EPM blend ratio.

| **Components** | **N-01** | **N-02** | **N-03** | **N-04** | **N-05** | **N-06** |
|---|---|---|---|---|---|---|
| m-EPM | 100 | 100 | 100 | 100 | 100 | 100 |
| PP | 60 | 60 | 60 | 60 | 60 | 60 |
| m-PP | 10 | 10 | 10 | 10 | 10 | 10 |
| Paraffinic oil | 25 | 25 | 25 | 25 | 25 | 25 |
| DCP (98%) | 0 | 1.0 | 1.5 | 2.0 | 2.5 | 3.0 |
| TAC (50%) | 0 | 4 | 4 | 4 | 4 | 4 |

**Table 3.6:** Mechanical properties of the TPV.

| **Properties** | **N-01** | **N-02** | **N-03** | **N-04** | **N-05** | **N-06** |
|---|---|---|---|---|---|---|
| TS (MPa) | 3.5 | 6.3 | 6.6 | 7.3 | 6.2 | 5.7 |
| EB (%) | 120.0 | 178.0 | 219.0 | 240.0 | 159.0 | 177.0 |
| Modulus at 50% (Mpa) | 3.5 | 3.9 | 4.0 | 4.1 | 4.2 | 4.3 |
| Modulus at 100% (Mpa) | 4.5 | 5.0 | 5.1 | 5.2 | 5.8 | 5.9 |
| Hardness (Shore A) | 60.0 | 65.0 | 68.0 | 70.0 | 72.0 | 73.0 |
| Tension set (%) | – | 16.1 | 14.2 | 12.2 | 10.2 | 8.2 |
| Tear strength (N/mm) | – | 20.1 | 35.0 | 42.4 | 45.8 | 52.1 |

### 3.2.1.4 Thermoplastic Vulcanisates based on Electron-induced Reactive Processing

The disadvantages of peroxide-cured TPV has increased the demand for alternative techniques to develop TPV. In this respect, dynamic vulcanisation *via* electron-induced reactive processing (EIReP) is a novel technique in which chemical reactions are induced by a spatial and temporal precise energy input *via* high-energy electrons under the dynamic conditions of melt mixing. A schematic representation of the unique set up of the EIReP process is demonstrated in Figure 3.9.

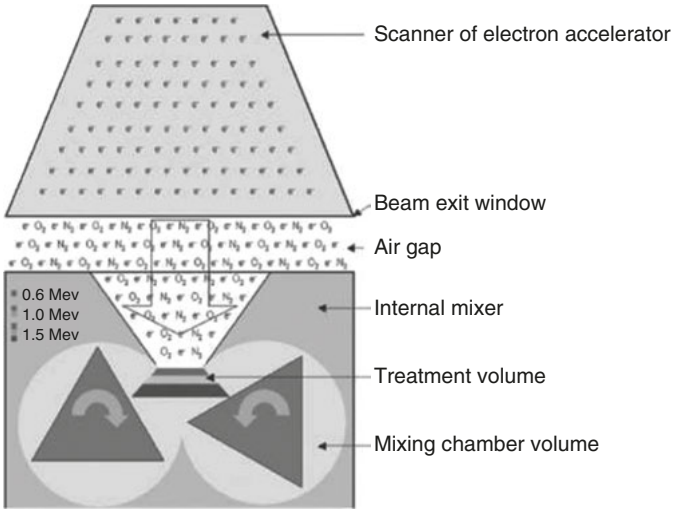


**Figure 3.9:** EIReP.

Naskar and co-workers investigated PP–EPDM TPV via EIReP [13]. All the TPV were developed using a batch process and during TPV preparation, the experimental variables were absorbed dose (25, 50 and 100 kGy), electron treatment time (15, 30 and 60 s) and electron energy (0.6 and 1.5 MeV). The physico-mechanical properties (E modulus, TS, EB) of the TPV are listed in Table 3.7.

The experimental data at 1.5 MeV and an electron treatment of 60 s shows that increasing the absorbed dose from 25 to 50 kGy, significantly improved the TS, EB and E modulus of the TPV. In the case of the untreated sample, the TS was only 4.7 ± 0.1 MPa and EB was 46 ± 5%. At 50 kGy, the TS was 9.2 ± 0.3 MPa and EB was 298 ± 35%. A further increase in dose to 100 kGy resulted in a small increase of TS to 9.8 ± 0.2 MPa, whereas EB remained constant (282 ± 28%). The experimental data at 1.5 MeV and 100 kGy shows that decreasing the electron treatment time from 60 to 15 s, further improved the TS and EB, whereas the

**Table 3.7:** PP–EPDM TPV produced *via* electron-induced reactive processing.

| Electron energy (MeV) | Dose (kGy) | Treatment time (sec) | *E* modulus (MPa) | TS (MPa) | EB (%) |
|---|---|---|---|---|---|
| 0.0 | 0 | 0 | 112 ± 12 | 4.7 ± 0.1 | 46 ± 5 |
| 1.5 | 25 | 60 | 159 ± 11 | 7.0 ± 0.1 | 135 ± 15 |
| 1.5 | 50 | 60 | 156 ± 4 | 9.2 ± 0.3 | 298 ± 35 |
| 1.5 | 100 | 60 | 173 ± 20 | 9.8 ± 0.2 | 282 ± 28 |
| 1.5 | 100 | 30 | 191 ± 8 | 9.5 ± 0.7 | 215 ± 80 |
| 1.5 | 100 | 15 | 176 ± 3 | 14.7 ± 0.5 | 624 ± 41 |
| 0.6 | 50 | 60 | 150 ± 35 | 8.2 ± 0.4 | 168 ± 42 |

*E* modulus remained constant at a level of 178 ± 2 MPa. Thus, the electron treatment time influences the dose rate as well as absorbed dose per rotation and are additional parameters controlling the stress–strain behaviour of the PP–EPDM TPV.

### 3.2.2 Polypropylene–Ethylene Octane Copolymer-based Thermoplastic Vulcanisates

Ethylene-α-olefins or polyolefin elastomers (POE), also known as plastomers, are a relatively new class of polymers that have emerged as a leading material for automotive interior and exterior applications, wires and cables, extruded and moulded goods, film applications, medical goods, adhesives, footwear, and foams and so on. Uniform intermolecular and intramolecular comonomer distribution results in a low-density product and the physical properties span the range between plastic and elastomeric behaviour [14].

Attempts have been made by Rajesh and co-workers to develop TPV based on a PP–ethylene octane copolymer (EOC) system [15]. A detailed investigation focused on a peroxide-cured PP–EOC TPV system, as phenolic resin is ineffective because it requires the presence of a double bond to form a crosslinked network structure. In the presence of peroxide, both the saturated and unsaturated polymer became crosslinked. In addition, the influence of structurally different peroxides with varying concentrations, at a fixed blend ratio of PP–EOC blends, during the preparation of peroxide-cured PP–EOC-based TPV has been investigated. A peroxide-cured TPV composition based on a PP–EOC blend is shown in Table 3.8.

Three structurally different peroxides, namely DCP, *tert*-butyl cumyl peroxide (TBCP) and DTBPIB were studied and the peroxide concentration (X phr) was varied from 0.5–7.0 milliequivalents.

In order to understand the effect of molecular characteristics (especially molecular mass) on the property enhancement of the prepared TPV, two types of EOC with the same octene content but different molecular masses were studied. It was found

**Table 3.8:** PP–EOC-based TPV composition (phr) at a fixed blend ratio.

| Component | Amount (phr) |
|---|---|
| EOC | 100.0 |
| PP | 50.0 |
| Peroxide | X |
| Co-agent (TAC) | 2.0 |

that DCP gives the best overall balance of properties for the PP–low-molecular weight EOC-based TPV, whereas TBCP is better for the PP–high-molecular weight EOC-based TPV.

Furthermore, the influences of different co-agents on the peroxide-cured PP–EOC-based TPV were investigated [16]. In general, co-agents are multifunctional vinyl monomers which are highly reactive towards free radicals either *via* the addition reaction and/or by hydrogen abstraction. Chain scission can be retarded *via* stabilising the PP macroradicals by the addition reaction across the double bond in the vinyl monomer (co-agent). It not only improves the end-use properties but also decreases the peroxide concentration and aids the flow characteristics during processing. TPV were prepared using three different co-agents, namely TAC, trimethylolpropane triacrylate (TMPTA) and *N*,*N*′-m-phenylene dimaleimide (MPDM). A typical recipe for PP–EOC-based TPV by varying the concentration of co-agents is given in Table 3.9.

**Table 3.9:** TPV composition (phr) with varying types and concentrations of co-agents at a fixed PP–EOC blend ratio.

| Component | Amount (phr) |
|---|---|
| EOC | 100.0 |
| PP | 50.0 |
| Peroxide (DCP) | 3.38 |
| Co-agent | Y |

The co-agent concentration (Y phr) was varied from 10.0–30.0 milliequivalents. It was observed that among the various co-agents used, TPV containing MPDM exhibited the best balance of mechanical properties, which is clearly shown in Figure 3.10.

Three different mixing procedures (as mentioned in Section 3.1.4) were also studied to develop PP–EOC-based TPV. The TPV made by adding an EOC-curative masterbatch to the molten PP (phase-mixing method) exhibited better mechanical

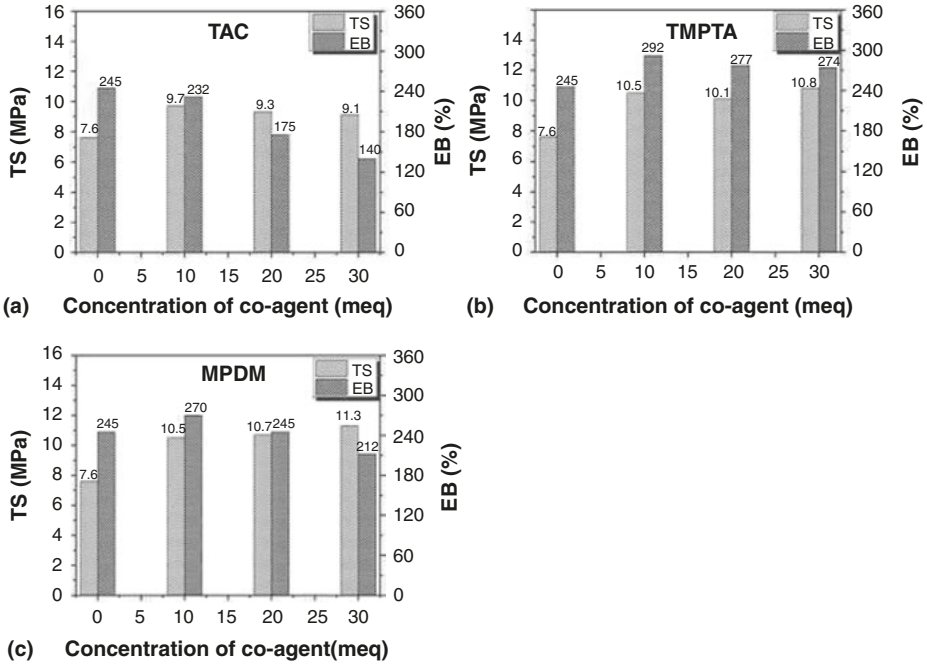


**Figure 3.10:** TS and EB as a function of concentration of different co-agents (a) TAC, (b) TMPTA and (c) MPDM of PP–EOC-based TPV.

properties and finer phase morphology than TPV prepared by pre-blending and the split addition method.

To eliminate the disadvantages of peroxide-cured TPV, similar to PP–EPDM TPV, EIReP was also applied for the production of PP–EOC TPV [17]. In this case, PP–EOC TPV at a 50:50 weight ratio were developed using a batch process. The experimental variable was exposure time (16, 32 and 64 s), while keeping the absorbed dose (100 kGy) and electron energy (1.5 MeV) constant. The samples were designated as polyethylene (PE)-control, PE-16 s, PE-32 s and PE-64 s for the PP–EOC blend treated with an exposure time of 0, 16, 32 and 64 s, respectively. The mechanical properties of PP–EOC TPV, prepared by EIReP at 1.5 MeV and 100 kGy in an oxygen atmosphere with varying exposure time, are summarised in Table 3.10.

It is evident from the table that the mechanical properties increased upon decreasing the exposure time. The gel content value also decreased upon increasing the exposure time, which can be clearly seen in Figure 3.11.

The maximum gel content value (18%) was observed for the sample irradiated at 16 s. Thus, the decrease in mechanical properties and lower gel content with longer electron exposure time can be related to the reduced crosslinking of the EOC phase in the presence of an oxygen atmosphere, as well as increased chain scission in both EOC and PP phases.

**Table 3.10:** Mechanical properties of PP–EOC uncrosslinked and EIReP-modified blends.

| Compound name | TS (MPa) | EB (%) | 100% modulus (MPa) |
|---|---|---|---|
| PE-c (control) | 10.8 ± 0.6 | 147 ± 12 | 10.6 ± 0.1 |
| PE-16 s | 11.0 ± 0.4 | 208 ± 10 | 10.6 ± 0.2 |
| PE-32 s | 9.4 ± 0.2 | 58 ± 12 | – |
| PE-64 s | 8.4 ± 0.5 | 23 ± 5 | – |

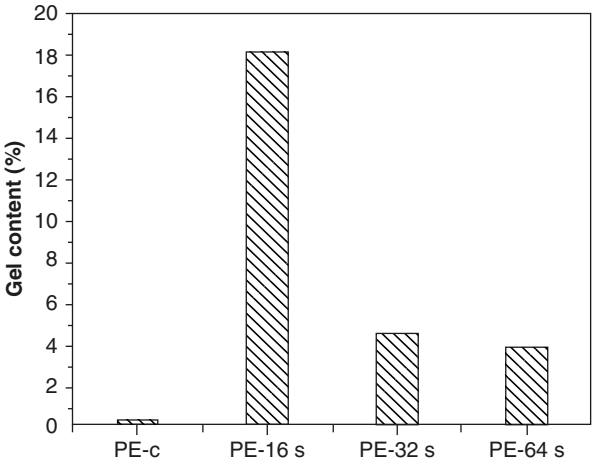


**Figure 3.11:** Gel content values of uncrosslinked and EIReP-modified blends.

Furthermore, PP–EOC TPV of a 30:70 weight ratio was also made using a batch process. In that case, the experimental variable was absorbed dose (25, 50 and 100 kGy), while keeping the exposure time (16 s) and electron energy (1.5 MeV) constant. D0, D25, D50 and D100 are the sample designations according to the absorbed dose. Stress–strain curves of the PP–EOC TPV with varying absorbed dose are shown in Figure 3.12.

From the figure it can be seen that as the absorbed dose increases, the 100% modulus and Young's modulus values steadily increase while EB decreases gradually. At the same time, the gel content value also increases at a higher dose.

## 3.2.3 Miscellaneous Thermoplastic Vulcanisates

With regards to the ongoing demand for commercial and industrial applications of TPV, several combinations of rubbers and thermoplastic blends have already been

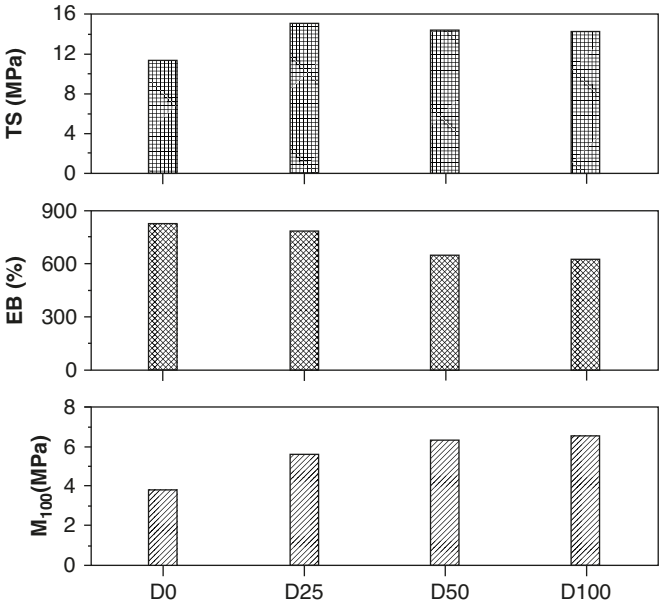


**Figure 3.12:** Stress–strain properties of unmodified and EIReP-modified PP–EOC samples.

tested. The list includes: natural rubber (NR), EPDM, isoprene isobutylene rubber/butyl rubber, styrene-butadiene rubber, polybutadiene rubber (BR), ethylene-vinyl acetate (EVA), alkyl acrylate copolymer/acrylate rubber, acrylonitrile-butadiene rubber (NBR), polychloroprene, chlorinated PE and so on, as rubber constituents; with PE, PP, polystyrene, styrene acrylonitrile (SAN), acrylonitrile-butadiene-styrene, polymethyl methacrylate, polybutylene terephthalate, PA and polycarbonate and so on, as thermoplastic counterparts. Unfortunately, only a few of the blends are suitable for commercial as well as industrial applications, as most of the blends are incompatible in nature. However, conventional TPV based on a PP matrix and a vulcanisated EPDM rubber or ethylene-α-olefins (or POE) have found limited use in automotive under-the-hood applications that require continuous use temperatures exceeding 135 °C and good oil resistance properties [18].

TPV based on a linear low-density polyethylene–polydimethyl siloxane (PDMS) blend system has been suggested by Giri and co-workers [19]. A TPV of silicone rubber and EOC has also been developed by researchers for a specific purpose [20]. However, it has limited use in automotive applications due to poor oil resistance properties associated with the olefinic thermoplastic matrices.

Subsequently, a new generation of TPV, based on crosslinked silicone rubber particles dispersed in a variety of engineering thermoplastic matrices, was developed. Chatterjee and co-workers explored the newly developed TPV based on silicone rubber (PDMS) and a PA12 thermoplastic matrix at a fixed blend ratio in the

presence of various peroxides [21]. Three structurally different peroxides, namely DCP, 3,3,5,7,7-pentamethyl-1,2, 4-trioxepane (PMTO) and cumyl hydroperoxide were chosen for investigation. It was observed that PMTO-crosslinked TPV exhibited superior mechanical, thermal and rheological behaviour compared with that of the other peroxide-crosslinked TPV. PMTO-crosslinked TPV led to a TS of 26.5 MPa and EB of 127%, whereas DCP-crosslinked TPV gave a TS of 19.6 MPa and EB of only 51%.

Following this, a new family of polar TPV, comprising of an ethylene acrylic dipolymer elastomer and PA12 at different blend ratios, was developed in the presence of peroxide and characterised in detail by Reffai and co-workers [22]. Although TPV possess superior heat and oil ageing behaviour, and also provide better thermal stability, poor mechanical behaviour and set properties were the main disadvantages of that particular system.

Recently, thermally-crosslinked and sulfur-cured soft TPV based on styrenic block copolymer styrene-ethylene-*co*-butylene-styrene (SEBS)/solution styrene-butadiene rubber (S-SBR) blends were reported by Dey and co-workers [23, 24]. A typical recipe of SEBS/S-SBR TPV is given in Table 3.11.

**Table 3.11:** SEBS/S-SBR based TPV composition (phr) at a fixed blend ratio.

| Component | Amount (phr) |
|---|---|
| S-SBR | 100.0 |
| SEBS | 100.0 |
| ZnO | 3.0 |
| Stearic acid | 2.0 |
| 2,2,4-Trimethyl-1,2-dihydroquinoline (antioxidant) | 1.0 |
| Sulfur | X |
| N-*tert*-butyl-2-benzothiazyl sulfenamide (accelerator) | Y |

Depending upon the semiefficient vulcanisation (SEV) and efficient vulcanisation (EV) system, the sulfur (X phr) and accelerator content (Y phr) were varied. Finally, the physico-mechanical properties of sulfur-cured TPV of SEBS/S-SBR-based TPV are shown in Table 3.12.

**Table 3.12:** Mechanical properties of a sulfur-cured TPV of a SEBS/S-SBR blend.

| System | TS (MPa) | EB (%) | 100% modulus | 200% modulus | 300% modulus | Hardness (Shore A) |
|---|---|---|---|---|---|---|
| SEV | 4.8 | 672 | 0.9 | 1.4 | 2.0 | 52 |
| EV | 4.9 | 533 | 1.1 | 1.7 | 2.6 | 55 |

### 3.2.4 End-use Applications of Thermoplastic Vulcanisates

TPV have found potential and proven applications in various areas including:

- Mechanical rubber goods applications: gaskets, seals, convoluted bellows, flexible diaphragms, tubing, mounts, bumpers, valves, housings, glazing seals, vibration isolators, plugs, connectors, caps, oil-well injection lines and so on.
- Under-the-hood applications in the automotive field: air conditioning hose cover, fuel line hose cover, vacuum tubing, vacuum connectors, seals, body plugs, bushings, protective sleeves, shock isolators and so on.
- Industrial hose applications: industrial tubing, hydraulic (wire braided), agricultural spray, paint spray, mine hose and so on.
- Electrical applications: wire and cable insulation, plug, bushings, enclosures, connectors and so on.
- Consumer goods: sporting goods, portable kitchen appliances, business appliances and so on [25].

## 3.3 Concept of Nanocomposites

### 3.3.1 Composites

Composite materials are solid multiphase materials that are made by the combination of more than one component with different structural, physical and chemical properties, which makes composite materials different from other multicomponent systems such as blends and alloys. This means composite materials are custom-tailored to obtain certain target properties that will meet special requirements for specific engineering applications. Thus, composite materials possess a combination of the properties of the component materials such as weight, strength, stiffness, permeability, electrical conductivity, biodegradability and optical properties, which are difficult to obtain by separate individual component materials [26].

It is well known that in a composite material the filler particles are in a well-dispersed state in a continuous matrix phase. Based on the nature of the matrix phase, composite materials can be divided into three categories:

- Metallic
- Ceramic
- Polymeric

Polymer materials have their advantages over metals and ceramics, including low cost, light weight, ease of processing and so on. Although the disadvantages of polymeric materials include lower modulus values and low strength properties, compared with metals and ceramics, the ongoing demand and commercial importance of these

materials has led to the continuous improvement of these properties to meet the required specifications. Thus, the development of polymeric composites is gaining considerable interest that will result in polymeric materials with improved properties while maintaining its light weight, low density and ductile behaviour.

### 3.3.2 Polymeric Composites

The combination of a polymer with a synthetic or natural filler leads to the formation of polymeric composites. Fillers are mainly used for two reasons:

- To fulfil the desired properties of the polymer.
- Simply to reduce the cost.

The improved mechanical, thermal and barrier properties, and flame-retardancy behaviour of polymer composites has led to a wide range of large-scale applications in various engineering fields. However, the application of a conventional filler (talc, calcium carbonate, fibres and so on) requires a large quantity of fillers in the polymer matrix to achieve significant improvements in the properties of the composite, which may result in some undesired properties such as brittleness or loss of opacity. The ultimate properties of the reinforced polymers (composites) are influenced by the nature, properties and loading of the components, dimensions of the components, interfacial interaction between the matrix and the dispersed phase, and also on the microstructure of the composite. The efficiency of the improvement in specific properties strongly depends on the properties of the filler, adhesion between the matrix and the filler, and especially on the aspect ratio of the filler. The aspect ratio of the filler plays a crucial role in the improvement of the composite's properties, such as electrical, mechanical and thermal. As a result, nanofillers with a high aspect ratio, such as layered clays, nanotubes and nanofibres, are gaining considerable interest for the development of polymeric nanocomposites.

### 3.3.3 Polymer Nanocomposites

In polymer nanocomposites, the nanoscale dispersion (well known as the nanoeffect) of the nanofiller (with at least one dimension in the nanometre range) within the polymer matrix leads to the tremendous improvement of certain properties, e.g., modulus, strength, toughness, barrier properties, flame retardancy and optical properties, compared with those of conventional microcomposites [27]. The presence of particle sizes in the nanometre dimension and large interfacial interactions between the polymer matrix and nanofillers results in a remarkable improvement of the performance properties of the polymer nanocomposites.

Hence, in the field of polymer science research and technology, polymer nanocomposites are gaining significant interest. Compared with the conventional filled polymer systems with loading levels from 10 to 40 wt%, low levels of nanofiller loading (<5 wt%) are sufficient to achieve superior properties of polymer nanocomposites. Light weight, low density and ease of processability of polymer nanocomposites, with respect to conventional composites, make them competitive with other materials for particular applications.

## 3.3.4 Various Types of Nanofillers for the Development of Polymer Nanocomposites

Based on the shapes of the nanofillers used to prepare polymer nanocomposites, they can be broadly categorised into three different classes, as shown in Figure 3.13.

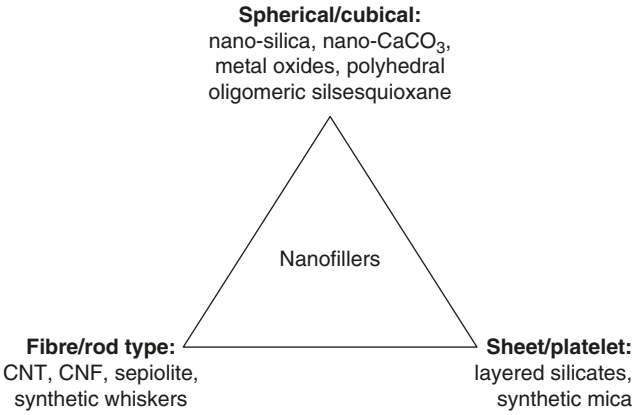


**Figure 3.13:** Classification of nanofillers [CNF: carbon nanofibre(s); CNT: carbon nanotube(s) and MMT: montmorillonite].

Among the above-mentioned nanofillers, nano-silica, CNT and specially layered silicates have potential applications [28].

### 3.3.4.1 Nano-silica

Nanoparticles of silicon dioxide, also known as silicon dioxide or nano-silica, are becoming an important nanofiller for polymer matrices. Nano-silica can be prepared *via* the sol-gel technique and it can be obtained in powder form. Nano-silica is a highly porous material and has a large surface area with a microstructure

network. The large surface area and size of the silica particles have played a key role in enhancing certain mechanical properties due to embedded silica in the polymer matrix [29].

#### 3.3.4.2 Carbon Nanotubes

As the word nanotube implies, the diameter of a nanotube is in the order of a few nanometres (approximately 50,000 times smaller than the width of a human hair) and can be up to several micrometres in length. CNT, a member of the fullerene structural family, are cylindrical carbon molecules with outstanding chemical, mechanical, thermal and electrical properties that enrich its use as a nanofiller for applications in various fields [30].

#### 3.3.4.3 Layered Silicates

Layered silicates are natural or synthetic minerals that consist of regular stacks of aluminosilicate layers with a high aspect ratio and high surface area. $(SiO_4)^{4-}$ tetrahedron is the basic chemical unit for silicates.

Based on the structure, silicates can be divided into the subclasses shown in Figure 3.14.

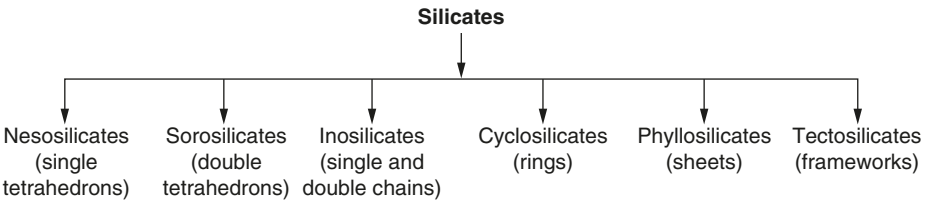


**Figure 3.14:** Classification of silicates.

Layered silicates mostly belong to the phyllosilicate group and usually consist of a layer of clay mineral, of about 1 nm thickness, and another layer of platelets of around 100 nm in width, which represents a significantly high aspect ratio. Layered silicates are usually clay minerals which assemble regularly with the unit crystalline layer on the nanoscale. According to the unit and ratio of crystal types, layered silicates can also be subcategorised into three classes, as shown in Figure 3.15.

However, the smectite group (2:1) clays are the most commonly used nanofillers for polymers. Table 3.13 depicts the chemical formula of MMT, hectorite and saponite, respectively.

**Table 3.13:** Smectite groups and their chemical structure.

| Smectite family | Chemical structure |
|---|---|
| MMT | $M_x(Al_{4-x}Mg_x)Si_8O_{20}(OH)_4$ |
| Hectorite | $M_x(Mg_{6-x}Li_x)Si_8O_{20}(OH)_4$ |
| Saponite | $M_xMg_6\ (Si_{8-x}Al_x)Si_8O_{20}(OH)_4$ |

M: Monovalent cation
x: Degree of isomorphous substitution

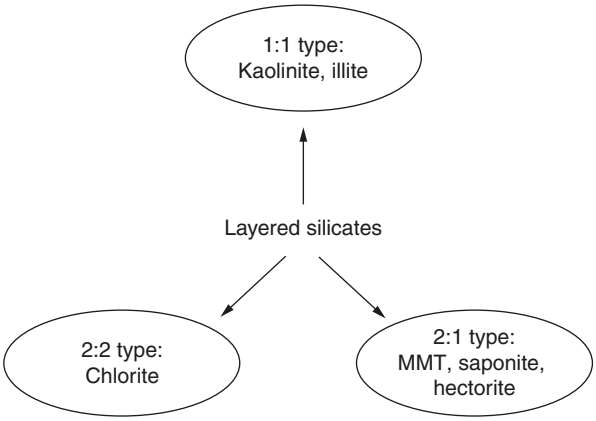


**Figure 3.15:** Classification of layered silicates.

Out of the smectite family, MMT is preferably used for the development of thermoplastic vulcanisate nanocomposite(s) (TPVN).

### 3.3.4.4 Montmorillonite

MMT belongs to the 2:1 type phyllosilicate group and has been the subject of considerable attention because of its unique features, including:

- Naturally abundant
- Suitable layered silicate structure
- Non-toxic
- Inexpensive
- Chemically and thermally stable

One layer of MMT consists of two tetrahedral layers of silica (SiO4), sandwiching an edge-shared octahedral sheet of alumina (AlO6), as shown in Figure 3.16. Due to weak binding and large spacing between the layered sheets, MMT can absorb water

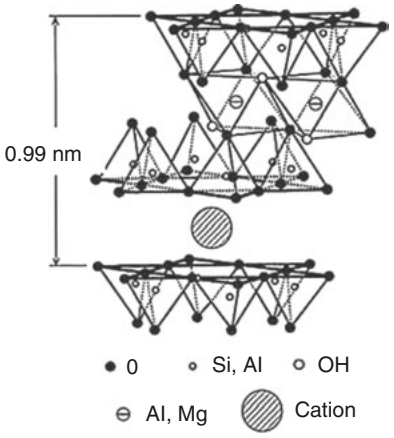


**Figure 3.16:** MMT clay.

between the charged layers, making it hydrophilic in nature [31]. Therefore, MMT is a water expandable clay mineral of the smectite family.

The hydrophilic nature of MMT clays hinders their interaction with organic polymers, which are hydrophobic in nature. In order to enhance the miscibility between the MMT clays and other organic polymers, organic modification or surface treatment is necessary. Therefore, it is essential to exchange the alkali ions ($Na^+$, $K^+$, $Ca^{+2}$) with cationic-organic surfactants, such as alkyl ammonium ions, to make organo-modified montmorillonite (OMMT) clay [27]. Thus, OMMT exhibits better compatibility with the hydrophobic polymer matrix. The classification of OMMT clay, according to the structure of intercalants used for the organic modification as well as the cation exchange capacity (CEC), is shown in Table 3.14.

**Table 3.14:** OMMT-based nanoclays and their features.

| Commercial name of OMMT | Alkyl ammonium groups | CEC (meq/100gm) |
|---|---|---|
| Cloisite® 10A | Dimethyl benzyl hydrogenated tallow | 110 |
| Cloisite® 15A | Dimethyl dihydrogenated tallow | 125 |
| Cloisite® 20A | Dimethyl dihydrogenated tallow | 95 |
| Cloisite® 30B | *Bis*(ethyl alcohol) methyl tallow | 90 |

Generally, the most commonly used organoclays are Cloisite® 10A, 15A, 20A and 30B, which can be used for the preparation of TPVN for use in automotive applications.

Polymer-layered silicate (PLS) composites can be classified into three categories, as shown in Figure 3.17, and these are:

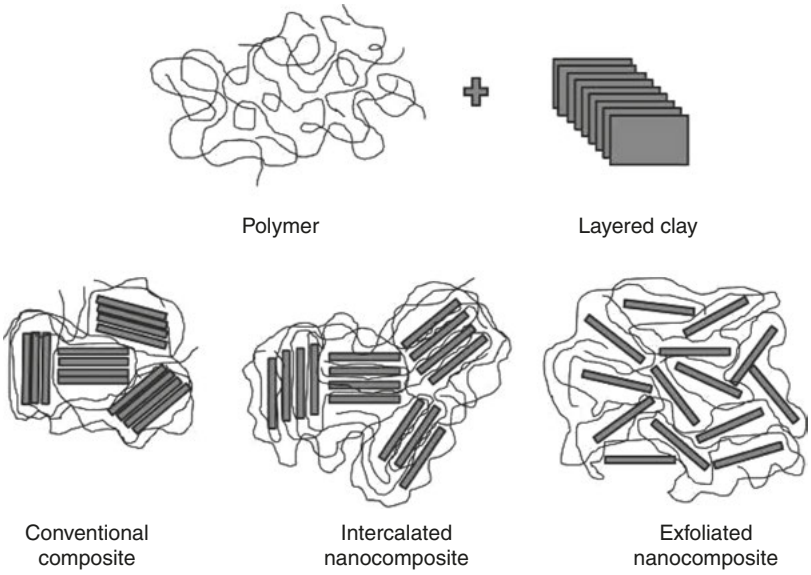


**Figure 3.17:** Schematic illustration of the PLS composite.

- Conventional composites: clay acts as a conventional filler and the clay layers remain stacked. The polymer chains remain attached to the surface of the clay layers instead of intercalating into the gallery of clay layers.
- Intercalated nanocomposites: the regular insertion of a polymer inbetween the clay layers. Although intercalation of the polymer chains into the gallery takes place, the layered structure remains unbroken.
- Exfoliated nanocomposites: delamination of the layers of clay leads to maximum polymer–clay interaction and makes the entire surface of the layers available to the polymer. The clay layers no longer remain stacked.

Compared with virgin polymers or conventional micro- and macrocomposites, the PLS nanocomposite exhibits a remarkable improvement in material properties, including higher modulus and strength properties, improvement in thermal resistance and decrease of gas permeability. As a result, over the last decade, the field of PLS nanocomposites has gained momentum and has been the focus of considerable interest.

## 3.3.5 Advantages of Nanocomposites

The insertion of nanoclay (NC) into the polymer matrix enhances certain properties in comparison to conventional composites. Polymer nanocomposites exhibit a substantial improvement in the following properties:

- Improvement in mechanical properties such as strength, modulus and dimensional stability.
- Improvement of thermal stability and heat distortion temperature.
- Improvement of flame retardancy and reduction of smoke emission.
- Reduced permeability of gases, hydrocarbons and so on, or other improved barrier properties.
- Provide better optical clarity compared with conventional composites.
- Improvement of surface appearance and chemical resistance [26, 32].

### 3.3.6 Requirements of Thermoplastic Vulcanisate Nanocomposites

Considering the advantages of polymer nanocomposites, it can be argued that over the past decade they have received considerable attention due to an unexpected improvement in properties, such as tensile modulus, TS, heat distortion temperature, barrier properties, solvent resistance, flame retardancy and so on, compared with pristine polymers. On the other hand, TPO and TPV have found a wider range of applications in the automotive industry, e.g., as cable applications, footwear packaging and so on. However, conventional reinforcing fillers (talc, mica, calcium carbonate) are generally mixed with TPO and TPV to increase the stiffness, heat distortion temperature and so on, which also increases the weight and melt viscosity of the composite and decreases the toughness, rendering the composite less attractive for aerospace and automotive applications [33]. At the same time, the higher loading (10–40 wt%) of conventional reinforcement causes adverse effects, such as processing difficulties. Moreover, a small amount of nanofiller loading (<5 wt%) is generally sufficient to improve the stiffness of the material and other valuable properties, such as barrier properties, solvent uptake and so on; hence, nanofillers are also cost-effective for automotive applications. As a result, TPVN is currently the prime concern to improve material properties such as strength, stiffness, permeability, fire retardancy, electrical and optical properties.

### 3.3.7 Preparation of Thermoplastic Vulcanisate Nanocomposites via the Melt-mixing Technique

Polymer nanocomposites can be prepared *via* three different techniques:

- *In situ* polymerisation
- Solution technique
- Melt intercalation or melt mixing

In general, TPVN are prepared using the last method, i.e., the melt-mixing technique [34]. In this method, nanofillers (nano-silica, layered silicates) are directly dispersed in the polymer melt. However, the silicates need to be modified via surface treatment prior to mixing with the polymer. The melt mixing of TPVN can be carried out in two ways: nanofillers can be melt mixed directly with the commercially-available TPV or nanofillers are allowed to mix with the thermoplastic phase only to form the thermoplastic nanocomposite; the elastomer phase is then added to the molten thermoplastic phase (with NC) and dynamic vulcanisation occurs in the presence of curatives during the melt-mixing process. A flow diagram of the melt-mixing technique of TPVN is given in Figure 3.18.

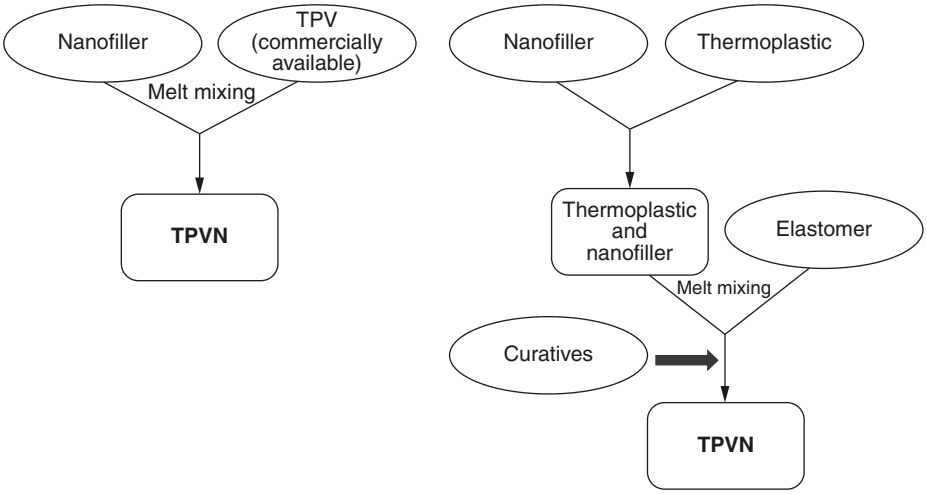


**Figure 3.18:** Flow diagram of the melt-mixing method of TPVN.

Among the above-mentioned techniques, melt mixing, or the melt-intercalation method, is most commonly used for the development of TPVN due to the following reasons:

- Melt intercalation is more flexible; meaning it is possible to melt-mix various polymer combinations which cannot be achieved using the solution-intercalation technique.
- It is much more 'green' than the other two routes due to the absence of solvents (the solution technique) and chemical reactions (the *in situ* polymerisation technique).
- The process is clean and environmentally friendly, and is economical from an industrial point-of-view. As a result, the process is commonly used by most industries.

## 3.4 Various Nanofilled Thermoplastic Vulcanisates

In recent years, TPVN have emerged as a new class of industrially acclaimed materials, in which reinforcing nanofillers are added to TPV in order to improve the properties of TPV. When nanofillers are added to a thermoplastic matrix, they increase the modulus value of the thermoplastic. At the same time, the incorporation of a nanofiller makes the thermoplastic matrix much more brittle. In order to achieve excellent impact properties, an elastomer phase is added to the thermoplastic matrix phase and when the elastomer becomes crosslinked, during melt mixing with the thermoplastic, the resulting material is known as TPVN.

### 3.4.1 Organoclay-filled Thermoplastic Vulcanisate Nanocomposites

#### 3.4.1.1 Thermoplastic Vulcanisate Nanocomposites based on Commercially Available Thermoplastic Vulcanisates

Mishra and co-workers explored the reinforcement of commercially-available PP–EPDM TPV (Santoprene® grades) in the presence of both nano-based (Cloisite® 20A) and microbased (talc) fillers [35, 36]. Both the fillers were melt blended with Santoprene®-grade TPV. Three TPVN were developed by varying the clay content from 2.5 to 7.5%, and a 20% talc-filled TPV microcomposite was also prepared.

Compared with pristine TPV, the tensile modulus of the TPV–Cloisite® 20A nanocomposite was found to be higher. The tensile modulus of pristine TPV is 120 kgf/cm2; while incorporation of 2.5% clay increased the tensile modulus to 202 kgf/cm2 (an 80% increase). It was found that the tensile modulus of 5.0% Cloisite® 20 A-filled TPVN was higher than that of the 20 wt% talc-filled microcomposite. The tensile modulus of the 5.0% TPV–Cloisite® 20A nanocomposite was 264 kgf/cm2 and was 227 kgf/cm2 for the 20% talc-filled TPV microcomposite. During the interaction between the Cloisite® 20A clay and polymer matrix, the intercalation of the polymer chains into the gallery of silicate layers resulted in a tremendous increment of the surface area, leading to a dramatic improvement of the tensile modulus value of the TPVN. In the case of the talc-filled microcomposite, the surface area of interaction is less. Thus, to improve the tensile modulus, a higher loading of talc or any other conventional filler is necessary, which is not cost-effective from an automotive application point-of-view, where minimising the material weight is a prime concern.

The incorporation of organoclay (Cloisite® 20A) also reduced the solvent uptake rate for the filled TPV system. At room temperature, the solvent uptake rate for pristine TPV was 48.7%, which reduced to 22.4% for 7.5% Cloisite® 20 A-filled TPVN.

Upon increasing the filler loading, the reduction of solvent uptake of the filled TPV system may be due to the better interaction between the filler (Cloisite® 20A) and TPV. This enhanced interaction between the filler and TPV leads to the formation of either physical crosslinks or bound polymer in close proximity to the reinforcing filler, which restricts solvent uptake.

In 2004, Lee and Goettler also explored TPVN based on commercially-available TPV (Santoprene® 101–80 elastomeric alloy) [37]. In the presence of organically modified NC, such as Cloisite® 20A and 30B which were modified with dimethyl dihydrogenated tallow quaternary ammonium and methyl tallow *bis*-2-hydroxyethyl quaternary ammonium salts, respectively, TPVN were developed. In order to develop TPVN, the clay loading was also varied from 2 to 8 wt%.

Studying the stress–strain behaviour, it was observed that upon increasing the concentration of organoclay, the tensile modulus of the TPV–Cloisite® 20A nanocomposite increased steadily, while the TS decreased gradually as a function of NC loading. On the other hand, the influence of NC loading was not as prominent in the TPV–Cloisite® 30B nanocomposite compared with the TPV–Cloisite® 20A nanocomposite. This may be due to the strong interaction between the TPV and Cloisite® 20A NC, whereas the interaction between the TPV and Cloisite® 30B NC is poor. In the case of commercially-available TPV, as the dispersed EPDM phase is already crosslinked, the layered silicates cannot penetrate into the dispersed phases. Layered silicates can only disperse in the continuous PP matrix and the compatibility mismatch between the layered silicates and PP continuous matrix would be the governing factor for the physico-mechanical behaviour of the TPVN. Thus, considering the physico-mechanical behaviour it can be stated that, in the case of the TPV–Cloisite® 20A nanocomposite, the proper dispersion of NC into the continuous PP matrix can occur, whereas large aggregate formation (similar to the microcomposite) may occur for the TPV–Cloisite® 30B nanocomposite. As a result, the enhancement of properties of the TPV–Cloisite® 20A nanocomposite is much higher than that of the TPV–Cloisite® 30B nanocomposite.

#### 3.4.1.2 Thermoplastic Vulcanisate Nanocomposites based on Polypropylene–Ethylene Propylene Diene Rubber Thermoplastic Vulcanisates

In 2006, Naderi and co-workers investigated the effects of the NC concentration, the viscosity ratio of PP–EPDM and dynamic vulcanisation on the microstructure and mechanical and thermal properties of the resulting PP–EPDM TPE [38, 39]. TPVN were developed using three different PP resins of different melt flow index at various loadings of NC. In the first step, the PP nanocomposite was prepared by mixing PP and NC (various loadings) in the presence of maleic anhydride-grafted-polypropylene (PPMA). The PP nanocomposite and EPDM was then melt mixed and dynamic vulcanisation occurred in the presence of a sulfur-accelerator system.

The tensile modulus of the TPVN increased from 20 to 90% depending upon the clay content and the viscosity ratio of PP–EPDM. For example, exfoliation of 2 wt% clay in a low viscosity PP-based TPVN resulted in a 92% improvement of tensile modulus, while the same amount of clay addition to a TPVN based on high-viscosity PP resulted in only a 23% improvement of tensile modulus over the unfilled one. This clearly suggests that the clay dispersion and exfoliation was better in the case of TPVN based on a low viscosity PP matrix.

Barrier properties, such as oxygen permeability, are another important feature of TPVN. Incorporation of NC also reduces the oxygen permeability of TPVN compared with the unfilled one, clearly indicating the improvement of the gas barrier property of TPVN.

#### 3.4.1.3 Polypropylene–Ethylene Propylene Diene Rubber Thermoplastic Vulcanisate Nanocomposites Produced by Electron-induced Reactive Processing

Thakur and co-workers studied the development of TPVN using EIReP. Three approaches were followed for the preparation of TPVN [40]:

- First approach: in a single step, PP, EPDM, NC and a coupling agent were melt mixed in an air atmosphere *via* EIReP to prepare TPVN under the same processing and EIReP parameters.
- Second approach: a two-step method. In the first step, PP–Cloisite® nanocomposites were prepared at 0.6 MeV/76 kGy/8.7 kGy per rotation, and then in the second step it was melt mixed again with EPDM to prepare TPVN *via* EIReP at 1.5 MeV/100 kGy/90 kGy per rotation.
- Third approach: in this process, the total charge input per time was kept constant and melt mixing was achieved in a nitrogen atmosphere and at a higher rotation per min.
- One-step process for preparing thermoplastic vulcanisate nanocomposites

In this process, PP and EPDM, in a blend ratio of 50:50, are taken with 5 wt% of NC and 3.4 wt% of a coupling agent. During mixing at 180 °C, dynamic vulcanisation was carried out with EIReP. During EIReP, an absorbed dose of 76 kGy and dose per rotation of 8.7 kGy were applied. The influence of electron energy (0.6 and 1.5 MeV) on the morphology and properties of TPVN were studied. Table 3.15 summarises the mechanical properties of TPVN, developed in the presence of two-electron energies.

The table clearly shows the influence of electron energy on the mechanical properties of TPVN. The TS and EB of the sample treated with 0.6 MeV electron energy were lower than the sample treated with 1.5 MeV electron energy, due to a decreased penetration depth of high-energy electrons, in the case of 0.6 MeV

**Table 3.15:** Mechanical properties of TPVN samples.

| Sample | E modulus (MPa) | TS (MPa) | EB (%) |
|---|---|---|---|
| TPVN_0.6 | 243 ± 34 | 9 ± 1 | 125 ± 73 |
| TPVN_1.5 | 204 ± 5 | 11 ± 0.5 | 333 ± 43 |

electron energy, which resulted in a lesser amount of crosslinked rubber particles and the homogeneity of crosslinking was also expected to be less. Since the penetration depth of electrons for the sample treated with 1.5 MeV electron energy was four times higher than the sample treated with 0.6 MeV electron energy, the EPDM rubber phase was efficiently crosslinked and the homogeneity of crosslinking was also higher for the sample treated with higher electron energy. As a result, the mechanical properties were much higher for 1.5 MeV electron energy-treated TPVN.

– Two-step Process for Preparing Thermoplastic Vulcanisate Nanocomposites

In the first step, PP nanocomposites were prepared at 0.6 MeV and 76 kGy and then melt mixed again with EPDM in the second step to prepare TPVN *via* EIReP at 1.5 MeV and 100 kGy. The blend ratio and processing conditions were kept the same as the one-step process. Table 3.16 shows the mechanical properties of TPVN made using the two-step approach.

**Table 3.16:** Mechanical properties of TPVN_2.

| Sample | *E* modulus (MPa) | TS (MPa) | EB (%) |
|---|---|---|---|
| TPVN_2 | 341 ± 12 | 8 ± 0.16 | 7 ± 1 |

2: Implies a two-step approach

This clearly reveals that the mechanical properties of the TPVN were significantly hampered compared with TPVN prepared *via* the one-step approach, due to the excessive chain scission of PP as a result of twice the thermal load and the double treatment with electron beams. Thus, the two-step approach was not suitable for preparing TPVN from a properties point-of-view.

– One-step Process of Preparing Thermoplastic Vulcanisate Nanocomposites at the Same Charge Input per Time

In this process, the charge input rate was kept constant for both samples treated with 0.6 and 1.5 MeV. Thus, for 0.6 MeV, the melt mixing was performed at 1.4 mA and 75 kGy and the treatment time was 300 s, while for 1.5 MeV, the melt mixing was performed at 4.1 mA and 113 kGy and the treatment time was 10 s. These EIReP

parameters were selected so that the charge input rate would be the same for both 0.6 and 1.5 MeV. Table 3.17 lists the mechanical properties of the two TPVN.

**Table 3.17:** Mechanical properties of TPVN_0.6/1.4 and TPVN_1.5/4.1 samples.

| Sample | *E* modulus (MPa) | TS (MPa) | EB (%) |
|---|---|---|---|
| TPVN_0.6/1.4 | 235 ± 18 | 17.0 ± 1.1 | 552 ± 40 |
| TPVN_1.5/4.1 | 205 ± 9 | 11.0 ± 1.7 | 272 ± 97 |

It was observed that at the same charge input rate, TPVN modified with 0.6 MeV and 1.4 mA under nitrogen and at 90 rpm exhibited excellent mechanical properties compared with TPVN modified with 1.5 MeV and 4.1 mA under nitrogen and at 90 rpm. This can be attributed to the better dispersion of nanoclay in TPV at 0.6 MeV as well as greater crosslinking of rubber at 90 rpm due to multiple modifications of the molten mass in the treatment zone. The coupling of NC to PP and EPDM along with crosslinked rubber resulted in superior TS (17 MPa) and EB (552%) values. This was also reflected in an enhanced *E* modulus (235 MPa) for 0.6 MeV, which can be attributed to more efficient coupling of filler particles to the polymer. At 1.5 MeV, although the charge input rate was the same as that of 0.6 MeV, the treatment time of 10 s may be too short for the homogeneous modification of TPVN. In addition, the total electron charges accumulated in the clay at 1.5 MeV within 10 s is 30-fold less compared with 0.6 MeV and 300 s. This resulted in less electrostatic repulsion in the clay layers and hence, the clay layers were not dispersed homogeneously.

Thus, the best set of mechanical properties was obtained with 0.6 MeV and at 1.4 mA with a treatment time of 300 s under nitrogen at 90 rpm.

#### 3.4.1.4 Styrene Acrylonitrile–Ethylene-Vinyl Acetate-based Thermoplastic Vulcanisate Nanocomposites

Patel and co-workers developed SAN–EVA-based TPVN in the presence of both unmodified (Cloisite® NA+) and modified (Cloisite® 10A) NC using the melt-intercalation technique [41, 42].

Table 3.18 shows the comparison of various physical properties of SAN–EVA blends filled with Cloisite® 10A and Cloisite® NA+ NC.

A greater improvement of physico-mechanical properties (TS, EB%, modulus and tension set value) was observed for the blends composed of Cloisite® NA+ NC compared with the blends filled with Cloisite® 10A NC. It can be suggested that, as Cloisite® NA+ is much more polar than Cloisite® 10A, it probably demonstrated

**Table 3.18:** TPV composition (phr) at a fixed SAN–EVA blend ratio and their corresponding properties.

| Component | SAN + EVA | SAN + EVA + Cloisite® 10A | SAN + EVA + Cloisite® NA+ | Dynamic vulcanisate of SAN + EVA | Dynamic vulcanisate of SAN + EVA + Cloisite® 10A | Dynamic vulcanisate of SAN+EVA + Cloisite® NA+ |
|---|---|---|---|---|---|---|
| SAN | 30 | 30 | 30 | 30 | 30 | 30 |
| EVA | 70 | 70 | 70 | 70 | 70 | 70 |
| Cloisite 10A (4 phr) | 0 | 4 | 0 | 0 | 4 | 0 |
| Cloisite® NA + (4 phr) | 0 | 0 | 4 | 0 | 0 | 4 |
| DCP (phr) | 0 | 0 | 0 | 2 | 2 | 2 |
| TAC (phr) | 0 | 0 | 0 | 1 | 1 | 1 |
| **Physico-mechanical properties** | | | | | | |
| TS (MPa) | 2.2 | 2.9 | 3.1 | 7.7 | 9.1 | 9.5 |
| EB (%) | 980 | 670 | 880 | 160 | 110 | 110 |
| 100% modulus (MPa) | 0.4 | 1.4 | 2.2 | 7.4 | 8.9 | 9.3 |
| 300% modulus (MPa) | 1.0 | 2.2 | 2.3 | – | – | – |
| Hardness (Shore D) | 14 | 17 | 18 | 21 | 27 | 30 |
| Tension set (%) at 25 °C | 8.0 | 6.0 | 4.0 | 2.5 | 2.5 | 2.0 |

better interaction with the polar SAN–EVA blend. Thus, the physico-mechanical properties were much improved for Cloisite® NA+-based SAN–EVA blends.

After dynamic vulcanisation, the TS, modulus and tension set properties improved tremendously for TPVN. Even after dynamic vulcanisation, the best physico-mechanical properties were observed for TPVN made of Cloisite® NA+, as shown in Table 3.18.

The values of the diffusion coefficient (D) of solvent (acetone) for TPE, TPE nanocomposites, TPV and TPVN-based SAN–EVA blends are reported in Table 3.19.

**Table 3.19:** Diffusion coefficient (D) of solvent (acetone) for various samples.

| Sample name | Diffusion coefficients ($D \times 10^{-3}$) ($cm^2/s$) at 25 °C |
|---|---|
| SE | 1.95 |
| SE10A | 1.91 |
| SENA+ | 1.58 |
| SE* | 1.18 |
| SE10A* | 1.18 |
| SENA+* | 1.01 |

* Implies for a dynamic vulcanisate

From the table, it can be clearly seen that the diffusion coefficient of solvent is lowest for the Cloisite® NA+-based nanocomposites. This also supports the better interaction of Cloisite® NA+ NC with the polar SAN–EVA blend and dynamic vulcanisation further reducing the diffusion coefficient value. This may be due to the more uniform dispersion of NC after dynamic vulcanisation, which restricts the passage of the solvent through the sample.

Although previous studies have highlighted the effectiveness of NC modification, this study clearly demonstrates that clay modification is not always necessary for nano-reinforcement.

## 3.4.2 Nano-silica-filled Thermoplastic Vulcanisates

Reinforcement of m-EPM-based TPV has been studied by Chatterjee and Naskar using various concentrations of nano-silica [43]. Due to the non-polar nature of PP and the large surface area of polar nano-silica particles, it was challenging to achieve a good dispersion of nano-silica in the polymer matrices. To improve the dispersion of nano-silica in PP, m-PP was used as a compatibiliser. All the TPV were prepared *via* the melt-mixing technique using a batch process and the TPV compositions are given in Table 3.20.

Upon increasing the incorporation of nano-silica, the physico-mechanical properties of TPV improved. With an increased loading (from 0 to 20 phr), there was a substantial improvement in the values of TS (from 6.1 to 7.7 MPa) and 100% modulus (from 5.2 to 6.9 MPa) for TPV, which is obvious from Table 3.21.

Hardness of the TPV also increased from 70 to 86 Shore A with an increase of nanofiller loading from 0 to 20 phr. Increasing the amount of nano-silica loading led to an improvement of physico-mechanical properties of various TPV, with the enhanced degree of reinforcement in the presence of nano-silica due to better polymer–filler interaction.

**Table 3.20:** TPV composition based on m-EPM–PP.

| Ingredients | phr |
|---|---|
| m-EPM | 100 |
| PP | 60 |
| m-PP | 10 |
| Paraffinic oil | 25 |
| Nanosilica | X |
| Si 69® | 1 |
| DCP (98%) | 2 |
| TAC (50%) | 4 |

**Table 3.21:** Physico-mechanical properties of m-EPM-based TPV at various nano-silica concentrations.

| Properties | Nano-silica content (phr) | | | | |
|---|---|---|---|---|---|
| | 0 | 5 | 10 | 15 | 20 |
| TS (MPa) | 6.1 | 6.5 | 6.6 | 7.6 | 7.7 |
| EB (%) | 184 | 180 | 189 | 190 | 150 |
| Modulus at 100% (MPa) | 5.2 | 5.4 | 4.6 | 6.2 | 6.9 |
| Hardness (Shore A) | 70 | 79 | 80 | 83 | 86 |
| Tear strength (N/mm) | 12.1 | 12.2 | 13.1 | 14.2 | 15.1 |

The addition of nano-silica also improved the thermal stability of the TPV and was dependent upon the amount of nano-silica added.

Peak degradation temperatures ($T_{max}$) of the TPV increased with nano-silica loading, which is summarised in Table 3.22. $T_{max}$ for pure TPV was 456 °C, whereas it increased to 466 and 468 °C for TPV containing 5 and 20 phr nano-silica loading, respectively.

**Table 3.22:** TGA data of nano-silica-filled TPV.

| Nano-silica content (phr) | $T_{max}$ (°C) |
|---|---|
| 0 | 456 |
| 5 | 466 |
| 10 | 467.5 |
| 15 | 468 |
| 20 | 468 |

Nano-silica loading also reduced the extent of swelling, in terms of the swelling ratio, of nanofilled TPV compared with that of unfilled TPV. The swelling ratio of pure TPV was 1.79, which reduced to 1.45 upon increasing the nano-silica loading up to 20 phr, as clearly shown in Figure 3.19.

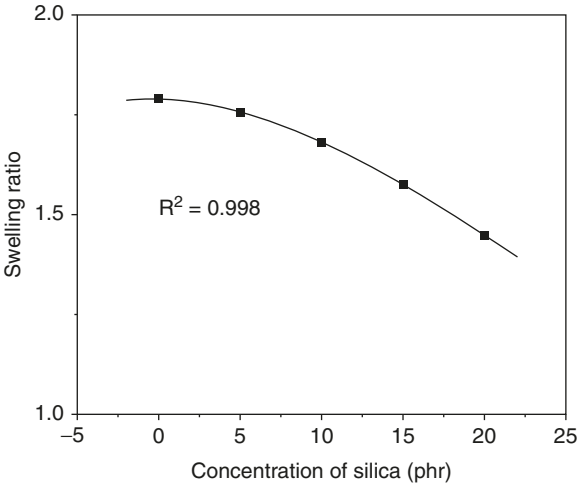


**Figure 3.19:** Swelling ratio of nano-silica-filled TPV as a function of nano-silica concentration.

Thus, the extent of swelling of nano-silica-filled TPV becomes reduced, meaning the solvent-resistance property of the filled TPV system improves, which may be due to the formation of physical crosslinks in the presence of nano-silica.

### 3.4.3 Graphite-based Thermoplastic Vulcanisate Nanocomposites

NC-reinforced TPV do not possess any significant electrical conductivity, magnetic or photonic properties like other functional polymer composites based on carbon black, carbon fibre, graphite and CNT. Conducting polymer composites have received considerable attention in applications of antistatic materials as well as pressure sensors. In general, carbon black, graphite, CNT and CNF are the most commonly used conducting fillers.

In 2007, Katbab and co-workers developed electrically-conductive TPVN based on graphite nanolayers and commercially-available TPV *via* the melt-mixing method [44]. TPVN have been prepared in the presence of natural graphite flakes (NGF), a graphite-intercalated compound (GIC) and expanded graphite (EG). Similar to layered silicates, NGF is composed of nanosheets with a spacing of 0.66 nm and

is a good electrical conductor, with a conductivity of $10^{+4}$ S/cm at room temperature. The presence of weak van der Waals forces between the carbon layers allows the intercalation of small molecules between the carbon layers, resulting in GIC. Exfoliation of the graphite nanolayers is carried out by subjecting the GIC to a sudden thermal shock at a very high temperature (>900 °C), which results in a large expansion of the graphite layers in the direction of the *c*-axis, called EG.

In the first step, a masterbatch of PPMA, used as an interfacial compatibiliser, was prepared separately with each graphite material *via* the melt-mixing process, it was then melt mixed with commercially-available Santoprene® TPV. Finally, TPVN based on TPV–PPMA–graphite nanolayers were prepared.

From the study of electrical conductivity (volume conductivity as a function of graphite content) of TPVN with each graphite material, it was seen that all the TPVN exhibited distinct percolation thresholds. TPVN based on EG nanolayers exhibited a percolation threshold at 6 phr (parts per hundreds resin) of EG, whereas the percolation threshold for TPVN based on NGF and GIC NC was approximately 20 phr of NGF and GIC, respectively. This clearly indicates that EG has a much higher potential to reduce the conductivity percolation threshold than NGF and GIC graphite. On the other hand, TPVN prepared by the melt mixing of TPV and EG in the absence of any interfacial compatibiliser, showed very little change in conductivity up to a 10 wt% loading of EG. At the loading of 15 wt% of EG, TPVN based on TPV–PPMA–EG exhibited a conductivity that was eight orders of magnitude higher than the TPV–EG counterpart. This clearly suggests the formation of infinite continuous conductive networks throughout the TPV matrix in the microstructure of the TPV–PPMA–EG nanocomposite. It also reveals better dispersion of the EG nanolayers with a higher aspect ratio, which results in an enhanced interaction between the compatibilised TPV matrix and functional groups existing on the surface of EG. In addition, PPMA facilitates the delamination of EG nanolayers and enhances the formation of interconnected conductive networks.

## 3.5 Applications of Thermoplastic Vulcanisate Nanocomposites

From the above-mentioned studies it can be seen that TPVN exhibit improved mechanical properties in terms of tensile modulus, TS and so on, compared with conventional composites. On the other hand, the insertion of NC improves the thermal properties in terms of thermal stability, heat distortion temperature and so on, which clearly enhances the use of TPVN in various automobile applications. Not only can TPVN improve mechanical and thermal properties, it also exhibits some unique features such as flame retardance, improved barrier properties, low solvent uptake and improved electrical properties. Thus, the uses of TPVN are gaining extensive

attention from many industrial application points-of-view. Besides the applications of simple rubber and thermoplastic-based nanocomposites, nowadays these kinds of materials are gaining considerable interest and have found many more potential applications, which include flame-retardant materials, electronics materials and so on.

## 3.6 Summary and Conclusion

Finally, considering the above-mentioned details regarding TPVN, it can be argued that most commercially-available TPV are based on PP–EPDM, and TPVN have mostly been developed by the incorporation of nanofillers into commercially-available PP–EPDM TPV or by the incorporation of nanofillers during the preparation of PP–EPDM TPV that also results in TPVN. Very few TPVN have been developed using other blend systems such as SAN–EVA.

In all cases, the reinforcement of TPV by nanofillers improves the physical properties (like tensile modulus, TS), thermal properties, flame-retardancy behaviour, barrier properties and swelling-resistance properties of TPVN. In some cases, the incorporation of expanded nanographite also improved the electrical properties of TPVN.

Considerable scope remains for the development of a new generation TPVN that possess enhanced properties. Although the TPV-based PP–EOC blend has been well investigated, it is still not commercially available. As a result, TPVN development based on the PP–EOC blend is a good option. On the other hand, a few TPV based on PP–NR and PP–NBR are slowly gaining commercial importance. The preparation of TPVN based on these blend systems is also highly appreciable. Currently, only a few soft TPV based on silicone rubber have been developed, hence TPVN development based on soft TPV is also a demanding aspect.

Finally, it can be concluded that, due to some unique properties, applications of TPVN are increasing in various commercial and industrial fields. In future, further development of TPVN will find several potential applications in various sectors and the development of new TPVN with superior properties is highly desired.

## References

1. J. Karger-Kocsis in *Polymer Blends and Alloys*, Eds., G.O. Shonaike and G.P. Simon, Marcel Dekker, New York, NY, USA, 1999, p.125.
2. R.R. Babu and K. Naskar, *Advances in Polymer Science*, 2011, **239**, 219.
3. S.K. De and A.K. Bhowmick in *Thermoplastic Elastomers from Rubber Plastic Blends*, Horwood, London, UK, 1990.
4. K. Naskar, *Rubber Chemistry and Technology*, 2007, **80**, 504.
5. R.M.A. l'Abee, M. van Duin, A.B. Spoelstra and J.G.P. Goossens, *Soft Matter*, 2010, **6**, 1758.

6. R.R. Babu, N.K. Singha and K. Naskar, *Journal of Polymer Research*, 2010, **17**, 657.
7. S. Abdou-Sabet and M.A. Fath, inventors; Monsanto Company, assignee; US4311628, 1982.
8. A.Y. Coran and R. Patel, *Rubber Chemistry and Technology*, 1980, **53**, 141.
9. J.B. Class, *Rubber & Plastics News*, 1995, 9th October.
10. K. Naskar and J.W.M. Noordermeer, *Rubber Chemistry and Technology*, 2003, **76**, 1001.
11. R.R. Babu, N.K. Singha and K. Naskar, *Express Polymer Letters*, 2008, **2**, 226.
12. K. Chatterjee and K. Naskar, *Express Polymer Letters*, 2007, **1**, 527.
13. K. Naskar, U. Gohs, U. Wagenknecht and G. Heinrich, *Express Polymer Letters*, 2009, **3**, 677.
14. T. McNally, P. McShane, G.M. Nally, W.R. Murphy, M. Cook and A. Miller, *Polymer*, 2002, **43**, 3785.
15. R.R. Babu, N.K. Singha and K. Naskar, *Journal of Applied Polymer Science*, 2009, **113**, 1836.
16. R.R. Babu, N.K. Singh and K. Naskar, *Journal of Applied Polymer Science*, 2009, **113**, 3207.
17. R.R. Rajeshbabu, U. Gohs, K. Naskar, M. Mondal, U. Wagenknecht and G. Heinrich, *Macromolecular Materials and Engineering*, 2012, **297**, 659.
18. S. Mani, P. Cassagnau, M. Bousmina and P. Chaumont, *Macromolecular Materials and Engineering*, 2011, **296**, 909.
19. R. Giri, K. Naskar and G.B. Nando, *Rubber Fibres Plastics International*, 2011, **6**, 97.
20. U. Basuli, T.K. Chaki and K. Naskar, *Express Polymer Letters*, 2008, **2**, 846.
21. T. Chatterjee, S. Wiessner, K. Naskar and G. Heinrich, *eXPRESS Polymer Letters*, 2013, **8**, 220.
22. S.M.R. Syed Ismail, T. Chatterjee and K. Naskar, *Journal of Applied Polymer Science*, 2015, **132**.
23. P. Dey, K. Naskar, G.B. Nando, B. Dash, S. Nair and G. Unnikrishnan, *Materials Today Communications*, 2014, **1**, 19.
24. P. Dey, K. Naskar, G.B. Nando, B. Dash, S. Nair and G. Unnikrishnan, *Journal of Applied Polymer Science*, 2014, **131**, 41182.
25. K. Naskar in *Dynamically Vulcanized PP/EPDM Rhermoplastic Elastomers: Exploring Novel Routes for Crosslinking with Peroxides*, University of Twente, Enschede, The Netherlands, 2004. [PhD Thesis].
26. A. Olad in *Advances in Diverse Industrial Applications of Nanocomposites*, Ed., B. Reddy, InTech, Rijeka, Croatia, 2011.
27. S.S. Ray and M. Bousmina, *Progress in Materials Science*, 2005, **50**, 962.
28. A.K. Chandra and V. Bhandari in *Advances in Elastomer II*, Springer Heidelberg, Germany, 2013, **12**, 183.
29. G. Wypych in *Handbook of Fillers*, 2nd Edition, ChemTec Publishing, New York, NY, USA, 1999.
30. H. Zengin, W. Zhou, J. Jin, R. Czerw, D.W. Smith, Jr., L. Echegoyen, D.L. Carroll, S.H. Foulger and J. Ballato, *Advanced Materials*, 2002, **14**, 1480.
31. M. Okamoto in *Handbook of Biodegradable Polymeric Materials and Their Applications*, American Scientific Publishers, Valencia, CA, USA, 2005.
32. J.W. Gilman, *Applied Clay Science*, 1999, **15**, 31.
33. S.S. Ray, P. Maiti, M. Okamoto, K. Yamada and K. Ueda, *Macromolecules*, 2002, **35**, 3104.
34. Y.H. Hyun, S.T. Lim, H.J. Choi and M.S. Jhon, *Macromolecules*, 2001, **34**, 8084.
35. J.K. Mishra, G.H. Kim, I. Kim, I.J. Chung and C.S. Ha, *Journal of Polymer Science: Part B: Polymer Physics*, 2004, **42**, 2900.
36. J.K. Mishra, J.H. Rhou, G.H. Kim, K.J. Hwang, I. Kim and C.S. Ha, *Materials Letters*, 2004, **58**, 3481.
37. K.Y. Lee and L.A. Goettler, *Polymer Engineering and Science*, 2004, **44**, 1103.
38. G. Naderi, P.G. Lafleur and C. Dubois, *Polymer Engineering and Science*, 2007, **47**, 207.
39. A. Mirzadeh in *Thermoplastic Vulcanizate Nanocomposites based on Polypropylene/Ethylene Propylene Diene Terpolymer (PP/EPDM) Prepared by Reactive Extrusion*, Université de Montréal, Québec, Canada, 2012. [PhD Thesis].

40. V. Thakur, U. Gohs, U. Wagenknecht and G. Heinrich, *Polymer Journal*, 2012, **44**, 439.
41. J. Patel, M. Maiti, K. Naskar and A.K. Bhowmick, *Rubber Chemistry and Technology*, 2005, **78**, 893.
42. J. Patel, M. Maiti, K. Naskar and A.K. Bhowmick, *Polymer and Polymer Composites*, 2006, **14**, 515.
43. K. Chatterjee and K. Naskar, *Polymer Engineering and Science*, 2008, **48**, 1077.
44. A.A. Katbab, A.N. Hrymak and K. Kasmadjian, *Journal of Applied Polymer Science*, 2008, **107**, 3425.

Dipak Kumar Setua and Yadavendra Nath Gupta

# 4 Elastomer–Clay Nanocomposites with Reference to their Automobile Applications and Shape-Memory Properties

## 4.1 Introduction

In recent years, both plastics and rubber product manufacturers have become increasingly interested in nanofillers due to their potential to replace conventional fillers, which are used in large quantities for reinforcement purposes.

Nanofillers, unlike conventional fillers, can significantly improve the functional properties of polymers, e.g., flame retardancy, impermeability and so on. However, these nanofillers are mostly inorganic in nature and also differ widely from conventional macrofillers in terms of their origin, structure, surface area and, in particular, the nature of the filler–matrix adhesion, which all generate a different set of structure–property relationships.

Different types of nanofillers are available commercially, e.g., carbon nanotubes (CNT), activated carbon nanofibres (CNF), natural clay (mined, refined, treated and so on), synthetic clay, silica, layered double hydroxide and calcium carbonate ($CaCO_3$), in addition to a variety of nanoparticles (NP), e.g., alumina, zinc oxide (ZnO), titanium dioxide, iron, iron oxides, iron carbonyls and so on.

However, layered silicates [e.g., nanoclays (NC)] are most commonly used in a variety of rubber products including tyres, tyre inner liners, tubes, V-belts, seals, gaskets and so on. NC, either alone or in combination with carbon black (CB), can significantly improve the mechanical, dynamic mechanical, tribological and thermal properties.

For example, the development of a high-performance tyre tread combining very good wet skid and low rolling resistance is possible. However, an important point to mention is that a few nano-sized carbon particles are always present in a bulk quantity of CB, which also influence the mechanical, reinforcement and morphological properties.

In nanocomposites, polymer chains have dimensions similar to those of nanofillers, which leads to an extensive filler–matrix interaction resulting in significant changes to their crystallinity, and optical and thermal properties, and so on. The extent of the filler–matrix adhesion, however, can be improved further by introducing functional chemical groups onto the filler's surface which interact with those present in a polymer backbone.

Hence, the blending of surface-functionalised clay platelets with a polymer matrix can yield a new class of hybrid materials commonly known as polymer–clay nanocomposites (PCN). Quite a few recent reviews are available on the synthesis,

https://doi.org/10.1515/9783110643879-004

characterisation techniques, mechanical properties and applications of PCN, particularly related to their applications in automotive and packaging industries [1–9].

Thermoplastic polyurethane (TPU) elastomers have established themselves as globally important due to their potential to exhibit many important properties, e.g., mechanical strength, elasticity, chemical resistance, optical properties, transparency and so on, for commercial exploitation. Furthermore, these properties can be monitored by varying the choice of the structural units and synthesis routes used. As a result, they are widely used in the automobile industry, and footwear and biomedical product sectors. TPU have also become significant due to their shape-memory property, which is an emerging trend in the fascinating field of smart and functional polymers.

TPU are multiblock copolymers and are sometimes called segmented, where the multiblocks are alternately distributed in a molecular chain as hard segments, comprised of diisocyanate and short-chain diols, and soft segments of long-chain diols of polyether, polyester or polycarbonate.

The hard segment bears the significance of generating the modulus, hardness, end- use temperature, wear and tear properties, while the soft segment is responsible for low-temperature flexibility, elongation at break, as well as chemical and water resistance. However, TPU have some drawbacks; they tend to become yellow upon prolonged exposure to visible and ultraviolet light and have poor flame retardancy, thermal stability and so on, which restricts their widespread application in high-quality products for outdoor use, e.g., interlayers or inner layers for automobiles, laminated windscreens, shatterproof coating for glass windows and so on.

These disadvantages of segmented polyurethanes (SPU) led to the development of SPU-based nanocomposite-filled NC. Naturally occurring montmorillonite (MMT) is extensively used as an NC and often organically surface modified so that the gallery spacing of the layered structure reaches the exfoliation stage, offering very good physico-chemical interaction with polymers for maximum reinforcement with a small percentage loading.

By using NC it is also possible to resolve the inherent microstructural problems of SPU, e.g., incompatibility between the hard and soft segments which induces phase separation resulting in a decrease of the amorphous nature of the material.

A one-off surface modification (singular type) of the NC via a chemical route has become a common trend to establish the desired polymer–filler interaction. Reported literature shows that an optimum thermal stability in TPU rubber can be achieved by adding 1 to 3 wt% of organo-modified montmorillonite (OMMT) [10, 11]. Laponite® is the synthetic counterpart of MMT and recent publications have shown that the dual modification of Laponite® is profitable [12–14]. Single modification is basically ionic modification, i.e., cationic exchange of $Na^+$ by organic amines of MMT, whereas in the dual-modification process, the singularly-modified clay is further modified by another surfactant to impart additional functionality. Inorganic

Laponite® RD has been ionically modified with cetyltrimethylammonium bromide using the standard ion exchange process [15].

Silanes are preferred over alky and aryl amines as a surfactant due to the use of the simple modification process. Thermogravimetric analysis (TGA) has been widely used to measure the thermal stability of nanocomposites both under isothermal and non-isothermal conditions. Exfoliated nanocomposites of SPU containing single- and dual-modified synthetic NC (Laponite®) have shown that the inclusion of NC imparts 3additional thermal stability, of approximately 20 °C, to SPU. Modulated thermogravimetric analysis (MTGA) has been found to be more accurate than the conventional technique, and reliable results can be obtained in a relatively short time span. The glass transition temperature ($T_g$), determined using thermomechanical analysis (TMA), could explain the interaction between NC and SPU. The crystallisation peak temperature ($T_p$) of the nanocomposites, determined by differential scanning calorimetry, is increased in the nanocomposites suggesting the nucleating effect of the nanofillers.

However, the results vary with the test methods and analytical approach used to evaluate the kinetic parameters, which is due to the complex degradation mechanism of these nanocomposites [16, 17]. Barick and Tripathy investigated the thermal stability and degradation kinetics of the polyurethane (PU) and Cloisite® type of NC in both inert and oxidative environments, and observed that the addition of Cloisite® imparts additional thermal stability to the nanocomposites [18]. Mishra and coworkers have made a similar observation in the case of Laponite® in SPU [19].

### 4.1.1 Shape-memory Effect in Polymers

Nature contains some amazing materials that are able to change their shape in response to environmental conditions, e.g., a sunflower. Mankind has relentlessly pursued how to mimic nature, which led to the discovery of the shape-memory effect (SME). The SME was first discovered by Chang and Read in 1932, which led to the development of shape-memory alloy(s) (SMA), e.g., Nitinol in 1962. A shape-memory material can be deformed and fixed into a temporary shape as long as desired and can regain its original shape upon exposure to an external stimuli such as heat, electricity, magnetic flux, light and so on. Nitinol, a shape-memory material, possesses important properties, such as high strength, and in the smart category it offers a short response time and extended fatigue cycles, which are attractive for a variety of applications including vibration damping, pipe coupling, electrical connectors, thermostats, actuators and so on.

However, despite the above attributes, SMA have disadvantages including: limited recoverable strains (less than 8%), inherently high stiffness, high density, high cost, inflexible transition temperature, and rigorous processing and programming practices. Alternatives were explored to overcome these drawbacks, which led to the development of shape-memory polymers (SMP). The discovery of PU in 1988 by

Mitsubishi Heavy Industries, Japan, that exhibited shape-memory behaviour led to the emergence of a new area of research. The versatile chemistry and industrial importance of PU coupled with their shape-memory characteristics led to the development of a new generation of advanced footwear, packaging and high-end engineered components for automotive applications.

Despite the numerous advantages of these SMP based on PU, there were still challenges due to low stiffness, poor dimensional stability and low recovery force compared with SMA and ceramics. Naturally, efforts were made to reinforce the SPU with different nanofillers to make SMP composites. To be precise, the SME is not an intrinsic property of materials such as polymers, i.e., they do not display the effect as such, but it results from a specific combination of polymer architecture and morphology which is carefully thermomechanically controlled and termed programming. For a polymer to exhibit shape-memory properties, the basic requirement is that it must possess a reversible phase and a fixed phase.

The latter is called a switching segment, while the reversible phase is described as a net point. The reversible phase activates molecular mobility both in the shape-fixing and shape-recovery stages. Whereas the fixed phase is essential for permanent shape retention and to avoid long-range chain slippage and flow during the deformation process.

## 4.1.2 Programming of Shape-Memory Polymers

For SMP to display the SME, precise thermomechanical programming is required and the process is schematically described in Scheme 4.1. First, the temperature is elevated above the thermal transition temperature ($T_s$) of the fixed phase, *via* conventional processing methods, resulting in the polymer attaining its permanent stage (in order to nullify the effect on the molecular architecture by changes in thermal history or intermittent deformation and so on), it is then equilibrated at room temperature (RT). Afterwards, the following thermomechanical programming steps are followed:

1. The temperature of the specimen is raised above the $T_s$ of the reversible phase and then a load is applied to generate the deformation. The sample is subsequently cooled below $T_s$ to a fixing temperature ($T_f$) (generally 20 °C below $T_s$) for complete phase transformation (while the load is still applied). The load is then removed after the sample is deformed to a desired temporary shape; this is termed the shape-fixing step, i.e., the shape remains fixed as along as temperature conditions remain unchanged.
2. When recovery to the original or permanent shape is desired, an external stimulus (e.g., heating) is applied to raise the temperature above the $T_s$ of the reversible phase. Beyond this temperature, the sample starts to regain its original shape, termed the shape-recovery step. Generally, the SME in SMP is triggered by a thermally induced process; however, electrical, magnetic, light, water,

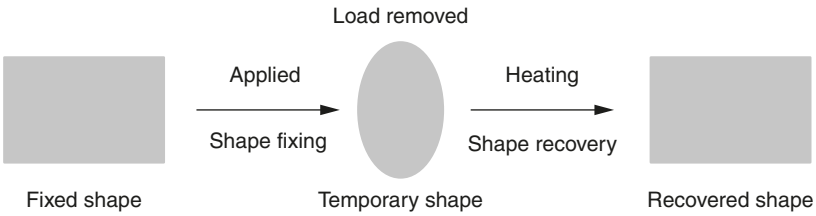


**Scheme 4.1:** Representation of the SME in polymers.

solvent and electromagnetic stimuli have also been used successfully. In general, the recovery step is carried out under constant stress.

Recovery under constant strain rate conditions is also possible. In constant stress recovery, there are two modes; the first mode is called a dynamic recovery experiment, where the material is held at a constant stress, and strain is allowed to recover during heating. During the second mode, i.e., the isothermal recovery experiment, the material is held at a constant strain during heating and the stress in the material increases owing to a strain constraint, which can be measured. Similarly, for the case of constant strain rate recovery experiments, it is possible to release the strained material at a constant strain rate and the resulting stress and stress rates can be monitored.

## 4.1.3 Figure of Merit

### 4.1.3.1 Shape Fixity

When an SMP is heated to a temperature above the $T_s$ of the reversible phase and a load is applied, the deformation can be fixed by cooling to a temperature below the $T_s$ of the switching segment. The quantitative parameter used to describe the extent of temporary shape fixing during the shape-memorisation process is termed shape fixity, '$R_f$', and defined as the ratio of the fixed deformation to the total deformation, as in Equation 4.1:

$$R_f = (\text{fixed deformation}/\text{total deformation}) \times 100\% \tag{4.1}$$

### 4.1.3.2 Shape Recovery

SMP in its temporary shape, or deformed shape, held at a temperature lower than the $T_s$ of the reversible phase can restore its original shape upon heating above the $T_s$ of the switching segment. The quantitative parameter used to define the extent of

shape recovery is termed the shape-recovery ratio, '$R_r$', and can be expressed as in Equation 4.2:

$$R_r = (\text{deformation recovered}/\text{fixed deformation}) \times 100\% \tag{4.2}$$

Another definition for '$R_r$' is also known, and is given in Equation 4.3:

$$\begin{aligned}\text{Shape recovery} = (&\text{deformation recovered by the sample over}\\ &\text{repeated cycles}/\text{deformation of the sample}\\ &\text{in the first cycle}) \times 100\%\end{aligned} \tag{4.3}$$

Other terms, like 'shape recoverability' or 'strain recovery' and so on, are used but are less common. A slight variation in definition, e.g., sometimes strain recovery is defined in place of shape recovery, is shown in Equation 4.4:

$$\begin{aligned}\text{Strain recovery} = (&\text{deformation recovered by the sample}\\ &\text{in this cycle}/\text{deformation of the sample}\\ &\text{in one cycle}) \times 100\%\end{aligned} \tag{4.4}$$

It is apparent, therefore, owing to the variation in definitions, different values of shape recovery will be reported by applying different formulae.

#### 4.1.3.3 Recovery Speed

The instantaneous recovery speed '$V_r$', is defined as time, 't', and a derivative of strain, 'ε' i.e., Equation 4.5:

$$V_r = (\partial\varepsilon/\partial t) \times 100\% \tag{4.5}$$

The $V_r$ is important for practical purposes but seldom reported as the absolute value of the shape $V_r$ is dependent on a variety of factors including: the thermal environment, thermal conductivity of the fillers and even the heating/cooling methods.

## 4.1.4 Molecular Mechanism of the Shape-Memory Effect in Polymers

#### 4.1.4.1 Chain Conformation

In the equilibrium state, polymer chains are randomly distributed with all possible conformations having equivalent internal energy. If the probability of a conformation is expressed by 'W', then the most probable state (a strongly coiled

conformation with maximum entropy) is given by the Boltzmann equation, i.e., Equation 4.6:

$$S = k\ln W \tag{4.6}$$

Where 'S' is the entropy and 'k' is Boltzmann's constant. This statistical relationship between the probability of chain conformation and entropy forms the basis of understanding the underlying principle behind the SME of SMP.

#### 4.1.4.2 Entropic Elasticity

In a glassy state, the long-chain cooperative movement of the polymer chains is frozen. However, upon application of thermal activation the chains regain mobility and undergo transition to an elastic rubbery state and thus, can be deformed in the direction of an applied external force. This act results in a loss of entropy from the system and variation of distance between the net points. As soon as the external force is withdrawn, the material reverts back to its original permanent shape and regains the lost entropy. However, if the external force is applied for a longer time, stress relaxation may occur which could create an irreversible deformation due to chain slippage and disentanglement. It is, therefore, imperative to prevent chain slippage or flow by crosslinking of the polymer chains either physically (e.g., H-bonding) or *via* chemical routes (using crosslinking agents, curing and so on).

Crosslinking enables the polymer chains to take up one of the possible energetically equivalent conformations without significantly disentangling, such that the majority of the macromolecules exhibit the random coil conformation, which is entropically favoured.

#### 4.1.4.3 Molecular Mechanism of Shape-Memory Polymers

The most probable chain conformations, as well as entropic elasticity, play a key role in the SME of SMP. When the temperature of the sample is raised above the $T_s$ of the reversible phase and a load is applied, the orientation of the molecular chains that occurs results in loss of entropy. In a particular situation, where the chains are frozen by cooling below Ts during the shape-fixing process, although the process is not entropically favoured the sample would remain in a deformed state provided the required temperature conditions were maintained. However, when the sample is exposed to an external stimulus (e.g., heating) that elevates the temperature above its $T_s$, the polymer recovers its original shape by regaining the entropy

lost during the deformation process. Therefore, the underlying mechanism of the SME of SMP is entropically driven.

## 4.2 Role of Rubber–Clay Nanocomposites in Automobile Applications

Different types of clays have commercial potential to serve as nanofillers as they are abundantly available in nature. Recently, rubber–clay nanocomposites (RCN) as well as rubber nanocomposites with other 0D, 1D and 2D nanofillers have also been the focus of attention amongst researchers and there are comprehensive reviews available with details on synthesis, processing methods for preparation, morphology, structural characterisation, filler surface modification, polymer–filler interaction, mechanical properties and their use in tyres and various other automotive, engineering and sports applications [20–24].

Nanocomposites are cost-effective and display excellent tensile strength (TS), very good gas barrier and dynamic mechanical properties, in addition to very good chipping/cutting/wear resistance, flame retardancy, high-temperature resistance, antifatigue properties and so on. RCN also fall into the category of organic–inorganic hybrid materials and they are suitable for a wide range of applications in automobile, construction, packaging and biomedical products, where the combination of the advantages of natural fillers/fibres and organic polymers and rubbers are utilised [25–27].

The addition of NC to a rubber compound can also improve tack, green strength and tribological properties, e.g., tear and wear resistance, to a greater degree than commercially-added resins used as tackifiers. There is also scope for combining two fillers to create a hybrid filler system, e.g., rubber together with an NC and CB in order to generate synergistic properties, e.g., tack and green strength of rubber [e.g., natural rubber (NR)] together with improved low rolling resistance, higher abrasion resistance, better wet grip and so on, required for advanced tyre treads.

A ternary filler system, e.g., CB/silica/*N,N*-dimethyldodecylamine-modified MMT, as an organic layered silicate, filled with styrene-butadiene rubber (SBR) has been used to formulate a tyre tread compound [28]. Calcium stearate (up to 0.5 phr) in place of stearic acid was found to be more effective at improving the filler–rubber interaction. The SBR–organoclay nanocomposites with this ternary filler system showed excellent dynamic properties and mechanical performance, combined with very good wear resistance and showed good potential as a tyre tread compound for passenger cars.

Various compatibilisation and dispersion techniques have been proposed for the homogeneous dispersion of either natural or synthetic NC in the elastomer matrix,

among them, latex compounding and melt-blending methods are the most common. The nanocomposites prepared by mixing NR latex with an aqueous dispersion of clay, pre-swollen using water, has been studied by Rezende and co-workers [29]. The mechanical properties, under uniaxial stretching, of non-vulcanised NR and dialised NR (obtained by dialysis of rubber latex with a 1% $NH_4OH$ solution)–clay nanocomposites have shown [studied by transmission electron microscopy (TEM) and small-angle neutron scattering] the morphology of a homogeneous filler dispersion with an excellent degree of exfoliation and coexistence of tactoids. The enhancement of mechanical properties was correlated with a high aspect ratio of exfoliated clay platelets inside the immobilised NR matrix and the strain-induced crystallisation of NR at high deformation. They also exhibited anisotropic behaviour, which increased with the clay concentration and extent of stretching of the samples. Braganca and co-workers employed this technique to design nanocomposites of styrene-acrylic (polystyrene-*co*-butyl acrylate-*co*-acrylic acid) latex containing cations of Li, K or Ca in Na-MMT and observed a 10-fold increase of elastic modulus and 2-fold increase in the TS [30]. Using a quantitative model, Valadares and co-workers showed that a strong association exists between the clay lamellae and the rubber matrix *via* electrostatic attraction at the organic–inorganic interface, which is as strong as a covalent bond [31]. Jacob and co-workers reported the effect of the interlayer distance 'd' spacing value, measured by X-ray analysis of NR latex-NC in RCN with a lower filler concentration [32]. Transport properties, e.g., sorption, diffusion and permeation coefficients, were studied using toluene at 30 °C, along with the barrier property, which were found to be dominated by the diffusion phenomenon in accordance with Nielson's model. The very good barrier property of these latex films has been claimed to have potential application for dipped packaging goods. A 50% increase in the TS and 150% increase in the tensile modulus at 300% elongation were reported for the NR–clay nanocomposites with 10% filler concentration [33].

Pal and co-workers reported the results of epoxidised natural rubber (ENR) and organoclay (Cloisite® 20A) nanocomposites prepared by the solution mixing technique [34]. The ENR–clay masterbatch was blended with NR–SBR blends with different types of CB and the morphology, curing behaviour, mechanical and thermal properties and so on, were evaluated. An intermediate super abrasion (ISAF) type of CB-filled nanocomposites showed an intercalated structure with a significant reinforcement effect of ISAF containing both SBR and NR phases; eventually helping to produce a highly abrasion-resistant tyre tread rubber compound. A rubber compound with 25 wt% SBR with ISAF CB showed the lowest heat build-up property.

Das and co-workers observed that by using stearic acid (in doses of 10 phr, higher than the normal 2 phr) premixed with OMMT in non-polar rubbers, e.g., NR and ethylene propylene diene monomer rubber (EPDM), the complete intercalation and exfoliation of clay platelets occurred, i.e., the formation of an ideal nanostructured composite

compared with standard non-polar clay conventional rubber composites prepared by melt mixing [35].

Besides stearic acid, a series of other long-chain fatty acids was also intercalated into OMMT–NR nanocomposites and a gradual expansion of the interlayer spacing was observed as the chain length of the fatty acid was increased [36].

Docosanoic acid (with 22 carbon atoms) was found to produce the highest interlayer spacing amongst all the fatty acids studied. Wide-angle X-ray diffraction (WXRD), Fourier–Transform infrared (FTIR) spectroscopy, contact angle measurements, scanning electron microscopy (SEM), TEM and so on, are commonly used to gain insight and evidence for enhanced intercalation, morphology, filler–matrix interaction, crystallinity and so on. Sadhu and Bhowmick have studied the effect of the addition of NC based on Na-MMT, bentonite, K-MMT and organic amines of varying chain lengths in SBR [37]. Increasing the chain length of the surface modifiers was found to profoundly influence both the mechanical as well as thermal properties. Das and co-workers have reviewed the RCN with special reference to their degree of dispersion, melt intercalation, masterbatch dilution, chemical modification and exfoliation of different layered clays in various rubbers [38].

They claimed that the melt-intercalation method is probably the most effective one if proper compounding techniques are carefully considered, in addition to the efficient curative package for vulcanisation and polarity between the different rubber phases (in the case of elastomer blends).

Wang and co-workers have prepared nanocomposites with styrene-vinylpyridine-butadiene, SBR 1500 and polybutadiene rubber (BR) 9000 using latex and solution methods [39]. The dispersion of clay in the rubber matrix at the nanometre level was ascertained by TEM and X-ray diffraction (XRD) techniques. A comparison of the efficacy of clay and CB, with respect to their reinforcing ability and mechanical properties, has also been made.

The structural characterisation of several rubber latexes, e.g., SBR, NR, acrylonitrile- *co*-butadiene rubber [acrylonitrile-butadiene rubber (NBR)] and carboxylated NBR co-coagulating directly with clay or clay in aqueous suspension, highlights the extensive swelling capability of clay in combination with water and latex. The characterisation performed by XRD and TEM showed that the nanocomposites possess a unique structure, i.e., the rubber molecules separated the clay particles into either individual layers or the silicate layers were aggregated at a nanometre-scale thickness without any intercalation of the rubber molecules.

This is unique structural information that differs greatly from intercalated and exfoliated clay–rubber nanocomposites [40]. The formation of this type of structure is based on the dispersion mechanism, where complete exfoliation of RCN occurred due to competition between the separation of the rubber latex particles and reaggregation of the single silicate layers during co-coagulation.

There is more bound rubber in SBR–clay nanocomposites than micrometre-scale clay filler–SBR nanocomposites. The gas permeability of an SBR–clay nanocomposite containing 20 phr NC decreased by 50% compared with conventional macrocomposites. The effect on vulcanisation, mechanical properties, thermal stability, ageing resistance and so on, of a modified Ca-MMT–NR latex masterbatch added into melt mixed SBR and ENR rubbers was investigated by Tan and co-workers [41]. An exfoliated structure of the masterbatch and coexistence of an intercalated–exfoliated structure in the vulcanisate were reported. The vulcanisation of the SBR and ENR systems in the presence of Ca-MMT was reportedly hindered, but improvement of TS, elongation, Shore A hardness, glass transition, storage modulus and so on, were also reported.

A novel process for preparing a coagulam of ternary fillers, e.g., CB, silica and NC incorporated into an NR latex masterbatch, has been reported by Alex and co-workers [42]. Dual-filled organoclay (e.g., Cloisite® 15A, 20A and 30B) and CB- loaded emulsion-polymerised SBR-based hybrid nanocomposites, using oil-extended carboxylated SBR as a compatibiliser, have been prepared [43]. Cloisite® 30B was found to be the best with respect to curing, mechanical, thermal and abrasion-resistant properties.

Using the latex compounding method, a high-performance two-step method was also designed in which the clay was dispersed at the nanoscale into SBR, which produced an 8-fold higher modulus at 300% strain and 7-fold higher TS compared with conventional SBR–clay vulcanisates [44]. 3-aminopropyltriethoxysilane (KH550) was simultaneously intercalated into clay galleries during co-coagulation and then *bis*(triethoxysilylpropyl) tetrasulfide (Si 69®) was incorporated into the above KH550- modified nanocompounds *via* mechanical blending, which showed the establishment of a chemical bridge between organically-modified clay and rubber through Si 69® during vulcanisation. RCN have also been prepared by a conventional two-roll mill method, using solid crumb NR and organically-modified smectite clays, and were compared with those produced by the latex method in terms of mechanical properties [45].

The nanocomposites prepared by the modified mill method were found to be superior as well as more effective for applications in biological systems. Isobutylene-isoprene rubber–OMMT clay nanocomposites were prepared by both solution and melt intercalation and the dispersion states of clay layers were studied by TEM and XRD [46].

The basal spacing was found to increase from 2.2 nm for the OMMT to 4.2 nm in the nanocomposite, and the mechanical and barrier properties were better when using the solution-intercalation method compared with melt intercalation. Brominated isobutyl-isoprene rubber (BIIR)–clay and EPDM RCN prepared by melt blending were studied to assess microstructural evolution, during curing, by WXRD and TEM. The WXRD results revealed that the intercalated structure of organo-modified clay (OMC) changed throughout the whole curing process [47].

The TEM results indicated that the spatial distribution of OMC is much better in BIIR (a polar rubber) than EPDM (a non-polar rubber). Therefore, the polarity of the rubber is the determining factor influencing the evolution of the intercalated structure in RCN. A series of highly filled (up to ~60 wt% of filler with respect to rubber) RCN based on EPDM, SBR and epichlorohydrin rubbers were prepared by melt blending, and the dynamic mechanical thermal analysis showed that a melt-like thermal transition of the alkyl chains of the surfactant of OMC still occurred in the intercalated filler structure [48].

Highly filled RCN also showed outstanding gas barrier properties. The preparation and properties of NC (bentonite) and its modified varieties, by adding organic amines of varying chain lengths (dodecylamine, hexadecylamine and octadecylamine) and an amine-terminated butadiene-acrylonitrile copolymer (ATBN), and the effect of their addition to natural and synthetic rubbers (SBR and NBR), were studied using FTIR, TEM, SEM, TGA and WXRD techniques [49]. X-ray results showed that the intergallery distance of the clay was increased due to intercalation by the amine and ATBN. The physico-mechanical properties were greatly improved at a low concentration of NC in comparison to those obtained with CB.

The characterisation of nanocomposites of an ethylene-vinyl acetate copolymer rubber and different types of NC, prepared in an internal mixer by melt blending, showed an optimum improvement of mechanical properties and permeability values at 3 wt% clay loading [50].

A novel NR–silicon dioxide ($SiO_2$) nanocomposite combining self-assembly and latex techniques was developed by Peng and co-workers [51]. $SiO_2$ NP at low concentration (e.g., <4 wt%) showed an assembled core-shell structure in NR, whereas employing poly(diallyldimethylammonium chloride), as a polymer with a molecular weight of approximately 100,000–200,000; 20 wt% dissolved in water as an intermedium led to only primary aggregates of $SiO_2$ being observed. Upon increasing the $SiO_2$ concentration, the secondary aggregation of NP occurred and the size of the NP increased quickly. A novel acid-free preparation of NR–clay nanocomposites has been reported by Nakason and co-workers [52].

As per the existing latex preparation techniques for nanocomposites, the co-coagulation of rubber latex and an aqueous suspension of clay was achieved with the assistance of acid, which generated a highly acidic rubber effluent resulting in environmental toxicity. Therefore, the authors first dispersed Na-MMT in distilled water using an ultrasonicator. The NR latex was gradually added to this suspension at RT with continuous stirring for 5 days or coagulated in a dilute formic acid solution, which was subsequently washed with water to neutral, crept through a mill and dried in a hot air oven. In both cases, the dried composites were compounded in an internal mixer, sheeted out using a two-roll mill and vulcanised in a hydraulic press.

The vulcanisates showed superior thermal resistance, tensile and modulus properties compared with the nanocomposites prepared by the conventional acid

coagulation process. The radiation crosslinking of NR–clay nanocomposites was studied where Na-MMT was modified with cationic surfactants, e.g., dodecylammonium chloride and octadecylamine (ODA) ammonium chloride and the melt-mixing method was adopted to produce NR–Na-MMT, NR–dodecylammonium chloride-MMT and NR–ODA-MMT nanocomposites [53]. An optimum electron beam dose of 250 kGy was used for crosslinking, and the gel content and tensile properties showed optimum values at a range of 3.0 to 5.0 phr NC content, respectively. A polar rubber-like ENR was used as a compatibiliser for better dispersion of Cloisite® 20A in SBR nanocomposites, which were prepared *via* solution mixing and cured with a sulfur-accelerator curative package [54]. The nanocomposites showed improved storage modulus and lesser damping properties. An NR latex–clay (MMT) nanocomposite was evaluated for mechanical and barrier properties and compared with those of conventional NR latex containing $CaCO_3$ [55]. The crosslink density was found to increase with clay concentration and a higher crosslink density offered better permeation resistance of NR-MMT compared with NR–$CaCO_3$ nanocomposites.

Blends of NR and SBR rubbers, reinforced with both short Nylon fibres and Cloisite® 15A NC, were used to prepare nanocomposites in an internal mixer followed by two-roll milling as an overall three-step mixing process [56].

The NC was used in place of conventional resorcinol, with hexamethylene tetramine and a hydrated silica-bonding system as a fibre-matrix adhesion promoter. The storage modulus and Tg increased remarkably with an increasing amount of organoclay and fibre loading. TGA showed greatly improved thermal stability of the organoclay nanocomposites coupled with good barrier properties. Activated nanokaolinite has also been impregnated in SBR using a dispersion kneader and two-roll milling followed by isostatic compression moulding [57].

The thermal conductivity of the nanocomposite was reduced by 41% while the thermal impedance of the composites was elevated by 31%. The thermal stability and endothermic capability were augmented with increasing filler concentration. The production of tailor-made poly(2-ethylhexyl acrylate) (PEHA), prepared *via in situ* living radical polymerisation at 90 °C using CuBr and Cu(O) as the catalyst and *N,N,N″,N″,N″*-pentamethyldiethylenetriamine (PMDETA) as a ligand, was achieved in the presence of layered silicates, e.g., Na-MMT, Cloisite® 15A and 30B, to prepare PCN [58].

The PEHA–clay nanocomposites exhibited intercalated morphology and better thermal properties than neat PEHA. Das and co-workers described the synergistic effects of expanded, stearic acid-modified organoclay and a CB hybrid system in NR-based truck-tyre compounds [59]. Stearic acid-modified clay was found to dominate the reinforcing ability compared with the unmodified version, as highlighted by the enhanced mechanical, dynamic mechanical and rolling resistance properties.

The fracture toughness of a series of Nylon 6/organoclay/maleic anhydride (MA)-grafted-polyethylene octene elastomer nanocomposites was evaluated using the J-integral method [60]. The fracture toughness increased with increasing

polyethylene octene elastomer-*g*-MA content at a fixed loading of organoclay, but reduced when the clay loading was increased. TEM in combination with a single-edge double-notch four-point bend test revealed the role of different factors, e.g., internal cavitation of the polyethylene octene elastomer-*g*-MA particles leading to crack-tip deviation under triaxial stress, crazing consisting of line arrays of the expanded voids and severe plastic deformation of the matrix resulting in a drastic increase of the fracture toughness. Fatigue life estimation of rubber parts, e.g., automotive engine mounts, is very important and is one of the critical issues that predicts the premature failure of the component during operation.

Woo and Park developed an environmentally friendly RCN, by inserting a nanofiller between the silicate layers over a temperature range of 70 to 100 °C, and after performing static and dynamic tests of the nanocomposites, they verified the mechanical properties were superior to the existing rubber composites [61]. Furthermore, a new method was developed to rapidly estimate the fatigue life time at an initial stage of design. Assuming the fatigue damage parameter is in the domain of the Green–Lagrange strain, they verified a relative match between expected life times of actual mounts *versus* results obtained by simulated fatigue tests. A reasonably good match was obtained between the predicted values and actual test results, thus saving development time while assuring, safety and reliability.

The structure–property relationship of an organoclay-filled NR–BR blend for tyre tread applications has been studied by Kim and co-workers [62]. Furthermore, the incorporation of layered silicates in an SBR solution has been used to develop green tyre compounds with low rolling resistance and high wet grip characteristics [63].

These compounds have also emerged as promising materials for tyre inner tubes, inner liners and off-road tyre tread, and have opened up new prospects in tyre tread formulations with the potential to replace a major portion of CB by only a few parts of layered silicate (e.g., 4–5 phr) [28].

The use of about 5 to 90 phr layered silicate modified with alkylammonium ions in tyre tread compounds with diene rubbers has been reported by Heinrich and co-workers [64].

Rooj and co-workers studied the impact of filler dispersion and rubber–filler interactions on the viscoelastic behaviour (Payne effect) of NR–clay nanocomposites, and introduced a process called the 'propping-open approach', in which the fractal dimensions of NP clusters and the extent of highly exfoliated structures of NP were assessed [65].

The incorporation of nanocomposites into tyre components is expected to increase their overall performance, in particular, with regards to increased fuel efficiency by virtue of improved rolling resistance, reduced heat build-up, improved traction, enhanced wear resistance and air retention, better reliability against premature failure and the potential of easy disposal. The successful use of NC in rubbers can ensure safety and an extended service life to tyres. NC used in the

preparation of RCN accounts for nearly 80% of the total volume of nanofillers used in the rubber industry.

NC are less expensive than other fillers and the rubber compounds made out of them exhibit acceptable toughness, excellent barrier properties, an enhanced heat distortion temperature, improved colourability, and superior scratch, flame and damage resistance.

NP also reduce strain vibration, which occurs when a tyre is used at high speed, and enables superior traction, especially on wet roads. CNF, multi-walled carbon nanotubes, polyhedral oligomeric silsesquioxanes and other polymorph varieties of carbon, e.g., graphene, are gaining importance in the automotive sector. Brominated isobutylene-*co*-paramethylstyrene rubber, for the development of tyre tread for winter traction tyres on icy/asphalt surfaces or on snowy glaciers, has been reported [66].

The rolling resistance of tyres can be improved using a CB-silane-treated silica combination, e.g., the stopping distance of a car on wet roads can be reduced by 15–20% along with a reduction of 5% in fuel consumption. Gopi and co-workers prepared SBR–clay nanocomposites with Cloisite® 15A *via* melt intercalation and observed that 6 phr of organoclay could replace 15 phr of CB in a conventional tyre tread compound [67]. They also observed that SBR (styrene content 23%) filled with 6 phr of Cloisite® 15A, in association with 25 phr of high abrasion furnace (HAF) CB, was effective for the development of tyre tread with better rolling and good abrasion resistance, good wet grip and lower heat build-up, and improved dynamic mechanical properties compared with a conventional SBR tyre tread compound containing 40 phr of HAF. Dynamic mechanical analysis revealed that the new tyre tread exhibited better rolling resistance, comparable wet grip and lower heat build-up properties.

Sanchez and co-workers reviewed the applications of hybrid organic–inorganic nanocomposites based on rubber–clay (vermiculite) and the potential to develop a core-sheath type of structure for improved gas barrier properties in tyres for bicycles, cars and trucks [26].

Rubber-toughened thermoplastics containing NC are more attractive than a conventional rubber–plastic blend for automotive applications. High surface nano – ZnO has been found to be more efficient as a cure activator than conventional ZnO for both NR and NBR compounds [68].

Hence, nanotechnology is opening up new avenues for the development of innovative products and applications in the automobile sector to achieve safety, comfort, fuel efficiency, durability and reduced carbon dioxide (CO2) emissions [69–72]. A dual phase CB- and NC-filled SBR compound has been developed for tyre tread which showed improved dynamic properties, e.g., good rolling and wet skid resistance at 3 phr loading of NC [73].

The improved properties were attributed to enhanced filler–rubber adhesion and the role of calcium stearate as a superior dispersion promoter for NC.

In addition to automotive components, sports equipment and consumer goods; nanotechnology and rubber nanocomposites have also received great interest for vital strategic and critical applications in the defence and aerospace sectors [64–66].

The major automotive tyre producers in the international market are Yokohama Tyre Corp., Japan; Pirelli S.P.A., Italy; Goodyear Tyre & Rubber Co., USA; Continental AG, Germany; InMat Inc., USA and so on.

## 4.3 Polyurethane–Clay (Attapulgite) Nanocomposites for Shape-memory Applications

### 4.3.1 Current Scenario and Literature Gap

In most published research, the study of shape-memory behaviour has been carried out using long-chain diols based on polycaprolactone, polylactic acid and other diols, and evaluated at ambient and higher temperatures [74–79]. Relatively few reports are available on the SME of SPU based on ether types of diol (e.g., polytetramethylene glycol) and aromatic diisocyanate [e.g., diphenylmethane diisocyanate (MDI)], although they possess many desirable attributes such as low-temperature flexibility, excellent thermal and thermo-oxidative stability along with biocompatibility [80–82]. SPU containing various nanofillers, such as NC, CNT, nano-ceramics and metal nanopowders, have been used as reinforcements and to significantly improve the mechanical and functional properties of SMP [6, 83–88].

However, most of the literature related to evaluating shape-memory behaviour under subambient conditions has been reported by our group [89–92].

Low-temperature shape-memory behaviour of SPU is important for automobile applications, e.g., in winter tyres with low skid resistance, and clothing materials for use in extremely cold weather, for instance, high-altitude areas.

Determination of the shape-memory properties of polymers involves assessing stress–strain measurements obtained under uniaxial extension in a universal testing machine (UTM), fitted with an environmental cabinet in order to vary temperature [77, 78, 93–97]. Some researchers have also utilised a dynamic mechanical analyser and nanoindenter for this purpose [98–101].

Stress–strain tests in a UTM require a large amount of material, in order to prepare a sufficient number of ‘dumbbell’ specimens, and the tests are conducted either at slower heating/cooling rates or at an isothermal temperature, which is time consuming. As an alternative, TMA could be used to monitor the dimensional changes of a sample upon being subjected to temperature variation at a controlled

rate and under a specific load, in either an inert or air environment. For this technique, a small quantity of sample (approximately 10–15 mg) could be subjected to heating/cooling at higher rates, resulting in reduced sample analysis time and also allowing the dimensional changes with temperature variation, as well as force ramp conditions for cyclic experiments, to be recorded.

SPU and its nanocomposites have been extensively examined for shape-memory performance under stress-free or unconstrained conditions by holding the sample at a constant elevated temperature or applying a continuous temperature increase until the strain is completely recovered [102–107]. In most published work, the single programming procedure has been applied and the resulting responses have been obtained under stress-free recovery or unconstrained conditions [108–119].

However, from a practical point-of-view a constraint-recovery condition, where a force is applied during the recovery process, is more important but scarcely reported [120]. The Vr and the timescale of the response depend on many factors including the thermal environment, deformation temperature, thermal conductivity of the fillers, shape Tf and heating/cooling rates.

An accurate estimation of Vr under both unconstrained and constrained conditions is also required in order to predict the correct SMP response. Therefore, the application of thermomechanical conditions in shape-memory programming is likely to bridge the above-mentioned technical gap and help to overcome the issue, which is due to molecular mobility and long-range chain slippages, and has the added benefit of a relatively faster timescale for the experiments.

### 4.3.2 Attapulgite – Segmented Polyurethane Nanocomposites

SPU consist of alternating hard and soft segments, which are microphase separated due to thermodynamic incompatibility, and are used in a wide range of applications in automotive adhesives and sealants, coatings, high-performance engineered components, sports goods and clothing [86, 121].

Relatively little attention has been paid to attapulgite (AT) NC, a natural hydrated magnesium–aluminum silicate with a structural formula $Mg_5Si_8O_20(OH)_2(OH_2)_4.4H_2O$, which has a fibre-like morphology and enables the adsorption of organics onto clay surfaces. They consist of a 3D network of densely packed rods with a diameter less than 100 nm and a length ranging from hundreds of nanometres to several micrometres. AT is relatively inexpensive and exhibits high rigidity and thermal stability, along with promising strength and toughening characteristics, and is mostly used as an adsorbent, adhesive, catalyst support and reinforcement for polymers. However, relatively few reports are available on the shape-memory properties of AT [122, 123]. When used in NR, AT enhances the curing rate and has the capacity to be a compatibiliser in immiscible blends of NR with other rubbers [80].

NR–AT-based RCN showed significant improvement in TS, wear resistance, thermal stability and solvent resistance.

An 8% solution of SPU in tetrahydrofuran (THF) was prepared in four round-bottom flasks and kept separately. AT loadings (with respect to SPU) of 1, 3 and 5 wt% were separately mixed in THF and sonicated for 15 min to minimise agglomeration. Thereafter, they were added individually into separate SPU solutions and stirred for 15 min followed by sonication for another 10 min to ensure homogeneous dispersion.

The mixtures were then poured into films in a Petri dish, evaporated to dryness at RT and kept in a vacuum oven at 40 °C until reaching a constant weight. The composite samples were named by prefixing PU before different wt% of AT, namely PUAT1, PUAT3 and PUAT5. Neat SPU, i.e., without any filler, was also treated in the same way and labelled PU, i.e., the control sample. Surface topographic images of the samples were collected using a low-vacuum SEM. WXRD data were collected using a D8 ADVANCE diffractometer (Cu Kα radiation, $\lambda$ =1.54056 nm) from BRUKER, Germany, with a tube voltage of 40 kV and a current density of 40 mA over a scanning range of $2\theta$ = 5–40°. The non-isothermal crystallisation data were collected using modulated differential scanning calorimetry (MDSC) (model – Q 200: TA Instruments, USA).

Approximately 5–10 mg of sample was heated at 10 °C/min from ambient to 200 °C and maintained isothermally for 2 min to remove any thermal history. Thereafter, the samples were cooled from 200 °C to ambient at 5 °C/min. A dynamic nitrogen flow of 50 ml/min was maintained throughout experimentation. For the thermal stability assessment, TGA data were collected in an inert argon environment using MTGA (model – Q500; TA Instruments, USA). A 60 and 40 ml/min purge flow of argon was maintained in the furnace and balance assembly of the instrument, respectively. In order to study the effect of the AT on Tg, TMA (model – TMA 2940; TA Instruments, USA) was used in the temperature range of –100 to 20 °C at 10 °C/min.

A 0.01 N force was applied with a nitrogen purge flow of 100 ml/min. The cyclic shape-memory experiments on the samples were conducted using modulated thermomechanical analysis (MTMA) (model – Q400EM; TA instruments, USA). In order to understand the effect of programming parameters on the shape-memory response, two sets of experiments were configured and performed on each sample. The first set of experiments corresponded to free or unconstrained recovery, whereas the second set was constrained recovery in a stress controlled mode.

In the first set of experiments, the following programming was applied:

1: Initial temperature 10.00 °C; 2: force 0.250 N; 3: ramp 10.00 °C/min to –80 °C; 4: force 0.001 N; 5: isothermal for 5 min; 6: ramp 10 °C/min to 20 °C and 7: end of method.

The minimum force (0.001 N) at sequence No.4 was applied to establish contact of the probe with the sample, it would otherwise be lost if the force at sequence No.4 was zero.

In the second set of experiments, the sequence was:

1: Initial temperature –10 °C; 2: strain 53%; 3: ramp 10 °C/min to –80 °C; 4: force 0.001 N; 5: isothermal for 5 min; 6: force 0.020 N; 7: ramp 10 °C/min to 20 °C and 8: end of method. The constraining force of 0.020 N at sequence No.6 was applied separately to each sample during the recovery process for the measurement of the extent of recovery.

For the first set of experiments, the sample was kept beneath the probe of the MTMA system and the temperature was equilibrated at an initial value of 10 °C. Once the sample reached the equilibrium temperature, the required force detailed at sequence No. 2 was instantaneously applied and the sample was then cooled at a cooling rate of 10 °C/min to –80 °C. Once the final temperature of –80 °C was reached, the load was removed and the sample was maintained isothermally for 5 min, completing the shape-fixing step.

After the isothermal period, the sample was again heated at 10 °C/min to reach a temperature of 20 °C; this step is called the shape-recovery process. During all these steps, the dimensional changes of the sample, with respect to both temperature and time, were recorded. For the second set, the experiments were performed in a similar way, but at sequence No.1 the deformation temperature was –10 °C and at sequence No.2 a predefined strain of 53% was imposed.

Figure 4.1 shows the SEM photomicrographs of the neat as well as the SPU–AT nanocomposites, where the appearance of the bright features correspond to AT evenly dispersed in the SPU matrix. However, there are some agglomerates that increase in size upon increasing the concentration of AT in the composites.

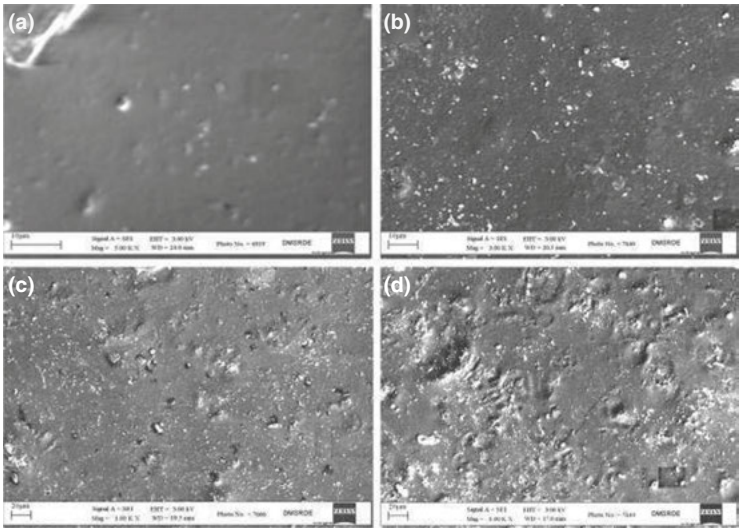


**Figure 4.1:** SEM image of (a) neat SPU; (b) PUAT1; (c) PUAT3 and (d) PUAT5.

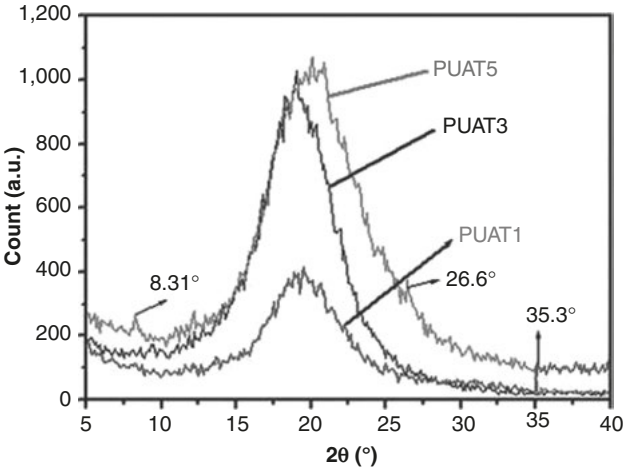


**Figure 4.2:** WXRD pattern of the composites.

Figure 4.2 illustrates the WXRD pattern of the composite samples in the 2θ range of 5 to 40°. A diffused diffraction peak centred at 20° is characteristic of the MDI–1,4- butanediol hard-segment reflection, indicating some aggregated hard domains resulting from the microphase separation and a lack of ordered crystal structure in these samples.

The intensity of the amorphous hallo increases and the peak becomes sharper upon increasing the AT content, whereas the location of the hallo is not shifted to any significant degree. However, at a higher concentration of AT, e.g., 5 wt%, some shoulder regions are observed at 8.31, 26.6 and 35.3° corresponding to crystal planes 110, 400 and 161, respectively, which are characteristic of AT.

Estimation of the crystallisation Tp and associated crystallisation enthalpy (ΔH) is essential in order to describe the crystallisation behaviour and the effect of the addition of nanofiller on the filler–matrix interaction. The analysed MDSC traces for samples PU, PUAT1, PUAT3 and PUAT5 at a cooling rate of 5 °C/min are presented in Figure 4.3. The results with respect to Tp and ΔH have been calculated and are detailed in Table 4.1. It can be noted that there is a change of the Tp (approximately 4 °C) of SPU due to the addition of AT, which indicates a moderate nucleating effect. At a higher AT concentration, the Tp decreases, although only slightly, showing a saturation level of the nucleating efficiency of AT during SPU crystallisation. The ΔH value of neat SPU is modified in the presence of AT and the extent of this modification is dependent upon the concentration of the filler. ΔH is highest for sample PUAT5 followed by PUAT3, PUAT1 and neat SPU.

Figure 4.4 depicts the comparison of thermal stability in an inert argon atmosphere and shows that inclusion of AT in the nanocomposites enhanced the thermal

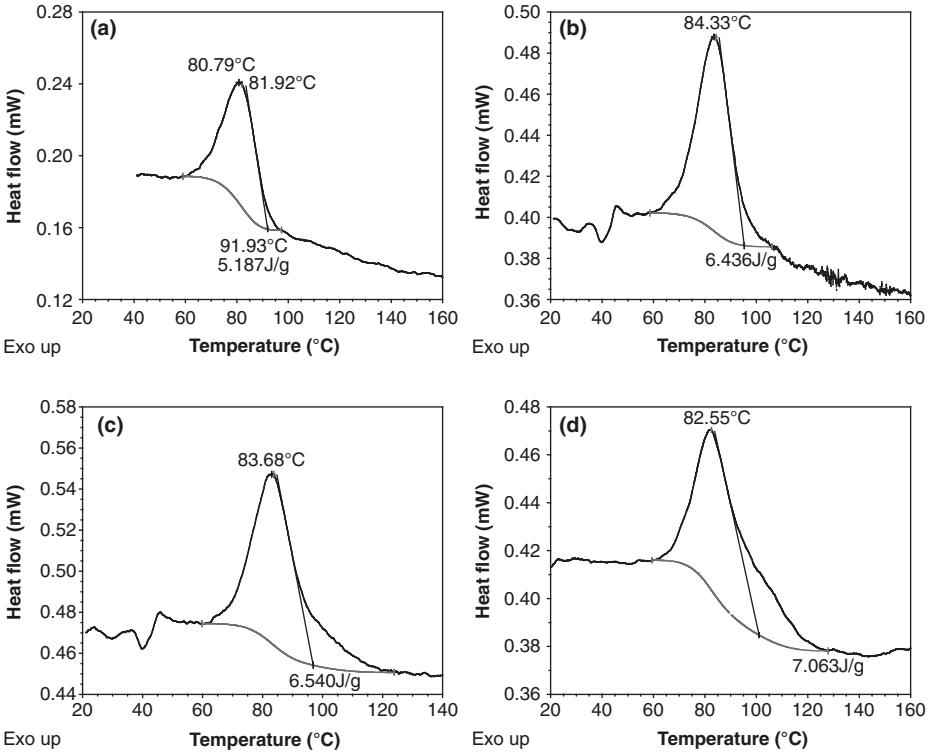


**Figure 4.3:** MDSC traces of (a) SPU; (b) PUAT1; (c) PUAT3 and (d) PUAT5.

**Table 4.1:** $T_p$, ΔH and $T_g$ values of the samples.

| Sample | $T_p$ (°C) | ΔH (J/g) | $T_g$ (°C) |
|---|---|---|---|
| PU | 80.79 | 5.187 | −48.47 |
| PUAT1 | 84.33 | 6.436 | −38.51 |
| PUAT3 | 83.68 | 6.540 | −33.35 |
| PUAT5 | 82.55 | 7.063 | −20.77 |

stability of the SPU. The high aspect ratio, the superior insulating and morphological properties of AT, and their uniform dispersion in the elastomer matrix, resulted in a more tortuous path for the passage of decomposed volatile products forced to move around in a random walk, thus hindering their escape. The overall improvement in the thermal stability is about 10 °C upon the addition of 3 wt% of AT and at a higher concentration, e.g., at 5 wt%, it does not show any further improvement in thermal stability.

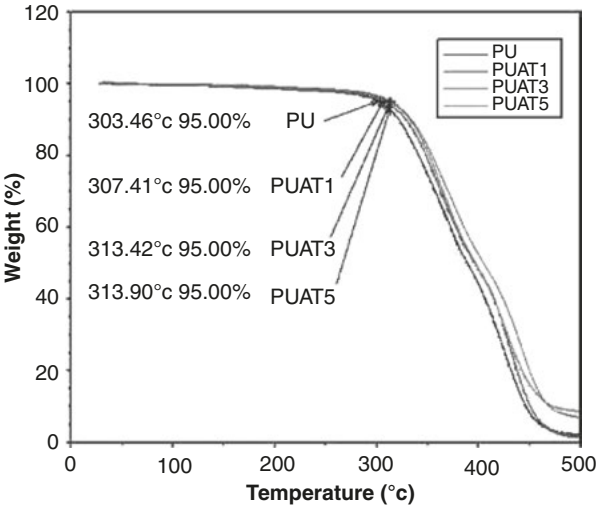


**Figure 4.4:** Assessment of the thermal stability of the samples.

Figure 4.5 shows TMA plots indicating dimensional change *versus* temperature for all the samples. The value of $T_g$ for each sample has been evaluated and is presented in Table 4.1. It can be noted that the $T_g$ of SPU shows a positive temperature shift upon inclusion of the AT and the overall improvement is about 28 °C for 5 wt% of clay. This is due to chain segments adjacent to the filler particles becoming highly restrained and thereby elevating the energy threshold needed for glass transition. The considerable increase in $T_g$ is desirable as these materials could be used in applications that withstand higher temperatures in comparison to virgin polymers. The AT offers excellent reinforcement of the SPU, even when present in a small amount, i.e., 5 wt%, due to the large surface area which is associated with imparting heterogeneous nucleation, i.e., making the material harder. The improvement in both the decomposition temperature as well as $T_g$ in the presence of AT indicates good dispersion and interaction of the clay with SPU.

Shape-memory experiments have been conducted with respect to time for neat as well as composite samples. At time zero, when the samples were at a deformation temperature of 10 °C, a 0.25 N load was applied and the samples were then cooled at a rate of 10 °C/min. At around 9 min, when the samples reached a temperature of –80 °C, the load was removed and the samples were maintained isothermally.

The step was termed the cooling/shape-fixing process. After the isothermal period, the samples were heated at a rate of 10 °C/min up to 20 °C, termed the heating/ recovery process. Figure 4.6 depicts the comparison of the extent of deformation upon applying an equal load to neat and composite samples. It can be observed that the deformation is less in the case of composite samples, which

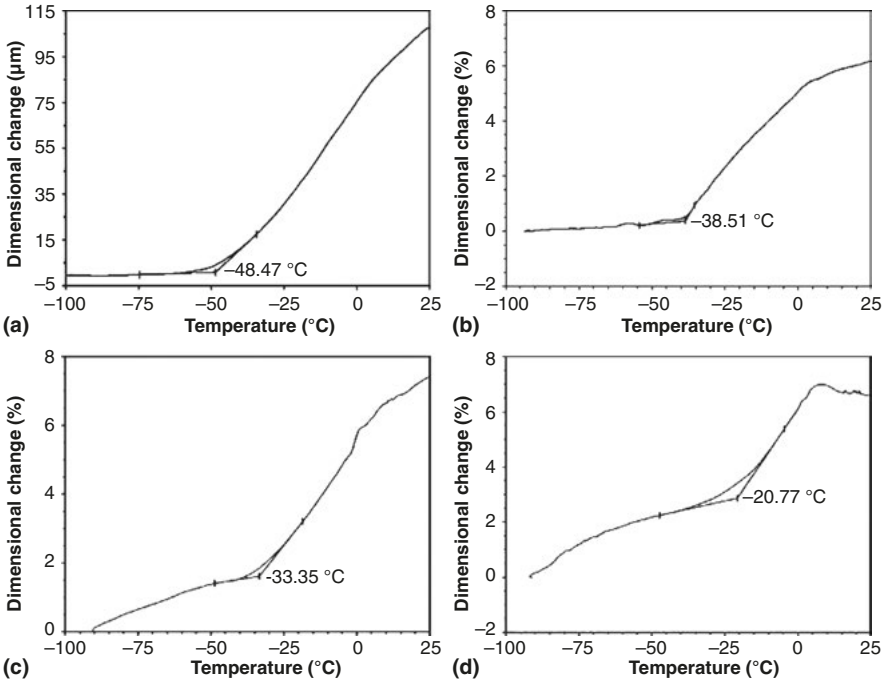


**Figure 4.5:** $T_g$ of (a) SPU; (b) PUAT1; (c) PUAT3 and (d) PUAT5.

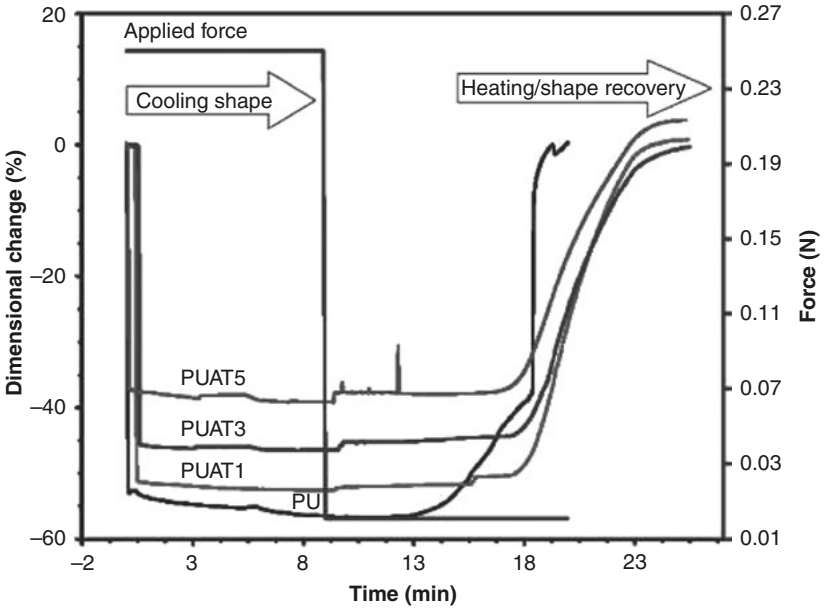


**Figure 4.6:** $R_f$ and recovery with respect to time.

indicates an improvement in the dimensional stability due to the addition of the filler. The improvement was greatest in sample PUAT5. This improvement in dimensional stability can be attributed to the reinforcing action of the AT and is in accordance with the increased $T_g$ and higher degree of crystallinity.

Figure 4.7 depicts the shape-memory profile of the samples with respect to temperature. It can be seen that when the samples are cooled to a temperature of −80 °C with an applied load, the deformed shape of the neat as well composite samples remain fixed. This phenomenon can be explained by considering the broad thermal transition or characteristic $T_g$ of the samples. The broad thermal transition can be considered to consist of an infinite number of sharp transitions continuously distributed over a broad $T_g$ and can be regarded as individual memory elements. Depending on the deformation temperature only, a fraction of memory elements available in the deformation temperature zone become activated and undergo orientation proportional to the reduction of the conformational entropy of the system. Freezing these memory elements in an oriented state results in the storage of energy in the glassy state of the material. In other words, the conformational rearrangement of the reversible phase induced by deformation is severely restricted at temperatures below $T_g$ and hence the chains cannot recover.

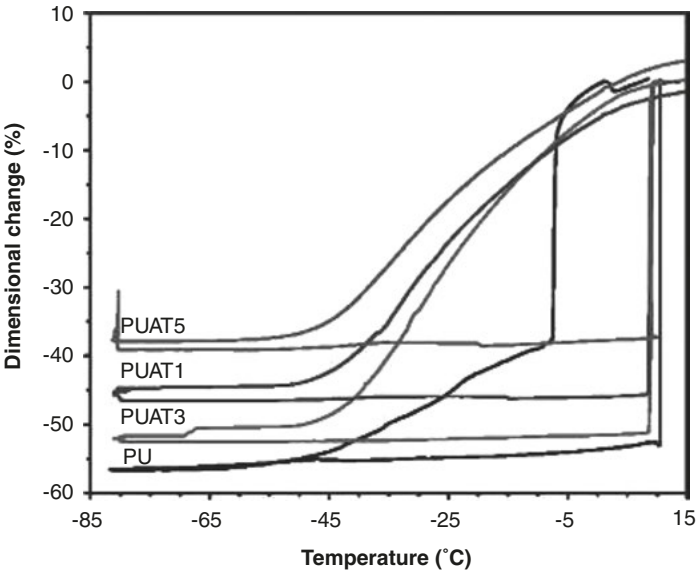


**Figure 4.7:** $R_f$ and recovery with respect to temperature.

After load removal, the samples show minute instantaneous recovery, which is attributed to a small fraction of memory units that preserve mobility even when the sample is cooled below the transition temperature. This is in accordance with the molecular dynamics of polymers, which shows that below $T_g$, segmental dynamics are present

within a static electrostatic network [103]. The entropic elasticity thus generates an instantaneous reverting force upon removal of the load. However, the magnitude of instantaneous recovery is not appreciable and $R_f$ for neat as well as composite samples is almost 100% under the chosen strain and thermomechanical conditions applied. Notably, the virgin sample of SPU and SPU–AT composites demonstrated a high $R_f$ and inclusion of AT had no significant effect on the $R_f$ of the SPU.

### 4.3.3 Shape Recovery under Unconstrained Conditions

Different types of interactions have been demonstrated between alternating soft and hard segments of SPU including: (1) hydrogen bonding between the carbamoyl group and carbonyl group of hard segments, (2) dipole–dipole interaction between carbonyl groups of hard segments, (3) induced dipole–dipole interaction between the aromatic rings of hard segments and hydrogen bonding among hard segments, and (4) dipole–dipole interaction between carbonyl groups [80]. During the recovery process, the destabilisation of these interactions upon heating initiates molecular mobility. However, AT serves as an additional fixed phase in the same manner as thermally stable crosslinking points. The oriented state, in which the conformational entropy of the system is reduced, is an entropically unfavourable state and, therefore, memory units already oriented during the $R_f$ process try to regain a more probable entropic state at each temperature and thereby, release elastic energy stored in the sample. This creates a restoring force in the sample, which reverts back to its permanent shape. In spite of the significant improvement in the dimensional stability of the composite samples, the shape-recovery profile showed little change from virgin SPU but complete recovery was still realised. However, neat SPU showed a sharp shape-recovery profile in comparison to composite samples due to the reinforcement action of AT.

### 4.3.4 Recovery Speed/Response Time under Unconstrained Conditions

The $V_r$ data are a very important aspect of product design for a particular application, but are rarely reported in the literature. The accurate estimation of $V_r$ data is difficult using conventional methods employed for the assessment of shape-memory performance. Figure 4.8 illustrates the comparison of $V_r$ of the neat and composite samples with respect to time, while Figure 4.9 depicts the same with respect to temperature. The peak recovery rate values for both cases are presented in Table 4.2. The $V_r$ graphs of Figure 4.8 show that the peak recovery rate is highest for neat SPU and decreases for the composites in the following order: PUAT1 > PUAT3 > PUAT5.

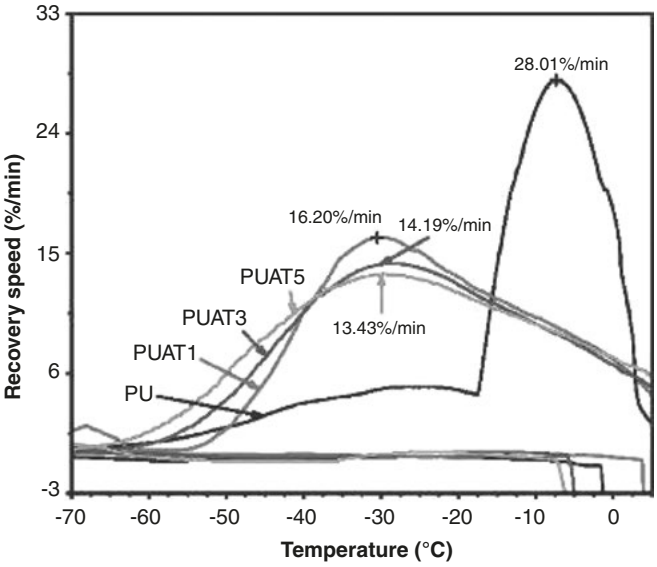


**Figure 4.8:** $V_r$ with respect to time.

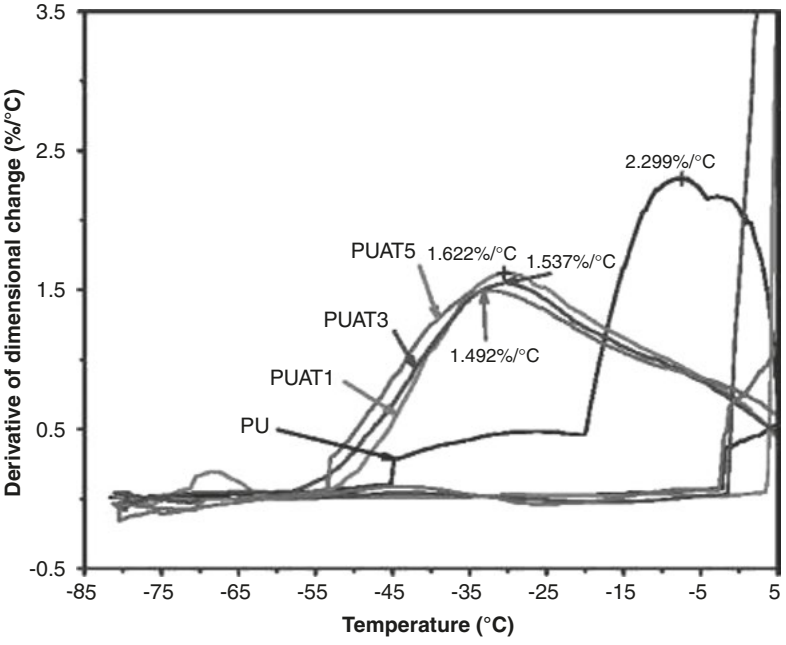


**Figure 4.9:** $V_r$ with respect to temperature.

**Table 4.2:** Peak recovery rate with respect to time and temperature under unconstrained conditions.

| Peak recovery rate | Sample name | | | |
|---|---|---|---|---|
| | PU | PUAT1 | PUAT3 | PUAT5 |
| With respect to temperature (%/°C) | 2.29 | 1.62 | 1.53 | 1.49 |
| With respect to time (%/min) | 28.01 | 16.20 | 14.19 | 13.43 |

This composite trend corresponds with the nature of interaction and dimensional stability of the AT-based composites. The higher the structural rigidity, the greater the hindrance during the recovery process. Although the recovery rate of the composite samples is retarded compared with neat SPU, full recovery was possible within the temperature interval set for experimentation.

The $V_r$ with respect to temperature in Figure 4.9 follows a similar trend to $V_r$ with respect to time as the experiments were carried out under temperature ramp conditions.

### 4.3.5 Shape Recovery under Constrained Conditions

Figure 4.10 depicts the recovery profile of the samples when they were subjected to a constraining load of 0.02 N during the recovery process. However, deformation was carried out under isostrain conditions at approximately 53%. It can be seen in Figure 4.10 that upon application of a minimum constraining force of 0.02 N, the neat sample was not able to recover appreciably due to poor strength; however, the composite samples showed a greater extent of recovery under the same constraining force.

This may be due to the fact that the composite samples are able to generate enough recovery force to counteract the constraining force during the recovery process. The higher recovery force generated in the composite samples resulted in a greater extent of recovery under the given constraining conditions, indicating reinforcement of the SPU in the presence of AT.

### 4.3.6 Recovery Speed/Response Time under Constrained Conditions

The recovery rate speed under an applied constraining force is important from a practical point-of-view in order to design products with a predetermined response

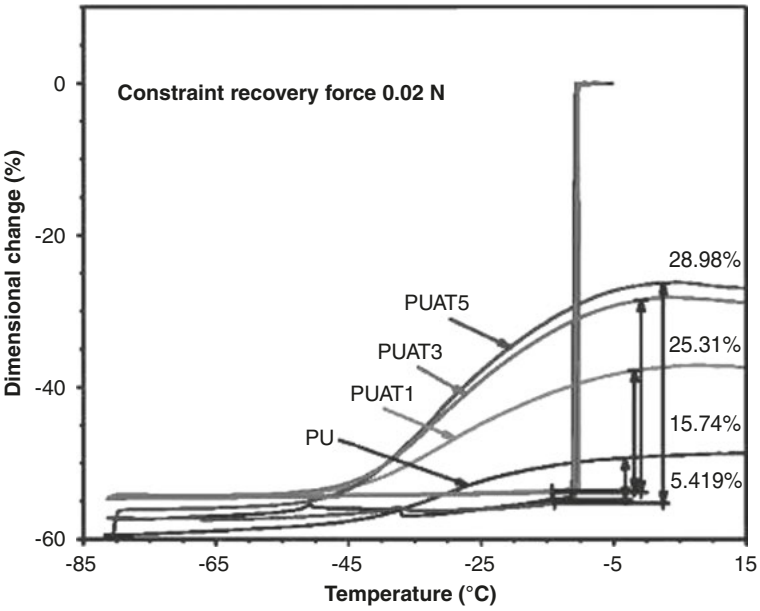


**Figure 4.10:** Constraint-recovery process of samples.

time. Figure 4.11 represents the comparison of constrained $V_r$ with respect to time for neat SPU and that of the composite samples at an applied constraining force of 0.02 N, while Figure 4.12 depicts the same with respect to temperature.

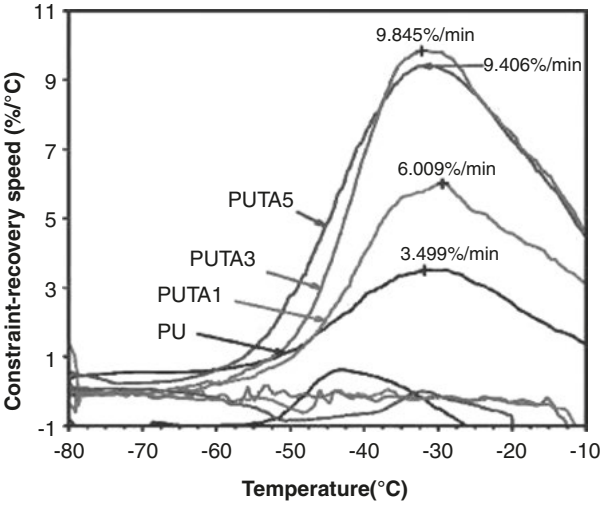


**Figure 4.11:** Comparison of constrained $V_r$ with respect to time.

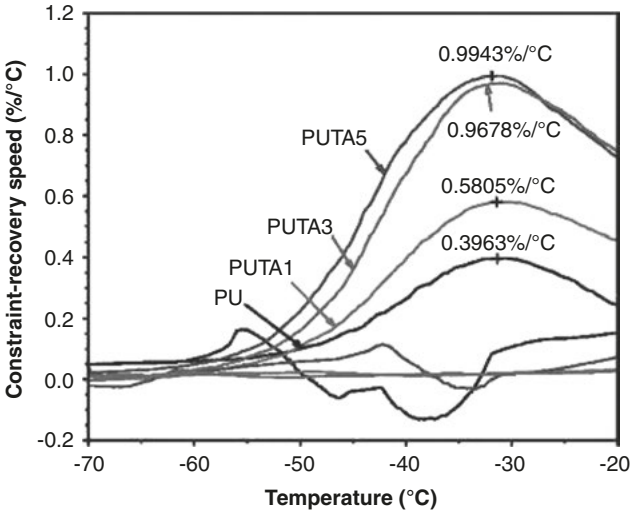


**Figure 4.12:** Comparison of constrained $V_r$ with respect to temperature.

**Table 4.3:** Peak recovery rate with respect to time and temperature under constrained conditions.

| Sample | Peak recovery rate | |
|---|---|---|
| | With respect to time (%/min) | With respect to temperature (%/°C) |
| PU | 3.49 | 0.39 |
| PUAT1 | 6.00 | 0.58 |
| PUAT3 | 9.40 | 0.96 |
| PUAT5 | 9.84 | 0.99 |

The summary presented in Table 4.3 indicates that the peak recovery rates of the composites are higher than the neat sample, which is contrary to that observed in the case of the stress-free or unconstrained conditions depicted in Table 4.2. This is because under the applied constraining force, the neat sample is not able to counteract the constraining force during the recovery process while the composite samples are able to do so. As loading increases, the extent of reinforcement also increases, thus generating more recovery force and hence increasing the peak recovery rate.

## 4.4 Summary and Conclusions

Despite the substantial progress made in the development of novel RCN, further studies are needed to investigate the effect of curing agents in the clay galleries in

order to develop *in situ*-cured rubber nanocomposites. More effective methods of ensuring NP are homogenised into the rubber matrix and understanding the interfacial properties of the rubber NP framework are also required. Furthermore, simulation and modelling studies to correctly predict the final mechanical properties of the material are of paramount importance.

The field of SMP and composites is growing at a very rapid pace and various applications, essentially for the automobile sector, are envisioned in the near future that have huge commercial potential.

**Acknowledgement:** The authors wish to thank the Director of the Defence Materials and Stores Research and Development Establishment (DMSRDE), Kanpur for his kind permission to publish the work as a book chapter.

# References

1. A.D. Katheria, E. Singh, R. Kumar, R. Srivastava and B.C. Yadav, *International Journal of Innovative Research in Science, Engineering and Technology*, 2016, **5**, 2, 1960.
2. G. Armstrong, *European Journal of Physics*, 2015, **36**, 6, 063001.
3. *Handbook of Polymernanocomposites: Processing, Performance and Application*, Volume A: Layered silicates, Eds., J.K. Pandey, K.R. Reddy, A.K. Mohanty and M. Misra, Springer, Berlin, Heidelberg, Germany, 2014, p.511.
4. L. Peponi, D. Puglia, L. Torre, L. Valentini and J.M. Kenny, *Materials Science and Engineering, R: Reports*, 2014, **85**, 1.
5. P.H.C. Camargo, K.G. Satyaanarayana and F. Wypych, *Materials Research*, 2009, **12**, doi:10.1590/51516-14392009000100002.
6. F. Hussain, M. Hojjati, M. Okamoto and R.E. Gorga, *Journal of Composite Materials*, 2006, **40**, 17, 1511.
7. J. Markarian, *Plastics, Additives and Compounding*, 2005, **7**, 6, 18.
8. W. Gacitua, A. Ballerini A. and J. Zhang, *Maderas: Ciencia y Tecnologia*, 2005, **7**, 3, 159.
9. P.C. LeBaron, Z. Wang and T.J. Pinnavaia, *Applied Clay Science*, 1999, **15**, 11.
10. F. Cao and S.C. Jana, *Polymer*, 2007, **48**, 13, 3790.
11. M. Mondal, P.K. Chattopadhyay, D.K. Setua, N.C. Das and S. Chattopadhyay, *Polymer International*, 2011, **60**, 9, 1334.
12. J. Wang, P.A. Wheeler, W.L. Jarrett and L.J. Mathias, *Journal of Applied Polymer Science*, 2007, **106**, 1496.
13. M. Mondal, P.K. Chattopadhyay, D.K. Setua, N.C. Das and S. Chattopadhyay, *Advanced Materials Research*, 2010, **123**, 435.
14. M. Mandol, P.K. Chattopadhyay, S. Chattopadhyay and D.K. Setua, *Thermochimca Acta*, 2010, **510**, 1, 185.
15. A.K. Mishra, G.B. Nando and S. Chattopadhyay, *Journal of Polymer Science, Part B: Polymer Physics*, 2008, **46**, 21, 2341.
16. M. Day, J.D. Cooney and M. MacKinnon, *Polymer Degradation and Stability*, 1995, **48**, 341.
17. A. Dannoux, S. Esnouf, J. Begue, B. Amekraz and C. Moulin, *Nuclear Instruments and Methods in Physics Research Section B*, 2005, **236**, 488.
18. A.K. Barick and D.K. Tripathy, *Materials Science and Engineering: A*, 2010, **527**, 3, 812.

19. A.K. Mishra, S. Chattopadhyay, P.R. Rajamohanan and G.B. Nando, *Polymer*, 2011, **52**, 4, 1071.
20. *Rubber Clay Nanocomposites: Science, Technology and Applications*, Ed., M. Galimberti, John Wiley & Sons, Hoboken, NJ, USA, 2011.
21. S. Bandyopadhyay, S. Chakraborty and R. Mukhopadhyay in *Rubber-Clay Nanocomposites: Science, Technology and Applications*, Ed., M. Galimberti, John Wiley & Sons, Hoboken, NJ, USA, 2011, p.525.
22. R. Sengupta, S. Chakraborty, S. Bandopadhyay, S. Dasgupta, R. Mukhopadhyay, K. Auddy and A.S. Deuri, *Polymer Engineering & Science*, 2007, **47**, 11, 1956.
23. *Rubber Nanocomposites: Preparation, Properties and Applications*, Eds., S. Thomas and R. Stephen, John Wiley & Sons (Asia) Pte Ltd., Singapore, 2010, doi:10.1002/9780470823477.
24. *Advanced Rubber Composites*, Ed., G. Heinrich, Advances in Polymer Science Series No.239, Springer-Verlag, Berlin, Heidelberg, Germany, 2011, p.314.
25. V.K. Modi, Y. Shrives, C. Sharma, P.K. Sen and S.K. Bohidar, *International Journal of Innovative Research in Science, Engineering and Technology*, 2014, **3**, 11, 17651.
26. C. Sanchez, B. Julian, P. Belleville and M. Popall, *Journal of Materials Chemistry*, 2005, **15**, 3559.
27. N. Saba, P.M. Tahir and M. Jawaid, *Polymers*, 2014, **6**, 2247.
28. W.S. Kim, D.H. Lee, I.J. Kim, M.J. Son, W. Kim and S.G. Cho, *Macromolecular Research*, 2009, **17**, 10, 776.
29. C.A. Rezende, F.C. Braganca, T.R. Doi, L.T. Lee, F. Gatembeck and F. Boue, *Polymer*, 2010, **51**, 16, 3644.
30. F.C. Braganca, L.F. Valadares, C.A.P. Leite and F. Galembeck, *Chemistry of Materials*, 2007, 19, 13, 3334.
31. L.F. Valadares, E.M. Linares, F.C. Braganca and F. Galembeck, *Journal of Physical Chemistry: Part C*, 2008, **112**, 23, 8534.
32. A. Jacob in *Rubber-Layered Clay Nanocomposites*, Cochin University of Science and Technology, Kochi, India, 2008 [PhD Thesis].
33. A. Jacob, P. Kurian and A.S. Aprem, *International Journal of Polymer Materials and Polymer Biomaterials*, 2007, **56**, 6, 593.
34. K. Pal, S.K. Pal, C.K. Das and J.K. Kim in *Recent Advances in Elastomeric Nanocomposites: Advanced Structured Materials*, Eds., V. Mittal, J.K. Kim and K. Pal, Springer-Verlag, Berlin, Heidelberg, Germany, 2011, **9**, 201.
35. A. Das, K.W. Stockelhuber, R. Jurk, D. Jehnichen and G. Heinrich, *Applied Clay Science*, 2011, **51**, 1, 117.
36. S. Rooj, A. Das, K.W. Stockelhuber, N. Mukhopadhyay, A.R. Bhattacharyya, D. Jehnichen and G. Heinrich, *Applied Clay Science*, 2012, **67**, 6, 50.
37. S. Sadhu and A.K. Bhowmick, *Rubber Chemistry and Technology*, 2003, **76**, 860.
38. A. Das, D.Y. Wang, K.W. Stockelhuber, R. Jurk, J. Fritzsche, M. Kluppel and G. Heinrich, *Advances in Polymer Science*, 2011, **239**, 85.
39. Y. Wang, L. Zhang, C. Tang and D. Yu, *Journal of Applied Polymer Science*, 2000, **78**, 1879.
40. Y.P. Wu, Y.Q. Wang, H.F. Zhang, Y.Z. Wang, D.S. Yu, L.Q. Zhang and J. Yang, *Composite Science and Technology*, 2005, **65**, 1195.
41. J. Tan, X. Wang, Y. Luo and D. Jia, *Materials and Design*, 2012, **34**, 825.
42. R. Alex, K. Sasidharan and J. Jacob, inventors; Rubber Research Institute of India, assignee; US20130079444A1, 2013.
43. A. Malas and C.K. Das, *Materials and Design*, 2013, **49**, 857.
44. Q.X. Jia, Y.P. Wu, Y.Q. Wang, M. Lu and L.Q. Zhang, *Composites Science and Technology*, 2008, **68**, 1050.
45. M.N. Qureshi and H. Qammar, *Materials Science and Engineering: C*, 2010, **30**, 590.

46. Y. Liang, Y. Wang, Y. Wu, Y. Lu, H. Zhang and L. Zhang, *Polymer Testing*, 2005, **24**, 12.
47. Y.L. Lu, F.Y. Ye, L.X. Mao, Y. Li and L.Q. Zhang, *eXPRESS Polymer Letters*, 2011, **5**, 9, 777.
48. Y.L. Lu, Z. Li, Z.Z. Yu, M. Tian, L.Q. Zhang and Y.W. Mai, *Composite Science and Technology*, 2007, **67**, 2903.
49. A.A. Yehia, A.M. Akelah, A. Rehab, S.H.E. Sabbagh, D.E.E. Nashar and A.A. Koriem, *Materials and Design*, 2012, **33**, 11.
50. D. Merinska, A. Kalendova, Z. Dujkova, M. Slouf and J. Simonik in *Recent Advances in Chemical Engineering, Biochemistry and Computational Chemistry*, 29–31st October, Paris, France, World Scientific and Engineering Academy and Society, 2013, p.35.http://www.wseas.us/e-library/conferences/2013/Paris/CHEM/CHEM-00.pdf.
51. Z. Peng, L.X. Kong, S.D. Li, Y. Chen and M.F. Huang, *Composite Science and Technology*, 2007, **67**, 3130.
52. C. Nakason, U. Sookyung, N. Vennemann and W. Thaijaroen in *Acid-free Preparation of Natural Rubber/Clay Nanocomposites*, Society of Plastics Engineers, SPE Plastics Research Online, Bethel, CT, USA, 2015, 10.2417/ spepro.005901. http://www.4spepro.org/pdf/005901/005901.pdf.
53. J. Sharif, W.M.Z.W. Yunus, K.Z. Hj, M. Dahlan and M.H. Ahmad, *Polymer Testing*, 2005, **24**, 211.
54. R. Rajasekar, G. Heinrich, A. Das and C.K. Das, *Research Letters in Nanotechnology*, 2009, Article ID:405153, doi:10.1155/2009/405153.
55. A. Amarasiri, U.N. Ratnayake, U.K. De Silva, S. Walpalage and S. Siriwardene, *Journal of Natural Science Foundation of Sri Lanka*, 2013, **41**, 4, 293.
56. M. Andideh, G. Naderi, M.H.R. Ghoreishy and S. Soltani, *Polymer-Plastics Technology and Engineering*, 2013, **52**, 10, 1016.
57. N. Iqbal, S.S. Iqbal, A.W. Anwar, S. Mustafa and S. Rashid, *International Journal of Advanced Technology in Engineering and Science*, 2014, **2**, 11, 244.
58. D.J. Haloi and N.K. Singha, *Journal of Polymer Science, Part A: Polymer Chemistry*, 2011, **49**, 1564.
59. A. Das, K.W. Stockelhuber, S. Rooj, D.Y. Wang and G. Heinrich, *Kautschuk Gummi Kunststoffe*, 2010, July/August,296.
60. S.H. Lim, A. Dasan, Z.Z. Yu, Y.W. Mai, S. Liu and M.S. Yong, *Composite Science and Technology*, 2007, **67**, 14, 2914.
61. C.S. Woo and H.S. Park in *Proceedings of the 21*st *European Conference on Fracture*, 20–24th June, ECF21, Catania, Italy, 2016.
62. S.K. Kim, J.H. Kang, Y. Choe and Y.W. Chang, *Macromolecular Research*, 2006, **14**, 2, 187.
63. *Elastomers II: Composites and Nanocomposites*, Eds., P.M. Visakh, S. Thomas, A.K. Chandra and A.P. Mathew, Springer, Heidelberg, Germany, 2013, **12**, p.183.
64. G. Heinrich, W. Herrmann, N. Kendziorra, T. Pietag and C. Recker, inventors; Continental Aktiengesellschaft, assignee; US6818693B2, 2004.
65. S. Rooj, A. Das, K.W. Stockelhuber, D.Y. Wang, V. Galiatsatos and G. Heinrich, *Soft Matter*, 2013, **9**, 14, 3798.
66. S.J. He, Y.Q. Wang, Y.P. Wu, X.H. Wu, Y.L. Lu and L.Q. Zhang, *Plastics, Rubber and Composites*, 2010, **39**, 1, 33.
67. J.A. Gopi, S.K. Patel, A.K. Chandra and D.K. Tripathy, *Journal of Polymer Research*, 2011, **18**, 6, 1625.
68. S. Sahoo, M. Maiti, A. Ganguly, J. Jacob-George and A.K. Bhowmick, *Journal of Applied Polymer Science*, 2007, **105**, 2407.
69. H. Kantamneni, A. Gollakota and S. Nimmagadda, *Advanced Materials Manufacturing Characterization*, 2013, **13**, 1, 195.

70. J. Jancar, J.F. Douglas, F.W. Starr, S.K. Kumar, P. Cassagnau, A.J. Lesser, S.S. Sternstein and M.J. Buehler, *Polymer*, 2010, **51**, 3321.
71. A.W. Myers in *Improved Fuel Efficiency from Nanocomposite Tire Tread*, Final Report, DE-FG36-04GO14323, US Department of Energy Inventions & Innovation Programme, USA, 2005. https://digital.library.unt.edu/ark:/67531/metadc873198/m1/1/.
72. D.G. Felix and G. Sivakumar, *Journal of Mechanical and Civil Engineering*, 2014, **11**, 4, 7.
73. T.R. Mohanty, V. Bhandari, A.K. Chandra, P.K. Chattopadhyay and S. Chattopadhyay, *Polymer Composites*, 2013, **34**, 2, 214.
74. I.S. Gunes, F. Cao and S.C. Jana, *Polymer*, 2008, **49**, 2223.
75. Y. Cai, J.S. Jiang, B. Zheng and M.R. Xie, *Journal of Applied Polymer Science*, 2013, **127**, 49.
76. C.P. Buckley, C. Prisacariu and A. Caraculacu, *Polymer*, 2007, **48**, 1388.
77. M. Nagata, and Y. Yamamoto, *Journal of Polymer Science, Part A: Polymer Chemistry*, 2009, **47**, 2422.
78. L. Peponia, I. Navarro-Baena, A. Sonsecac and E. Gimenez, *European Polymer Journal*, 2013, **49**, 893.
79. W. Wang, P. Ping, X. Chen and X. Jing, *European Polymer Journal*, 2006, **42**, 1240.
80. B.S. Lee, B.C. Chun, Y-C. Chung, K.I. Sul and J.W. Cho, *Macromolecules*, 2001, **34**, 6431.
81. J.R. Lin and L.W. Chen, *Journal of Applied Polymer Science*, 1998, **69**, 1563.
82. J.R. Lin and L.W. Chen, *Journal of Applied Polymer Science*, 1998, **69**, 1575.
83. T. Gong, W. Li, H. Chen, L. Wang, S. Shao and S. Zhou, *Acta Biomaterialia*, 2012, **8**, 3, 1248.
84. R. Libanori, F.H.L. Münch, D.M. Montenegro and A.R. Studart, *Composite Science and Technology*, 2012, **72**, 3, 435.
85. F.A. Sheikha, M.A. Kanjwalb, S. Saran, W.J. Chung and H. Kim, *Applied Surface Science*, 2011, **257**, 3020.
86. B. Xu, W.M. Huang, Y.T. Pei, Z.G. Chen, A. Kraft, R. Reuben, J.T.M. De Hosson and Y.Q. Fu, *European Polymer Journal*, 2009, **45**, 7, 1904.
87. B. Xu, Y.Q. Fu, W.M. Huang, Y.T. Pei, Z.G. Chen, J.T.M. De Hosson, A. Kraft and R.L. Reuben, *Polymer*, 2010, **2**, 31.
88. P.S. Goh, A.F. Ismail and B.C. Ng, *Composites Part A: Applied Science and Manufacturing*, 2014, **56**, 103.
89. Y.N. Gupta, S.M. Abbas, R.B. Sharma and D.K. Setua, *Journal of Thermal Analysis and Calorimetry*, 2015, **119**, 2, 1393.
90. Y.N. Gupta, S.M. Abbas, R.B. Sharma and D.K. Setua, *Journal of Thermal Analysis and Calorimetry*, 2016, **124**, 1449.
91. Y.N. Gupta, A.K. Pandey, T. Bhave, R.B. Sharma and D.K. Setua, *Polymer Engineering & Science*, 2016, **56**, 11, 1248.
92. Y.N. Gupta, T. Bhave, M. Chandra, R.B. Sharma and D.K. Setua, *Rubber Chemistry and Technology*, 2017, **90**, 1, 159.
93. S.K. Lee, S.H. Yoon, I. Chung, A. Hartwig and B.K. Kim, *Journal of Polymer Science, Part A: Polymer Chemistry*, 2011, **49**, 3, 634.
94. F.L. Ji, J.L. Hu and S.S. Chui, *Polymer Engineering & Science*, 2012, **52**, 5, 1015.
95. Q. Meng, J. Hu, L.Y. Yeung and Y. Hu, *Journal of Applied Polymer Science*, 2009, **111**, 1156.
96. S. Chen, J. Hu, H. Zhuo, C. Yuen and L. Chan, *Polymer*, 2010, **51**, 1, 240.
97. X. Gu and P.T. Mather, *Polymer*, 2012, **53**, 25, 5924.
98. T. Xie, K.A. Page and S.A. Eastman, *Advanced Functional Materials*, 2011, **21**, 11, 2057.
99. C. Poilanea, P. Delobellea, C. Lexcellent, S. Hayashib and H. Tobushic, *Thin Solid Films*, 2000, **379**, 156.
100. D. Zhang, W.L. Burkes, C.A. Schoener and M.A. Grunlan, *Polymer*, 2012, **53**, 14, 2935.
101. E. Wornyo, K. Gall, F. Yang and W. King, *Polymer*, 2007, **48**, 11, 3213.

102. B. Yan, S. Gu and Y. Zhang, *European Polymer Journal*, 2013, **49**, 2, 366.
103. F. Khan and K. Singh, *Polymer Testing*, 2016, **49**, 82.
104. R.B. Trinca and M.I. Felisberti, *European Polymer Journal*, 2015, **62**, 77.
105. S.L. Phua, L. Yang, S. Huang, G. Ding, R. Zhou, J.H. Lew, S.K. Lau, X. Yuan and X. Lu, *European Polymer Journal*, 2014, **57**, 11.
106. G.Q. Li and M. John, *Composite Science and Technology*, 2008, **68**, 15–16, 3337.
107. Q.Q. Ni, C.S. Zhang, Y.Q. Fu, G.Z. Dai and T. Kimrura, *Composite Structures*, 2007, **81**, 176.
108. J. Leng, X. Lan, Y. Liu and S. Dua, *Progress in Materials Science*, 2011, **56**, 7, 1077.
109. Y. Zhu, J. Hua and K. Yeung, *Acta Biomaterialia*, 2009, **5**, 9, 3346.
110. H. Lu, Y. Liu, J. Leng and S. Du, *European Polymer Journal*, 2010, **46**, 1908.
111. J.W. Cho and S.H. Lee, *European Polymer Journal*, 2004, **40**, 7, 1343.
112. C. Azra, Y. Ding, C.J.G. Plummer and J.E. Månson, *European Polymer Journal*, 2013, **49**, 1, 184.
113. S. Han and B.C. Chun, *Composites Part A: Applied Science and Manufacturing*, 2014, **58**, 65.
114. J. Xu, W. Shi and W. Pang, *Polymer*, 2006, **47**, 1, 457.
115. L. Liu and W. Cai, *Materials Letter*, 2009, **63**, 20, 1656.
116. F. Cao and S.C. Jana, *Polymer*, 2007, **48**, 13, 3970.
117. B. Yang, W.M. Huang, C. Li and L. Li, *Polymer*, 2006, **47**, 1348.
118. T. Pretsch, I. Jakob and W. Muller, *Polymer Degradation & Stability*, 2009, **94**, 1, 61.
119. J.D. Merline, C.P.R. Nair, C. Gouri, R. Sadhana and K.N. Ninan, *European Polymer Journal*, 2007, **43**, 8, 3629.
120. M. Souri, Y.C. Lu, A. Erol, S.S. Pulla and H.E. Karaca, *Polymer Testing*, 2015, **41**, 231.
121. P.C. LeBaron, Z. Wang and T.J. Pinnavaia, *Applied Clay Science*, 1999, **15**, 1–2, 11.
122. G.H. Pan, W.M. Huang, Z.C. Ng, N. Liu and S.J. Phee, *Smart Materials and Structures*, 2008, **17**, 4, 045007.
123. J. Wang and D. Chen, *Journal of Nanomaterials*, 2013, Article ID:496584, doi:10.1155/2013/496584.

Jiji Abraham, Hanna J. Mariya and Sabu Thomas

# 5 The Role of Ionic Liquids in Carbon Nanotube–Rubber Composites

## 5.1 An Overview of Carbon Nanotube–Elastomer Composites

One of the most exceptional materials of the 21st century that has found a unique position in the scientific world is carbon nanotubes (CNT). The excellent thermal, electrical and mechanical properties of CNT, which also exhibits an ultrahigh Young's modulus of around 1 TPa and tensile strength (TS) varying from 11–63 GPa, makes it a promising reinforcement material in high-performance polymer matrix composites. However, as they exist in the form of aggregates or agglomerates, the desired property is not always achieved. According to experts in the field, four goals must be met in order to create effective CNT composites:

- They must be aligned in rows.
- The nanotubes must be long in order to effectively carry loads.
- There must be a high ratio of CNT to the polymer or resin used to hold them together.
- Nanotubes must be as straight as possible for the material to bear weight evenly.

Once this is achieved, this allotrope of carbon, which is a cylindrical nanostructure material, could theoretically offer the same strength as carbon fibre at one-tenth the weight, or the same weight at 10 times the strength [1]. Large numbers of polymers have been employed as matrices to prepare CNT polymer nanocomposites, such as epoxy polyamide, polyethylene, polyvinyl chloride (PVC), polyvinyl acetate and many others [2–7]. In this chapter, current advances involving CNT and their composites will be presented based on CNT-filled elastomeric nanocomposites. Bismark and coworkers, in their review of CNT-reinforced elastomeric nanocomposites, showed the recent trend of research activity involving CNT-related elastomeric composites over the years [7].

It has been a long time since elastomeric polymers and rubbers were first used in various industrial applications such as tyres, electrical goods, seals, shock-absorbing mounts and gaskets, and so on [8–16]. Elastomers are usually reinforced with minerals in order to maximise their potential use, and the extent of property improvement depends upon several parameters including the size of the particles, their aspect ratio, their degree of dispersion and orientation in the matrix, and the degree of adhesion with the polymer chains [17].

https://doi.org/10.1515/9783110643879-005

A considerable amount of work has been performed in order to achieve the fabrication of effective CNT elastomer nanocomposites. The effective interfacial interaction between the filler and the elastomer, *via* the good dispersion of CNT in the elastomeric matrix and the covalent and non-covalent modification/functionalisation of the CNT, paved the way for many high-performance CNT-based elastomer nanocomposites. Adopting different mixing techniques, such as solution mixing, melt mixing and *in situ* polymerisation, is also effective for the dispersion of CNT, while the other factors to consider for CNT dispersion are the CNT type and concentration, modification of CNT, type of polymer matrix and so on.

Recently, Subramaniam and co-workers attempted to improve the dispersion of CNT in elastomers. Employing a simplified mixing technique, using ionic liquids (IL), they studied the effect of modified tubes and IL on polar polychloroprene rubber (CR) and non-polar solution styrene-butadiene rubber (SBR) and could achieve enhanced dispersion and networking of CNT, which resulted in highly conducting composites [18]. In another study by Lee and co-workers, thermoplastic polyurethane (TPU) and ethylene propylene diene monomer rubber (EPDM) were melt mixed with multi-walled carbon nanotubes (MWCNT) and the changes in the surface resistivity of the nanocomposites during annealing at room temperature (RT) were examined [19]. The surface resistivity of TPU–MWCNT nanocomposites and uncrosslinked EPDM–MWCNT nanocomposites has been analysed by Gavrilov and co-workers, and the mechanical properties of a crosslinked elastomer filled with surface-functionalised CNT were investigated under uniaxial stretching, by employing a mesoscale coarse-grained model and dissipative particle dynamics, and were found to depend upon nanotube length and bulk density, and crosslink density. They suggested that for composites with chemical couplings between the polymer and fillers, different regimes of elastomer reinforcement exist, manifesting in the stress–strain response, which is completely dependent on the nanotube length and the characteristic network mesh size [20]. In another study by Gavrilov and co-workers, they investigated the structural changes in unfilled and filled elastomers during uniaxial deformation *via* a large-scale dissipative dynamics simulation, which helped to shed some light on the underlying reasons for filler reinforcement in rubber nanocomposites [21]. Galantini and co-workers reported work on MWCNT, where it was first functionalised by grafting either acrylonitrile or diurethane monoacrylate oligomers, and then dispersed into a polyurethane matrix to make dielectric elastomer composites. An effective improvement in the actuation strain was observed for samples loaded with functionalised CNT [22]. Composites of styrene-butadiene-styrene (SBS) block copolymers containing MWCNT were processed by Costa and co-workers using solution casting in order to investigate the influence of filler content, the different ratios of styrene butadiene in the copolymer and the architecture of the SBS matrix on the electrical, mechanical and electromechanical properties of the composites. It was found that the filler content and elastomer matrix architecture influenced the percolation threshold and consequently, the overall

electrical conductivity of the composites [23]. The mechanical properties were mainly affected by the styrene and filler content. The main mechanism for composite conduction is proposed to be movement between the nearest fillers, with the variation of electrical resistivity being linear with the deformation. This fact, together with the gauge factor values in the range of 2–18, led to some of these composites being used as (large) deformation sensors. Choi and co-workers reported work which introduced reversibly deformable and high-performing solid-state yarn supercapacitors. They reported that mesoporous, pseudocapacitive $MnO_2$ was electrochemically deposited on the microcoiled yarn electrodes, resulting in core (CNT)–shell ($MnO_2$) structured electrodes. The yarn supercapacitors can be woven into energy textiles that can effectively power various wearable electronics in the future [24]. Gaharwar and co-workers fabricated stiff, elastomeric nanocomposites from polyglycerol sebacate (PGS) and CNT. They reported that the addition of 1% CNT resulted in a 5-fold increase in the tensile modulus and a 6-fold increase in compression modulus compared with PGS alone, which is far superior to the previously reported studies for CNT-based nanocomposites; in addition, they stated that the elasticity of the network was not compromised and the resulting nanocomposites showed more than 94% recovery [25]. Zhang and co-workers investigated the resistivity response, under cyclic loading, of TPU MWCNT elastomeric nanocomposite films fabricated by a solution process, and reported enhanced nanotube dispersion and a lower percolation threshold (~0.35 wt%) [26].

## 5.2 Carbon Nanotubes – A Brief History

CNT are comparatively new nanomaterials that have received special interest over the last 20 years, but their history goes back to the 1950s. CNT were discovered in 1952 by Radushkevich and Lukyanovich [27] and the single- (or double-) walled CNT were observed by Oberlin and co-workers in 1976, with the discovery of commercially important MWCNT credited to Iijima in 1991 [28–30]. Depending on the process used for CNT fabrication, CNT can be classified into single-walled carbon nanotubes (SWCNT) and MWCNT [31–33]. SWCNT consist of a single graphene layer rolled up into a seamless cylinder, whereas MWCNT are comprised of two or more concentric cylindrical shells of graphene sheets coaxially arranged around a central hollow core with van der Waals forces between adjacent layers. Both SWCNT and MWCNT tend to aggregate into ropes, or bundles, due to their surface interactions as a result of the van der Waals force of attraction between individual tubes. For SWCNT, the morphology varies with nanotube diameter and chirality, individual nanotube length, end configuration (capped or uncapped), atomic-level defects as well as the aggregation of nanotubes into bundles. Similarly, MWCNT morphology varies with changes in the outer diameter of the nanotube, number of concentric

walls, growth-induced structure, such as internal caps of nanotube walls, and other defects in the graphitic structure.

CNT are made up of graphene sheets that have been rolled into a tube. A graphene sheet can be in rolled in different ways, generating different types of CNT. The bonding in CNT is $sp^2$ and consists of honeycomb lattices with each atom joined to three neighbours, as in graphite. This bonding structure, which is stronger than the $sp^3$ bonds found in diamond, provides the molecules with their unique strength. The orientation of graphene sheets upon rolling has a considerable effect on the final structure of CNT. This can be specified by a vector (called a chiral vector), which defines how the graphene sheet is rolled up. CNT have three chiralities: armchair, zigzag and a chiral one depending on the rolling angle of the graphene sheet. The chirality of the tube is defined by the chiral vector, $C_h=na_1 + ma_2$, where the integers (n, m) are the number of steps along the unit vectors ($a_1$ and $a_2$) of the hexagonal lattice. Using this (n, m) naming scheme, the three types of orientation of the carbon atoms around the nanotube circumference are specified. If n=m, the nanotubes are called 'armchair', if m=0, the nanotubes are called 'zigzag', otherwise, they are called 'chiral'. The chirality of nanotubes has a significant impact on their transport properties, and in particular, the electronic properties. For a given (n, m) nanotube, if (2n + m) is a multiple of 3, then the nanotube is metallic, otherwise the nanotube is a semiconductor. Each MWCNT contains a multilayer of graphene, and each layer can have different chiralities, so predicting the physical properties of MWCNT is more complicated than that of SWCNT.

Traditional synthesis techniques for CNT include high-temperature preparation techniques such as arc discharge or laser ablation. Recently, these methods have been replaced by low-temperature chemical vapour deposition (CVD) techniques (<800 °C). The advantages of this modern technique include complete control of the orientation, alignment, nanotube length, diameter, purity and density of CNT [31]. CVD and the most current fluidised bed CVD method has advantages in terms of its price/unit ratio due to excellent heat and mass transfer, which ensures a homogeneous product, inherent scalability and comparatively low cost. The types of impurities produced during the synthesis of CNT depend on the method employed for its production. Final products of the above-mentioned techniques produce powders that contain both CNT and other carbonaceous particles, such as nanocrystalline graphite, amorphous carbon and fullerenes, and different metals (typically Fe, Co, Mo or Ni, which were introduced to accelerate the synthesis). These unwanted impurities have a negative impact on the desired properties of CNT and seriously impede detailed characterisation and applications. Various synthesis routes for the production of MWCNT are depicted in Figure 5.1. Other methods such as the high-pressure carbon monoxide disproportionation process, flame synthesis, plasma torch method, electrolysis and solar energy methods, have also been proposed for the synthesis of CNT and, in particular, for the synthesis of SWCNT.

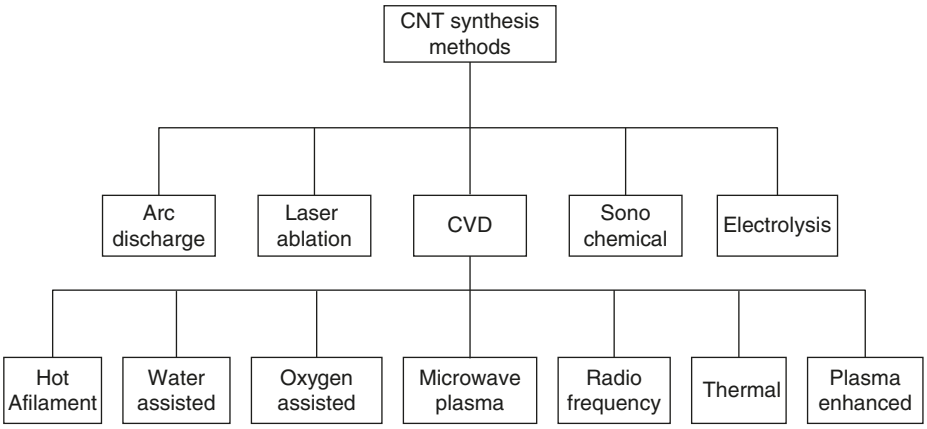


**Figure 5.1:** Currently used methods for CNT synthesis.

CNT possess high flexibility, low mass density and a large aspect ratio (typically >1,000). The chemical bonding of CNT is composed entirely of $sp^2$ carbon – carbon bonds. Theoretical and experimental results have shown unusual mechanical properties of CNT with a Young's modulus as high as 1.2 TPa and a TS of 50–200 GPa, making CNT the strongest and stiffest materials on Earth [34]. They have a higher TS than steel and Kevlar. Due to the greater strength of the atomic bonds in CNT, they not only survive high temperatures but have also been shown to be very good thermal conductors, withstanding up to 750 and 2,800 °C at normal and vacuum atmospheric pressures, respectively. Individual SWCNT can be metallic or semiconducting; the latter can transport electrons over long distances without significant interruption, which makes them more conductive than copper. In addition, CNT have unique mechanical, electrical, magnetic, optical and thermal properties [35] that offer great potential for use in a wide range of applications including: field emission, conducting plastics, thermal conductors, energy storage, conductive adhesives, thermal interface materials, structural materials, fibres, catalyst supports, biological applications, air and water filtration, ceramics and so on.

Due to these outstanding properties, CNT are ideal reinforcing agents for high-performance polymer composites. Schadler and co-workers introduced polymer nanocomposites, based on CNT as a reinforcing agent [36], leading to a subsequent dramatic increase in the number of articles and patents on CNT-based polymer composites. A wide variety of polymer matrices can be used to prepare composites, including thermoplastics, thermosetting resins, elastomers, liquid crystalline polymers, fibres, water-soluble polymers and conjugated polymers. The presence of CNT can improve the overall properties of a composite including TS, tensile

modulus, toughness, glass transition temperature ($T_g$), thermal conductivity, electrical conductivity, solvent resistance, optical properties and so on.

## 5.3 Ionic Liquids

IL are salts with melting points below 100 °C, which are composed of asymmetric cations and anions and possess unique properties. There are also room temperature ionic liquids (RTIL) and, as the majority of IL have melting points below RTIL, there has been great interest in IL over the last few years by both academic and industrial sectors, as they can be considered to be a green solvent. Specific properties such as chemical stability, thermal stability, low-saturated vapour pressure, non-flammability and good ionic conductivity make them ideal candidates for a wide range of applications in the chemical industry. The combination of one asymmetric cation and one anion is referred to as a primary IL but is more commonly referred to as simply IL [37, 38]. There are around 106 potential primary IL. The two important properties common to all IL are (i) that the substance is liquid (its $T_g$ and/or melting point are <99.85 °C) and (ii) that it contains ions and therefore exhibits ionic conductivity. The main difference between IL and simple molten salts is that IL are composed of bulky, asymmetrical ions that can't properly arrange into a regular crystal lattice. However, in the case of simple molten salts, the proper arrangement of ions in the crystal lattice is possible due to the symmetric nature of both ions. Synonyms for materials that meet this definition of IL include RT molten salt (also known as RTIL), low-temperature molten salt, ambient temperature molten salt, ionic fluid, Coulombic fluid and liquid organic salt [39, 40]. Table 5.1 provides an overview of a comparison between the properties of organic solvents and IL.

### 5.3.1 Origin of Ionic Liquids

Research on IL flourished very recently even though they were discovered in the early 20th century. According to the literature, the first IL was an ammonium salt, ethylammonium nitrate (formula $EtNH_3NO_3$), with a melting point below 100 °C [41]. However, it was really in the 1970s that the first IL were synthesised to any great degree and used in batteries for nuclear warheads [42]. Wilkes and other scientists continued to use IL as electrolytes in batteries and studied different properties [43]. Then during the 1980s, a new class of IL emerged: the imidazolium salts. The anionic part of this IL is chloroaluminate. However, utilisation of this IL was limited due to the high reactivity between the chloroaluminate anion and water or air.

**Table 5.1:** Comparison of organic solvents with IL.

| Property | Organic solvents | IL |
|---|---|---|
| Number of solvents | >1,000 | >1,000,000 |
| Applicability | Single function | Multifunctional |
| Catalytic ability | Rare | Common and tuneable |
| Chirality | Rare | Common and tuneable |
| Vapour pressure | Obeys the Clausius–Clapeyron equation | Negligible vapour pressure under normal conditions |
| Flammability | Usually flammable | Usually non-flammable |
| Solvation | Weakly solvating | Strongly solvating |
| Polarity | Conventional polarity concepts apply | Polarity concept questionable |
| Tuneability | Limited range of solvents available | Virtually unlimited range means 'designer solvents' |
| Cost | Normally cheap | Typically between 2 and 100 times the cost of organic solvents |
| Recyclability | Green imperative | Economic imperative |
| Viscosity (cP) | 0.2–100 | 22–40,000 |
| Density (g/cm–3) | 0.6–1.7 | 0.8–3.3 |
| Refractive index | 1.3–1.6 | 1.5–2.2 |

The interest of researchers in IL increased substantially after the synthesis of imidazolium salts, particularly 1-butyl-3-methylimidazolium tetrafluoroborate ($BmimBF_{4-}$) and 1-butyl-3-methylimidazolium hexafluorophosphate ($PF_{6-}$), which were water and air stable.

## 5.3.2 Structure of Ionic Liquids

IL can reduce the use of many organic solvents because of their unique characteristics. An IL is made up of an organic cation associated with an organic or inorganic anion, which makes it tuneable for specific applications [44].

### 5.3.2.1 Effect of Cations

There are several types of IL and their function depends upon the chemical nature of the cation, which is usually a bulk organic structure with low symmetry. Most IL are based on different organic cations such as: ammonium, imidazolium, phosphonium, pyridinium, pyrazolium, thiazolium, oxazolium

or pyrolidium. In the literature, many other cations have been studied and functionalised using various groups including: amine, acid, thiol, ester, acrylate and nitrile.

#### 5.3.2.2 Effect of Anions

Changing the anion results in an increasing number of alternative IL with various properties. There are two types of anions that are commonly reported in the literature: fluorinated anions, such as hexafluorophosphate ($PF_6$-), tetrafluoroborate ($BmimBF_4$-) and trifluoromethanesulfonate ($CF_3SO_3$-), and conventional anions such as bromide (Br-), chloride (Cl-), iodide (I-) and chloroaluminate ($AlCl_4^{-1}$). The end properties of IL depend on the nature of the anion used. Indeed, whatever the type of cation used, significant differences are observed according to the associated anion. In some cases, the anion is responsible for decreasing or increasing the melting temperature and thermal stability [45]. For example, IL 1-methyl-2-butyl-imidazolium tetrafluoroborate exhibits better thermal stability than the same salt in the presence of a bromide anion. The chemical nature of the anion also determines the solubility of IL, e.g., 1-methyl- 2-butyl-imidazolium tetrafluoroborate is soluble in water whereas the same cation with the $PF_6$- anion is totally immiscible in water. The choice of anion also influences the viscosity and density of molten salts. $BmimBF_4$- and $PF_6$- anions are the most commonly used in a wide range of applications, especially in electrolytes and batteries. Although they have advantages, there are some limitations, e.g., in the presence of air or heat they produce unwanted hydrogen fluoride; as a result, researchers have focused on the use of other anions such as $CF_3SO_3$- and $(CF_3SO_3)_2N$-.

### 5.3.3 Properties of Ionic Liquids

Unlike conventional solvents based on organic molecules, IL are a combination of asymmetric cations and anions. Most IL have melting temperatures below 100 °C and could be classed as RTIL as they are liquid at RT. This advantage is useful for many applications in various sectors. Low-melting temperature IL are emerging from the combination of large, asymmetric organic cations and inorganic anions, which leads to a decrease of the lattice energy making the required arrangement of both ions in the crystal lattice impossible. Today, they are considered to be 'green' solvents and environmentally friendly components due to their recyclability and reusability. The important characteristics of IL include:

- Excellent thermal stability, i.e., about 300 °C and even higher when using fluorinated anions.
- Low saturated vapour pressure to prevent evaporation.
- They are non-inflammable and polar.

- Good thermal and electrical conductivities, making them excellent candidates in the electrochemical environment sector.
- It is possible to synthesise IL for a wide range of applications by varying the combination of anions and cations, with their properties being easily adjusted by changing one of the ions [46].
- IL can be used as solvents for many substances such as proteins, carbohydrates, polysaccharides, deoxyribonucleic acid, crude oil and plastic materials [47, 48].

### 5.3.4 Applications of Ionic Liquids

The attractive macroscopic properties of many IL include a very large range are in the liquid state, a wide electrochemical window, the ability to solubilise a wide range of solutes and negligible vapour pressure; hence, they can be used in various fields where the use of molecular solvents is not possible [49, 50]. Due to the interesting and tuneable properties of IL, there are many potential applications including: solvent replacement, catalysis, electrodeposition, electrolytes in different devices, chromatography and lubricants. The opportunities for industrial applications are almost boundless, and it is clear that IL are not yet being used to their full potential [51]. In their capacity as green and designable solvents, IL have been very useful in organic reactions, polymerisation, catalysis, biotransformations, self-assembly media, electrochemistry, supercritical fluid and lubricants and so on. In particular, various crystalline nanoparticles with specific functions have been successfully synthesised in the presence of IL, as a result of the high polarity and self-organisation ability of IL.

IL could play a key role in the field of polymer nanocomposites. Several studies have reported that IL can be used to disperse CNT, graphene, clay, silica, layered double hydroxides (LDH) and so on, in a polymer matrix. Some years ago, Fukushima and co-workers found that RTIL are capable of dispersing CNT [52, 53]. Ma and co-workers found that CNT can be successfully modified by IL containing long alkyl-substituted groups, including 1-docosanyl-3-methylimidazolium bromide and 1-docosanyl-3- methylimidazolium hexafluorophosphate [54]. Initially, ammonium IL were the most commonly used intercalating agents for layered silicates; however, new surfactants have recently emerged, with the use of pyridinium, imidazolium and phosphonium salts that have better thermal stability (at about 300 °C) than ammonium-based IL. Moreover, the use of IL has a positive impact on the mechanical, thermal and electrical conductivity properties of nanocomposites. Livi and co-workers found that clay can be modified by IL and successfully dispersed in a fluorinated matrix [55]. A series of novel organic–inorganic nanohybrid materials were obtained by the intercalation in interlamellar spaces of the clay mineral

kaolinite using IL based on imidazolium derivatives [56, 57]. Fontana and co-workers evaluated the role of an IL as an organophilisation agent for montmorillonite (MMT) for the production of acrylonitrile-butadiene rubber (NBR) nanocomposites [58]. They found that incorporation of IL in the ammonium-based organoclays led to better compatibility with the elastomeric matrix (NBR). Hong and co-workers developed a new one-pot technique, where the hydrophilic sodium-MMT layers were decorated with hydrophobic 1-dodecyl-3-methylimidazolium hexafluorophosphate ($C_{12}$mim$PF_6$) IL *in situ*, during melt blending with polymethyl methacrylate (PMMA), with the subsequent intercalation of polymer chains [59]. Inspired by the successful exfoliation of CNT with IL, the use of IL for the dispersion of graphene sheets was the focus of several research groups. In a recent work reported by Pandey and co-workers, a graphene-based solid-state supercapacitor was successfully fabricated by a gel electrolyte consisting of 1-butyl-3-methylimidazolium tetrafluoroborate and polyvinylidene fluoride (PVDF)-*co*-hexafluoropropene [60]. Yang and co-workers reported a different covalent approach utilising nucleophilic attack by an amine-terminated IL to open the epoxy groups on graphene oxide. The graphene nanosheets obtained were well dispersed and showed long-term stability in water, dimethylformamide and dimethyl sulfoxide, i.e., for more than 3 months [61]. The non-covalent approach is probably superior to the covalent method since graphenes are able to maintain their intrinsic properties [62]. In another study, Livi and co-workers presented IL based on tetraalkyl phosphonium salts combined with different anions (decanoate and dodecylsulfonate), which were used as intercalating agents for LDH *via* ion exchange [63].

Gayet introduced IL-modified silica into a PMMA matrix and studied its enhanced mechanical and thermal properties [64]. A polyhedral oligomeric silsesquioxane-bound imidazolium surfactant was used to exchange MMT for the preparation of polymer nanocomposites of polystyrene (PS), poly(ethylene-*co*-vinyl acetate) and Nylon 6, using a melt-blending technique, by Fox and co-workers [65]. Cellulose–nano-hydroxyapatite composite scaffolds with extensive porosity were successfully prepared by PMMA particulate leaching. In this study, IL was used for the better dissolution of cellulose [66]. Soheilmoghaddam prepared novel regenerated cellulose/sepiolite nanocomposite films using an environmentally friendly IL, 1-butyl-3-methylimidazolium chloride, through a simple, cost-effective and 'green' method [67].

### 5.3.5 Main Limitations of Ionic Liquids

Even though IL have many advantages and unique properties, as well as the multiple combinations of cations and anions that can be achieved, the price of these new materials is their main disadvantage. The current cost per kilogram of IL is tens of thousands of euros, more than common organic solvents such as acetone; however,

this cost can be significantly reduced [68]. In the case of imidazolium IL, Wagner and co-workers predicted a price of around €50–100 per kg if produced on a large scale [69]. Another limitation is that the synthesis of IL involves the use of conventional organic solvents such as acetonitrile, toluene and tetrahydrofuran. The global aim is to reduce the use of conventional organic solvents, which cannot be achieved *via* the traditional synthesis of IL as it requires these solvents. However, the emergence of new synthesis methods that avoid the use of conventional solvents has been welcomed, e.g., supercritical medium and microwave synthesis [70]. A further disadvantage is the high viscosity of IL in comparison to organic solvents, which can be avoided by changing the nature of the anion, increasing the temperature or using a supercritical medium at very high pressure. The limitations of IL can be overcome and IL show great potential in many sectors, especially in the case of polymer processing.

### 5.3.6 Future of Ionic Liquids

Due to the close cooperation between academia and industry, the field of IL has grown extremely quickly. The range and number of commercial applications is quite astounding and is a result of their increasing number and wide diversity. As the concepts of IL are relatively new they are still not fully accepted in the wider community, as it is very difficult for conservative scientists to change from the traditional concepts of conventional molecular solvents. However, there are now many laboratories all over the world, especially in China, that work with IL.

## 5.4 Carbon Nanotube–Ionic Liquid Polymer Composites

Advanced polymeric composites have various potential applications and are critical for the development of innovative polymeric materials and finding solutions for a sustainable future. The use of IL as functional building blocks is one of the state-of-the-art methods for designing and creating new polymer materials with improved properties. The combination of these materials leads to unique properties which are unachievable using traditional materials [71, 72]. The use of IL in polymer science has advanced from their use as solvents, or as surfactants of nanoparticles, and has become focused on using IL as functional additives to polymer matrices [73–75].

IL can act as ionic conducting agents for polymer electrolytes, in particular, imidazolium- and phosphonium-based IL have been widely investigated [76–78]. Thus,

various polymeric matrices have been used in the design of electrolytes, such as polyethylene oxide, polyacrylonitrile, PVDF and its copolymers, and PMMA. IL can also be used as processing aids and compatibilisers of polymer blends, biopolymers and thermoplastic starch [79–82].

In the plastics industry, IL are used as plasticisers to increase processability, flexibility and ductility of rigid polymers. IL are excellent candidates to replace conventional plasticisers used in the production of polylactic acid, PMMA, PVC, thermoplastic starch and PVDF [83–86]. The advantages of IL over conventional plasticisers include excellent thermal stability and low volatility. It is also possible to modify their chemical structures and molecular weights by introducing different functional groups on the cations, or on the counterions, that control the degree of plasticisation of polymeric materials. IL have huge potential in the plasticiser industry; however, their high price limits their applications in many fields, especially when combined with polymers that are very cost-effective. Nevertheless, for specific applications, such as in biomedicine, their application has been realised.

Cellulose, the most abundant natural polymer in nature, is renewable, biodegradable and biocompatible. Cellulose is difficult to process in solution, or as a melt, because of its large proportion of intra- and intermolecular hydrogen bonds; however, this issue can be overcome by using RTIL, which are considered to be desirable green solvents [87]. Studies have also been conducted on the use of RTIL to lower polymer friction and the wear of polymers against steel [88].

### 5.4.1 Mechanism behind the Exfoliation of Nanofillers by Ionic Liquids

IL contain a cationic part and an anionic part. The versatile interactions between IL and fillers have been confirmed to be cation–π, π–π, van der Waals, hydrogen bonding and delocalised electron interactions [89–96].

Several reviews are available on the functionalisation of CNT using IL [97, 98]. IL interacts with CNT through cation–π and/or π–π interactions. According to Du and co-workers, the adsorption of IL significantly changes the Raman spectrum of CNT [99]. While in the spectrum of purified CNT, the disorder-induced D-band at 1,340 $cm^{-1}$ is negligible, its intensity increases significantly in the case of modified CNT. This is attributed to overlapping Raman features coming from the added layers on CNT. However, Price and co-workers argued that the cation–π interaction was very weak and that the weak van der Waals interaction was responsible for the interactions between IL and SWCNT [100]. In order to understand the molecular packing of IL immobilised on MWCNT surfaces, Zhao and co-workers took composite samples with different

weight ratios of IL and characterised them using X-ray photoelectron spectroscopy, differential scanning calorimetry, X-ray diffraction and Fourier–Transform infrared spectroscopy [101]. Their study showed that the rings of imidazolium cations of IL were nearly parallel to the MWCNT surfaces and the packing orientation was determined by the substituent groups on the imidazolium ring; with anions occupying an adjacent area to the imidazolium cation to form a neutral surface layer. Studies have reported the theoretical understanding of CNT–IL composite systems *via* molecular dynamics simulations [102–105]. Figure 5.2 represents the scheme of 1-butyl-3-methylimidazolium chloroauric acid ([Bmim][AuCl4]) on the MWCNT surface and the distinctive first external solvation shell of cylindrical symmetry with imidazolium stacked on the exterior wall of the nanotube.

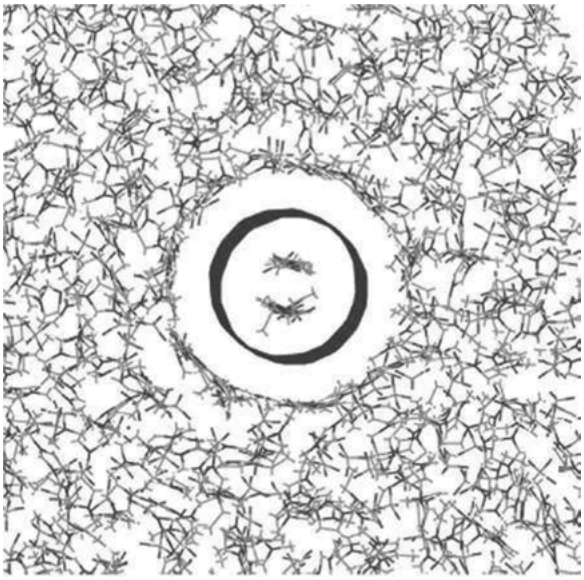

**Figure 5.2:** Scheme of [Bmim][$AuCl_4$] on the MWCNT surface and distinctive first external solvation shell of cylindrical symmetry with imidazolium stacked on the exterior wall of the nanotube. Reproduced with permission from Y. Shim and J.K. Hyung, *ACS Nano*, 2009, **3**, 1693. ©2009, American Chemical Society [102].

When MWCNT are mixed with IL, CNT are dispersed as shown in Figure 5.3. The cationic part of IL interacts with the π-electronic network on the MWCNT, which results in the reduction of the van der Waals force of attraction between the individual tubes. When MWCNT is mixed with IL by grinding in an agate mortar the shear force detaches bundles of MWCNT into individual ones and the MWCNT are

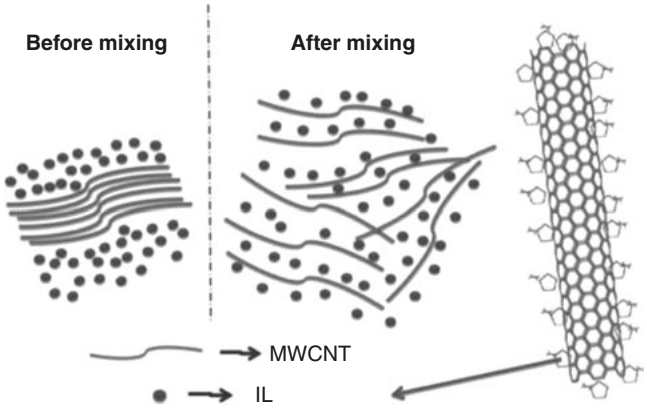


**Figure 5.3:** Schematic representation of the dispersion of MWCNT using IL. Reproduced with permission from J. Abraham, M.P. Arif, L. Kailas, N. Kalarikkal, S.C. George and S. Thomas, *RSC Advances*, 2016, **6**, 32,493. ©2016, Royal Society of Chemistry [106].

covered by IL *via* a cation–π interaction between the cationic part of the IL and the MWCNT surface. It is proposed that the π–π stacking interactions of nanotubes are shielded by the high dielectric constants of IL restricting them from rebundling.

### 5.4.2 Advantages of Ionic Liquid-mediated Surface Modification of Multi-walled Carbon Nanotubes over Other Methods

Chemical functionalisation involves the formation of a covalent bond between the CNT surface and the incoming group or creation of a defect on the surface of CNT *via* oxidative treatment [107, 108]. Functionalisation of CNT using covalent methods can provide useful functional groups on the CNT surface. However, these methods have two major drawbacks: firstly, during the functionalisation reaction a large number of defects are inevitably created on the CNT sidewalls and, in some extreme cases, CNT are fragmented into smaller pieces. These damaging effects result in severe degradation of the mechanical properties of CNT, as well as disruption of the π-electron system in the nanotubes, leading to failure of the electrical properties. Covalent functionalisation has been used to try and improve the interfacial properties of the tubes [109]. Chemical functionalisation destroys the π-electronic conjugation of the tubes, but the rubber–filler interaction is said to be improved at the cost of electrical conductivity. IL ensure better CNT–elastomer compatibility and recent studies have revealed the importance of these materials in achieving effective CNT dispersions. It is an alternative method to chemical treatment that avoids vigorous

oxidation or damage to the nanotubes. Compared with the physical method of surfactant addition, these IL can act both as dispersing and reinforcing agents.

## 5.4.3 Novel Materials based on Ionic Liquid-modified Carbon Nanotubes

CNT modified with IL exhibit improved compatibility and stability, and hence can be used for a wide range of applications. Since IL can act as both a dispersing agent and green solvent, the use of harmful organic solvents can be avoided, i.e., it is an environmentally friendly method. Many other functionalisation methods, such as covalent functionalisation using acids, require tedious experimental conditions, expensive instruments and are not 'green' procedures. The resulting compounds retain the original properties of each component. Moreover, combining other independent components into the functionalisation reaction results in the formation of multifunctional compounds. CNT–IL hybrids have been extensively studied in the fields of electrochemistry, catalysis and composite materials. Potential applications include sensors, actuators, supercapacitors, dye-sensitised solar cells, elastic conductors, supports for metal nanoparticles, additives for lubricants and polymer nanocomposites. IL can function as a dispersant and/or binder for CNT, iin addition ot being a major component in the final hybrid or composite.

## 5.4.4 Fabrication of Ionic Liquid-modified Carbon Nanotube Polymer Nanocomposites

Fabrication methods have focused on improving nanotube dispersion in the polymer matrices as this leads to enhanced properties. In order to be an effective reinforcement for high-strength polymer composites, CNT should be prevented from agglomerating and must be well dispersed to achieve improved interfacial interaction with the matrix. An optimised interfacial interaction between the CNT sidewalls and the matrix should result in an efficient load transfer to the 'hard' component of the composite *via* reinforcement. Methods of fabricating polymer nanocomposites include solution blending, melt blending and *in situ* polymerisation. In addition, latex technology, solid-state shear pulverisation and coagulation spinning methods are also used for the production of CNT-based polymer nanocomposites.

### 5.4.4.1 Solution Processing of Carbon Nanotubes and Polymers

Solution processing of CNT, the most widely used method for the fabrication of polymer nanocomposites, is based on mixing nanotubes and a polymer in a

suitable solvent and then evaporating the solvent to obtain the composite film [110–113]. The general strategy for all solution processing methods includes the dispersion of CNT powder in a liquid medium, by vigorous stirring and/or sonication, followed by mixing the CNT dispersion with a polymer solution and then the controlled evaporation of the solvent with or without vacuum conditions. The most efficient and fine dispersion of tubes during the first step is achieved by magnetic stirring, shear mixing, reflux, or more commonly, ultrasonication, which can be provided in two forms: mild sonication in a bath or high-power sonication using a tip, and the major benefit of this method is that agitation of the nanotube powder in a solvent facilitates nanotube deaggregation and dispersion.

#### 5.4.4.2 Melt Mixing

Melt blending uses a high temperature and large shear forces to disperse nanotubes in a polymer matrix and is widely employed in current industrial practices. Melt processing has been a very efficient technique for the fabrication of CNT-based composites, as thermoplastic semicrystalline polymers soften when heated above their melting point. This method is suitable for polymers that cannot be processed *via* solution techniques due to the insolubility of many polymers in common solvents. Examples of the melt-blending process include SWCNT–PMMA, MWCNT–PMMA, MWCNT–polycarbonate, MWCNT–Nylon 6, SWCNT–polypropylene (PP) and SWCNT–polyimide composites [114–118]. However, compared with solution-blending methods, melt blending is generally less effective at dispersing nanotubes in polymers and is limited to lower concentrations due to the high viscosities of the composites at higher nanotube loadings.

#### 5.4.4.3 Bulk Mixing

Milling is a mechanical process that is used to shorten the lengths of carbon nanostructures [119]. A solid-state mechanochemical pulverisation process, namely pan milling, has been used to prepare a CNT–PP composite powder [120]. High-energy ball milling has been utilised to incorporate CNT, at a satisfactory level of dispersion, into polymer matrices to enhance the overall performance of the composites [121].

#### 5.4.4.4 In Situ Polymerisation

This fabrication strategy starts by dispersing nanotubes in a monomer followed by polymerising the monomers. The main advantage of this method is that it produces

polymer grafted tubes, which are mixed with free polymer chains. The homogeneity of the resulting composite materials is much higher than mixing CNT and polymer chains in solution due to the small size of the monomeric molecules. Hence, this method allows the preparation of composites with a high CNT weight fraction. This technique is especially important for the preparation of insoluble and thermally unstable polymers, which cannot be fabricated by solution or melt processing. *In situ* radical polymerisation was first applied for the synthesis of PMMA composites by Jia and co-workers [122]. *In situ* epoxidation has also been used for the preparation and processing of epoxy–polymer composites [36, 123, 124].

#### 5.4.4.5 Other Methods

Freeze drying is a method of fabricating porous structures during which polymer solutions are frozen in a cold bath and then the frozen solvents are removed *via* sublimation under vacuum. CNT–PS latex composites have been synthesised *via* freeze drying followed by the compression-moulding method by Yu and co-workers [125]. The suspension of CNT in an elastomer can be converted to CNT–elastomer powder composites *via* the spray-drying process. Zhou and co-workers produced SBR powders containing CNT with uniform diameters of about 5–10 nm using the spray-drying process [126]. The formation of crosslinks in the polymer chains of rubber latex can be achieved by adding compounding ingredients such as sulfur in the presence of ZnO, stearic acid, tetramethylthiuram disulfide or 2,2′-dithiobis(benzothiazole). Curing agents were well mixed with latex using milling methods, and then the compounded latex was mixed with CNT [127]. The heterocoagulation method was also successfully employed by Peng and co-workers while preparing functionalised multi-walled carbon nanotube (f-MWCNT)–NR composites, which involved binding *via* the interaction between the charged particles to give well-dispersed composite materials [128].

### 5.4.5 Different Roles of Ionic Liquids in Carbon Nanotubes/ Rubber Composites

#### 5.4.5.1 Coupling Agents between Rubber and Carbon Nanotubes

IL can act as a coupling agent between rubber and CNT. In order to ensure better rubber–MWCNT compatibility and to enhance the dispersibility, a series of IL has been tested by Das and co-workers with regard to an improved interaction between rubber and CNT [129]. They found that in the presence of one particular IL, namely, 1-allyl-3-methylimidazolium chloride (AMIC), a remarkable improvement in the TS

was achieved with only 3 wt% MWCNT loading as a result of the chemical coupling between CNT and the rubber chains *via* IL. It was also found IL not only acted as a coupling agent but also a dispersing agent. As IL behaves like a coupling agent between CNT and the rubber chains, the twisted structure of CNT holds a specific amount of rubber polymer and also forms three-dimensional interactions with the rubber matrix.

#### 5.4.5.2 Dispersant for Carbon Nanotubes in a Rubber Matrix

Several studies have reported the role of IL as a new dispersant for CNT. Fukushima and co-workers found that imidazolium-based RTIL can be employed to disperse SWCNT by means of the cation–π/π–π interaction. It was demonstrated that the highly entangled SWCNT bundles were exfoliated, resulting in much finer bundles and aiding better dispersion. This new approach with IL offers possibilities for various elastomer applications, e.g., to produce a rubber-like stretchable active matrix using elastic conductors [130]. A vinylidene fluoridehexafluoropropylene copolymer–SWCNT composite coated with polydimethyl siloxane rubber was prepared and the elongation at break was found to be 134%. Subramaniam and co-workers developed a simple eco-friendly approach to develop CR composites with high electrical conductivity. A CR composite containing MWCNT modified using 1-butyl-3-methyl imidazolium *bis*(trifluoromethylsulfonyl)imide (BMI) exhibited an electrical conductivity of 0.1 S/cm with a stretchability of >500% due to the physical interaction between the IL and the MWCNT, as evidenced by Raman spectroscopy. From viscoelastic studies it is also clear that more MWCNT networks are formed in the presence of IL. Transmission electron microscopy (TEM) images of modified CNT-based composites showed less agglomerates compared with unmodified composites. This is due to the fact that bundles of MWCNT were perturbed, due to the reduced intertubular attraction between CNT in the presence of IL, and upon increasing the proportion of IL, the filler–filler networks were found to be improved and exhibited well-dispersed MWCNT.

Subramaniam and co-workers investigated the effect of IL-modified CNT on the dielectric and electrical properties of CR composites and found that the presence of BMI not only increased the alternating current (AC) electrical conductivity and polarisability of the composites but also improved the state of dispersion of the tubes, as observed from dielectric spectroscopy and TEM, respectively [131]. The improved AC conductivity of composites with modified tubes is due to the synergic effect of CNT and IL, and also due to the formation of additional networks of CNT in the presence of IL. The secondary interaction between IL and CNT with modified tubes decreases the van der Waals attraction among the tubes, which in turn leads to disentanglement of CNT and thus, the formation of CNT networks is enhanced. The formation of these additional networks in the presence of IL was determined by amplitude sweep

measurement. Abraham and co-workers reported the facile synthesis of a conducting polymer nanocomposite by incorporating non-covalent f-MWCNT containing IL into an SBR matrix and achieved a shielding efficiency of approximately 35.06 dB at 18 GHz (i.e., ~99.99% shielding attenuation) [132]. A significant enhancement in the shielding effectiveness ($S_E$) of the polymer nanocomposite with different loadings of f-MWCNT is shown in Figure 5.4.

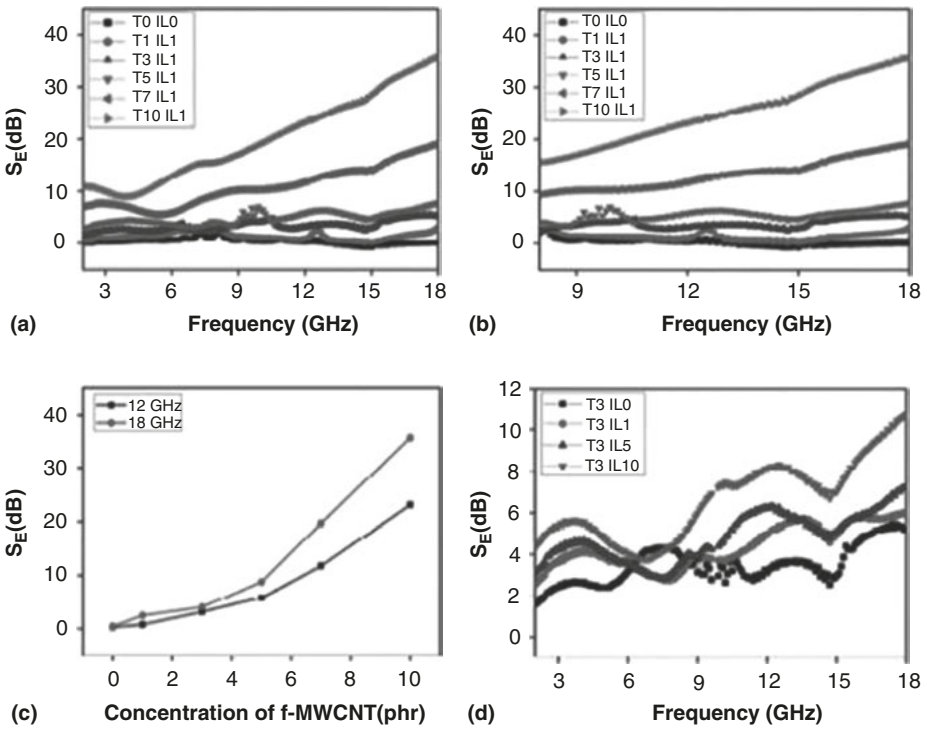


**Figure 5.4:** (a) Total $S_E$ as a function of the frequency for composites; (b) total $S_E$ as a function of the frequency for composites in the X and Ku band (8–18 GHz); (c) variation in total $S_E$ with MWCNT loading at two different frequencies and (d) electromagnetic $S_E$ as a function of frequency for SBR–MWCNT composites with fixed MWCNT containing different amounts of IL. Reproduced with permission from H.H. Le, K. Oßwald, S. Wießner, A. Das, K-W. Stöckelhuber, R. Boldt, G. Gupta, G. Heinrich and H-J. Radusch, *Polymer*, 2013, **54**, 7009. ©2013, Elsevier [133].

In further studies, the authors investigated the thermal degradation of CR composites based on IL-modified CNT. Due to the better dispersion, as well as improved interfacial interactions in the presence of IL, the thermal stability was found to be enhanced for IL-assisted systems. The composites showed three and four stages of degradation behaviour in nitrogen and air, respectively. The flame retardancy of the composites remained unchanged after the incorporation of IL [134]. Optical microscopy, TEM and

atomic force microscopy provided qualitative information regarding the morphological development and localisation of the dispersing agent in the nanocomposites, whereas a quantitative understanding is obtained using the wetting concept [133]. It was found that the dispersing agents used exerted a positive influence on the filler dispersion, and selective wetting of the filler surface by the dispersing agent and rubber matrix was controlled by various thermodynamic and kinetic factors. A model using the surface energy data of polymer components (rubber and dispersing agent) and the filler was used in order to determine the thermodynamic equilibrium state of filler wetting, which was found to be dependent upon the filler – polymer affinity and the dispersing agent/matrix mass ratio.

The dispersion of MWCNT in the presence of IL in an ethylene acrylic rubber matrix has been analysed by Sahoo and co-workers [135]. They found that no agglomeration occurred in the presence of AMIC IL, but MWCNT agglomerations were found at higher filler loadings. From a dynamic mechanical analysis study, it was observed that the storage modulus increased with increased MWCNT loading and increased in the presence of IL due to the better dispersion of MWCNT. The effect of the non-covalent modification of carboxylated MWCNT by a carboxylated IL, 1-carboxyethyl-3-methylimidazolium *bis*(trifluoromethylsulfony)imide, on polymer–filler interactions, filler dispersion, thermal stability, and mechanical and dielectric properties of CR–MWCNT composites were studied [136]. The filler dispersion in the polymer matrix was characterised visually by TEM images. A reduction in the number of agglomerates of MWCNT in the SBR matrix was observed due to the non-covalent functionalisation by IL (Figure 5.5). The substantial dispersion of modified MWCNT with fewer agglomerates throughout the SBR matrix was attributed to the molecular ordering of IL between individual tubes. In this case, the surface treatment of MWCNT with IL reduced the surface energy, in addition, modified MWCNT loading resulted in the formation of continuous percolating networks with no agglomeration of the MWCNT. It is well known that the shielding effect of IL against the π–π stacking interaction among MWCNT plays a key role in dispersing MWCNT. IL interact with MWCNT through weak van der Waals interaction, whereas the interactions between modified MWCNT and rubber chains are mainly due to interfacial adhesion between the nanofiller and elastomer matrix.

#### 5.4.5.3 Cure Accelerator

The rheometric study of elastomers measures the torque response over time during the curing process. The measured torque is related to the modulus of the composite. Figure 5.6 shows the vulcanisation curves of neat SBR–MWCNT and the SBR–MWCNT–IL compounds. From the figure, it can be seen that there is a remarkable increase in the torque for SBR–MWCNT composites, which is due to the immobilisation of polymer chains in the rigid MWCNT

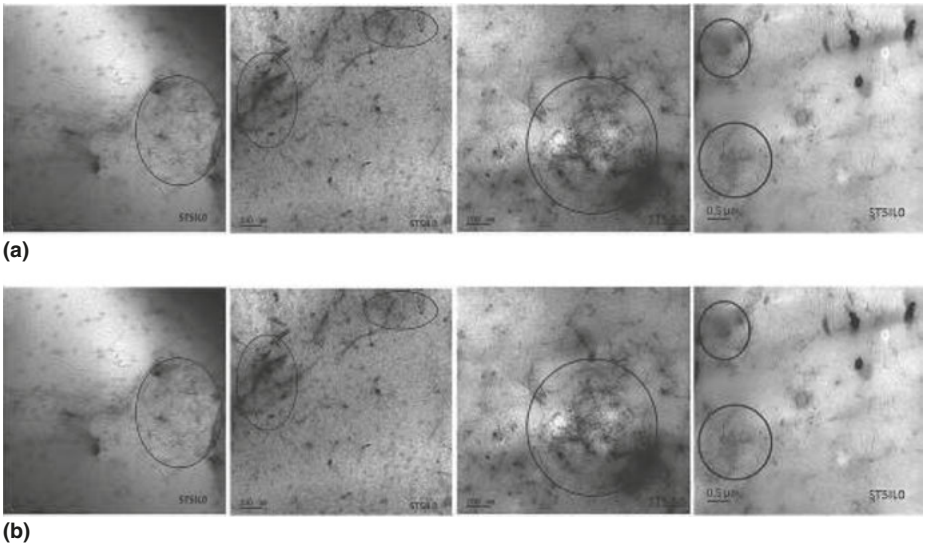


**Figure 5.5:** TEM images of (a) unmodified and (b) modified composites at different magnifications. Reproduced with permission from J. Abraham, M.P. Arif, L. Kailas, N. Kalarikkal, S.C. George and S. Thomas, *RSC Advances*, 2016, **6**, 32,493. ©2016, Royal Society of Chemistry [106].

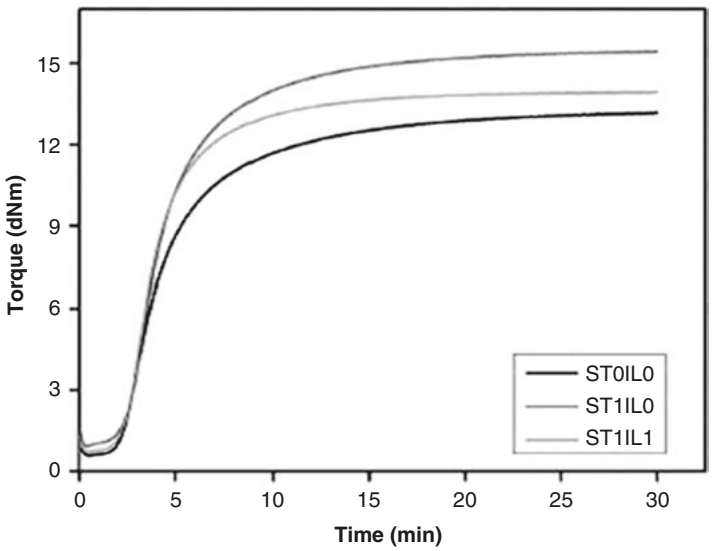


**Figure 5.6:** Rheographs of neat SBR and its composites. ST0IL0: neat rubber; ST1IL0: rubber containing 1 phr unmodified MWCNT and ST1IL1: rubber containing 1 phr modified MWCNT. Reproduced with permission from J. Abraham, M. Arif, L. Kailas, N. Kalarikkal, S.C. George and S. Thomas, *RSC Advances*, 2016, **6**, 32,493. ©2016, Royal Society of Chemistry [106].

region [106]. A large specific surface area of CNT results in high stiffness and torque of the composites. It was also noted that the presence of IL in the rubber composites influenced the cure kinetics by reducing the torque value, which is important from a processing point-of-view. This could be due to the fact that IL act both as a plasticiser and as a catalyst of the interface crosslinking reactions, thus speeding up the cure reaction [83]. Curatives must dissolve in the rubber and diffuse to the active sites in order to react effectively for the efficient crosslinking of rubber. It can be concluded that IL improved the dispersion of curing agents, particularly zinc oxide in the polymer matrix, so their presence in the rubber composites contributed to a considerable decrease in vulcanisation time and an increase in the crosslinking efficiency.

#### 5.4.5.4 Plasticiser

The effect of IL as a plasticiser in rubber composites was investigated by Subramaniam and co-workers. In this study, after the incorporation of IL-modified MWCNT, a decrease in mechanical performance was observed, which was correlated with the plasticising effect of IL [137].

## 5.5 Conclusion

This review provides an overview of research on the role of IL as a coupling agent, dispersant and cure accelerator for rubber nanocomposites, with particular emphasis on the dispersion of nanofillers with the aid of IL, in addition to discussing bulk property changes of the composites. It has also been shown that good filler dispersion leads to an improvement in properties. Furthermore, it has been shown that an IL has a surface energy which is closely related to the surface energy of MWCNT, resulting in the possibility of non-covalent interaction between CNT and IL. This is an environmentally friendly method to develop composites with better mechanical, thermal, electrical and tribological properties at a low concentration of nanofiller. Additionally, the use of IL significantly influences the cure behaviour of polymer nanocomposites. Even though IL can impart some incredible properties to the polymer matrix, some challenges remain including: (i) lack of understanding of the interactions between IL and the matrix polymer, (ii) the cost and accessibility of the original IL structure and (iii) the intensification of work on combinations of multiple IL.

**Acknowledgements:** The authors would like to thank the Council for Scientific and Industrial Research (CSIR), Delhi, India for the financial support.

# References


1. J. Sandler, M.S.P. Shaffer, T. Prasse, W. Bauhofer, K. Schulte and A.H. Windle, *Polymer*, 1999, **40**, 5967.
2. F.H. Gojny, J. Nastalczyk, Z. Roslaniec and K. Schulte, *Chemical Physics Letters*, 2003, **370**, 820.
3. J.K.W. Sandler, S. Pegel, M. Cadek, F. Gojny, M. Van Es and J. Lohmar, *Polymer*, 2004, **45**, 2001.
4. F. Li, H.M. Cheng, S. Bai, G. Su and M.S. Dresselhaus, *Applied Physics Letters*, 2000, **77**, 3161.
5. A.B. Dalton, S. Collins, E. Munoz, J.M. Razal, V.H. Ebron, J.P. Ferraris, J.N. Coleman, B.G. Kim and R.H. Baughman, *Nature*, 2003, **423**, 703.
6. M.S.P. Shaffer and A.H. Windle, *Advanced Materials*, 1999, **11**, 937.
7. M. Bismark, H.G. Kim, J. Lee, S. Arepalli and C. Nah, *International Journal of Smart and Nano Materials*, 2015, **6**, 211.
8. A. Shanmugharaj, J. Bae, K. Lee, W. Noh, S. Lee and S. Ryu, *Composites Science and Technology*, 2007, **67**, 1813.
9. D. Steinhauser, *Express Polymer Letters*, 2012, **6**, 927.
10. G. Sui, W.H. Zhong, X.P. Yang and Y.H. Yu, *Material Science Engineering: A*, 2008, **485**, 524.
11. G. Sui, W.H. Zhong, X.P. Yang, Y.H. Yu and S.H. Zhao, *Polymers for Advanced Technologies*, 2008, **19**, 1543.
12. M.A.A. Tarawneh, S.H. Ahmad, R. Rasid, S.Y. Yahya, S.A.R. Bahri, S. Ehnoum, K.Z. Ka and L.Y. Seng, *Sains Malaysiana*, 2011, **40**, 725.
13. T.T.N. Dang, S.P. Mahapatra, V. Sridhar, J.K. Kim, K.J. Kim and H. Kwak, *Journal of Applied Polymer Science*, 2009, **113**, 1690.
14. S.K. Yadav, S.S. Mahapatra and J.W. Cho, *Journal of Applied Polymer Science*, 2013, **129**, 2305.
15. G. Scherillo, M. Lavorgna, G.G. Buonocore, Y.H. Zhan, H.S. Xia, G. Mensitieri and L. Ambrosio, *ACS Applied Materials & Interfaces*, 2014, **6**, 2230.
16. K. Subramaniam, A. Das, D. Steinhauser, M. Klüppel and G. Heinrich, *European Polymer Journal*, 2011, **47**, 2234.
17. L. Bokobza, *Polymer*, 2007, **48**, 4907.
18. K. Subramaniam, A. Das, K.W. Stöckelhuber and G. Heinrich, *Rubber Chemistry and Technology*, 2013, **86**, 367.
19. S.Y. Lee and G.H. Kim, *Polymer Composites*, 2016, doi:10.1002/pc.23953.
20. A.A. Gavrilov, A.V. Chertovich, P.G. Khalatur and A.R. Khokhlov, *Soft Matter*, 2013, **9**, 4067.
21. A.A. Gavrilov, A.V. Chertovich, P.G. Khalatur and A.R. Khokhlov, *Macromolecules*, 2014, **47**, 5400.
22. F. Galantini, S. Bianchi, V. Castelvetro and G. Gallone, *Smart Materials and Structures*, 2013, **22**, 5, 055025.
23. P. Costa, J. Silva, A. Ansón-Casaos, M.T. Martinez, M.J. Abad, J. Viana and S. Lanceros-Mendez, *Composites Part B: Engineering*, 2014, **61**, 136.
24. C. Choi, H.J. Sim, G.M. Spinks, X. Lepró, R.H. Baughman and S.J. Kim, *Advanced Energy Materials*, 2016, **6**, 1.
25. A.K. Gaharwar, A. Patel, A. Dolatshahi-Pirouz, H. Zhang, K. Rangarajan, G. Iviglia and A. Khademhosseini, *Biomaterials Science*, 2015, **3**, 46.
26. R. Zhang, H. Deng, R. Valenca, J. Jin, Q. Fu, E. Bilotti and T. Peijs, *Composites Science and Technology*, 2013, **74**, 1.
27. L.V. Radushkevich and V.M. Lukyanovich, *Russian Journal of Physical Chemistry*, 1952, **26**, 88.
28. A. Oberlin, M. Endo and T. Koyama, *Journal of Crystal Growth*, 1976, **32**, 335.
29. S. Iijima, *Nature*, 1991, **354**, 56.
30. D.S. Bethune, C.H. Klang and M.S. De Vries, *Nature*, 1993, **363**, 605.

31. M.S. Dresselhaus, G. Dresselhaus and R. Saito, *Carbon*, 1995, **33**, 883.
32. P.C. Ma, N.A. Siddiqui, G. Marom and J.K. Kim, *Composites Part A: Applied Science and Manufacturing*, 2010, **41**, 1345.
33. P. Jan, D. Jana, C. Jana, H. Jaromir, J. Ondrej, A. Vojtech and K. Rene, *Journal of Material Chemistry*, 2011, **21**, 15872.
34. D. Qian, G.J. Wagner, W.K. Liu, M.F. Yu and R.S. Ruoff, *Applied Mechanics Reviews*, 2002, **55**, 495.
35. X. Xiao-Lin, M. Yiu-Wing and Z. Xing-Ping, *Materials Science and Engineering*, 2005, **49**, 89.
36. L.S. Schadler, S.C. Giannaris and P.M. Ajayan, *Applied Physics Letters*, 1998, **73**, 3842.
37. G. Annat, D.R. MacFarlane and M. Forsyth, *The Journal of Physical Chemistry B*, 2007, **111**, 9018.
38. J.N.C Lopes, T.C. Cordeiro, J.M.S.S. Esperanc H.J.R. Guedes, S. Huq, L.P.N. Rebelo and K.R. Seddon, *The Journal of Physical Chemistry B*, 2005, **109**, 3519.
39. T. Tsukasa, T. Tetsuya, O. Ken-ichi and K. Susumu, *Advanced Materials*, 2010, **22**, 1196.
40. V.P. Natalia and R.S. Kenneth, *Chemical Society Reviews*, 2008, **37**, 123.
41. J.S. Wilkes, J.A. Levisky, R.A. Wilson and C.L. Hussey, *Inorganic Chemistry*, 1982, **22**, 1263.
42. J. Gorman, *Science News*, 2001, **160**, 156.
43. A.A. Fannin, Jr., D.A. Floreani, L.A. King, J.S. Landers, B.J. Piersma, D.J. Stech, R.L. Vaughn and J.S. Wilkes, *Journal of Physical Chemistry*, 1984, **88**, 2614.
44. S. Lee, *Chemical Communications*, 2006, **10**, 1049.
45. W.H. Awad, J.W. Gilman, M. Nyden, R.H. Harris, T.E. Sutto, J. Callahan, P.C. Trulove, H.C. DeLong and D.M. Fox, *Thermochimica Acta*, 2004, **409**, 3.
46. A.S. Larsen, J.D. Holbrey, F.S. Tham and C.A. Reed, *Journal of American Chemical Society*, 2000, **122**, 7264.
47. J.G. Huddleston, H.D. Willauer, R.P. Swatloski, A.E. Visser and R.D. Rogers, *Chemical Communications*, 1998, **16**, 1765.
48. L. Cammarata, S.G. Kazarian, P.A. Salter and T. Welton, *Physical Chemistry Chemical Physics*, 2001, **3**, 5192.
49. M.J. Earle, S.P. Katdare and K.R. Seddon, *Organic Letters*, 2004, **6**, 707.
50. V.I. Pârvulescu and C. Hardacre, *Chemical Reviews*, 2007, **107**, 2615.
51. M. Armand, F. Endres, D.R. MacFarlane, H. Ohno and B. Scrosati, *Nature Materials*, 2009, **8**, 621.
52. T. Fukushima, A. Kosaka, Y. Ishimura, T. Yamamoto, T. Takigawa and N. Ishii, *Science*, 2003, **300**, 2072.
53. T. Fukushima and T. Aida, *Chemistry – A European Journal*, 2007, **13**, 5048.
54. H. Ma, X. Chen, B.S. Hsiao and B. Chu, *Polymer*, 2014, **55**, 160.
55. S. Livi, J. Duchet-Rumeau and J. Gerard, *Journal of Colloid and Interface Science*, 2012, **369**, 111.
56. L. Sadok and D. Christian, *Journal of Material Chemistry*, 2007, **17**, 1476.
57. L. Sadok and D. Christian, *Journal of Material Chemistry*, 2005, **15**, 4734.
58. J.P. Fontana, F.F. Camilo, M.A. Bizeto and R. Faez, *Applied Clay Science*, 2013, **83**, 203.
59. X. Hong, T. Fangfang, Y. Jian, W. Lixiong and Z. Jun, *Polymer International*, 2012, **61**, 1382.
60. G.P. Pandey and A.C. Rastogi, *MRS Online Proceedings*, 2012, doi:10.1557/opl.2012.1279.
61. H. Yang, C. Shan, F. Li, D. Han, Q. Zhang and L. Niu, *Chemical Communications*, 2009, p.3880.
62. X. Zhou, T. Wu, B. Hu, G. Yang and B. Han, *Chemical Communications*, 2010, **46**, 3663.
63. S. Livi, V. Bugatti, L. Estevez, J. Duchet-Rumeau and E.P. Giannelis, *Journal of Colloid and Interface Science*, 2012, **388**, 123.
64. F. Gayet, L. Viau, F. Leroux, Mabille, S. Monge, J. Robin and A. Vioux, *Chemistry of Materials*, 2009, **21**, 5575.

65. D.M. Fox, R.H. Harris, Jr., S. Bellayer, J.W. Gilman, M.Y. Gelfer, B.S. Hsaio, P.H. Maupin, P.C. Trulove and H.C. De Long, *Polymer*, 2011, **52**, 5335.
66. C. Tsioptsias and C. Panayiotou, *Carbohydrate Polymers*, 2008, **74**, 99.
67. M. Soheilmoghaddam, M.U. Wahit, A.A. Yussuf, M.A. Al-Saleh and W.T. Whye, *Polymer Testing*, 2014, **33**, 121.
68. P. Wassersheid and M. Haumann in *Catalyst Separation, Recovery and Recycling: Chemistry and Process Design*, Eds., D.J. Cole-Hamilton and R.P. Tooze, Springer, Dordrecht, Germany, 2006.
69. M. Wagner and M. Uerdingen in *Multiphase Homogeneous Catalysis*, Eds., B. Cornils, W.A. Herrmann, I.T. Horvath, W. Leitner, S. Mecking, H. Olivier-Bourbigou and D. Vogt, Wiley-VCH, Weinheim, Germany, 2005.
70. R. Martinez-Palou, *Journal of the Mexican Chemical Society*, 2007, **51**, 252.
71. S. Livi, V. Bugatti, B.G. Soares and J. Duchet-Rumeau, *Green Chemistry*, 2014, **16**, 3758.
72. M.P. Scott, M. Rahman and C.S. Brazel, *European Polymer Journal*, 2003, **39**, 1947.
73. P. Kubisa, *Progress in Polymer Science*, 2004, **29**, 3.
74. J. Lu, F. Yan and J. Texter, *Progress in Polymer Science*, 2009, **34**, 431.
75. A. Noda, K. Hayamizu and M. Watanabe, *The Journal of Physical Chemistry B*, 2001, **105**, 4603.
76. H. Sakaebe and H. Matsumoto, *Electrochemistry Communications*, 2003, **5**, 594.
77. A. Lewandowski and A. Swiderska, *Solid State Ionics*, 2004, **169**, 21.
78. W. Zhai, H.Z. Chen, R.Y. Ma and J. Chin, *Beijing University of Chemical Technology*, 2007, **34**, 138.
79. E. Leroy, P. Jacquet, G. Coativy, A.L. Reguerre and D. Lourdin, *Carbohydrate Polymers*, 2012, **89**, 955.
80. S.S. Ray, J. Bandyopadhyaj and M. Bousmina, *Macromolecular Materials and Engineering*, 2007, **292**, 729.
81. J. Chen, Y. Shi, J. Yang, N. Zhang, T. Huang and Y. Wang, *Polymer*, 2013, **54**, 464.
82. A. Sankri, A. Arhaliass, I. Dez, A.C. Gaumont, Y. Grohens, D. Lourdin, I. Pillin, Rolland-Sabate and E. Leroy, *Carbohydrate Polymers*, 2010, **82**, 256.
83. M.P. Scott, C.S. Brazel, M.G. Benton, J.W. Mays, J.D. Holbrey and R.D. Rogers, *Chemical Communications*, 2002, **13**, 1370.
84. M. Rahman and C.S. Brazel, *PMSE Preprints*, 2008, **98**, 788.
85. K.I. Park and M. Xanthos, *Polymer Degradation and Stability*, 2009, **94**, 834.
86. P. Bernado, J.C. Jansen, F. Bazzarelli, F. Tasselli, A. Fuoco, K. Friess, P. Izak, V. Jarmarova, M. Kacirkova and G. Clarizia, *Separation and Purification Technology*, 2012, **97**, 73.
87. H. Zhang J. Wu, J. Zhang and J.S. He, *Macromolecules*, 2005, **38**, 8272.
88. V. Totolin, N. Ranetcaia, V. Hamciuc, N. Shore, N. Dörr, C. Ibanescu, B.C. Simionescu and V. Harabagiu, *Tribology International*, 2013, **67**, 1.
89. T. Fukushima, K. Asaka, A. Kosaka and T. Aida, *Angewandte Chemie International Edition*, 2005, **44**, 2410.
90. Y. Zhou, J.H. Schattka and M. Antonietti, *Nano Letters*, 2004, **4**, 477.
91. K. Baba, T. Kaneko, R. Hatakeyama, K. Motomiya and K. Tohji, *Chemical Communications*, 2010, **46**, 255.
92. N. Maleki, A. Safavi and F. Tajabadi, *Analytical Chemistry*, 2006, **78**, 3820.
93. J. Wang, H. Chu and Y. Li, *ACS Nano*, 2008, **2**, 2540.
94. H. Zhang, Z.G. Wang, Z.N. Zhang, J. Wu, J. Zhang and H.S. He, *Advanced Materials*, 2007, **19**, 698.
95. K. Dong, G. Zhou, X. Liu, X. Yao, S. Zhang and A. Lyubartsev, *Journal of Physical Chemistry C*, 2009, **113**, 10013.

96. Y. Zhang, Y. Shen, J. Li, L. Niu, S. Dong and A. Ivaska, *Langmuir*, 2005, **21**, 4797.
97. L. Polo-Luque, B.M. Simonet and M. Valcárcel, *Trends in Analytical Chemistry*, 2013, **47**, 99.
98. T. Meltem, D. Jérôme and S. Philippe, *Carbon*, 2012, **50**, 4303.
99. P. Du, S. Liu, P. Wu and C. Cai, *Electrochimical Acta*, 2007, **52**, 6534.
100. B.P. Price, J.L. Hudson and J.M. Tour, *Journal of American Chemical Society*, 2005, **127**, 14867.
101. C. Zhao, B. Ren, Y. Song, J. Zhang, L. Wei, S. Chen and S. Zhang, *RSC Advances*, 2014, **4**, 31, 16267.
102. Y. Shim and H.J. Kim, *ACS Nano* 2009, **3**, 1693.
103. A. Santiago and A. Mert, *Journal of Physical Chemistry C*, 2012, **116**, 12055.
104. Z. Hua, R. Michael, F. Guang, S.L. Sang, D. Hugh, F. Paul and T. Peter, *ACS Nano*, 2012, **6**, 9818.
105. M. Morteza and F. Masumeh, *Physical Chemistry Chemical Physics*, 2013, **15**, 2482.
106. J. Abraham, M. Arif, L. Kailas, N. Kalarikkal, S.C. George and S. Thomas, *RSC Advances*, 2016, **6**, 32493.
107. K.F. Kelly, I.W. Chiang, E.T. Mickelson, R.H. Hauge, J.L. Margrave, X. Wang, G.E. Scuseria, C. Radloff and N.J. Halas, *Chemical Physics Letters*, 1999, **313**, 445.
108. K. Esumi, M. Ishigami, A. Nakajima, K. Sawada and H. Hond, *Carbon*, 1996, **34**, 279.
109. Y.P. Sun, K. Fu, Y. Lin and W. Huang, *Accounts of Chemical Research*, 2002, **35**, 1096.
110. M. Cadek, J.N. Coleman, V. Barron, K. Hedicke and W.J. Blau, *Applied Physics Letters*, 2002, **81**, 5123.
111. M. Cadek, J.N. Coleman, K.P. Ryan, V. Nicolosi, G. Bister, A. Fonseca, J.B. Nagy, K. Szostak, F. Beguin and W.J. Blau, *Nano Letters*, 2004, **4**, 353.
112. F. Dalmas, L. Chazeau, C. Gauthier, K. Masenelli-Varlot, R. Dendievel, J.Y. Cavaillé and L. Forró, *Journal of Polymer Science, Part B: Polymer Physics*, 2005, **43**, 1186.
113. R. Haggenmueller, H.H. Gommans, A.G. Rinzler, J.E. Fischer and I. Winey, *Chemical Physics Letters*, 2000, **330**, 219.
114. Z. Jin, K.P. Pramoda, G. Xu and S.H. Goh, *Chemical Physics Letters*, 2001, **337**, 43.
115. P. Potschke, T.D. Fornes and D.R. Paul, *Polymer*, 2002, **43**, 3247.
116. T. Liu, I.Y. Phang, L. Shen, S.Y. Chow and W.D. Zhang, *Macromolecules*, 2004, **37**, 7214.
117. A.R. Bhattacharyya, T.V. Sreekumar, T. Liu, S. Kumar, L.M. Ericson, R.H. Hauge and R.E. Smalley, *Polymer*, 2003, **44**, 2373.
118. E.J. Siochi, D.C. Working, C. Park, P.T. Lillehei, J.H. Rouse, C.C. Topping, A.R. Bhattacharyya and S. Kumar, *Composites Part B: Engineering*, 2004, **35B**, 439.
119. N. Pierard, A. Fonseca, Z. Konya, I. Willems, G. van Tendeloo and J.B. Nagy, *Chemical Physics Letters*, 2001, **335**, 1.
120. H. Xia, Q. Wang, K. Li and G.H. Hu, *Journal of Applied Polymer Science*, 2004, **93**, 378.
121. S. Ghose, K.A. Watson, K.J. Sun, J.M. Criss, E.J. Siochi and J.W. Connell, *Composite Science and Technology*, 2006, **66**, 1995.
122. Z. Jia, Z. Wang, C. Xu, J. Liang, B. Wei and D. Wu, *Materials Science and Engineering: A*, 1999, **271**, 395.
123. F.H. Gojny, M. Wichmann, U. Kopke, B. Fiedler and K. Schulte, *Composite Science and Technology*, 2004, **64**, 2363.
124. J. Zhu, H. Peng, F. Rodriguez-Macias, J.L. Margrave, V.N. Khabashesku, A. Imam, K. Lozano and E.V. Barrera, *Advanced Functional Materials*, 2004, **14**, 643.
125. J. Yu, K. Lu, E. Sourty, N. Grossiord, C.E. Koning and J. Loos, *Carbon*, 2007, **45**, 2897.
126. X. Zhou, Y. Zhu, Q. Gong and J. Liang, *Materials Letters*, 2006, **60**, 3769.
127. D. Ponnamma, S.H. Sung, J.S. Hong, K.H. Ahn, K.T. Varughese and S. Thomas, *European Polymer Journal*, 2014, **53**, 147.
128. Z. Peng, C. Feng, Y. Luo, Y. Li and L.X. Kong, *Carbon*, 2010, **48**, 4497.

129. A. Das, K.W. Stockelhuber, R. Jurk, J. Fritzsche, M. Kluppel and G. Heinrich, *Carbon*, 2009, **47**, 3313.
130. T. Sekitani, Y. Noguchi, K. Hata, T. Fukushima, T. Aida and T. Someya, *Science*, 2008, **321**, 1468.
131. K. Subramaniam, A. Das and G. Heinrich, *Composites Science and Technology*, 2011, **71**, 1441.
132. J. Abraham, P. Xavier, S. Bose, S.C. George, N. Kalarikkal and S. Thomas, *Polymer*, 2017, **112**, 102.
133. H.H. Le, K. Oßwald, S. Wießner, A. Das, K-W. Stöckelhuber, R. Boldt, G. Gupta, G. Heinrich and H-J. Radusch, *Polymer*, 2013, **54**, 7009.
134. K. Subramaniam, A. Das, L. Häussler, C. Harnisch, K.W. Stöckelhuber and G. Heinrich, *Polymer Degradation and Stability*, 2012, **97**, 776.
135. P. Sahoo, K. Naskar and D.K. Tripathy, *Polymer Composites*, 2016, **37**, 2568.
136. G. Jiang, S. Song, Y. Zhai, C. Feng and Y. Zhang, *Composites Science and Technology*, 2016, **123**, 171.
137. K. Subramaniam, A. Das, F. Simon and G. Heinrich, *European Polymer Journal*, 2013, **49**, 345.

Mangala Joshi and Bapan Adak

# 6 Nanotechnology-based Textiles: A Solution for the Emerging Automotive Sector

## 6.1 Introduction

Nanotechnology deals with dimensions of less than 100 nm, which is achieved *via* the precise manipulation of individual atoms and molecules to create nanomaterials and nanodevices with exciting new properties [1]. By virtue of the high surface area to volume ratio (SVR) of nanostructured materials or nanomaterials, they are capable of tremendously enhancing the properties of a material to which they are added. Recently, nanomaterials and nanotechnology have shown a very wide range of potential applications in many fields of science and technology. The textile industry is also benefitting from the advantages of nanotechnology in its various fields of applications [2].

Nowadays, nanotechnology-based textile products, from nanofibres (NF) or nanocomposite fibres to functional nanofinishing, nanocoatings or polymer nanocomposite coatings, are the focus of considerable interest for the development of smart, functional and high-performance textiles [3]. Applications of nanoparticles (NP) in conventional chemical processing, such as finishing, dyeing and coatings, markedly improve the performance of textiles. Modern nanotechnology-based coating techniques, such as layer-by-layer (LbL), sol-gel, plasma polymerisation, dip/spray coating and so on, are capable of producing multifunctional, smart and intelligent fabrics [2, 4]. Great repeatability, durability of acquired functionality, reliability and robustness are the main benefits of nanotechnology-based developments in textiles. At present, the automotive industry is one of the major consumers of nanotechnology-enhanced textiles [5].

Textiles are of great importance in the automotive sector and are mainly used in upholstery, interior covers and panels (seat covering, doors and pillars, dashboards, carpets, headliners, safety belts, airbags, trimmings and so on), air/liquid filtration, tyre application and structural body components. The use of textile products in the automotive industry results in: weight reduction, increased fuel efficiency, good aesthetic and visual impression, increased sound absorption and product reachability, and also ensures safety and comfort to drivers and passengers [6]. The automotive industry is potentially a major beneficiary of nanotechnology-based developments which promise to improve performance at various levels providing stronger, lighter, harder materials, improved engine efficiency, reduced environmental impact, reduced consumption of fuel, extended service life, and improved safety and comfort [7].

https://doi.org/10.1515/9783110643879-006

The automotive industry is a material-intensive industry involving the use of a wide variety of materials (metals, textiles, polymers and fillers). The commercialisation of any automotive component made of these materials depends on fulfilling specific requirements, in addition to their overall performance and cost [8]. The application of nanotechnology in automotive textiles is intended to bridge the gap between superior technical performance and cost fluctuation. This chapter mainly focuses on the potential application of specific nanotechnology-based textiles in the automotive industry. However, before discussing the use of nanotechnology for automotive textiles, it is very important to know where textile materials are used in automotives. Therefore, the first section of this chapter will highlight the major uses of textiles in the automotive industry.

## 6.2 Textiles used in Automobiles

### 6.2.1 Automotive Textiles: Market Scenario

Innovations and product development, enhanced product properties, such as strength and durability, and the growth and advancement of the global automotive industry are the major factors that have driven the present market for technical textiles in the automotive sector. The global demand for technical textiles reached US$ 162.3 billion by 2016, up from an estimated US$ 155.3 billion in 2015, where the market share of mobiltech is anticipated to reach 13.7% by 2020, up from 13.3% in 2014 [9]. A study conducted in 1997 indicated that about 20 kg of textiles are used in a midsize car, which include approximately 3.5 kg for seat covers, 4.5 kg for carpets, 6.0 kg for glass fibre composites and 6.0 kg for other interior parts and tyres [10]. According to the Textiles Intelligence report [11], the average weight of textile materials in a midsize car has increased from 20 to 26 kg today, and by the end of 2020 it is expected to reach 35 kg. The increase stems from a rise in demand for greater comfort and safety, and effort focused on reducing the weight of a vehicle in order to lower fuel consumption and carbon dioxide ($CO_2$) emissions [11]. Moreover, as travelling has become an integral part of everyone's life, safety and comfort are of the utmost priority. The combined effect of all these factors indicate a bright prospect for technical textiles in the automotive sector [12]. At present, almost two-thirds of automotive textiles are used in carpets, seat covers, upholstery, interior trims, and roof and door liners. Other applications of automotive textiles include: tyres, safety belts, hoses, air bags, battery separators, filters, and textile-reinforced flexible and hard composites for structural components [13]. Figure 6.1 details the use of textiles in different automotive parts, whereas Table 6.1 summarises the use of textiles in different automotive parts and their percentage share.

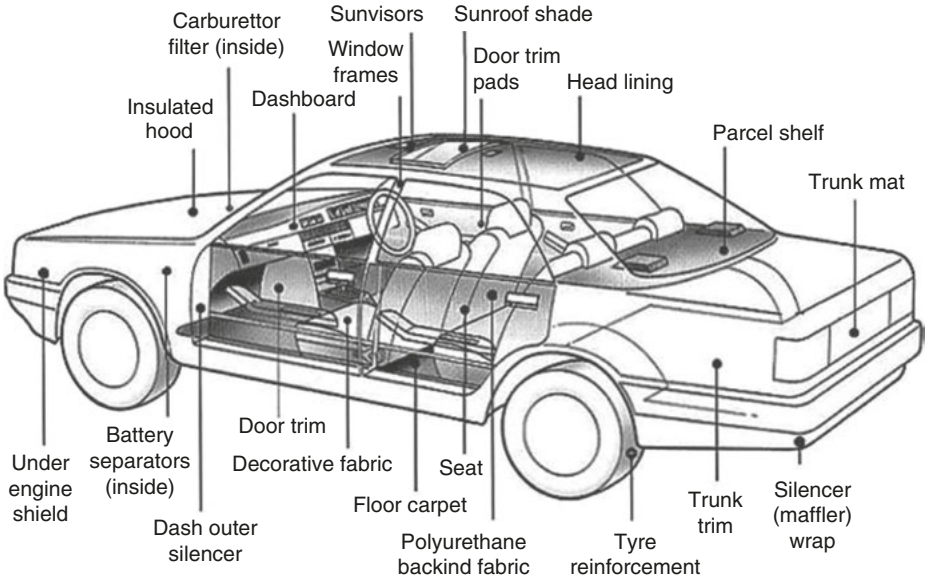


**Figure 6.1:** Applications of textiles in different parts of a car.

**Table 6.1:** Use of textiles in the automotive industry.

| Serial No. | Different automotive textiles | Percentage share (%) |
|---|---|---|
| 1 | Carpets (including car mats) | 33.3 |
| 2 | Upholstery (seating fabric) | 18 |
| 3 | Preassembled interior components | 14 |
| 4 | Tyres | 12.8 |
| 5 | Safety belts | 8.8 |
| 6 | Air bags | 3.7 |
| 7 | Others | 9.4 |
| Total | | 100 |

Adapted from K. Singh, *Journal of Safety Engineering*, 2012, **1**, 1, 7 [14] and S. Viju and A. Mukhopadhyay, *Asian Textile Journal*, 2006, **15**, 5, 49 [16]

## 6.2.2 Textile Fibres used in Automobiles

Different synthetic fibres [mainly polyester, polypropylene (PP), Nylon 6, Nylon 6,6, acrylic and mod-acrylic], natural fibres (mainly cotton, jute, wool, sisal and hemp) and man-made cellulosic fibres (mainly viscose rayon) are potentially used in the automotive industry. Apart from these, some high-temperature-resistant

and high-performance fibres, such as Aramid (Nomex®, Kevlar®, DuPont), Panox (Lantor Universal Carbon Fibres), polybenzimidazole (PBI) fibre (Hoechst), Inidex (Courtaulds), ultrahigh molecular weight polyethylene and glass fibres, are also used for some special automotive applications [15]. Table 6.2 highlights the use of different fibres in various automotive applications and the properties suitable for that particular application.

**Table 6.2:** Various fibres used in automotive interiors and their properties.

| Serial No. | Application | Fibre used | Properties required |
|---|---|---|---|
| 1 | Seat covers | Polyester, Nylon, PP, wool | UV resistance and abrasion resistance, attractive design and texture |
| 2 | Seat belts | Polyester | Good tensile strength and extension (up to 25–30%), UV resistance and abrasion resistance |
| 3 | Seat fire barriers | Panox, Aramid (Nomex, Kevlar), PBI, Inidex | High strength, highly fire resistant, low HRR, low toxicity, opacity of fumes |
| 4 | Carpets | Nylon, polyester, PP | Light fastness, soil and abrasion resistance |
| 5 | Airbags | Nylon 6,6 and Nylon 4,6 | Resistance to high-temperature inflation of gases, good tear strength, durability to storage over many years |
| 6 | Door trim | PP, Nylon, polyester | UV resistance and abrasion resistance, colour retention, attractive design and texture |
| 7 | Trunk liner | Polyester blends, PP | Attractive design and texture, moulding ability, light weight and low cost |
| 8 | Sewing threads | Nylon 6,6 | Abrasion resistance, heat resistance, durability, elastic recovery and wet strength |

HRR: heat release rate
UV: ultraviolet
Adapted from K. Singha, *Journal of Safety Engineering,* 2012, **1**, 1, 7 [14]; W. Fung in *Handbook of Technical Textiles,* Eds., A.R. Horrocks and S.C. Anand, Woodhead Publishing Limited, Boca Raton, 2000 [15]; S. Viju and A. Mukhopadhyay, *Asian Textile Journal,* 2006, **15**, 5, 49 [16]; and *Application of Technical Textiles in Car Industry,* The Apparel, 14th September 2015 [17]

## 6.2.3 Textile Structures used in Automobiles

Automotive textiles for interior furnishing are primarily made of woven, warp-knitted, weft-knitted, tufted, non-woven and laminated fabrics. The design, aesthetics, handle/feel and comfort are very important considerations for textiles used in automobile interiors. At present, in the global automobile fabric arena, woven and knitted fabrics dominate the market. Moreover, among different woven fabric structures, dobby

weaves and jacquard weaves hold the main share. Woven fabrics have a profitable market mainly in the making of seat covers, door covers, air bags and headrests [6].

Circular warp-knitted fabrics and spacer fabrics are used in car interiors including seat covers, door covers, headliners, boot covers, headrests, sunroofs and parcel shelves. Knitted fabrics also have a good application potential in this area due to their high elasticity, flexibility, comfort while travelling and high-grade visual quality [13].

Among other textile-based structures, non-wovens and composites closely trail woven and knitted fabrics. However, the use of non-woven fabrics is gradually increasing in the automotive sector due to certain advantages over woven or knitted fabrics. Non-wovens are used globally for applications such as carpets, floor coverings, headliners, boot linings, parcel shelves, door panels, roof linings, dashboard panels, battery separators, car seats, acoustic insulation and many more [6, 17]. Moreover, special braided structures [both two-dimensional (2D) and three-dimensional (3D)] and 3D fabrics are currently gaining importance for many automotive applications. Multilayered 3D woven fabrics are being used in impact-charged multilayer composite structures such as automobile floor components [18].

### 6.2.4 Interior Automotive Textiles

It has been estimated that approximately 45 $m^2$ of textiles are used in a car interior including: seating area, carpets, headliners, side panels, trunk liners, door trim and dash mats [17]. The materials, structure and specific requirements for different interior automotive textiles are detailed in Table 6.3.

### 6.2.5 Textiles for Tyre Cord Applications

Tyres are a highly engineered complex structural composite material made of tyre cord fabrics, bead wires and rubber, along with carbon black (CB) and other chemical compounds. They consist of a tread and a body, where the tread provides traction while the body provides containment for a quantity of compressed air. The tyre cords and bead wires determine the load-bearing capacity and dynamic behaviour of the tyre. The performance and endurance from cyclic loading/unloading of an automotive tyre depends on the material or composition of the tyre cord, which continuously comes into contact with the road. The main desirable properties for an automotive tyre are: required grip, low rolling resistance, slip-proof, high abrasion resistance, low heat generation, and good thermal stability, air retention, resistance against tear or cut propagation, and ride comfort [20, 21].

Specially prepared and processed woven fabrics are used to reinforce automotive tyres. Tyre cords are made of yarns which in turn come from filaments that have a tensile strength of about 6–10 g/denier. The filaments are ‘Z’ twisted and the

**Table 6.3:** Interior automotive textiles: desired properties and suitable materials.

| Serial No. | Automotive interiors | Required properties or special features | Textile-based materials |
|---|---|---|---|
| 1 | Automotive seats | Good resistance against abrasion, tear, pilling, wrinkle, light and UV degradation, colour fading water, oil, stain, dirt, chemicals and flames<br>Good aesthetic property | Generally, it is a trilaminate containing a face fabric, PU foam in the middle and a scrim backing<br>Mainly Nylon, polyester, PP or wool are used<br>Coconut fibres are frequently used for seat cushioning which has a good breathing propertycushioning which has a good breathing property |
| 2 | Seat belts | Light weight<br>Good load-bearing capacity (up to 1,500 kg)<br>Extensibility up to 25–30%<br>Good resistance against abrasion, light and heat<br>Capability of being unfastened and put back in place easily<br>Smooth surface and good retraction behaviour | Nylon and polyester fibres are widely used for making seat-belt webbing<br>Different weave patterns such as plain, twill and satin are utilised to manufacture seat belts. However, the 2/2 twill structure are commonly used<br>In inflatable seat belts, a polyester fabric or warp-knitted structure is used in the face fabric, while the folded envelop is coated with rubber or made of urethane |
| 3 | Airbags | It slows the passenger's forward motion as quick as possible and within a fraction of a second | The air bag fabric is generally made of a Nylon 6,6 multifilament yarn<br>The fabric may be uncoated or coated with silicon or neoprene |
| 4 | Floor covering/ carpets | The carpets play a significant role in sound and vibration damping in cars | The carpets which are used for automotive floor coverings are mainly three types: tufted loop-pile carpet, tufted cut-pile carpet and needle-felt carpet<br>These are usually coated with SBR or acrylic latex |

| | | | |
|---|---|---|---|
| 5 | Interior trims | Good resistance from heat, sunlight and staining<br>Good colour fastness property<br>Good sound absorbing property<br>Good texture | Generally made of a two to three layered textile material<br>Fot the long run, coconut fibres are being used<br>In a modern car's roof trim, tricot and PET needle-punched non-woven are used<br>Polyester foam sheets and fibre-reinforced porous polymer sheets are used as a base material of roof trims |
| 6 | Door casing | Soft touch<br>Resistance from UV light, abrasion, pilling, colour fading, oil, water, stain, dirt and flames | Generally, in a particular car the face fabric of the door casing is made of the same fabric as used for the seat covers<br>Most of the door casings are manufactured by traditional methods of moulding and lamination, using woven fabric and foam<br>A textile/PUF laminate is almost invariably used in door casing in combination with a film or foil made of thermoplastic PU, thermoplastic PO or PVC |
| 7 | Headliners | It is important as a sound-damping property, vibration insulation and good aesthetics<br>Thin profile but rigid without a buckling tendency, light weight, flexible, dimensionally stable, decorative, aesthetically pleasing or soft to the touch | The centre core is generally made of semi-rigid thermomouldable PUF phenolic-resinated waste fibres/100% non-woven based on polyester<br>In the adhesive layer, a hot-melt powder or hot-melt film is used to join the layers together in a flat-bed laminator<br>The chopped glass/roving is used to impart rigidity in the structure and also absorb sound |
| 8 | Boot or trunk liners | Must be decorative and functional<br>Good noise absorption capability<br>Mouldable, light weight and low cost | Needle-punched polyester or PP are mainly used in coverings of boot liners<br>Sometimes, trunk liners are made from natural fibres such as hemp and sisal and also shoddy waste fibres. These materials not only increase noise absorption but also reduce cost |
| 9 | Bonnet liners | Absorb and reduce engine noise | Generally, a textile-based laminated structure is used<br>Commonly made of PET- and PP-based needle-punched non- woven sheets bound by PUF |

(continued)

**Table 6.3** (continued)

| Serial No. | Automotive interiors | Required properties or special features | Textile-based materials |
|---|---|---|---|
| 10 | Dashboards | Low gloss, non-odorous, non-fogging, soft touch, pleasant aesthetics and resistance from UV radiation, heat ageing, temperature and abrasion | At present, a very limited number of car models use textiles for this special automotive application<br>The structure of dashboard being very complex and curved, only knitted or 3D-knitted fabric can be effectively used |
| 11 | Sun visors | It is an adjustable hinged flap to protect the driver and passengers from sunlight | Raised warp-knit fabrics or PVC is generally used<br>In this area, the textiles, especially non-wovens, have great opportunities to produce a recyclable product |
| 12 | Parcel shelves | Resistance against abrasion, liquids, dirt and flames with good strength and dimensional stability | Nowadays, parcel shelves or package trays are almost invariably covered with polyester- or PP-based needle-punched non-wovens |

PET: Polyethylene terephthalate
PO: Polyolefin
PU: Polyurethane
PUF: Polyurethane foam PVC: Polyvinyl chloride
SBR: Styrene-butadiene rubber
Adapted from W. Fung and M. Hardcastle in *Textiles in Automotive Engineering,* Volume 13, Woodhead Publishing, Cambridge, UK, 2001 [12]; R.S. Kumar in *Textiles for Industrial Applications,* CRC Press, Boca Raton, FL, USA, 2013 [13]; W. Fung in *Handbook of Technical Textiles*, Eds., A.R. Horrocks and S.C. Anand, Woodhead Publishing Ltd, Boca Raton, FL, USA, 2000 [15]; *Application of Technical Textiles in Car Industry,* The Apparel, 14th September 2015 [17]; and M. Singha and K. Singha, *Marine Science,* 2012, **2**, 6, 110 [19]

yarns are back twisted ('S' twist) to form the tyre cord. The twists in filaments and yarns influence the property of the tyre cords, such as tensile strength, initial modulus, elongation at break, rupture energy, cyclic tension fatigue resistance and cyclic compression fatigue resistance [13]. The textile fibres/filaments which are used to produce tyre cords are mainly polyester, Nylon, viscose rayon, Aramid and steel. A comparison of properties of these fibres are shown in Table 6.4. Multifilament Nylon 6 yarns have extensive applications in the tyre industry to reinforce rubbers; however, for better heat stabilisation, for example, in airplane tyres, Nylon 6,6 are used [22].

**Table 6.4:** Different tyre-grade reinforcing fibres and their advantages/disadvantages.

| Reinforcing fibres | Advantages | Disadvantages |
|---|---|---|
| PA (Nylon 6 and Nylon 6,6) | Good strength and heat resistance; high elastic recovery, good abrasion and fatigue resistance, lower creep | More flat-spotting tendency, long-term service growth |
| Polyester | High strength, low shrinkage, better flat-spotting resistance than Nylon, low service growth and low cost | Lower elastic recovery and higher loss modulus than Nylon, poor fatigue resistance |
| Viscose rayon | Heat resistant, stable dimensions, good handling characteristics | Highly sensitive to moisture, expensive and environmental issues during manufacturing |
| Aramid | Very high strength and stiffness, heat resistant | Very expensive, processing constraints (difficult to cut) |
| Steel cord | High belt strength and stiffness improves wear and handling | Special processing is required, heavy, more sensitive to moisture |

PA: Polyamide
Adapted from R.S. Kumar in *Textiles for Industrial Applications,* CRC Press, Boca Raton, FL, USA, 2013 [13]; A.K. Naskar, A.K. Mukherjee and R. Mukhopadhyay, *Polymer Degradation and Stability,* 2004, **83**, 1, 173 [21]; and V.B. Gupta and V.K. Kothari in *Manufactured Fibre Technology,* Springer Science & Business Media, Dordrecht, Germany, 2012 [23]

## 6.2.6 Textiles for Automotive Filter Applications

Filters play an important role in preventing solid contaminants like dirt, dust and grit from entering the engine or cabin of any vehicle. Both fuel mileage and engine performance can suffer from dirty or clogged automotive filters. The filtration efficiency mainly depends on the physical structure of the filter (pore size, fibre fineness, matrix structure, thickness and so on), size range of the particles to be collected, chemical characteristics of the filter surface (active chemical group present on the surface, surface free energy and so on), flow rate of air/oil through the filter and pressure drop [24].

The different types of filters (mainly air, oil, fuel and cabin) used in vehicles are all basically textile-based products made of 100% cellulosic fibre or 100% synthetic fibre or a combination of these two. However, the structure of the products that are used as filter media may vary (fabric, non-woven, fibre webs, paper, composite-layered structure and so on) depending on specific requirements (Table 6.5) [16, 25]. To obtain good filtration efficiency, the right choice of filter media is very important. Recently, an NF-based material has gained importance in automotive filtration applications, which will be discussed later in detail.

**Table 6.5:** Different types of automotive filters and typical filter media for their preparation.

| Serial No. | Filter type | Types of filter media (conventional) |
|---|---|---|
| 1 | Carburettor air filter | Mainly different types of non-woven (dry laid, wet laid, needle punched or spun bound) |
| 2 | Fuel tank filters | Activated carbon, woven saran monofilament or resin impregnated, wet laid filter paper |
| 3 | Engine oil filter | Resin-impregnated wet laid non-woven, paper |
| 4 | Cabin interior filter | Electrostatically charged fibre media, non-wovens, speciality paper, activated carbon |
| 5 | Antilock braking system wheel/ brake filters | Metal or fibre woven screens |
| 6 | Diesel/soot filters | Porous ceramic materials with magnesia/ alumina/silica composition |
| 7 | Power steering filters | Mainly screen fabrics |
| 8 | Transmission filters | Needle felts or woven fabrics |
| 9 | Wiper washer screen filters | Woven fabrics |
| 10 | Crank case breathe filters | Non-wovens |
| 11 | Air-conditioning recirculation filters | Non-wovens or activated carbon |

Adapted from S. Viju and A. Mukhopadhyay, *Asian Textile Journal,* 2006, **15**, 5, 49 [16] and P. Ganesan, L. Sasikala, S. Sundaresan, K. Gowri and R. Senthilkumar, *Pakistan Textile Journal,* 2007, http://www.ptj.com.pk/Web-2009/07-09/P.Ganesan.htm [25]

## 6.2.7 Textiles in Automotive Battery Separators

In general, rechargeable batteries are used in the automotive industry that convert chemical energy to electrical energy. A battery is an electric cell or electrochemical device that consists of a negative electrode, an electrolyte that conducts ions, a separator and a positive electrode. The battery separator is a porous membrane that is placed between two oppositely charged electrodes [26]. A separator plays an important role in batteries as it permits the ionic

flow but restricts the electric contact of electrodes. A separator must be an electrical insulator and should have good mechanical and thermal stability and resistance to chemical degradation by electrolytes. A variety of materials have been used to produce battery separators over the years including: cellophane and cellulosic papers to non-woven fabrics (mainly PO based), ion exchange membranes, foams, wet laid glass fibres and polymeric microporous flat sheets. Recently, the separators have become more sophisticated and complex with the introduction of new battery chemistries. Generally, PP-based wet laid non-woven felts are used as the separation materials of a nickel/hydrogen battery [13]. In alkaline-manganese batteries, a wide range of fibres including polyvinyl alcohol (PVA), vinyon and rayon fibre-based materials are used to produce separators [26].

### 6.2.8 Textiles in Automotive Fuel Cells

A fuel cell is an electrochemical device that converts the chemical energy from fuel into electricity *via* a chemical reaction of positively charged hydrogen ions with oxygen or another oxidising agent. Textile materials can potentially be used in the electrodes and separators of a fuel cell. The electrode of a fuel cell must have high gas permeability and electric conductivity. Carbon fibre sheets and activated carbon fibres show good potential for use in electrodes, whereas non-wovens exhibit potential for use in membrane systems or the separators of fuel cells [13, 26]. Nowadays, electrospun NF are used as potential materials for electrodes of fuel cells and batteries, which will be discussed in detail later.

### 6.2.9 Textile-reinforced Composites for Automotive Structural Components

Using the beneficial properties of textiles, such as flexibility, light weight, strength, toughness and availability of different structures, textile-reinforced composites have found many structural applications in automobiles. Textile-reinforced structural composites are uniquely suitable for automotive composite components due to the ease of large scale-up manufacturing, mouldability and low-cost manufacturing. The utilisation of textile-reinforced composite materials has been identified as the main factor that will lead to a reduction of the structural weight of automobile body and chassis components compared with earlier passenger vehicles [6]. The different textile structures used for composite reinforcements are shown in Figure 6.2.

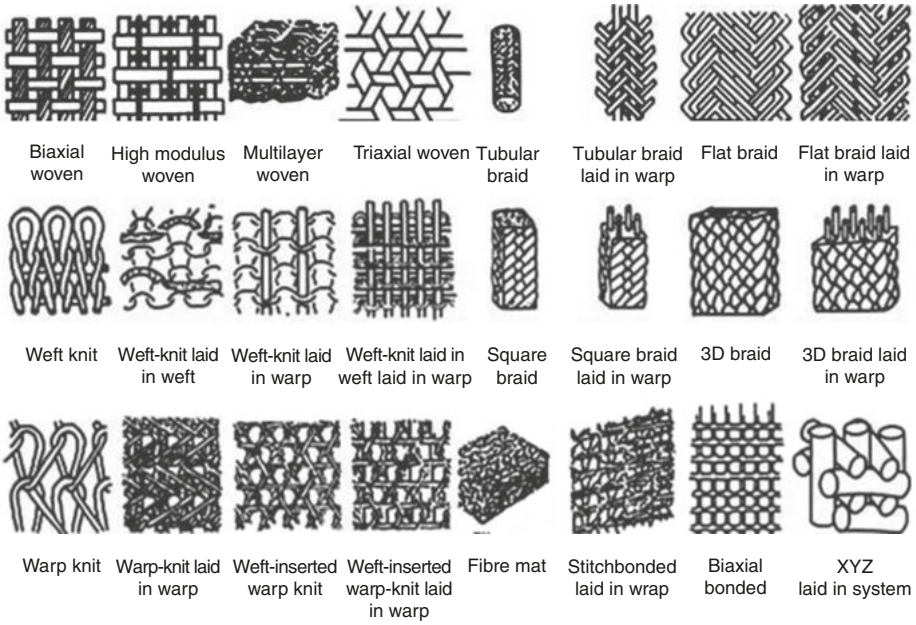


**Figure 6.2:** Textile structures for composite reinforcements. Reproduced with permission from M. Singha and K. Singha, *Marine Science*, 2012, **2**, 6, 110. ©2012, Scientific & Academic Publishing [19].

### 6.2.10 Other Miscellaneous Applications of Textiles in Automobiles

There are many other textile items that are used in cars, in addition to the major components, such as sewing threads, fastening devices, flocked fabric on window seals, hoses and belts, brake and clutch linings, gaskets, window frames, under-engine shield, sunroof and safety devices [6, 15]. Conventional textiles are commonly employed in the automotive sector, but can have limited use in some fields; nano-enabled textiles might be suitable for such applications and will be discussed in the following section.

## 6.3 Nanotechnologies for Automotive Textiles

### 6.3.1 Applications and Market Potential

Nanotechnology is one of the key drivers for the latest innovations in the automotive industry. Nanostructured textiles are becoming increasingly popular in

order to overcome the deficiencies of conventional automotive textiles. Recently, considerable research has been undertaken in the automotive field to use nano-enabled textiles for different automobile applications. As a result, nanofinishing, nanocoating, nanocomposite coatings on textiles, polymeric NF, nanocomposite fibres have been investigated for their potential application in various automotive components.

The main potential of nanotechnology relies on the sudden and profound change in the properties of a material when the particle size is reduced to the nanometre level. Incorporation of different nanomaterials into the textiles *via* finishing or coating, can impart several multifunctional properties such as strength, antimicrobial property, self-cleaning, electrical conductivity, UV-resistance property, flame retardant (FR) property and so on [2].

Nowadays, several polymer nanocomposites are extensively used in the automotive industry. The characteristics of any polymer system change drastically with the size, shape and distribution of nanomaterials in the polymer matrix. Nanomaterials can be distributed in the polymer matrix *via* a chemical or mechanical process. In many cases, these materials are not compatible with the polymer matrix and modification of the nanomaterials or matrix improves the properties of the polymer nanocomposites as well as the final products (polymer nanocomposite coatings or fibres). A good polymer nanocomposite coating on a fabric can improve several functionalities such as: barrier property, optical property, mechanical strength, thermal stability, fire resistance, antistatic property, antimicrobial property and many more. At present, polymeric NF also have extensive applications in the automotive field. NF can be defined as fibres with a diameter in the range of less than 1,000 nm, and are characterised as having a high specific SVR and a small pore size in web form [6].

The development of high-performance automotive textile materials depends on tailoring and controlling the properties of materials at the nanoscale level. Nanotechnology plays a vital role in the automobile industry by improving the performance characteristics of different components of cars or vehicles. Today, the automobile industry is one of the major recipients of developments in the field of nanotechnology with promising enhancements and benefits at different levels providing harder, stronger and lighter materials with reduced fuel consumption, improved fuel efficiency, safety and comfort, and reduced environmental impact. Traditional textiles used for automotive interiors face several major challenges such as wear and tear, protection from dust and dirt, durability, ventilation, bacterial resistance and fire resistance, all of which call for new high-tech textiles providing enhanced functionalities. Nano-enabled textiles may have novel solutions and also address several functional requirements for automotive textiles [7]. Figure 6.3 summarises the different areas where nanotechnology can be used in automotive textiles and will be discussed in the next part of this chapter.

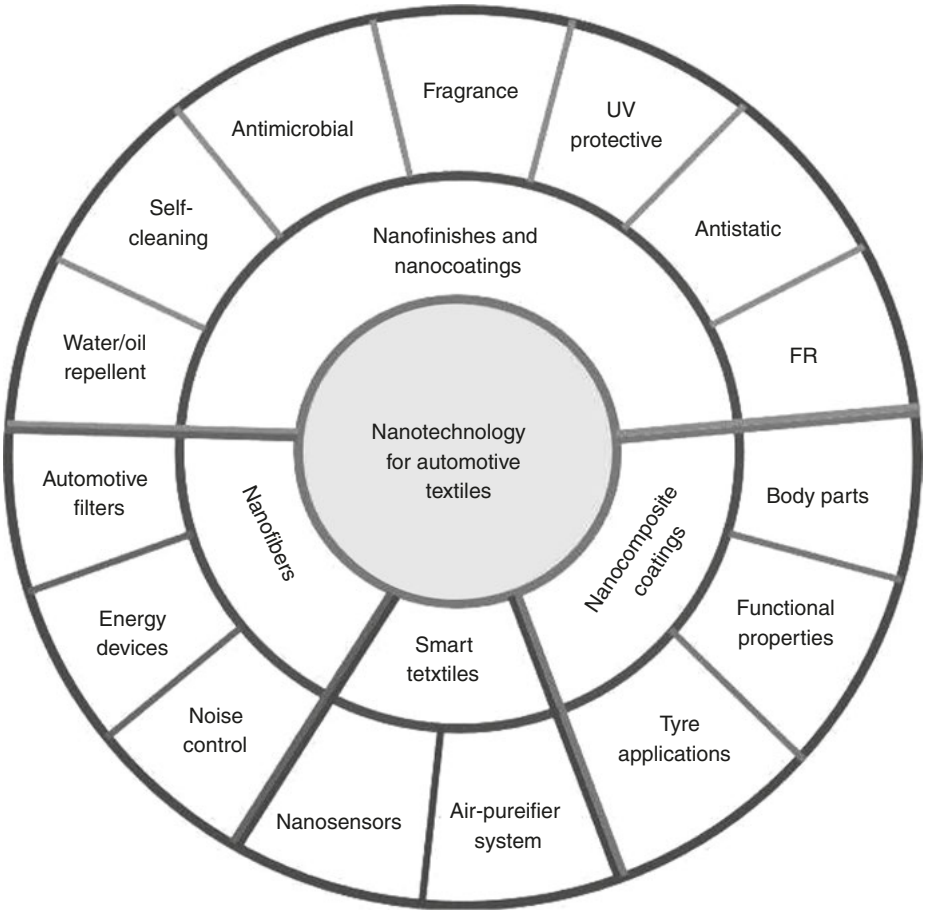


**Figure 6.3:** Different applications of nanotechnology for automotive textiles.

## 6.3.2 Nanofinishing and Nanocoatings to produce Functional Automotive Fabrics

Recently, textile finishing and coating has become more functional and precise due to the innovative techniques of nanotechnology. Functional nanofinishing and nanocoating on textiles substantially increase the potential applications of textiles in the automotive sector.

### 6.3.2.1 What is Nanofinishing?

Nanofinishing is a finishing technique where ultrafine NP are applied on to the material to develop a specific functionality without affecting the feel or comfort of the

textile substrate. Nanofinishing of textiles can be broadly classified in two major areas: a) application of NP using a conventional finishing method and b) development of a nanostructured surface onto the fabric using a specific finishing composition. The main advantages of nanofinishing over conventional finishes are:

- NP having large SVR and high surface energy, and most nanofinishes are highly durable.
- Requirement of a very low amount of nanomaterials.
- Nanofinishing does not affect the handle/feel, breathability and comfort of the fabric.
- Some specific textile properties, which can be obtained easily by nanofinishing are not possible using conventional finishes.

Generally, most nanofinishes are applied onto textile materials in the form of nanoemulsions (oil/water emulsion or water/oil emulsion) or nanosols, where the average droplet size in the nanoemulsion is about 100–500 nm [2]. Table 6.6 summarises some commercial nanofinishes that have been launched by different companies.

**Table 6.6:** Commercially available functional finishes.

| Serial No. | Name of the finish | Properties | Developed by (company) |
|---|---|---|---|
| 1 | Nanocare® | Washes the stain easily | Nano-Tex |
| 2 | Coolest Comfort™ | Breakthrough moisture wicking and comfort properties | Nano-Tex |
| 3 | Resists Spills™ | Water repellent and stain resistant | Nano-Tex |
| 4 | Odour Neutralizer® | Excellent odour resistance | Nano-Tex |
| 5 | Wrinkle Defense® | Durable press effect with less loss of strength with great flexibility | Nano-Tex |
| 6 | Ultra-Fresh™ | Provides an excellent antimicrobial property in textiles | Thomson-Research Associates |
| 7 | NanoSphere® | Repels water and oil drops and prevents soil particles from attaching themselves on the fabric surface | Schoeller Textil AG |
| 8 | Nuva FW | Excellent oil and water-repellent effects on textiles made from synthetic and cellulose fibres | Clariant |
| 9 | Zyvere® | Self-cleaning paint surface | Nanovere Technologies |
| 10 | Zonyl® | Water-repellent fluorinated PU as a soil-release finish | DuPont |

Adapted from M. Joshi and A. Bhattacharyya, *Textile Progress,* 2011, **43**, 3, 155 [2] and B.L. Deopura, R. Alagirusamy, M. Joshi and B. Gupta in *Polyesters and Polyamides,* Woodhead Publishing Limited, Cambridge, UK, 2008 [22]

#### 6.3.2.2 What is Nanocoating?

Nanocoating is the technique of depositing a very thin film (<100 nm) on the surface of the substrate to impart some functionality. Conventional coatings have many drawbacks such as improper adhesion property, strength loss, less durability, less flexibility and poor abrasion resistance [27], which can be easily overcome by nanocoatings. There are several widely used nanocoating techniques such as [2, 4]:

- Plasma assisted/ion-beam assisted techniques
- Vapour deposition techniques
- Sol-gel coating
- Self-assembly
- LbL coating
- Dip coating
- Spin coating
- Magnetron sputtering
- Pulsed laser deposition
- Electrochemical deposition

In recent years, by virtue of nanofinishes and nanocoatings, different functionalities can be incorporated into interior automotive textiles including: antimicrobial, antiodour, antistatic, FR, UV-blocking and even self-cleaning attributes. These developments can provide further product convenience and satisfaction to automotive drivers and passengers.

#### 6.3.2.3 Water- and Oil-repellent Nanofinishes and Nanocoatings for Automotive Textiles

In order to develop water- and oil-repellent properties on fabrics, it has to be finished or coated with a material that has a low surface energy. There are many commercially available water- and oil-repellent chemicals that can be classified into two categories: fluorocarbon based or non-fluorocarbon based. Although a silicon (Si)-based finish gives textiles good water repellency, they are not oil repellent. Fluorocarbon-based chemicals are the most popular to impart oil- and water-repellent properties to the fabric; however, these chemicals are very costly and cause environmental pollution. Furthermore, conventional finishing/coating causes the fabric to lose its original feel and the effect is not durable. Recently, nanotechnology-based novel and innovative nanofinishes/nanocoatings have been effectively fulfilling customer/market demands.

Nano Care®, NanoPel®, Resist Spills™ and so on are some commercial nanofinishes that protect fabrics from both water- and oil-based stain. These nanofinishes

can be effectively applied onto natural fibre (cotton, wool and silk) as well as onto synthetic fibre (polyester, Nylon, acrylic and so forth)-based fabric [2].

Plasma polymerisation enables the deposition of a very thin (<100 nm) nanostructured coating onto textiles to impart several functional properties. Low-pressure plasma polymerisation of unsaturated fluorohydrocarbons ($C_3F_6$ and $C_4F_8$) on particular fabrics has been industrially achieved using a semicontinuous process to impart stain repellency [28].

#### 6.3.2.4 Self-cleaning Automotive Fabrics

The development of efficient water-, oil- and dirt-repellent fabrics is a great challenge for textile scientists and manufacturers. Recently, the fields of textiles, botany and nanotechnology have united to explore the new concept of 'self-cleaning textile', where textile surfaces have the potential to be cleaned by any laundering treatment. At present, the automotive sector is one of the major consumers of self-cleaning fabrics to cover different interior parts of a car and to be used in upholstery. There are two distinct methods for developing self-cleaning textiles:

- The Lotus effect
- Photocatalytic action

The inspiration for developing self-cleaning textiles first came from nature. In 1990, Wilhelm Barthlott discovered that the lotus leaf has a self-cleaning behaviour, i.e., when water rolls-out on the surface of a lotus leaf it removes dirt particles and makes the surface clean. This phenomenon happens due to the very low surface energy of the lotus leaf, which comes from dual-size surface roughness, i.e., microscale bumps of epidermal cells and nanoscale hair-like waxy crystal structures present on the lotus leaf (Figure 6.4) [29, 30].

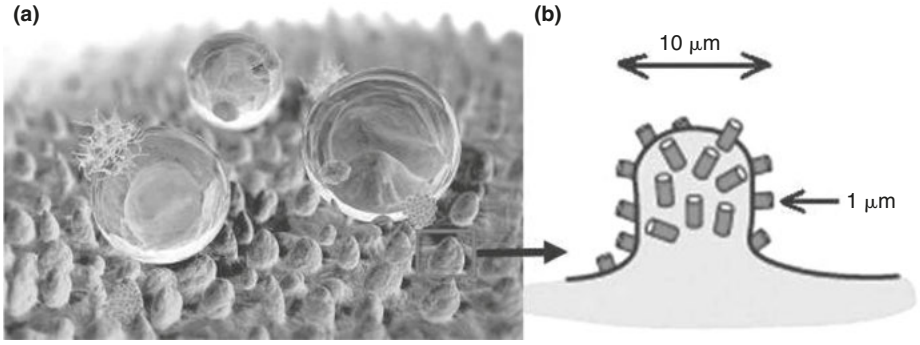


**Figure 6.4:** (a) Computer graphic of a lotus leaf surface and (b) dual-size surface roughness of a lotus leaf. Reproduced with permission from William Thielicke. ©2007, William Thielicke [30].

Based on these observations, researchers have developed the self-cleaning phenomenon on textiles using nanotechnology, which is called the 'Lotus effect'. The main requirements for obtaining the 'Lotus effect' on textiles are [31–33]:

- Superhydrophobic surface (contact angle close to or higher than 150°).
- Very low surface energy (below 10 dyne/cm).
- Dual-size surface roughness.
- Low sliding angle or tilting angle (less than 10°).

The hydrophilicity or hydrophobicity of any material is governed by surface roughness and the chemical composition of the material surface. A superhydrophobic surface can be produced by modifying the surface chemistry or changing the surface topography using specific nanofinishings or nanocoatings. Generally, a silica, zirconia or surface- modified carbon nanotube(s) (CNT)-based nanocoating is used to generate the 'Lotus effect' on textile fabrics. Figure 6.5 shows a schematic representation of the 'Lotus effect'.

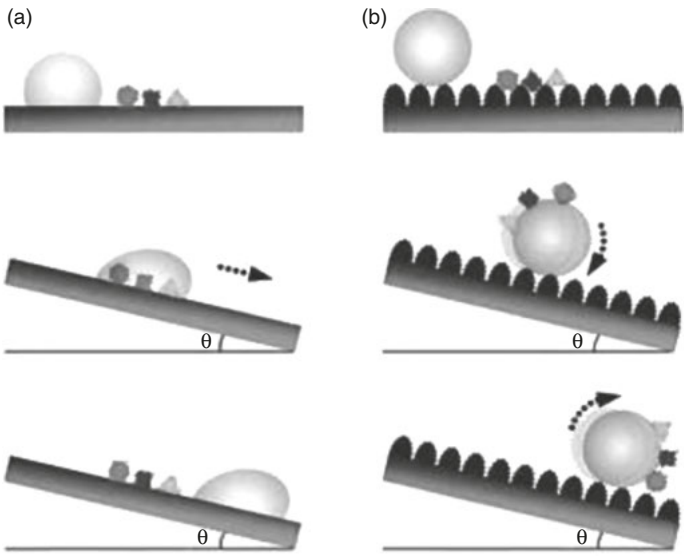


**Figure 6.5:** A schematic representation of the self-cleaning mechanism: (a) a normal smooth surface water rolling-out without taking the dirt particles when tilted to a certain angle, denoted as θ and (b) the Lotus effect water is rolling-out on a superhydrophobic fabric surface taking the dirt particles, resulting in a self-cleaned surface. Reproduced with permission from Y.L. Zhang, H. Xia, E. Kim and H.B. Sun, *Soft Matter*, 2012, **8**, 44, 11217. ©2012, Royal Society of Chemistry [33].

Bae and co-workers [34] showed that a superhydrophobic cotton fabric can be produced *via* the combined treatment of nano-silica (synthesised by the sol-gel method)

and a perfluoroacrylate-based water-repellent agent (0.1 wt% concentration). The treatment was also cost-effective compared with a fluorinated silane-based water/ oil-repellent finish [34]. In an interesting study, Joshi and co-workers [35] successfully developed the 'Lotus effect' on cotton fabric by applying nano-silica and clay-based nanocomposite coatings *via* dip coating and LbL self-assembly. The nano-silica performed better at creating nano-roughness on a cotton fabric without affecting the air permeability of the fabric. The water contact angle (WCA) of the 2 wt% fluoro-emulsion (Nuva HPU)-treated cotton fabric increased from 115 to 155, when the fabric was pretreated with 0.5 wt% nano-silica emulsion. Moreover, the water repellency of the 0.16 wt% nano-silica along with 2 wt% Nuva HPU-treated fabric was comparable to the 4 wt% Nuva HPU-treated cotton fabric [35].

Xue and co-workers [36] coated an epoxy-functionalised cotton fabric with an amino- functionalised and an epoxy-functionalised silica NP to produce dual-size roughness on cotton fabric. The coated fabrics were further treated with a 1H,1H,2H,2H- perfluorodecyl-trichlorosilane and stearic acid to obtain a durable, superhydrophobic surface (WCA 170°) [36]. Very recently, Das and co-workers [37] developed a superhydrophobic cotton fabric using a zirconia-based nanocoating, which exhibited the 'Lotus effect' (Figure 6.6).

For this, they first synthesised a fsZr by the sol-gel method and applied it onto the cotton fabric using the immersion method. The superhydrophobic surface possessed a very high WCA (163 ± 1°) and low hysteresis (about 3.5°). The coating resulted in the fabric being extremely durable to abrasion and laundering treatment, up to 20 times, due to the strong covalent bonding between the zirconia-based nanocoating and fabric [37].

Among the currently available commercialised products, textiles finished with the NanoSphere® finishing technology, produced by Schoeller, represent a naturally self-cleaning effect showing a potential to be used in automotive interiors [38].

#### 6.3.2.4.1 Photocatalytic Self-cleaning Nanofinishing or Nanocoating

The mechanism of obtaining a photocatalytic self-cleaning fabric is totally different from a 'Lotus effect' fabric. In this case, the fabric is coated or finished with nano-titanium dioxide ($TiO_2$), nano-zinc oxide (ZnO) or nano-$TiO_2$–ZnO-based formulations. Nano-$TiO_2$ or nano-ZnO are basically semiconductor oxides with a band gap of about 3.2 and 3.37 eV, respectively. In the presence of light (which has a higher energy than the band gap energy of these semiconductors), an electron from the valance band of the semiconductor oxide jumps to the conduction band creating a hole in the valance band. These excited electrons react with oxygen atoms present in the air and form oxygen free-radicals by breaking the double bond of oxygen. Furthermore, the hole present in the valance band of the nano-$TiO_2$ or nano-ZnO crystal reacts with moisture present in the air and produces hydroxyl radicals. In the next step, these oxygen and

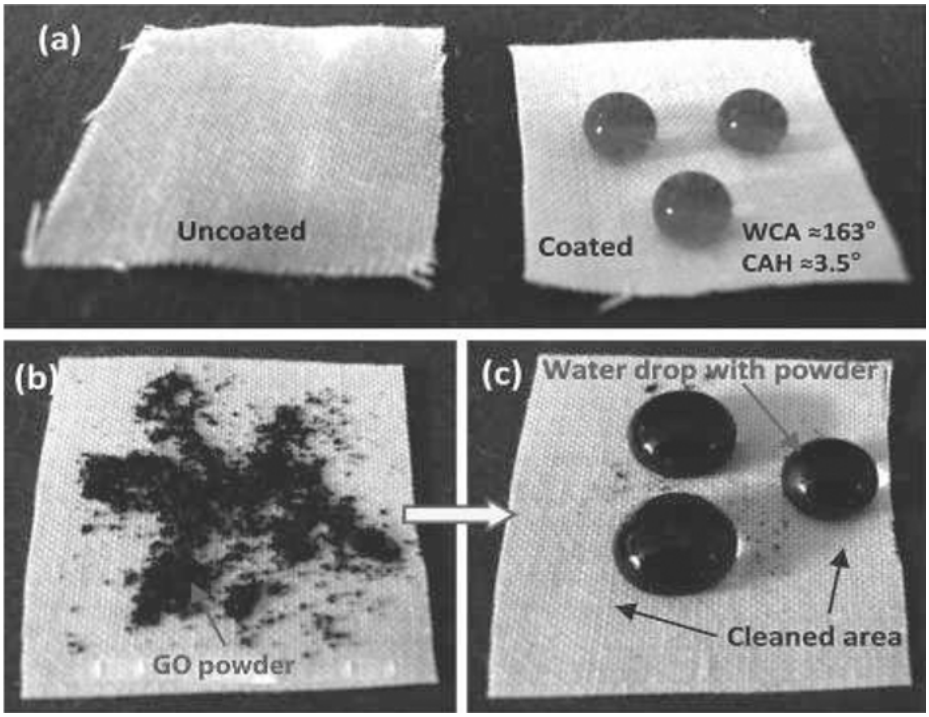


**Figure 6.6:** Photographs of the uncoated and fluorinated silyl-functionalised zirconia (fsZr)-coated fabrics: (a) the dyed (Rhodamine B) water drops on uncoated and fsZr-coated cotton fabrics, where the coated fabric showed a higher water contact angle (WCA) and lower contact angle hysteresis (CAH). (b) Graphene oxide (GO) powder on the coated superhydrophobic fabric. (c) Water drops with GO powder showing the self-cleaning ability of the fsZr-coated fabric. Reproduced with permission from I. Das and G. De, *Scientific Reports*, 2015, **5**, 1. ©2015, Nature Publishing Group [37].

hydroxyl free-radicals attack absorbed organic species (dirt, microbes or pollutants) causing them to decompose [39, 40]. Here, nano-$TiO_2$ or nano-ZnO act as a catalyst, so they are never used up. The photocatalytic effect of nano-$TiO_2$ is shown in Figure 6.7.

$TiO_2$ or ZnO NP can be applied onto textile fabrics by padding (finishing) or coating. However, a coated fabric exhibits a slightly lower photocatalytic activity, due to the binder used in the coating formulation to reduce the exposure of the $TiO_2$ nanoparticle on the fabric surface, and hence reduces its self-cleaning and pollution control activity [41]. Yuranova and co-workers [42] applied a highly dispersed 1:1 mixture of nano-$TiO_2$ and $SiO_2$ colloids onto cotton fabric using the dip-coating technique and sequential thermal treatment of the cotton fabric. The $TiO_2$–silicon dioxide ($SiO_2$)-coated fabric exhibited better photocatalytic activity compared with only $TiO_2$-coated ones, showing the efficient discolouration of red wine [42].

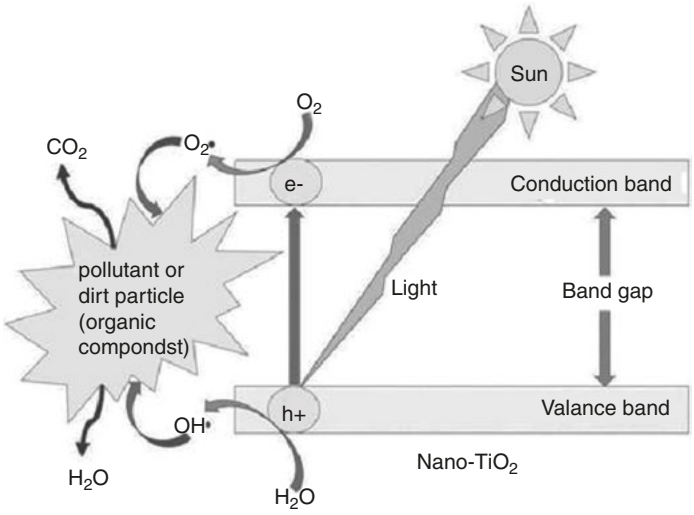


**Figure 6.7:** Mechanism of the photocatalytic action of nano-$TiO_2$.

Wang and co-workers [43] developed an advanced visible-light driven self-cleaning cotton fabric by treatment with a gold (Au)/$TiO_2$/$SiO_2$ photocatalyst. The synthesised- $TiO_2$ nanosol and Au/$TiO_2$/$SiO_2$ nanosol were applied onto cotton fabric *via* various processes, such as dip-pad-cure, dip-coating and spraying. In comparison to a $TiO_2$- coated fabric, the Au/$TiO_2$/$SiO_2$-coated fabric exhibited a better self-cleaning effect in the presence of visible light, showing the reduction of staining intensity (Figure 6.8). The self-cleaning effect of an Au/$TiO_2$/$SiO_2$-coated fabric

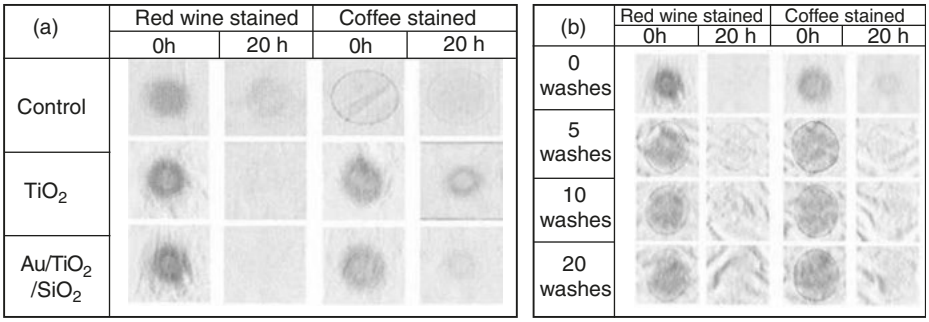


**Figure 6.8:** (a) Degradation results of red wine and a concentrated coffee stain, respectively, on control (pristine cellulosic fabrics), a $TiO_2$-coated cellulosic fabric and an Au/ $TiO_2$/$SiO_2$-coated cellulosic fabric before and after 20 h visible light irradiation using a SUNTEST® solar simulator with light intensity of 6,460 lux (lx). (b) Wash- fastness effect on the degradation of stains on an Au/ $TiO_2$/$SiO_2$-coated cellulosic fabric before and after 20 washes, assessed using the same visible light source. Reproduced with permission from R. Wang, X. Wang and J.H. Xin, *ACS Applied Materials & Interfaces*, 2010, **2**, 1, 82. ©2010, American Chemical Society [43].

was durable for up to 20 washes. There was also a huge improvement in the UV-blocking property after coating with nanosols. However, the fabric coated with only $TiO_2$ showed better a UV-blocking property compared with the $Au/TiO_2/SiO_2$-coated fabric. This reduction in the UV-blocking property of the $Au/TiO_2/SiO_2$-coated fabric might be caused by hydrophilic modification by $SiO_2$ [43].

These nanofinished or nanocoated self-cleaning fabrics can be potentially used as upholstery and interiors of a car.

#### 6.3.2.5 Antimicrobial and Antiodour Nanofinished/Nanocoated Automotive Fabrics

Most textile fabrics, especially cellulosic fibre-based fabrics, are very susceptible to attack by microbes, such as bacteria, fungi, protozoa, algae or viruses, during their service life. This is due microorganisms utilising them as food, which destroys the fabric. The presence of sweat and moisture/humidity in interior textiles creates a suitable environment for the growth of different pathogenic and non-pathogenic microbes, resulting in the generation of bad odours, causing different diseases and also affecting the colour and aesthetic feel of the textile materials. Nowadays, due to increasing concern of the hygiene and health of automotive drivers and passengers, an antimicrobial property has become a basic requirement for interior automotive textiles. Nevertheless, the durability and effectiveness of the antimicrobial property is a very important criteria for interior automotive textiles. Although there are different bioactive agents that give antimicrobial properties to textiles, material scientists are currently taking considerable interest in nanostructured antimicrobial agents, mainly due to three reasons:

1. Better antimicrobial activity compared with conventional antimicrobial agents due to the higher surface area of nanoantimicrobial agents.
2. A very low quantity of a nanoantimicrobial agent is required to obtain good antimicrobial properties.
3. Finishing with nanoantimicrobial agents does not affect the feel and other textile properties.

The application of NP-based finishes on automotive textiles will impart antimicrobial properties that can remove unpleasant odours and create a hygienic atmosphere inside the car. Several metal and metal oxide NP such as silver (Ag), copper (Cu), Au, titanium (Ti), zinc, silver oxide, $TiO_2$, copper oxide, ZnO, calcium oxide and magnesium oxide (MgO) have been identified as exhibiting antimicrobial activity [44]. There are several factors that determine the antimicrobial activity of these nanomaterials, which are mainly: crystal structure, size, shape and surface area of the nanomaterial. The exact mechanisms behind the antimicrobial properties of these nanomaterials are still under investigation; however, two popularly accepted mechanisms are: a) generation of free metals ions from the surface of the NP and b) oxidative stress *via* the

generation of reactive oxygen species on the NP surface [44]. The metal ions are believed to bind with the protein molecules of microorganisms and inhibit their cellular metabolism, causing microbial death. Researchers have studied the biocidal action of different metal NP [especially silver nanoparticles (AgNP)] using scanning electron microscopy and transmission electron microscopy (TEM). Their results confirmed that the interaction of AgNP with the cell walls of the bacteria/microbes caused damage due to the formation of 'pits' in the cell wall [45]. Figure 6.9 shows how AgNP damages the microbial cell wall using a step-by-step action [46].

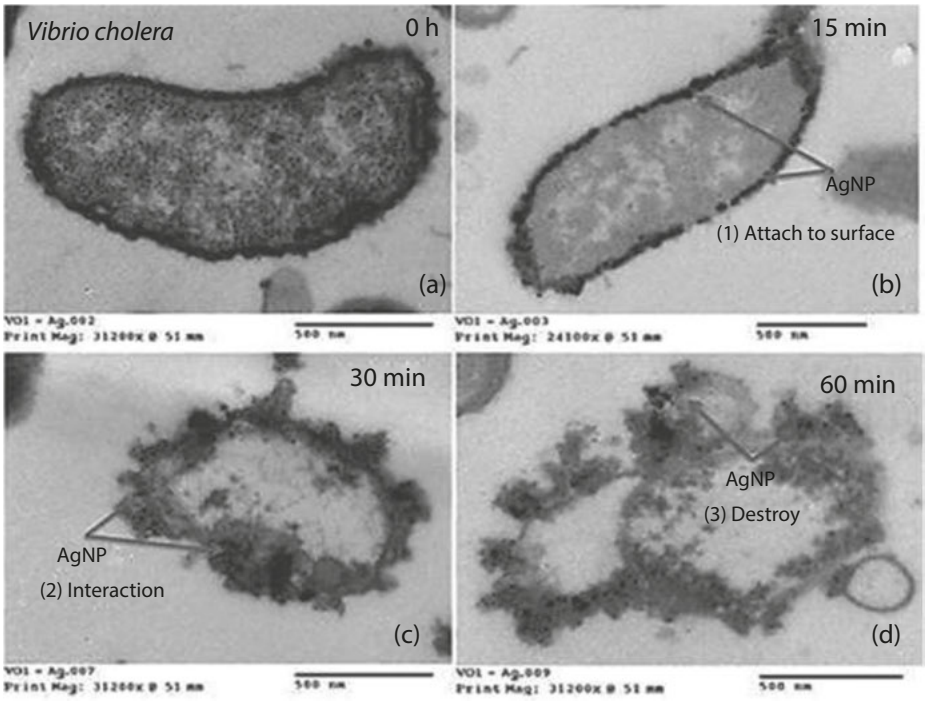


**Figure 6.9:** TEM images showing the steps involved in damaging the cell wall of a Gram-negative bacteria (*Vibrio cholera*) in the presence of AgNP: (a) at the start, (b) after 15 min, (c) after 30 min and (d) after 1 h. Reproduced with permission from M. López-Heras, I.G. Theodorou, B.F. Leo, M.P. Ryan and A.E. Porter, *Environmental Science: Nano*, 2015, **2**, 4, 312. ©2015, Royal Society of Chemistry [46].

The nanoantimicrobial agents (metal or metal oxide NP) can be applied on polymeric or textile materials using different techniques such as [2, 4, 47, 48]:

- Incorporation of antimicrobial agents during polymerisation
- Addition during the preparation of spinning dope
- Nanofinishing
- Microencapsulation
- Nanocoating

Among these techniques nanofinishing (the pad-dry-cure or exhaust method) and nanocoating (sol-gel application, LbL method, dip-coating or spray coating) are currently the most popular for producing antimicrobial textiles.

Research activities in this field have shown that among the different metal or metal oxide NP, nanosilver is the best or most effective antiseptic, disinfectant and antimicrobial agent [2]. Consequently, nanosilver applications have been widely explored for the production of antimicrobial textiles to be used in the health sector, automotive industry, apparel industry and many more. Nanosilver exhibits a very high antimicrobial efficacy and has been successfully applied on many natural and synthetic fibre-based textile materials. Jeong and co-workers [49] incorporated nano- and micron-sized Ag particles into PP by melt mixing in a twin-screw extruder. Their investigation showed that the AgNP-containing PP exhibited a much better antimicrobial efficacy than the PP-containing micron-sized particles. Furthermore, in the case of the micron-sized particles, more than a 5-fold increase in concentration was required to equal the antimicrobial activity exhibited by nanosilver [49]. Lee and co-workers [50] reported that the application of a colloidal solution of nanosilver using the pad-dry-cure method led to a highly effective antimicrobial property of cotton and polyester fabrics. The efficacy of the antimicrobial property was largely retained even after several laundering treatments [50]. Ki and co-workers [51] obtained antimicrobial, mothproofing and antistatic properties in wool by applying a sulfur and nanosilver-based colloidal solution containing a very low Ag content [51]. There is extensive published research work covering the use of AgNP as an antimicrobial agent. In fact, at present, there are a wide variety of AgNP-based products readily available on market [2].

There is a great deal of research that covers the antimicrobial properties of metal and metal oxide NP other than Ag. Teli and co-workers [52] in their study, utilised a bamboo rayon fabric grafted with acrylamide as a backbone to immobilise Cu NP. This product showed excellent antimicrobial properties for both Gram-positive and Gram-negative bacteria, which was effective for up to 50 washes [52].

A considerable amount of research has focused on the combined effects of two metallic NP in order to obtain better antimicrobial properties in textiles or to develop multifunctional textiles. Very recently, Paszkiewicz and co-workers [53] prepared five impregnation solutions containing Ag and Cu in the form of bimetallic (alloy and core-shell) NP and ionic species. These five compositions ($Ag/Cu_{alloy}$, $Ag_{core}/Cu_{shell}$, $CuNP/Ag^{+}$, $AgNP/Cu^{2+}$ and $Ag^{+}/Cu^{2+}$) were used to impregnate cotton-polyester fabrics and their antimicrobial and antifungal properties were tested. All five composites showed very strong and durable antimicrobial properties against *Escherichia coli* and *Staphylococcus aureus* for up to 20 washes.

The textile sample impregnated in the solutions containing $Ag^{+}/Cu^{2+}$ and $AgNP/Cu^{2+}$ exhibited 99.99% (after 5 washes) and 100% (after 15 washes) antifungal efficiency, respectively [53].

Berendjchi and co-workers [54] synthesised silica-sol using the sol-gel method, which were doped with 0.5 and 2% wt/wt CuNP. The Cu-doped silica-sols were applied onto cotton fabric using the impregnation-dry-cure method. Some samples were further treated with an alkyl-silane (hexadecyltrimethoxysilane) to block some hydroxyl groups. The surface of these cotton fabrics became superhydrophobic with the highest static water contact angle (SWC) of approximately 155.9° for the cotton fabric treated with 0.5% Cu-doped silica-sol. However, doping of silica-sol with 2% Cu led to the most slippery smooth cotton fabric surface, resulting in a slight reduction of the SWC to 147°. All cotton fabrics with a Cu-coated surface showed very efficient antimicrobial properties against both Gram-positive and -negative bacteria [54].

Ali and co-workers [55] investigated the antimicrobial property of cotton fabric coated *via* the LbL method using poly(sodium-4-styrenesulfonate) and chitosan (CS) (bulk and NP). Excellent antimicrobial efficacy was obtained in the case of the nano-CS-based coating using a very low (only 0.1 w/v%) concentration of CS [55].

The application of a tourmaline NP-based finishing on textiles results in the elimination of odour. Tourmaline is a natural mineral substance which, when in contact with oxygen, carbon monoxide and water molecules in the environment, enables electrolytic dissociation and emits negative ions. These negative ions create a magnetic field and inhibit the growth of bacteria causing elimination of bad odours and lowering the risk of skin infection. This nanofinish can remove up to 99.99% of bacteria, 90% of odour and 75% of the sticky moisture within the cloth [56, 57].

#### 6.3.2.6 Fragrance-finished Automotive Fabrics

Fragrance finishing is a process that enhances the value of a product by applying aromas or perfumes to the textile material. During the lifespan of a car, the interior undergoes minimal cleaning that may lead to the generation of malodour, which is unhygienic and problematic. Therefore, a fragrance-finishing treatment on interior automotive textiles may neutralise the chance of malodour occurring, keeping the vehicle environment fresh and restricting microbial growth. The treatment of textiles with a nanoemulsion of fragrant material, or coating containing a nano-encapsulated fragrant material, causes deep penetration of the fragrance into the fabric resulting in an increased fragrance retention property.

Jing and co-workers [58] developed a sustained release aroma-finished cotton fabric by applying a finish of rose fragrance nanocapsules directly onto the cotton fabric. They also studied the effect of nanocapsule size on the fragrance retention property and observed that smaller nanocapsules resulted in a better, sustained release property [58].

Polyester fabrics are predominantly used as interior automotive textiles. Islam and co-workers [59] successfully applied microencapsulated fragrance oil onto 100% polyester fabrics (knitted and woven), in combination with CS, to develop a durable

perfume/fragrance finish. CS acted as a binder for the uniform application of a micro-encapsulated fragrance oil, which resulted in high fragrance retention in the 100% polyester automotive fabric. The polyester fabrics, especially the woven one, showed good fragrance retention against abrasion. The coated fabrics also exhibited excellent antimicrobial efficacy due to the inherent antimicrobial property of CS [59].

More recently, Priyadarshinirajkumar and co-workers [60] developed an eco-friendly nanofinishing technique to produce durable mosquito-repellent and fragrance-finished cotton fabrics. The extracted herbal solution from medicinal plants such as *Eucalyptus globulus*, *Santalum album* and *Hemidesmus indicus* were applied onto cotton fabric using three different methods: a) conventional finishing method, b) using an ultrasonic atomiser and c) converting the solution to NP and then applied using a nanospray- dryer. The herbal-finished fabric showed an excellent mosquito-repellency property and also imparted good fragrance, which came from the natural fragrance of the medicinal plants. The durability of the herbal finishing was increased in the case of nanofinishing [60]. This type of perfume-finished fabric is called 'aromatherapy fabric' and can be potentially used to cover automotive interiors.

#### 6.3.2.7 Ultraviolet-protective Nanofinished/Nanocoated Automotive Fabrics

The colour and strength of textile fabrics are very adversely affected upon long-time exposure to UV radiation, which comes to the earth from the sun. UV radiation can break down the chemical bonds of dyes and fibres, resulting in fading the colours of textile fabrics, in addition to reducing its strength. Therefore, in modern cars, a UV-protective finishing is a special requirement for some interior automotive textiles, for example, seat covers, door casings, sun visors and sunroofs. The main function of the sun visor is to block or absorb harmful UV rays and protect the driver and passengers; therefore, the fabric used in sun visors should exhibit a good UV-absorbing characteristic. Other interior cover fabrics should have good resistance against UV degradation. The inherent UV-absorbing property of any textile fabric depends on several factors including: type of fibre used, fabric construction and tightness, thread density, cover factor, porosity, thickness, colour or dye used, and also chemicals used during fabric processing [61]. The treatment of textile fabrics with certain UV absorbers ensures protection from harmful UV radiation, and the efficacy of UV protection of the textile fabric is measured using the ultraviolet-protection factor (UPF) – the higher the UPF value equates to higher protection from UV.

Some metal oxide NP such as ZnO and $TiO_2$ are very strong and stable UV blockers compared with other organic UV-blocking agents. These nanomaterials enhance the UV absorption property due to their very high surface area and intense absorption in the UV range. Yadav and co-workers [62] coated bleached cotton fabric with ZnO NP using an acrylic binder, which resulted in approximately 75% UV blocking

with a very low concentration (2%) of ZnO NP [62]. Z-Cote® is a very popular commercialised-nano-ZnO dispersion with a long-lasting UV-blocking property [63].

#### 6.3.2.8 Antistatic-nanofinished Automotive Fabrics

Synthetic fibres such as polyester and Nylon are prone to the accumulation of static charge due to their low moisture regain exhibiting a poor antistatic property. Inside a car, due to friction between interior textiles and the human body, or any other object, static charge accumulation is a very common issue, especially in the winter season. Therefore, in modern cars, the carpets, upholstery fabrics, air bags, seat covers and so on are generally finished or coated with some electrically conductive nano-sized materials or antistatic agents. Researchers have reported that the application of nano- sized ZnO whiskers, $TiO_2$, silane nanosols and antimony-doped tin oxide could impart a good antistatic property to synthetic fibres [64–66]. ZnO and $TiO_2$ NP exhibit a good electroconductive property and readily dissipate the static charge generated in synthetic fibres. This kind of conducting nanofiller-based finish also reduces the static charge generated in the synthetic fabric. Any functional group present in the nanofiller, responsible for hydrogen bond formation, can reduce the tendency of static charge accumulation by increasing the moisture content of the fabric. As silane compounds contain hydroxyl (OH) and amine ($NH_2$) groups, a finishing treatment with silane nanosols can significantly improve the antistatic property of synthetic fibre-based fabrics. These approaches have yet to be considered by the automotive textile industry but could be a viable alternative in future applications.

#### 6.3.2.9 Flame-retardant Nanofinished/Nanocoated Fabrics

Although some special fibres show inherent FR property, most textile materials are highly flammable and are primary sources of ignition. However, treatment with some FR chemicals (FR agents) can inhibit or suppress the combustion process of textile materials. To obtain a conventional FR finish, the chemicals mainly used include: inorganic compounds (aluminium trihydroxide, antimony trioxide, zinc borate and so on), halogen compounds (chlorine and bromine based), phosphorus-based compounds (ammonium polyphosphate and red phosphorus) and nitrogen-based compounds (i.e., melamine) [13, 67]. Sometimes, the combination of any two systems can result in a synergistic FR property. Flame retardancy is a basic requirement for aircraft and automotive interior textiles, especially for upholstery, carpets and seat covers, along with other automotive components.

Although conventional FR are extensively used to impart FR property to textiles, the combinations of halogen-antimony and phosphorus-bromine have many environmental issues and implications. Therefore, environmental regulations have

restricted the use of these conventional FR and replaced them with some environmentally-friendly alternatives, which has galvanised the interest of nanoscientists.

In contrast to this, nanocomposites containing organically-modified clay dispersed in selected polymer matrices have attracted considerable attention for their ability to impart flame resistance. A very low concentration of clay (5 wt% or less) has been shown to result in effective flame retardancy [68]. Furthermore, researchers have attempted to find other nanomaterials that exhibit an FR property, such as CNT, polyhedral oligomeric silsesquioxane (POSS) and nano-colloidal antimony pentoxide [5, 69, 70]. In particular, some commercial colloidal antimony pentoxide sols (NYACOL® A1530, NYACOL® A1540N and NYACOL® A1550) can be potentially used to impart effective flame retardancy to automotive textiles [69]. Most current research in this field has been limited to the application of nano-FR agents, in a polymer melt or solution, to produce FR fibres but very few applications have been reported for the FR finishing of fabrics. In a recent and interesting study, El- Hady and co-workers [71] developed novel FR and UV-protective cellulosic fabrics (100% cotton and 65/35% cotton/polyester) *via* treatment with ZnO NP in the presence of sodium hypophosphite as a catalyst and different polycarboxylic acids (1,2,3,4-butanetetracarboxylic acid and succinic acid) through the conventional pad-dry-cure method [71].

However, organically-modified nanoclay, POSS, colloidal antimony pentoxide, CNT, nano-ZnO are currently very expensive, compared with traditional FR agents, and do not offer a significantly higher level of fire protection. Therefore, even if they are more environmentally friendly compared with conventional FR agents, their current use is very limited. Reducing the cost of nano-FR agents, further improvement in their performance or both would likely change this situation in the future [7].

### 6.3.3 Polymer Nanocomposites in Automobiles

Polymer nanocomposites are the latest and most advanced class of composite materials where the nanofillers or NP have at least one dimension smaller than 100 nm and are dispersed in a polymer matrix. Due to the very large SVR of NP, the interfacial interaction between the polymer matrix and NP increases exponentially. Therefore, polymer nanocomposites show much improved properties over conventional composites even at low nanofiller loading (<5 wt%) [22]. The interest in polymer nanocomposites is also governed by the fact that they are light weight, compared with conventional composites, due to low filler loading, and usually transparent due to the very low scattering of light from the nanomaterials (having nanoscale dimensions) embedded in the polymer matrix. With these improved set of properties, polymer nanocomposites show promising applications in the development of advanced textile materials, such as nanocomposite fibres, NF and nanocomposite coatings, for making a wide range of smart and intelligent textiles. However, the main issues involved in the preparation of polymeric nanocomposite-based

coatings and laminates are: (i) matrix- filler compatibility, (ii) dispersion, (iii) exfoliation, (iv) orientation, (v) reaggregation and (vi) interfacial interaction [2].

#### 6.3.3.1 Polymer Nanocomposites in Automotive Body Parts

Polymer nanocomposites are used in different vehicle components to fulfil specific requirements. In collaboration with Ube Industries, Toyota Motors Corporation first commercialised a Nylon 6–clay hybrid nanocomposite in 1991, for making timing belt covers as an engine component of Toyota Camry cars. The belt covers showed a huge increase in heat distortion temperature, tensile strength and modulus with a significant reduction of weight due to using a lower amount of clay [13, 72]. Very shortly, the Japanese company Unitika Ltd. introduced a Nylon 6 nanocomposite as an engine cover on Mitsubishi's Gasoline Direct Injection engines [73]. Nylon 6-based nanocomposites have also been used in oil reservoir tanks, engine covers and fuel hoses of vehicles due to a significant increase in thermal stability, and barrier and mechanical properties [13]. However, these Nylon 6-based nanocomposites were not able to retain their position in the highly competitive automotive market due to their very high cost. Therefore, the main focus was switched to the use of polyimide (PI)-based nanocomposites to fulfil the required gas barrier properties in automotive parts [73]. Later, Ube developed the 'ECOBESTA' line incorporating a PA (Nylon 12, Nylon 6, Nylon 6,6) nanocomposite-based multilayered system for automotive fuel lines and fuel system components to replace polyvinylidene fluoride (PVDF), ethylene vinyl alcohol and other traditional barrier materials [74].

In 2002, General Motors launched a clay–PO nanocomposite-based step-assist automotive component in collaboration with Basell (formerly Montell) for GMC Safari and Chevrolet Astro vans and replaced conventional talc-reinforced materials [75]. Incorporating the highly exfoliated ultrapure clay into a PO matrix resulted in a more than 10% reduction in weight and improvement in appearance, stiffness and ductility at cold temperature [73]. It was followed by the application of clay–PO nanocomposites for structural seat backs in the Honda Acura and in the doors of Chevrolet Impalas [76, 77]. In 2009, General Motors commercialised nanoclay-enhanced sheet moulded compounds (SMC) for their Pontiac Solace, which were developed by Moulded Fibre Glass Companies, Ohio, USA. This technology has also been used on General Motors' Chevrolet Corvette Coupe and Corvette ZO6. The nanofilled SMC has a lower density compared with conventional SMC, which resulted in a huge reduction in weight and improved fuel efficiency [77].

The research on polymer–clay nanocomposites has resulted in the remarkable improvement of a wide range of physico-chemical properties compared with neat polymers. The Toyota research team reported the use of various types of clay nanocomposites based on polymers such as PA, PO, polystyrene (PS), PI, acrylic, epoxy resin and elastomers using a similar approach [78]. Different polymer

nanocomposites can be advantageously used in several automotive applications, such as engines and power trains, chassis and body parts, exhaust systems, catalytic converters, protective paints and coatings, lubrications, tyres, electric and electronic equipment. Recently, extensive research has focused on increasing the use of polymer nanocomposites for automotive applications. Figure 6.10 shows the different automotive parts that are composed of polymer nanocomposites.

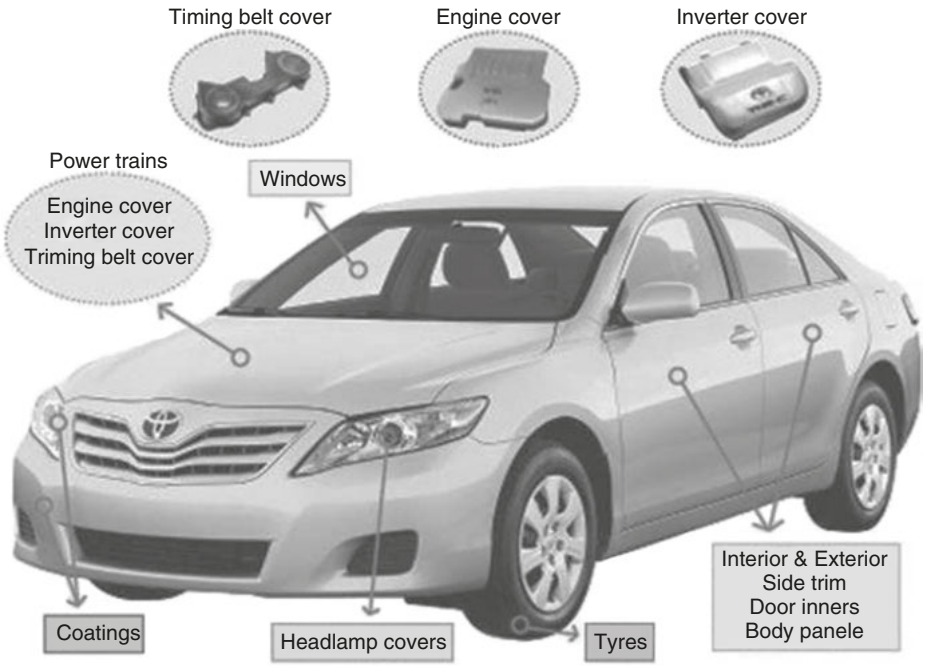


**Figure 6.10:** The most important parts of a car where polymer nanocomposites are used. Reproduced with permission from *Polymer Nanocomposites Drive Opportunities in the Automotive Sector*, Nanowerk, 2012. ©2012, Nanowerk [78].

### 6.3.3.2 Polymer Nanocomposites for Tyre Applications

The tyre is one of the first application areas where nanostructured materials were introduced in automobiles. Novel nano-reinforcement materials and effective structures have the capability to protect tyres from environmental hazards, enable auto-responsiveness to the changing environment and improve tyre life [6]. Recently, different polymer nanocomposites have been extensively used in tyre applications in order to provide extended tyre life, lower rolling resistance, abrasion resistance, reduced friction, wet traction, lower weight, improved air retention, safety and superior

performance. There are three main ways in which nanomaterials can be incorporated to improve tyre performance:

- Incorporation of nanomaterials in filaments to be used for the production of tyre cords.
- Incorporation of nanomaterials into rubber compounds.
- Interlayer nanocomposite coatings to improve tyre performance.

#### 6.3.3.2.1 Polymer Nanocomposite-based Fibres for Tyre Cord Application

Polyester (PET) and Nylon filaments are extensively used in tyre cords; however, neat polyester and Nylon cord have certain drawbacks in this particular application that can be improved by using nanocomposite filaments. PET–clay nanocomposite-based tyre cords have many advantages including: high strength, low heat emission, good heat resistance and good adhesion with rubber, which are required for tyre manufacturing [22]. Recently, Joshi and co-workers [79] prepared Nylon 6–clay nanocomposite filaments for tyre cord applications by incorporating sodium (Na) montmorillonite (MMT) and two differently modified clays (Claytone® HY and silane-MMT) into a Nylon 6 matrix. The nanocomposite filaments showed significant improvement in tensile properties (about 10%) and creep-resistant behaviour (20%). Furthermore, the Nylon– clay nanocomposite cords showed an increase of 7–21% in tensile strength, as well as an approximately 34–55% improvement in the cord to rubber adhesion property [79].

#### 6.3.3.2.2 Rubber Nanocomposites for Tyre Applications

In the tyre manufacturing industry, the fillers that are commonly mixed with rubber are CB, precipitated silica, precipitated calcium carbonate ($CaCO_3$), clay, talc and other chemicals [80]. When the size of these fillers is reduced to the nanolevel, a huge improvement is observed in the properties of the rubber–filler nanocomposites compared with neat rubber. In 1904, the first nano-CB was introduced as an effective reinforcing filler for rubber. After that, rubber–CB nanocomposites were widely used in different tyre products. Currently, in addition to this, polymer–clay nanocomposites have gained a strong momentum in the tyre industry due to the possibility of excellent exfoliation, easy processing, remarkable improvement in material propertiesand the better cost/performance ratio compared with macro/microcomposites [80, 81].

Elastomeric nanocomposite materials are currently gaining popularity in the automotive industry, especially for tyre applications, due their lower weight and rolling resistance, enhanced durability and superior performance in the form of fuel saving [82]. Cataldo and co-workers [83] reported that incorporating alkyammonium Na-MMT nanoclay into a rubber compound [carbon filled in natural rubber (NR)/SBR] the hysteresis loss and heat build-up problem of the rubber compounds reduced significantly [83]. Kojima and co-workers [84] reported that the tensile

strength (at 100% elongation) of the rubber–clay nanocomposite containing a 10 vol% MMT loading was equal to that of a rubber–CB composite with 40 phr CB. Furthermore, in the case of rubber–clay hybrid composites, a 70% reduction in hydrogen and water vapour permeability was observed with only a 3.9 vol% clay loading compared with pristine rubber [84]. For advanced rubber technology, this reduction in gas permeability of nanocomposites is considered to be the most important factor for tyre-inner liner applications [85]. Different layered clay nanominerals dispersed in the elastomeric matrix (NR, isoprene, copolymers of isobutylene, polybutadiene and its copolymers) allow the production of tyre-inner liners with sufficiently low air permeability [80].

Mishra and co-workers [86] studied the properties of nano-$CaCO_3$ of different particle sizes (9, 15 and 20 nm) and fly ash-reinforced SBR. The mechanical properties, swelling index, flame retardancy and abrasion resistance of SBR/$CaCO_3$ nanocomposites improved drastically compared with fly-ash-filled SBR and commercial $CaCO_3$. Reducing the particle size of $CaCO_3$ led to further property enhancement due to the better dispersion of $CaCO_3$ in the polymer matrix (SBR) [86]. Wang and co-workers [87] developed a novel rubber composition for use in tyre production by incorporating nano-sized metal particles, such as aluminium hydroxide, in rubber. This new rubber composition exhibited significantly improved rubber properties including bonding property, tensile strength, tear strength and wet traction [87]. Exfoliated nanosheets of graphite (thickness 100–400 nm) in elastomers (polybutadiene, polyisoprene, SBR) have great potential for the manufacture of pneumatic tyres for motorcycles, passenger cars and trucks [80, 88].

#### 6.3.3.2.3 Polymer Nanocomposite-based Interlayer Coatings

The inside steel belt of a tyre becomes rusted due to the migration of oxygen through the vehicle tyre resulting in a decrease service life of the tyre, to prevent this situation the inner tubes and inner liners should exhibit good gas barrier properties [89]. In 2001, Wilson Sporting Goods introduced a special double core tennis ball where the inner core of the ball was coated with a butyl rubber/clay nanocomposite, in which vermiculite was exfoliated in the rubber matrix. This inner core coating significantly reduced air permeability by increasing the travel path of air through the polymer–clay nanocomposite, resulting in retention of air pressure. The patented coating technology, known as Air D-fence®, was developed by InMat, Inc. [90] and was also applied to the bicycle and automotive tyre industry. In case of tyres, the butyl rubber–vermiculite nanocomposite-based inner layer coating reduced the permeation of oxygen inside the tyre, which resulted in an increased service life of the tyre, better pressure retention and improvement in fuel efficiency [89].

An interesting European patent, EP1418199 [91] reports the invention of a 'tubeless tyre'. In this study, an air chamber was formed between the inner face of the tyre body and the rim, where the tyre body was mounted to the periphery of the

rim. On the inner face of the tyre body, a polymer nanocomposite-based gas barrier layer was used that contained an inorganic-layered compound (maximum particle size 5 μm and aspect ratio of 50 to 5,000) and a resin. This internal polymer nanocomposite coating resulted in a significant decrease in air permeability.

#### 6.3.3.3 Polymer Nanocomposite-coated and Laminated Automotive Textiles

Polymer nanocomposite-coated and laminated textiles can be potentially used in automotive interiors to introduce several functional properties, such as water/oil/dirt repellency, flame retardancy, abrasion resistance, antimicrobial antistatic properties, UV protection and many more. The major classes of polymeric materials used for conventional fabric coatings are: natural and synthetic rubber, Si rubber, PU, PVC, polyacrylics and Teflon [28]. The development of nanomaterials and different coating techniques has opened new scope for scientists to develop miscellaneous polymer nanocomposite-based coatings on textile substrates with satisfactory or enhanced properties and durability. The dimensions of the nanofillers and compatibility with the polymer matrix greatly influence the nanocomposite morphology and polymer-coating quality. Therefore, the suitable modification (physical or chemical) of nanofillers can improve compatibility with the polymer matrix, enhance dispersion of nanomaterials in the polymeric matrix and also improve the properties of the coated fabrics [92].

##### 6.3.3.3.1 Polymer–Clay Nanocomposite Coatings

Pristine-layered silicate (clay) is a highly hydrophilic material and is therefore not compatible with most hydrophobic polymer matrices. However, in the case of organically-modified nanoclay, the surface energy of the clay-inorganic host is significantly reduced, leading to improvement in the wetting characteristics or compatibility with the polymer resulting in much improved properties [2]. Many scientists have reported that the proper dispersion or exfoliation of clay platelets in the polymer matrix boosted several properties, such as mechanical strength, thermal stability, flame retardancy and barrier properties of the polymers [93]. A PU–clay nanocomposite coating improves flame retardancy, abrasion resistance and the gas barrier property of textiles, and can be potentially used in automotive seat-cover back coatings [94, 95, 96].

##### 6.3.3.3.2 Polymer–Silica Nanocomposite Coatings

Nano-silica is one of the most promising nanomaterials for the creation of nanoscale roughness on textile substrates, resulting in a superhydrophobic surface and the ‘Lotus effect’. Daoud and co-workers [97] developed an interesting low-temperature silica nanocomposite coating to create superhydrophobic textiles.

In this study, the coating was applied to a cotton fabric *via* co-hydrolysis and polycondensation of a mixture containing tetraethoxyorthosilcate, hexadecyltrimethoxysilane and 3-glycidyloxypropyl-trimethoxysilane [97]. Basu and co-workers [98] fabricated a superhydrophobic sol-gel nanocomposite coating (spin coating and spray coating) where sol-gel matrices, prepared with methyltrimethoxy silane and acid-catalysed tetraethoxy silane, were used to disperse hydrophobically-modified silica nanoparticles. By controlling the process parameters and concentration of silica NP in the coating, they were able to achieve a WCA of 166° with a roll-off angle of less than 2° [98]. Recently, Guo and co-workers [99] fabricated a superhydrophobic surface by applying a Nylon 6,6/$SiO_2$ nanocomposite coating using a facile casting process. The WCA of the nanocomposite-coated surface was always higher than 159° and the sliding angle reduced from 33.4 to 1° [99].

Nano-silica also possess very high thermal stability and flame retardancy. Polymethyl methacrylate (PMMA)–nano-silica-based nanocomposites can be used to develop FR automotive textiles [100]. Furthermore, the presence of silica NP can reduce friction and wear of PU- and Nylon 6-based nanocomposite coatings [101, 102].

#### 6.3.3.3.3 Polymer–Carbon Nanotube Nanocomposite Coatings

Single- and multi-walled carbon nanomaterial-based polymer nanocomposite coatings enable the attainment of several unique textile properties, such as exceptional mechanical properties, high thermal and electrical conductivity, and enhanced friction and wear properties [2]. CNT-based different polymer (PMMA, epoxy and PS) nanocomposite coatings can significantly improve the tribological performance of automotive textiles using a very low (1–1.5 wt%) CNT loading [103]. The application of CNT–polymer nanocomposite coatings to automobile upholstery make it conductive, which could result in the elimination of static charge in the winter season.

#### 6.3.3.3.4 Other Polymer Nanocomposite Coatings

Several other nanocomposite coatings, containing different NP, also have the potential to overcome the limitations of conventional polymeric coatings and impart various functionalities on textile fabrics.

Nano-$TiO_2$ or nano-aluminium oxide ($Al_2O_3$)-based polymeric coatings on textile fabrics significantly reduce the friction and wear properties, resulting in increased service life of the fabric [104, 105]. This reduction in friction and wear can be explained by the contact being among three bodies (NP, polymer and fabric), as opposed to the direct surface contact between the polymer and fabric, leading to reduced abrasive force between the material pairs with the positive rolling effect of NP [106].

$TiO_2$ and ZnO NP exhibit a strong UV-absorbing capability, and can be used in different polymeric-coating formulations to impart UV-resistance to fabric. Katangur and co-workers [107] reported that these NP embedded in acrylic coatings protect the base fabric from sun-induced degradation [107]. Nano-Ag–CS or Ag:ZnO NP–CS biocomposite-based coatings on cotton or cotton/polyester blend (50/50%) textiles reach 95% antimicrobial activity [47].

Automotive seat covers are generally back-coated with a PU-based FR coating. Bourbigot and co-workers [95] reported that incorporating polysilsosesquioxanes and nanoclay in a PU coating led to the peak HRR of a PU-coated knitted polyester fabric being significantly reduced [95], and showing a much improved FR property. In a similar study, Devaux and co-workers [96] also reported a promising FR property of PU–clay and PU–POSS-coated polyester or cotton fabrics that are suitable for automotive applications [96].

## 6.3.4 Nanofibres in Automotive Applications

There are various methods of NF production, such as electrospinning, island-in sea (for bicomponent NF), melt fibrillation, gas jet technique, self-assembly and nanolithography [108]. Among these, the electrospinning techniques are gaining more importance due to several advantages, such as low cost, high production rate, higher porosity, capability of production of NF exhibiting the required diameter and morphology (beaded, ribbon, porous, aligned, core-shell and so on) [108, 109]. In particular, compared with melt-blown webs, electrospun NF have 3–4 times smaller diameter, substantially greater surface area and smaller micropores [110]. These make electrospun NF more suitable for many potential applications in automotives.

### 6.3.4.1 Electrospun Nanofibre-based Automotive Filters

Novel filters made of NF (diameter 50–300 nm) have the potential to offer superior performance, compared with conventional products, and exhibit better removal of harmful substances, and greatly improved air quality and safety (Figure 6.11). The first image of Figure 6.11 highlights the cross-section of a nanofilter where a nanofibrous web has been used on a conventional non-woven-based filter material, resulting in improved filtration efficiency. Therefore, NF-based webs are currently gaining huge importance in automotive filtration applications as they are even capable of filtering nanoparticulates (pollutants, dust particles and so on). These NF-based webs can be used in soot filters, air filters and cabin filters of automobiles, which will provide very high efficiency due to their low density, highly porous structure, tight pore size and large SVR [5, 110].

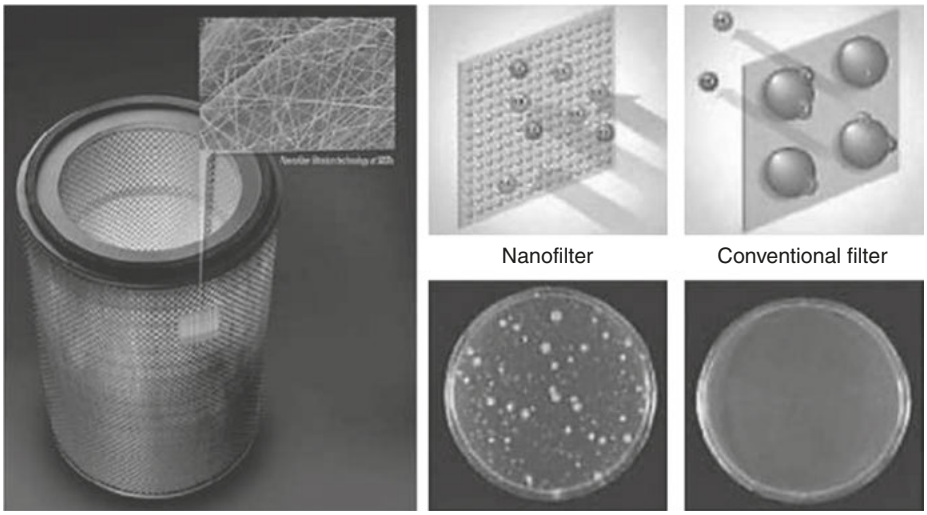


**Figure 6.11:** NF-based filters for air cleaning in a car interior. Reproduced with permission from M. Mohseni, B. Ramezanzadeh, H. Yari and M.M. Gudarzi in *New Advances in Vehicular Technology and Automotive Engineering*, Eds., J.P. Carmo and J.E. Ribeiro, InTech, Rijeka, Croatia, 2012, Chapter 1. ©2012, InTech [5].

QualiFlo® Gradient Polyester Filtration Media is excellent for automotive intake filtration with exceptional dirt holding capacity and low pressure drop. Its pore size varies from top to bottom, hence it relies on depth and gradient filtration to remove dust particles from the air. It has also introduced an FR version [111]. Other advancements in air filtration include cellulose fibre-based fabrics or papers covered with NF webs to improve the dust holding capacity, and minimise dust penetration and the rate of binding by facilitating surface filtration rather than depth filtration (Figure 6.12) [112, 113].

#### 6.3.4.2 Application of Electrospun Nanofibres in Automotive Energy Devices

Electrospun NF have a high SVR, lower pore size and higher porosity, and are gaining momentum for use in automotive energy-harvesting and storage devices.

##### 6.3.4.2.1 Electrospun Nanofibres for Rechargeable Lithium-ion Batteries

NF are very promising materials for lithium-ion batteries (LIB) due to their good electrochemical activity, high specific surface area and high mechanical strength. The recent advancements in the use of electrospun nanofibres as anode, cathode and separator materials for LIB are briefly summarised below.

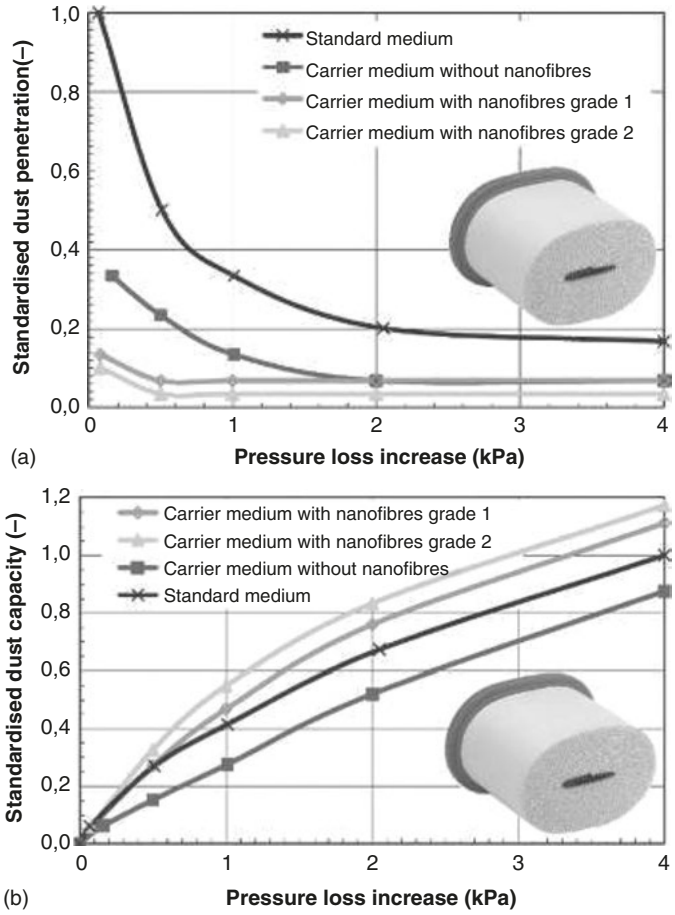


**Figure 6.12:** (a) Improvement in efficiency for NF-coated carrier papers compared with non-coated carrier paper and standard paper and (b) improvement in dust holding capacity for NF-coated carrier papers compared with non-coated carrier paper and standard paper. The test was conducted according to International Organization for Standardizations' ISO 5011 with coarse ISO test dust. Reproduced with permission from P. Trautmann, M. Durst, A. Pelz and N. Moser in the *Proceedings of the AFS 2005 Conference and Expo*, 10–13th April, Ludwigsburg, Germany, 2005. ©2005, American Filtration & Separations Society [113].

Carbon nanofibres (CNF) are used as a typical anode material in LIB due to certain advantages such as easily available, low cost and long service life. However, CNF also have some disadvantages, such as a relatively low specific capacity and rate capability [114]. Therefore, researchers have taken many initiatives to replace CNF with other composite NF such as carbon–polyacrylonitrile (PAN) NF, carbon–tin NF, carbon–Si NF and carbon–manganese oxide NF to enhance battery performance [115–118].

Generally, lithium cobalt oxide ($LiCoO_2$) is used as a cathode in LIB due to its high voltage, high specific capacity and long lifecycle. Nanostructured electrospun $LiCoO_2$ fibres exhibit increased lithium-ion and electron conductivity, high power density and good rate capability. The core-shell $LiCoO_2$–MgO composite NF are capable of solving the problem of poor cycling stability of electrospun $LiCoO_2$ NF [114]. Utilising the power of electrospinning, researchers have performed many trials to prepare and use other NF, such as vanadium(V) oxide ($V_2O_5$), lithium iron phosphate and lithium manganese dioxide ($LiMn_2O_4$) NF, as cathode material to solve certain issues and enhance performance [119–121].

Separator material plays a crucial role in controlling the performance of a battery, which is the reason electrospun polymeric NF membranes are gaining momentum in this field. The main advantages behind the excellent performance of these NF membranes as separator materials are: large specific surface area, high porosity and better interconnected conduction pathway for ions within the membrane. PVDF NF membranes can also provide good thermal stability, good electrochemical stability, stable cycle performance and high ionic conductivity at room temperature [122]. Further research in this area covers the use of composite NF such as PVDF-*co*-chlorotrifluoroethylene, PVDF-*co*-hexafluoropropylene (HFP), $SiO_2$–Nylon 6,6 and so on to replace commercial microporous membrane-based battery separators [121, 123, 124]. Recently, Jayaraman and co-workers [121] developed a high-performance LIB where they used Ti-niobium oxide NF, $LiMn_2O_4$ NF and a PVDF–HFP NF membrane as the anode, cathode and separator material, respectively (Figure 6.13) [121].

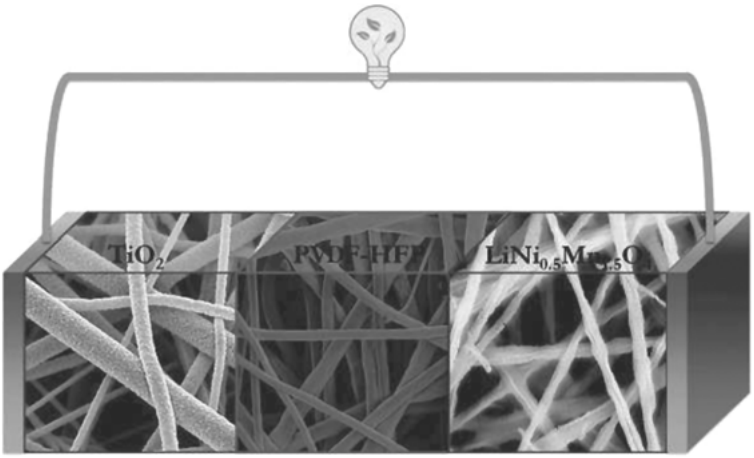


**Figure 6.13:** Schematic representation of LIB where the components (anode, cathode and separator) are made of NF. Reproduced with permission from S. Jayaraman, V. Aravindan, P.S. Kumar, W.C. Ling, S. Ramakrishna and S. Madhavi, *ACS Applied Materials & Interfaces*, 2014, **6**, 11, 8660. ©2014, American Chemical Society [121].

#### 6.3.4.2.2 Elecrospun Nanofibres for Supercapacitors

Supercapacitors (SC) are one of the most promising energy-storage devices in modern vehicles. They are mainly two types: electrically double layer capacitors (EDLC) and pseudocapacitors (PC). Highly porous electrospun CNF are mainly used in high- performance EDLC. Different polymers such as PAN, PBI and PI have been extensively investigated as precursor materials, with coaxial electrospun NF recently attracting more attention for this application. Some researchers have also explored the use of ruthenium(IV) oxide and $V_2O_5$ NF as PC due to their high electrical conductivity, high capacitance and high electrochemical stability. However, considering the higher cost and toxicity of ruthenium, researchers are focusing more on conducting polymers such as polyaniline (PANI) (currently the most promising), polypyrrole and poly(*p*-phenylene) [114].

Recently, the Volvo Car Group has developed a revolutionary concept where the car's body panels serve as a battery (Figure 6.14). They developed a very thin, light weight structural energy-storage component in combination with CNF, nanostructured batteries and SC that could enhance the energy usage of upcoming electric vehicles. It requires less space in the car, offers lighter energy storage, enables options for a cost-effective structure, would be able to replace the car's steel panels and is eco- friendly. In this material, the reinforced carbon fibres sandwich the new battery and are moulded and formed to fit around the chassis, such as the roof,

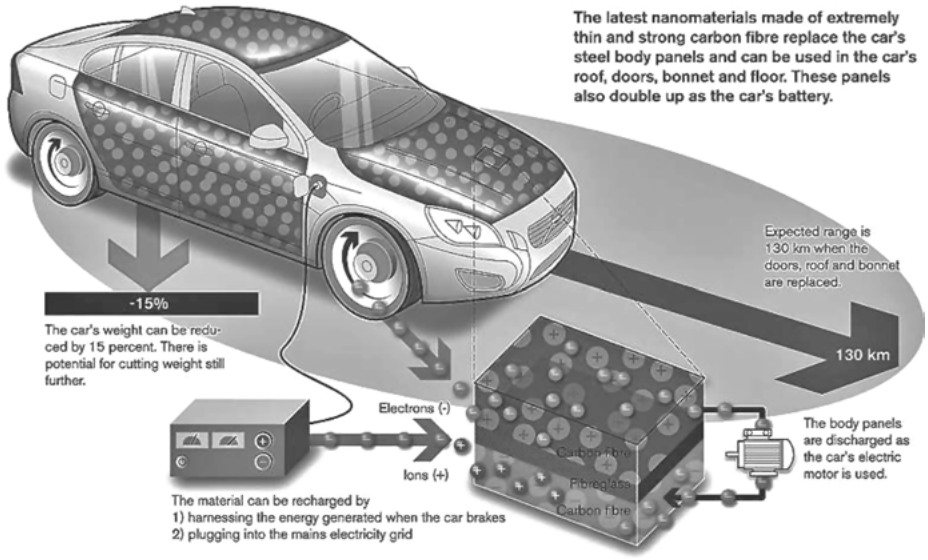


**Figure 6.14:** Concept in which the car's body panels serve as a battery, developed by the Volvo Car Group. Reproduced with permission from J. Shiry in *Carbon Fibre could make Electric Vehicle Batteries a Thing of the Past*, Composites Today, 24th October 2013. ©2013, Composites Today [125].

door panels, bonnet and floor. The material is recharged and energised *via* brake energy regeneration in the car or by plugging into a mains electrical grid. It then transfers the energy to the electric motor which is discharged as it is used around the car [125].

#### 6.3.4.2.3 Elecrospun Nanofibres for a Hydrogen Generator and Storage Device of Hydrogen Cars

A hydrogen generator, also called a HHO generator or Brown gas generator, is a device that splits water into its base molecules (two hydrogen and one oxygen) and then separates hydrogen from oxygen. Hydrogen is a highly flammable material when it is mixed with fuel vapour, creating a combustible material that can effectively power gasoline and diesel engines [126, 127]. Hydrogen energy is one of the new alternative fuel sources in 21$^{st}$ century cars.

Electrospun NF exhibit larger SVR and higher crystallinity, and have shown enhanced photocatalytic activity in the splitting of water and generation of more hydrogen. Electrospun NF also provide very high hydrogen storage capacity due to their larger SVR, higher porosity and smaller pore size. For example, CNT and CNF with tailored morphologies revealed a very high hydrogen storage capacity [128]. Researchers further extensively investigated improving the hydrogen storage capacity *via* electrospun NF by developing core-shell nanocomposite fibres such as PS–ammonia borane NF, PMMA–ammonia borane NF, carbon-coated lithium nitride NF with controllable pore size, and various morphologies [129–131].

#### 6.3.4.2.4 Elecrospun Nanofibres for an Automotive Fuel Cell

Among the different types of fuel cells, the proton exchange membrane fuel cells (PEMFC) and direct methanol fuel cells (DMFC) are currently the most popular. In recent years, researchers have focused on using novel nanostructured carbon materials such as CNF and CNT for platinum-catalyst support in electrodes of DMFC [132, 133]. Due to the one-dimensional morphology, large SVR and high porosity, these nanostructured materials can improve the stability of the supporting materials, enhance catalytic activity and the overall battery performance. PAN, PI and PANI are widely used as precursor materials to prepare CNF and CNT with controlled diameters and structures using the electrospinning technique [114].

In PEMFC, electrospun Nafion® NF are very important in the production of electrolyte membranes. However, electrospinning of the Nafion® perfluorosulfonic acid polymer alone is very difficult due to its insolubility in alcohol/water solutions and in most common organic solvents [134]. Therefore, electrospinning Nafion® requires the presence of some high-molecular weight carrier polymer such as polyacrylic acid, polyethylene oxide or PVA. However, the presence of such a carrier polymer

reduces the proton conductivity and therefore, more recent studies have focused on minimising the carrier polymer content [114]. Tamura and co-workers [135] synthesised a composite electrolyte membrane for PEMFC that was composed of sulfonated PI and sulfonated PI NF. This composite electrolyte membrane showed remarkably higher proton conductivity than the cast films without NF [135].

#### 6.3.4.3 Nano-enabled Automotive Textiles for Noise Control

Nanotechnology is also gaining importance for car interior acoustic applications. Nano- and microfibres have a highly porous structure capable of absorbing noise. Freundenberg's nano-modified microfilament structure named Evolon®, is used for headliners, doors, carpet backing, dashboard and the underbody shield, and enables an approximately 10–30-fold reduction in thickness and weight, along with a better noise absorption capacity (2,000 Hz or more) [136]. The NanoSpider™ acoustic web produced by Elmarco offers a similar sound reduction, in addition to weight reduction and heat insulation. The multiple layers of this NF web-coated high loft substrate increases acoustic performance [137].

### 6.3.5 Nanosensors in Automotive Textiles

Car interior smart textiles with nanosensors could be used to detect different actions, in particular, to recognise the posture of the driver and passengers and their gestures. Furthermore, when these sensors are connected to computing facilities and a control unit, they may recognise a situation and its context for a better interpretation of reality, or may also be used to record the health of a driver and passengers in a broad sense and to raise an alert if necessary.

Textile-based nanosensors have been discussed in order to highlight the development and integration possibilities of smart textile structures specifically designed for car interiors. Many researchers are working on different applications of smart fabric-based nanosensors inside a car. For example, the aforementioned airbag control system contains sensors and actuators interconnected *via* the apparatus for controlling airbag deployment [6].

Cochrane and co-workers [138] developed a smart flexible sensor adapted to textile structures in order to measure their strain deformation. A thermoplastic elastomer (Evoprene™) and CB NP-based nanocomposite prepared *via* a solution (chloroform) process was used to manufacture the sensor. After the total evaporation of chloroform, the final concentration of CB NP in the Evoprene™ polymer matrix was 27.6 vol%, exhibiting a good conducting network throughout the composite. This sensor displayed general mechanical properties that are strongly compatible with any soft and flexible material, such as a textile structure, offering

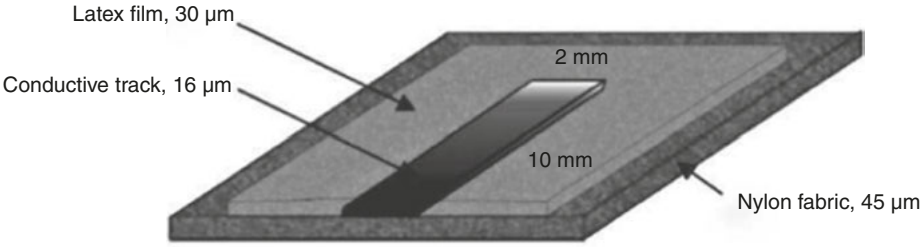


**Figure 6.15:** Schematic representation of the structure and dimensions of the sensor integrated on the fabric. Reproduced with permission from C. Cochrane, V. Koncar, M. Lewandowski and C. Dufour, *Sensors*, 2007, **7**, 4, 473. ©2007, MPDI [138].

great potential for use in car interiors. They applied a protective latex film between the sensor and a light weight Nylon fabric, as shown in Figure 6.15. The authors suggested that the textile-based nanosensor can be used in automotive airbags and seats [6, 138].

In a recent study, Ramasamy and co-workers [139] developed a flexible wearable headband system (Figure 6.16) along with real-time monitoring software to monitor a driver's condition (drowsiness and alertness). A specially designed textile-based nanosensor-containing electrode and electronics module was used that continuously acquired and transmitted signals (mainly electroencephalogram and electrooculogram type of information) through a bluetooth module to the monitoring station. The software placed in the monitoring station decoded the signal into meaningful information to detect the driver's alertness and drowsiness. This technological design can be used as a prototype to introduce advancements and modifications in structural design, software development and communication protocol in the near future to improve system performance [139].

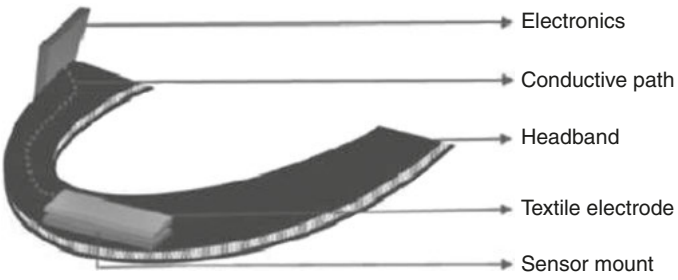


**Figure 6.16:** Headband and sensor architecture. Reproduced with permission from M. Ramasamy, S. Oh, R. Harbaugh and V.K. Varadan in *Real Time Monitoring of Driver Drowsiness and Alertness by Textile based Nanosensors and Wireless Communication Platform*, Forum for Electromagnetic Research Methods and Application Technologies, 2013. ©2013, FERMAT [139].

### 6.3.6 NanoBreeze$^{TM}$ Car Air Purifier

The NanoBreeze$^{TM}$ air filter is one of the latest, high-tech innovations of NanoTwin Technologies, Inc. (USA) to replace traditional air filters [140]. The functioning of this filter is very similar to the photocatalytic action of a self-cleaning fabric finished with $TiO_2$ NP. Inside this type of filter there is a fluorescent light tube, which emits UV-A light. The tube is wrapped by fibreglass coated with a nanolevel thin semiconductive layer of anatase $TiO_2$ NP (band gap of 3.2 eV) of approximately 40 nm. The coating of $TiO_2$ NP is achieved by the sol-gel method, which has been described in US6336998B1 [141]. As the energy of emitted UV-A light is higher than the band gap of $TiO_2$ NP, the electrons present within the crystal structure of $TiO_2$ are excited from the valance band to the conduction band causing a hole in valance band. These excited electrons and electron-holes react with oxygen and water resulting in the formation of oxygen radicals and hydroxyl radicals, respectively. The oxygen and hydroxyl free-radicals further attack other molecules (airborne dirt, pollen, harmful gases, cigarette smoke, mould spores, viruses, bacteria and so on) breaking them down *via* the oxidation–reduction reaction. The $TiO_2$ NP acts a catalyst here and is never used up, making the filter last until the light tube burns out. One main advantage of this air filter is the life of the fluorescent bulb is more than 5,000 h and no other maintenance is required [25, 140]. The working mechanism of the NanoBreeze$^{TM}$ car air purifier is shown in Figure 6.17.

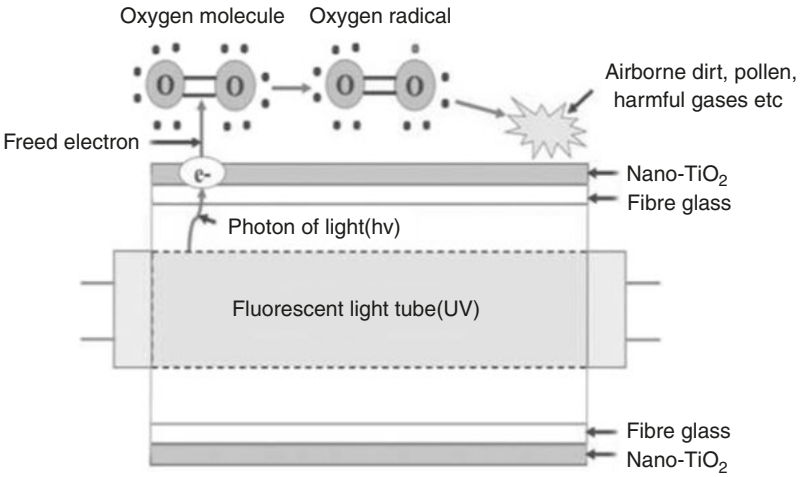


**Figure 6.17:** Schematic of the working mechanism of the NanoBreeze$^{TM}$ car air purifier.

## 6.4 Current Difficulties/Challenges for Nano-enhanced Automotive Textiles

Obtaining comfort, safety, cost-effectiveness, improved fuel efficiency, along with superior automobile characteristics and performance, is the main current challenge for the automotive industry. In spite of being a field of ambitious ideas, nanotechnology is facing many challenges in the automotive sector to successfully replace well-established/commercialised technologies or products [1]. The use of nanotechnology in automotive textiles is limited due to certain disadvantages of nanotechnology itself, i.e., nanotechnology is one the most expensive technologies worldwide. Therefore, the application of nanotechnology and use of new nanomaterials in automotive textiles may be capable of improving product characteristics, aesthetics and comfortable behaviour, but at an increased cost. The automotive industry is mostly driven by cost and reliability; therefore, the advantageous features provided by nanotechnology have to be balanced with cost-effective and reliable mass production. Since the price/performance ratio is a key driver for the market and demand of textiles in the automotive sector, the current cost of nano-enabled products could slow its widespread adoption [7]. For example, although it may be possible to achieve high filtration efficiency using NF filtration systems, it is currently cost prohibitive to be mass produced, which has limited its use.

Current research has highlighted that certain nanomaterials exert a negative impact on the environment due to the creation of many toxins and pollutants. Nanotechnology has also increased the risk to health and due to their small size, nanomaterials can cause inhalation problems and many other fatal diseases. Therefore, the development of safe nanotechnology-based approaches is a daunting task [142]. Currently, most research and development involving nanotechnology is limited to the lab-scale level. Thus, the scale up of lab-developed process technologies for application in automotive manufacturing is a big challenge. Mass production and the application of nano- enabled textiles in cars may be cost-effective; however, in today's competitive world, it is a big challenge for the automotive industry.

## 6.5 Future Scope of Nanotechnology-enhanced Automotive Textiles

The application of nanotechnology-enhanced textiles in the automotive sector is still in the under-development stage. However, it is expected that in the near future nano-enabled textiles will create a critical link between macroscopic phenomena and the nanoscale effect, enabling a pathway for the utilisation of nanomaterials for practical large-scale automotive applications. At present, considerable research is ongoing in

the automotive field to explore the potential of nano-enabled textiles for various applications in automobiles. Though nanofinishing or nanocoated textiles are capable of introducing various functionalities to automotive interior textiles, this process has not been fully commercialised. The previously discussed wide variety of functional property improvements, such as self-cleaning, antimicrobial property, flame retardancy, abrasion resistance, UV resistance and so on, has only been accepted by a few automotive manufacturers. Hence, there is a great opportunity for nano-enhanced multifunctional textiles to increase its market share in the automotive sector.

With more intensive research, in the near future the limiting factor of the high cost of nanotechnology might be eliminated, enabling the widespread commercialisation of nano-enabled textiles in automotive applications including:

- The electrically conductive nanocoatings of nano-sized materials like $TiO_2$, ZnO and antimony-doped tin(II) oxide, have been proved to be very effective in dissipating accumulated static charge, and could potentially be used in automotive interiors in the near future.
- NP such as $Al_2O_3$-, $SiO_2$-, ZnO- and CNT-based polymer nanocomposite coatings could be widely used to improve tear/wear resistance of automotive textiles.
- The hydrophilic coating of textiles using $TiO_2$ NP, or plasma treatment, may provide good moisture wicking as well as transpiration absorption that are valuable for comfortable driving, and could be commercialised in the automotive sector in the near future.
- Nanocomposites containing organically-modified clay or POSS dispersed in selected polymer matrices have attracted considerable attention for imparting flame resistance in modern and futuristic cars.
- Electrospun NF-based novel filters have the potential to offer superior filtration capabilities compared with conventional products, effectively removing harmful substances and greatly improving the air quality and safety. These filters can be widely used in automotive cabin filters and air filters in future to provide highly efficient particulate filtration.
- In futuristic cars, one of the most important requirements will be complete comfort using dirt repellent and antimicrobial textile surfaces. The application of AgNP or CuNP to the textile surface will impart antimicrobial properties that could improve hygiene within the car interior as well as contribute to eliminating unpleasant odours.
- The application of $TiO_2$, silica and zirconia NP in textiles will introduce the 'self-cleaning effect' or 'Lotus effect' providing potential applications in automotive interiors.
- Tencel™-based on nanofibrils of cellulose produced by Lenzing, which combines good moisture management, breathability, cool and dry feel to the touch, reduced bacterial growth, good heat-absorbing and insulation properties (warm and dry) compared with common polyester, make the material a suitable candidate for seat car covers [13, 143].

## 6.6 Summary/Conclusion

The traditional fabrics used in automotive interiors face various challenges such as durability, protection from dirt and dust, ventilation, fire resistance, antimicrobial activity, wear and tear resistance, and many more. Nano-enabled developments have the potential to offer novel solutions for new high-tech textiles with multiple functionalities. The automotive industry can benefit from nano-enabled textiles, both in terms of passenger needs (safety and comfort) and environmental impact, along with its prolonged service life. The increased use of textiles in modern vehicles contributes to weight reduction and hence reduced fuel consumption and CO2 emissions. Nano-enabled technical textiles offering unique and innovative features could favour the tendency of a more widespread use of textiles by the automotive industry.

NF and nano-enabled textiles enable the production of materials with reduced weight, noise absorbency, adequate insulation and other desired functionalities for accessories such as air filters, boot carpets, the cabin roof, airbags, safety belts, airbags, tyre cords and trimmings. Moreover, these textiles can be recycled easily and also have the potential to replace conventional hard surface structures.

As discussed earlier, nano-enabled textiles have the potential to provide new and innovative solutions for car upholstery with properties such as: self-cleaning, moisture wicking, water/oil/dirt repellency, wear/tear resistance, antimicrobial and antistatic activity, and noise reduction. Passenger safety can also be enhanced using nano-enabled textiles by incorporating flame-resistance or UV-resistance properties into them.

Moreover, in the near future, nanotechnology-enhanced 'smart textiles' may monitor many variables such as the driver's health; however, privacy issues may have to be overcome. Recently, several nano-enhanced innovative automotive textiles have been commercialised to compete with commercial/established products. However, the current high cost of nano-enhanced technical textiles have slowed down the widespread adoption by the automotive industry. Currently, the European automotive industry holds the most advanced and competitive position in the world. It is expected that it will continue to drive and fulfil the demand for cutting-edge technology and this is likely to inspire future nano-enabled textile industry developments to provide a competitive edge for Europe as well as worldwide.

## References

1. A.S. Malani, A.D. Chaudhari and R.U. Sambhe, *International Journal of Mechanical, Aerospace, Industrial, Mechatronic and Manufacturing Engineering*, 2016, **10**, 1, 36.
2. M. Joshi and A. Bhattacharyya, *Textile Progress*, 2011, **43**, 3, 155.
3. M. Joshi, A. Bhattacharyya and S.W. Ali, *Indian Journal of Fibre and Textile Research*, 2008, **33**, 3, 304.

4. M.P. Gashti, *Journal of Textile Science & Engineering*, 2014, **4**, 2.
5. M. Mohseni, B. Ramezanzadeh, H. Yari and M.M. Gudarzi in *New Advances in Vehicular Technology and Automotive Engineering*, Eds., J.P. Carmo and J.E. Ribeiro, InTech, Rijeka, Croatia, 2012.
6. R. Shishoo in *Textile Advances in the Automotive Industry*, Woodhead Publishing Ltd, Cambridge, UK, 2008.
7. *Textiles: Nano-enable Automotive Textiles*, observatoryNANO Project, December 2011. http://www.nanotec.it/public/wp-content/uploads/2014/04/ObservatoryNano_BRIEFING_No24_Nano-enabledAutomotiveTextiles.pdf [Accessed on 20th May 2016].
8. J.M. Garces, D.J. Moll, J. Bicerano, R. Fibiger and D.G. McLeod, *Advanced Materials*, 2000, **12**, 23, 1835.
9. *Global Technical Textiles Market Expected to Reach US$ 162.3 Billion by 2016*, EuroPlat.org, 25th January 2016. http://www.europlat.org/global-technical-textiles-market-expected-to-reach-us-162-3-billion-by-2016.htm [Accessed on 29th July 2016].
10. L. Benisek in *Global Focus at Man-made Fibre Event*, Textile Month, November, 1997, **8–16**, 3.
11. *The Use of Textiles in the Automotive Industry is set for Significant Growth*, Textiles Intelligence, 2012. https://www.textilesintelligence.com/til/press.cfm?prid=466 [Accessed on 20th May 2016].
12. W. Fung and M. Hardcastle in *Textiles in Automotive Engineering*, Volume 13, Woodhead Publishing, Cambridge, UK, 2001.
13. R.S. Kumar in *Textiles for Industrial Applications*, CRC Press, Boca Raton, FL, USA, 2013.
14. K. Singha, *Journal of Safety Engineering*, 2012, **1**, 1, 7.
15. W. Fung in *Handbook of Technical Textiles*, Eds., A.R. Horrocks and S.C. Anand, Woodhead Publishing Ltd, Boca Raton, FL, USA, 2000.
16. S. Viju and A. Mukhopadhyay, *Asian Textile Journal*, 2006, **15**, 5, 49.
17. *Application of Technical Textiles in Car Industry*, The Apparel, 14th September 2015. http://theapparel.biz/application-of-technical-textile-in-car-industry/ [Accessed on 14th May 2016].
18. D. Brookstein, *International Journal of Materials and Product Technology*, 1994, **9**, 1–3, 116.
19. M. Singha and K. Singha, *Marine Science*, 2012, **2**, 6, 110.
20. K. Pal, S.K. Pal, C.K. Das and J.K. Kim in *Recent Advances in Elastomeric Nanocomposites*, Eds., V. Mittal, J.K. Kim and K. Pal, Springer, Berlin, Heidelberg, 2011.
21. A.K. Naskar, A.K. Mukherjee and R. Mukhopadhyay, *Polymer Degradation and Stability*, 2004, **83**, 1, 173.
22. B.L. Deopura, R. Alagirusamy, M. Joshi and B. Gupta in *Polyesters and Polyamides*, Woodhead Publishing Ltd, Cambridge, UK, 2008.
23. V.B. Gupta and V.K. Kothari in *Manufactured Fibre Technology*, Springer Science & Business Media, Dordrecht, Germany, 2012.
24. J. Fang, X. Wang and T. Lin in *Nanofibres – Production, Properties and Functional Applications*, Eds., T. Lin, InTech, Rijeka, Croatia, 2011.
25. P. Ganesan, L. Sasikala, S. Sundaresan, K. Gowri and R. Senthilkumar, *Pakistan Textile Journal*, 2007. http://www.ptj.com.pk/Web-2009/07-09/P.Ganesan.htm [Accessed on 19th July, 2017].
26. *Nonwovens in Batteries and Electronic Applications*, Textile World, 1st December 2004. http://www.textileworld.com/textile-world/nonwovens-technical-textiles/2004/12/nonwovens-in-batteries-and-electronic-applications/ [Accessed on 20th May 2016].
27. I. Holme, *International Journal of Adhesion and Adhesives*, 1999, **19**, 455.
28. A.K. Sen in *Coated Textiles: Principles and Applications*, Woodhead Publishing Ltd, Cambridge, UK, 2001.

29. W. Barthlott and C. Neinhuis, *Planta*, 1997, **202**, 1, 1.
30. https://en.wikipedia.org/wiki/Lotus_effect#/media/File:Lotus3.jpg [Accessed on 11th November 2016].
31. X. Zhang, M. Järn, J. Peltonen, V. Pore, T. Vuorinen, E. Levänen and T. Mäntylä, *Journal of the European Ceramic Society*, 2008, **28**, 11, 2177.
32. S.L. Sanjay, B.G. Annaso, S.M. Chavan and S.V. Rajiv, *Journal of Surface Engineered Materials and Advanced Technology*, 2012, **2**, 76.
33. Y.L. Zhang, H. Xia, E. Kim and H.B. Sun, *Soft Matter*, 2012, **8**, 44, 11217.
34. G.Y. Bae, B.G. Min, Y.G. Jeong, S.C. Lee, J.H. Jang and G.H. Koo, *Journal of Colloid and Interface Science*, 2009, **337**, 1, 170.
35. M. Joshi, M.A. Bhattacharyya, N. Agarwal and S. Parmar, *Bulletin of Materials Science*, 2012, **35**, 6, 933.
36. C.H. Xue, S.T. Jia, J. Zhang and L.Q. Tian, *Thin Solid Films*, 2009, **517**, 16, 4593.
37. I. Das and G. De, *Scientific Reports*, 2015, **5**, 1.
38. http://www.schoeller-textiles.com/en/technologies/nanosphere [Accessed on 25th May 2016].
39. G. Abdulraheem, O.N. Peter, A.B. Kasali and A.K. Kasali, *Journal of Environmental Protection*, 2012, **3**, 9, 1063.
40. A. Bozzi, T. Yuranova, I. Guasaquillo, D. Laub and J. Kiwi, *Journal of Photochemistry and Photobiology A: Chemistry*, 2005, **174**, 2, 156.
41. K.K. Gupta, M. Jassal and A.K. Agrawal, *Research Journal of Textile and Apparel Project*, 2007, **11**, 3, 1.
42. T. Yuranova, R. Mosteo, J. Bandara, D. Laub and J. Kiwi, *Journal of Molecular Catalysis A: Chemical*, 2006, **244**, 1, 160.
43. R. Wang, X. Wang and J.H. Xin, *ACS Applied Materials & Interfaces*, 2010, **2**, 1, 82.
44. S.M. Dizaj, F. Lotfipour, M. Barzegar-Jalali, M.H. Zarrintan and K. Adibkia, *Materials Science and Engineering: C*, 2014, **44**, 278.
45. I. Sondi and B. Salopek-Sondi, *Journal of Colloid and Interface Science*, 2004, **275**, 1, 177.
46. M. López-Heras, I.G. Theodourou, B.F. Leo, M.P. Ryan and A.E. Porter, *Environmental Science: Nano*, 2015, **2**, 4, 312.
47. M. Buşilă, V. Muşat, T. Textor and B. Mahltig, *RSC Advances*, 2015, **5**, 28, 21562.
48. S.K. Ghosh in *Functional Coatings: By Polymer Microencapsulation*, John Wiley & Sons, Weinheim, Germany, 2006.
49. S.H. Jeong, S.Y. Yeo and S.C. Yi, *Journal of Materials Science*, 2005, **40**, 20, 5407.
50. H.J. Lee, S.Y. Yeo and S.H. Jeong, *Journal of Materials Science*, 2003, **38**, 10, 2199.
51. H.Y. Ki, J.H. Kim, S.C. Kwon and S.H. Jeong, *Journal of Materials Science*, 2007, **42**, 19, 8020.
52. M.D. Teli and J. Sheikh, *International Journal of Biological Macromolecules*, 2013, **61**, 302.
53. M. Paszkiewicz, A. Goł biewska, L. Rajski, E. Kowal, A. Sajdak and A. Zaleska-Medynska, *Journal of Nanomaterials*, 2016, **2016**, 1.
54. A. Berendjchi, R. Khajavi and M.E. Yazdanshenas, *Nanoscale Research Letters*, 2011, **6**, 1, 594.
55. W. Ali, M. Joshi and S. Rajendran in *Proceedings of the AATCC International Conference*, 18–20th May, Atlanta, GA, USA, 2010.
56. Md. Ruhul Amin in *Application of Nanotechnology in Textile Finishing*, Textile Learner. http://textilelearner.blogspot.in/2013/04/application-of-nanotechnology-in.html [Accessed on 18th May 2016].
57. P. Aravin Prince and P. Raja in *Nano-Finishing of Textiles (TT-03)*, Fibre2Fashion.com. http://www.fibre2fashion.com/industry-article/1505/nano-finishing-of-textiles? [Accessed on 18th May 2016].

58. H.U. Jing, X.I.A.O. Zuobing, Z.H.O.U. Rujun, M.A. Shuangshuang, W.A.N.G. Mingxi and L.I. Zhen, *Chinese Journal of Chemical Engineering*, 2011, **19**, 3, 523.
59. S. Islam, O. Troynikov and R. Padhye in *Sustainable Automotive Technologies 2012*, Eds., A. Subic, J. Wellnitz, M. Leary and L. Koopmans, Springer, Heidelberg, Germany, 2012.
60. A. Priyadarshinirajkumar and N.V. Raja, *International Journal of Fibre and Textile Research*, 2015, **5**, 3, 44.
61. A. Majumdar, A. Das and P. Hatua, *Fibres and Polymers*, 2015, **16**, 5, 1163.
62. A. Yadav, V. Prasad, A.A. Kathe, S. Raj, D. Yadav, C. Sundaramoorthy and N. Vigneshwaran, *Bulletin of Materials Science*, 2006, **29**, 6, 641.
63. http://www2.basf.us [Accessed on 25th May 2016].
64. Z. Zhou, L. Chu, W. Tang and L. Gu, *Journal of Electrostatics*, 2003, **57**, 3, 347.
65. Y. Wu, Y.B. Chi and J.X. Nie, *Journal of Functional Polymers*, 2002, **15**, 1, 43.
66. P. Xu, W. Wang and S.L. Chen, *Melliand International II*, 2005, **11**, 56.
67. A.R. Horrocks, *Polymer Degradation and Stability*, 2011, **96**, 3, 377.
68. P. Kiliaris and C.D. Papaspyrides, *Progress in Polymer Science*, 2010, **35**, 7, 902.
69. http://www.nyacol.com/products/antimony-pentoxide/ [Accessed on 25th May 2016].
70. J. Alongi, G. Brancatelli and G. Rosace, *Journal of Applied Polymer Science*, 2012, **123**, 1, 426.
71. M.A. El-Hady, A. Farouk and S. Sharaf, *Carbohydrate Polymers*, 2013, **92**, 1, 400.
72. T. Kurauchi, A. Okada, T. Nomura, T. Nishio, S. Saegusa and R. Deguchi, *SAE Technical Paper Series*, 1991, Paper No.910584.
73. C. Edser, *Plastics Additives and Compounding*, 2002, **4**, 1, 30.
74. M. Biron in *Thermoplastics and Thermoplastic Composites*, 2nd Edition, William Andrew, Oxford, UK, 2013.
75. H. Cox, T. Dearlove, W. Rodgers, M. Verbrugge and C.S. Wang in *Proceedings of the 4*th *World Congress in Nanocomposites*, 1st–3rd September, EMC, San Francisco, CA, USA, 2004.
76. T. Patterson in *Proceedings of the 4*th *World Congress in Nanocomposites*, 1st–3rd September, EMC, San Francisco, CA, USA, 2004.
77. F. Bergaya and G. Lagaly in *Handbook of Clay Science*, 2nd Edition, Elsevier, Amsterdam, The Netherlands, 2013.
78. *Polymer Nanocomposites Drive Opportunities in the Automotive Sector*, Nanowerk, 2012. http://www.nanowerk.com/spotlight/spotid=23934.php [Accessed on 27th May 2016].
79. M. Joshi, D. Biswas, A. Sarvanan, R. Purwar and R. Mukhopadhaya, *Journal of Applied Polymer Science*, 2012, **125**, S1, E224.
80. S. Thomas and R. Stephen in *Rubber Nanocomposites: Preparation, Properties and Applications*, John Wiley & Sons, Singapore, 2010.
81. A.K. Chandra and V. Bhandari in *Advances in Elastomers II*, Eds., P.M. Visakh, S. Thomas, A.K. Chandra and A.P. Mathew, Springer, Heidelberg, Germany, 2013.
82. K.K. Kar, S. Rana and J.K. Pandey in *Handbook of Polymer Nanocomposites: Processing, Performance and Application*, Springer, Heidelberg, Germany, 2015.
83. F. Cataldo, *Macromolecular Symposia*, 2007, **247**, 1, 67.
84. Y. Kojima, K. Fukumori, A. Usuki, A. Okada and T. Kurauchi, *Journal of Materials Science Letters*, 1993, **12**, 12, 889.
85. B. Rogers, R. Webb and W. Wang in *Proceedings of the 39*th *ACS Central Regional Meeting*, 16–20th May, Frankenmuth, MI, USA, 2006, p.16.
86. S, Mishra and N.G. Shimpi, *Journal of Scientific and Industrial Research*, 2005, **64**, 10, 744.
87. X. Wang and G.G. Böhm, inventors; Bridgestone Corporation, assignee; US7560510, 2009.
88. A. Lechtenboehmer, inventor and assignee; US20060229404, 2006.
89. M. Joshi, K. Banerjee, R. Prasanth and V. Thakare, *Indian Journal of Fibre & Textile Research*, 2006, **31**, 1, 202.

90. S. Parsowith in *These Balls could Bounce All the Way to Profit*, Business News, 13th November 2001, p.13.
91. K. Muraoka, K. Nishioka, N. Osaki and N. Yagi, inventors; Sumitomo Rubber Industries, Ltd., assignee; EP1418199, 2004.
92. D.K. Chattopadhyay and K.V.S.N. Raju, *Progress in Polymer Science*, 2007, **32**, 352.
93. Y.H. Yu, J.M. Yeh, S.J. Liou and Y.P. Chang, *Acta Materialia*, 2004, **52**, 2, 475.
94. I. Jones and G.K. Stylios in *Joining Textiles: Principles and Applications*, Woodhead Publishing Ltd, Cambridge, UK, 2013.
95. S. Bourbigot, E. Devaux, M. Rochery, X. Flambard and J.H. Koo in *Proceedings of the 47*th *International SAMPE Symposium and Exhibition*, 12–16th May, Long Beach, CA, USA, 2002, p.1108.
96. E. Devaux, M. Rochery and S. Bourbigot, *Fire and Materials*, 2002, **26**, 4–5, 149.
97. W.A. Daoud, J.H. Xin and X. Tao, *Journal of the American Ceramic Society*, 2004, **87**, 9, 1782.
98. B.J. Basu, V. Hariprakash, S.T. Aruna, R.V. Lakshmi, J. Manasa and B.S. Shruthi, *Journal of Sol-Gel Science and Technology*, 2010, **56**, 3, 278.
99. Y. Guo, Q. Wang and T. Wang, *Journal of Materials Science*, 2011, **46**, 11, 4079.
100. T. Kashiwagi, A.B. Morgan, J.M. Antonucci, M.R. Vanlandingham, R.H. Harris, W.H. Awad and J.R. Shields, *Journal of Applied Polymer Science*, 2003, **89**, 8, 2072.
101. H.J. Song, Z.Z. Zhang and X.H. Men, *Composites Part A: Applied Science and Manufacturing*, 2008, **39**, 2, 188.
102. M. Garcia, M. De Rooij, L. Winnubst, W.E. van Zyl and H. Verweij, *Journal of Applied Polymer Science*, 2004, **92**, 3, 1855.
103. N.R. Choudhury, A.G. Kannan and N.K. Dutta, *Tribology and Interface Engineering Series*, 2008, **55**, 501.
104. C. Friedrich, G. Berg, E. Broszeit and C. Berger, *Surface Coating Technology*, 1998, **98**, 816.
105. Y. Wang, S. Lim, J.L. Luo and Z.H. Xu, *Wear*, 2006, **260**, 976.
106. L. Chang, Z. Zhang, H. Zhang and A.K. Schlar, *Composite Science and Technology*, 2006, **66**, 3188.
107. P. Katangur, P.K. Patra and S.B. Warner, *Polymer Degradation and Stability*, 2006, **91**, 2437.
108. S. Ramakrishna, K. Fujihara, W.E. Teo, T. Yong, Z. Ma and R. Ramaseshan, *Materials Today*, 2006, **9**, 3, 40.
109. P.S. Kumar, J. Sundaramurthy, S. Sundarrajan, V.J. Babu, G. Singh, S.I. Allakhverdiev and S. Ramakrishna, *Energy & Environmental Science*, 2014, **7**, 10, 3192.
110. R.R. Hegde, A. Dahiya and M.G. Kamath in *Nanofibre Nonwovens*, Department of Materials Science & Engineering, University of Tennessee, TN, USA, 2005.
111. http://www.fiberwebfiltration.com/QualiFlo.cfm [Accessed on 25th May 2016].
112. *Proven Fibers Make a Big Difference*, Donaldson Filtration Solutions, Bloomington, MN, USA. https://www.donaldson.com/en/engine/filters/air-intake/replacement-filters/donaldson-blue-filters.html [Accessed on 25th May 2016].
113. P. Trautmann, M. Durst, A. Pelz and N. Moser in *Proceedings of the AFS 2005 Conference and Expo*, 10–13th April, Ludwigsburg, Germany, 2005.
114. X. Shi, W. Zhou, D. Ma, Q. Ma, D. Bridges, Y. Ma and A. Hu, *Journal of Nanomaterials*, 2015, **2015**, 122.
115. C. Kim, K.S. Yang, M. Kojima, K. Yoshida, Y.J. Kim, Y.A. Kim and M. Endo, *Advanced Functional Materials*, 2006, **16**, 18, 2393.
116. Y. Yu, Q. Yang, D. Teng, X. Yang and S. Ryu, *Electrochemistry Communications*, 2010, **12**, 9, 1187.
117. H.S. Choi, J.G. Lee, H.Y. Lee, S.W. Kim and C.R. Park, *Electrochimica Acta*, 2010, **56**, 2, 790.
118. Z. Lin, L. Ji, M.D. Woodroof and X. Zhang, *Journal of Power Sources*, 2010, **195**, 15, 5025.

119. L. Mai, L. Xu, C. Han, X. Xu, Y. Luo, S. Zhao and Y. Zhao, *Nano Letters*, 2010, **10**, 11, 4750.
120. O. Toprakci, L. Ji, Z. Lin, H.A.K. Toprakci and X. Zhang, *Journal of Power Sources*, 2011, **196**, 18, 7692.
121. S. Jayaraman, V. Aravindan, P.S. Kumar, W.C. Ling, S. Ramakrishna and S. Madhavi, *ACS Applied Materials & Interfaces*, 2014, **6**, 11, 8660.
122. L. Yinzheng, S. Cheng, J. Zhao, C. Zhang, S. Sun, N. Zhou, Y. Qiu and X. Zhang, *Journal of Power Sources*, 2013, **240**, 204.
123. H. Lee, M. Alcoutlabi, J.V. Watson and X. Zhang, *Journal of Applied Polymer Science*, 2013, **129**, 4, 1939.
124. M. Yanilmaz, M. Dirican and X. Zhang, *Electrochimica Acta*, 2014, **133**, 501.
125. J. Shiry in *Carbon Fibre could make Electric Vehicle Batteries a Thing of the Past*, Composites Today, 24th October 2013. http://www.compositestoday.com/2013/10/carbon-fibre-could-make-electric-vehicle-batteries-a-thing-of-the-past/ [Accessed on 25th May 2016].
126. *What is a Hydrogen Generator?* wiseGEEK. http://www.wisegeek.com/what-is-a-hydrogen-generator.htm [Accessed on 25th May 2016].
127. *How to Assemble a HHO Generator and Why It Works*, instructables.com. http://www.instructables.com/id/How-to-assemble-a-HHO-Generator-and-why-it-works/ [Accessed on 25th May 2016].
128. A.D. Lucking, L. Pan, D.L. Narayanan and C.E.B. Clifford, *Journal of Physical Chemistry: B*, 2005, **109**, 26, 12710.
129. Z. Kurban in *Electrospun Nanostructured Composite Fibres for Hydrogen Storage Applications*, Department of Physics and Astronomy University College, London, UK, 2011 [PhD Thesis].
130. J. Alipour, A.M. Shoushtari and A. Kaflou, *e-Polymers*, 2014, **14**, 5, 305.
131. X. Guanglin, D. Li, X. Chen, Y. Tan, Z. Tang, Z. Guo, H. Liu, Z. Liu and X. Yu, *Advanced Materials*, 2013, **25**, 43, 6238.
132. J.Y. Jhan, Y.W. Huang, C.H. Hsu, H. Teng, D. Kuo and P.L. Kuo, *Energy*, 2013, **53**, 282.
133. S. Kang, S. Lim, D.H. Peck, S.K. Kim, D.H. Jung, S.H. Hong, H.G. Jung and Y. Shul, *International Journal of Hydrogen Energy*, 2012, **37**, 5, 4685.
134. J.B. Ballengee and P.N. Pintauro, *Journal of the Electrochemical Society*, 2011, **158**, 5, B568.
135. T. Tamura and H. Kawakami, *Nano Letters*, 2010, **10**, 4, 1324.
136. *Acoustics – Evolon®: Sound Absorption at the Highest Level*, evolon.com. http://www.evolon.com/acoustics-absorption-material,10731-en.html [Accessed on 25th May 2016].
137. *Elmarco: Nano Technology and its Industrial Applications*, Elmarco, 2012. http://www.ptj.com.pk/Web-2012/02-2012/February-2012/Spinning-Elmarco.pdf [Accessed on 25th May 2016].
138. C. Cochrane, V. Koncar, M. Lewandowski and C. Dufour, *Sensors*, 2007, **7**, 4, 473.
139. M. Ramasamy, S. Oh, R. Harbaugh and V.K. Varadan in *Real Time Monitoring of driver Drowsiness and Alertness by Textile based Nanosensors and Wireless Communication Platform*, Forum for Electromagnetic Research Methods and Application Technologies, 2013. https://www.e-fermat.org/files/articles/15328a6b91cee4.pdf.
140. *NanoBreeze Car Air Purifier*, The Cutting Edge Magazine. http://cutcat.com/item/NanoBreeze_Car_Air_Purifier/407/c26 [Accessed on 18th May 2016].
141. W. Wei-Hong, inventor; Chung Shan Institute of Science and Technology and Taiwan Fluorescent Lamp Co., Ltd., assignee; US6336998B1, 2002.
142. R.C. Wernette, *Westlaw Journal Automotive*, 2010, **30**, 10, 1.
143. H. Firgo, K.C. Schuster, F. Suchomel, J. Männer, T. Burrow and M. Abu Rous, *Lenzinger Berichte*, 2006, **85**, 22.

# Abbreviations

| | |
|---|---|
| [Bmim][$AuCl_4$] | 1-Butyl-3-methylimidazolium chloroauric acid |
| 12C-MMT | Dodecylamine-intercalated montmorillonite |
| 3D | Three-dimensional |
| AC | Alternating current |
| ACM | Acrylic rubber (ester based) |
| ACN | Acrylonitrile |
| AEM | Acrylic rubber (ether based) |
| AgNP | Silver nanoparticle(s) |
| AMIC | 1-Allyl-3-methylimidazolium chloride |
| ASTM | American Society for Testing and Materials |
| AT | Attapulgite |
| ATBN | Amine-terminated butadiene-acrylonitrile copolymer |
| BIIR | Brominated isobutyl-isoprene rubber |
| BIMS | Brominated polyisobutylene-*co*-*para*-methylstyrene |
| BMI | 1-Butyl-3-methyl imidazolium *bis*(trifluoromethylsulfonyl)- imide |
| $BmimBF_{4-}$ | 1-Butyl-3-methylimidazolium tetrafluoroborate |
| BR | Polybutadiene rubber |
| $CaCO_3$ | Calcium carbonate |
| CAH | Contact angle hysteresis |
| CB | Carbon black(s) |
| CEC | Cation exchange capacity |
| $CeO_2$ | Cerium(IV) oxide |
| CG | Coal gangue |
| CIIR | Chlorinated isobutyl-isoprene rubber |
| CNC | Cellulose nanocrystals |
| CNF | Carbon nanofibre(s) |
| CNT | Carbon nanotube(s) |
| CR | Polychloroprene rubber |
| CRI | Cure rate index |
| CS | Chitosan |
| CSM | Chlorosulfonated polyethylene |
| CTP | Cyclohexylthiopthalimide |
| CVD | Chemical vapour deposition |
| DCP | Dicumyl peroxide |
| DDA | *N,N*-dimethyldodecylamine |
| DMFC | Direct methanol fuel cells |
| DSC | Differential scanning calorimetry |
| DTBPH | 2,5-Dimethyl-2,5-di(*tert*-butylperoxy)hexane |
| DTBPHY | 2,5-Dimethyl-2,5-di(*tert*-butylperoxy)hexyne-3 |
| DTBPIB | Di-(2-*tert*-butylperoxyisopropyl)benzene |
| DTG | Differential thermogravimetric analysis |
| DTGA | Derivative thermogravimetic analysis |
| EB | Elongation at break |
| ECO | Epichlorohydrin rubber |
| EDLC | Electrically double layer capacitor(s) |
| EG | Expanded graphite |
| EIReP | Electron-induced reactive processing |

https://doi.org/10.1515/9783110643879-007

| | |
|---|---|
| ENR | Epoxidised natural rubber |
| EOC | Ethylene octane copolymer |
| EPDM | Ethylene propylene diene monomer rubber |
| EV | Efficient vulcanisation |
| EVA | Ethylene-vinyl acetate |
| FG | Functionalised graphene |
| f-MWCNT | Functionalised multiwalled carbon nanotubes |
| FR | Flame retardant/resistant |
| fsZr | Fluorinated silyl-functionalised zirconia |
| FTIR | Fourier–Transform infrared |
| FVMQ | Fluoro vinyl methyl silicone rubber |
| GE | Graphene |
| GIC | Graphite-intercalated compound |
| GO | Graphene oxide |
| GON | Graphite oxide nanosheets |
| HAF | High abrasion furnace |
| Hc | Hectorite |
| HFP | Hexafluoropropylene |
| HNBR | Hydrogenated acrylonitrile-butadiene rubber |
| HNT | Halloysite nanotube(s) |
| HRR | Heat release rate |
| HRTEM | High-resolution transmission electron microscopy |
| IIR | Isobutyl-isoprene rubber |
| IL | Ionic liquids |
| ISAF | Intermediate super abrasion |
| ISO | International Organization for Standardization |
| KH550 | 3-Aminopropyltriethoxysilane |
| LbL | Layer-by-layer |
| LDH | Layered double hydroxide(s) |
| LIB | Lithium-ion batteries |
| LPG | Liquefied petroleum gas |
| LRD | Laponite® RD |
| MA | Maleic anhydride |
| m-CG | Modified coal gangue |
| MDI | Diphenylmethane diisocyanate |
| MDSC | Modulated differential scanning calorimetry |
| MEG | Modified expanded graphite |
| MEK | Methyl ethyl ketone |
| m-EPM | Maleated-ethylene propylene rubber |
| MK | Modified kaolin |
| MMT | Montmorillonite |
| MPDM | *N,N′*-m-phenylene dimaleimide |
| m-PP | Maleated-polypropylene |
| MTGA | Modulated thermogravimetric analysis |
| MTMA | Modulated thermomechanical analysis |
| MVQ | Methyl vinyl siloxane |
| MW | Molecular weight |
| MWCNT | Multi-walled carbon nanotube(s) |
| Na-MMT | Sodium montmorillonite |

| | |
|---|---|
| NBR | Acrylonitrile-butadiene rubber |
| NC | Nanoclay(s) |
| NF | Nanofibres |
| NGF | Natural graphite flake(s) |
| NP | Nanoparticles |
| NR | Natural rubber |
| OC | Organoclay(s) |
| ODA | Octadecylamine |
| O-Hc | Hectorite modified by octadecylamine |
| OMC | Organo-modified clay |
| OMMT | Organo-modified montmorillonite |
| ORD | Organo-modified Laponite® RD |
| OS-Hc | Hectorite modified by both O-Hc and S-Hc |
| PA | Polyamide(s) |
| PAN | Polyacrylonitrile |
| PANI | Polyaniline |
| PAT | Purified attapulgite |
| PBI | Polybenzimidazole |
| PC | Pseudocapacitors |
| PCN | Polymer–clay nanocomposites |
| PDMS | Polydimethyl siloxane |
| PE | Polyethylene |
| PEG | Polyethylene glycol |
| PEHA | Poly(2-ethylhexyl acrylate) |
| PEMFC | Proton exchange membrane fuel cells |
| PET | Polyethylene terephthalate |
| PGS | Polyglycerol sebacate |
| PI | Polyimide |
| PLS | Polymer-layered silicate |
| PMDETA | *N,N,N′,N″,N‴*-Pentamethyldiethylenetriamine |
| PMMA | Polymethyl methacrylate |
| PMTO | 3,3,5,7,7-Pentamethyl-1,2,4-trioxepane |
| PO | Polyolefin |
| POE | Polyolefin elastomer(s) |
| POSS | Polyhedral oligomeric silsesquioxane |
| PP | Polypropylene |
| PPMA | Maleic anhydride-grafted polypropylene |
| PS | Polystyrene |
| PU | Polyurethane(s) |
| PUF | Polyurethane foam |
| PVA | Polyvinyl alcohol |
| PVC | Polyvinyl chloride |
| PVDF | Polyvinylidene fluoride |
| RCN | Rubber–clay nanocomposites |
| $R_f$ | Shape fixity |
| RG | Reduced graphene |
| rGO | Reduced graphene oxide |
| RHP | Rice husk powder |
| rNBR | Recycled acrylonitrile-butadiene rubber |

| | |
|---|---|
| rPET | Recycled polyethylene terephthalate |
| $R_r$ | Shape recovery ratio |
| RT | Room temperature |
| RTIL | Room temperature ionic liquids |
| SA | Sorbic acids |
| SAN | Styrene acrylonitrile |
| SBR | Styrene-butadiene rubber |
| SBS | Styrene-butadiene-styrene |
| SC | Supercapacitors |
| $S_E$ | Shielding effectiveness |
| SEBS | Styrene-ethylene-*co*-butylene-styrene |
| SEM | Scanning electron microscopy |
| SEV | Semiefficient vulcanisation |
| S-Hc | Hectorite grafted by a silane coupling agent |
| SiO2 | Silicon dioxide |
| SMA | Shape-memory alloy(s) |
| SMC | Sheet moulded compounds |
| SME | Shape-memory effect(s) |
| SMP | Shape-memory polymers |
| SMR | Standard Malaysian Rubber |
| SPU | Segmented polyurethanes |
| SRSO | Sodium salt of rubber seed oil |
| S-SBR | Solution styrene-butadiene rubber |
| SVR | Surface area to volume ratio |
| SWC | Static water contact angle |
| SWCNT | Single-walled carbon nanotubes |
| TAC | Triallyl cyanurate |
| TAG | Tannic acid functionalised graphene |
| TBCP | *Tert*-butyl cumyl peroxide |
| $TC_{90}$ | Optimum cure time |
| TEM | Transmission electron microscopy |
| $T_f$ | Fixing temperature |
| $T_g$ | Glass transition temperature |
| TGA | Thermogravimetric analysis |
| THF | Tetrahydrofuran |
| TMA | Thermomechanical analysis |
| $T_{max}$ | Peak degradation temperatures |
| TMPTA | Trimethylolpropane triacrylate |
| $T_p$ | Peak temperature |
| TPE | Thermoplastic elastomer(s) |
| TPO | Thermoplastic polyolefin(s) |
| TPU | Thermoplastic polyurethane(s) |
| TPV | Thermoplastic vulcanisate(s) |
| TPVN | Thermoplastic vulcanisate nanocomposite(s) |
| TS | Tensile strength |
| $T_s$ | Thermal transition temperature |
| $TS_2$ | Scorch safety time |
| TTTP | 3,6,9-Triethyl-3,6,9-trimethyl-1,4,7-triperoxonane |
| UPF | Ultraviolet-protection factor |

| | |
|---|---|
| UTM | Universal testing machine |
| UV | Ultraviolet |
| VMQ | Methyl silicone rubber |
| vNR | Virgin natural rubber |
| $V_r$ | Recovery speed |
| vSBR | Virgin styrene-butadiene rubber |
| WCA | Water contact angle |
| WCB | White carbon black |
| WXRD | Wide-angle X-ray diffraction |
| XNBR | Carboxylated nitrile rubber |
| XRD | X-ray diffraction |
| XSBR | Carboxylated styrene-butadiene rubber |
| ZnO | Zinc oxide |
| ΔH | Enthalpy |

# Index



https://doi.org/10.1515/9783110643879-008